INVESTIGATION ON PATH LOSS FOR 5G WIRELESS COMMUNICATION IN AN INDOOR ENVIRONMENT

A thesis submitted in fulfillment of the requirements for the degree of Doctor of Philosophy

by

Tolulope Tunji Oladimeji

COLLEGE OF AGRICULTURE, ENGINEERING AND SCIENCE
UNIVERSITY OF KWAZULU-NATAL
DURBAN-4041 SOUTH AFRICA

2023

INVESTIGATION ON PATH LOSS FOR 5G WIRELESS COMMUNICATION IN AN INDOOR ENVIRONMENT

Tolulope Tunji Oladimeji

218048938

A thesis submitted in fulfillment of the requirements for the degree of Doctor of Philosophy: Electronic Engineering

Discipline of Electrical, Electronic and Computer Engineering

School of Engineering, College of Agriculture, Engineering and Science

University of Kwazulu-Natal, Durban, South Africa

Supervisor: Prof. Pradeep Kumar

As the candidate's supervisor, I agree to the submission of this thesis.

Signed: [redacted] _____ Date: 08-06-2023

Name: Prof. Pradeep Kumar

DECLARATION 1: PLAGIARISM

I, Tolulope Tunji Oladimeji, with student number 218048938 declare that this thesis titled **"Investigation on Path Loss for 5G Wireless Communication in an Indoor Environment"** declare that;

1. The research reported in this thesis, except where otherwise indicated, is my original work.
2. The thesis has not been submitted for any degree or examination at any other University.
3. This thesis does not contain other persons' data, pictures, graphs, or information, unless specifically acknowledged as being sourced from other persons.
4. This thesis does not contain other persons' writings, unless specifically acknowledged as being sourced from other researchers. Where other written sources have been quoted, then:
    a) Their words have been re-written, but the general information attributed to them has been referenced,
    b) Where their exact words have been used, their writing has been placed inside quotation marks, and referenced.
5. This thesis does not contain text, graphics or tables copied and pasted from the internet unless specifically acknowledged, the source being detailed in the thesis and in the references section.

Signed……[redacted]……. Date: 08-06-2023

Tolulope Tunji Oladimeji

DECLARATION 2: PUBLICATIONS

I, **Tolulope. T. Oladimeji** declare that the following is the list of publications from this dissertation: under listed journal and conference articles which is either published, accepted or under review are gotten from the research work and constitutes the topics of the research work discussed in various chapters of this thesis.

[Chapter Two]

[1] T. T. Oladimeji, P. Kumar, and N. O Oyie, "Propagation Path Loss Prediction Modeling in Enclosed Environments for 5G Networks: A Review", *Heliyon,* vol. 8. Issue 11, pp. 1-16. 2022, https://doi.org/10.1016/j.heliyon.2022.e11581.

[Chapter Three]

[2] T. Oladimeji, P. Kumar, and M. K. Elmezughi, "Path loss measurements and model analysis in an indoor corridor environment at 28 and 38 GHz", *Sensors,* vol. 22, no. 19, pp. 1-33, 2022, https://doi.org/10.3390/s22197642.

[Chapter Four]

[3] Tolulope T. Oladimeji, Pradeep Kumar, Mohamed K. Elmezughi, "Performance Analysis of Improved Path Loss Models for Millimeter-Wave Wireless Network Channels at 28 GHz and 38 GHz", *PLOS ONE,* vol. 18, no. 3, pp. 1-27, 2023, https://doi.org/10.1371/journal.pone.0283005.

[4] Tolulope Oladimeji, Pradeep Kumar and Mohamed Elmezughi, "Performance Analysis of High Order Close-In Path Loss Model at 28 and 38 GHz" *2023 Conference on Information Communications Technology and Society (ICTAS 2023),* pp. 1-5, 2023, https://doi.org/10.1109/ICTAS56421.2023.10082746.

[Chapter Five]

[5] Tolulope T. Oladimeji, Pradeep Kumar, Mohamed K. Elmezughi, "Path Loss Modeling Evaluation in the 28 and 38 GHz Frequency Bands", *Telecommunication Systems,* 2023 (under review).

[Chapter Six]

[6] Tolulope Oladimeji, Pradeep Kumar and Mohamed Elmezughi, "An Improved Path Loss Model for 5G Wireless Networks in an Enclosed Hallway", *Wireless Networks*, 2023 (under review).

DEDICATION

This thesis is dedicated to:

Almighty God, my Glory, the Bishop of my soul and Lifter of my head. – Who made this research work possible.

ACKNOWLEDGEMENT

I give all the glory to God, my maker, my sustainer, and my keeper for his mercy, protection, provision, guidance and most importantly the fulfillment of His word upon my life and this program *"Not by might, nor by power, but by my spirit says the Lord of hosts"* ***Zechariah 4:6 (King James Version)***

I would like to express my heartfelt gratitude to my supervisor, Professor Pradeep Kumar, whose influence on this work and my life has been enormous. You have been a true mentor, supporter, and trainer in the art of being the best at almost everything.

My thanks to everyone in the Radio Propagation research group at the University of KwaZulu- Natal's Discipline of Electrical, Electronic, and Computer Engineering, Howard Campus, Durban, for their cooperation, companionship, and shared enthusiasm for valuable research, this has been a buoy for me during this program.

I have no words to express my gratitude to Tertiary Education Trust Fund (TETFUND) and Federal Polytechnic, Ado-Ekiti for funding my PhD program. I would also like to thank all of the Electrical & Electronics Engineering staff at Federal Polytechnic Ado-Ekiti for their support and assistance.

I owe my deepest gratitude to Mrs. Ebunoluwa Oladimeji, my loving wife, and my wonderful daughter, Inioluwa Oladimeji: for your Love, prayers, support, encouragement and belief that I could do it. You've all given up so much for me to be able to do this. No words can express how grateful I am. May God grant us many years so that I can repay it in kind.

I am appreciative to my wonderful parents and siblings, father-in-law, mother-in-law, sisters-in-law, and brothers-in-law for their prayers, words of encouragement, and support. To Elder and Deaconess Oladimeji, Elder and Deaconess Raji, Mr and Mrs Dahunsi, Engr and Dr. (Mrs.) Ogbeye, Engr and Mrs Olaolu Oladimeji, Engr and Mrs Olusola Oladimeji, Mr and Mrs Titi Famakinwa, Mr and Mrs Muyiwa Raji, Mr Iyioluwa Raji, Mr and Mrs Oluwaseun Raji, Dr and Dr (Mrs) Bodunde, Engr and Pharm Idowu, Surveyor and Mrs Adegboyega, Dr and Mrs Bamisaye, Prof and Engr (Mrs) Adebayo, Engr and Mrs Adewale, Evang and Mrs Emmanuel, Pastor and Mrs Fasuan, Pastor and Mrs Alokan, Dr (Mrs) J.O. Omoniyi, Mr. Oluwafisayo Akinwumi and numerous other friends who have supported me along the way, I say thank you. It was great having you guys around to collaborate with, especially Nicholas, Mohammed, Okiki, Bukola, Elliot, Femi, Bamidele, Feroza, and many others from UKZN. Thank you for your kind words.

ABSTRACT

Large scale path loss modeling is critical in both mobile and fixed broadcasting system design. Predicting a system's radio coverage area is not standardized. As a result, before installing a wireless system, the channel surroundings, frequency range, as well as preferred radio coverage range must all be considered. Path loss estimation is critical in link characterization and predicting cell coverage in mobile radio systems. Increased subscriber numbers, particularly in urban areas, necessitate the addition of more base stations as well as channels. To achieve highest effectiveness from the spectrum sharing concept in contemporary communication network, interference at cell boundaries must be completely removed. An accurate path loss prediction method is used to properly determine the cell size. Beginning with signal propagation physical processes and basic path loss models, this thesis aims to demonstrate various precise path loss prediction models that can be utilized for fifth generation (5G) wireless indoors networks. For a thorough analysis, the single frequency close in (CI) references free space and floating intercept (FI) path loss models are used for continuous radio wave propagation in an enclosed corridor.

This study analyses the large-scale path loss models for an indoor corridor environment at frequencies of 28 and 38 GHz. The measurement environment consists of an indoor corridor with both line-of-sight (LOS) and non-line of sight (NLOS) scenarios using vertical–vertical (V–V) and vertical–horizontal (V–H) antenna polarizations. The single-frequency CI, FI, free space large-scale path loss models and measured data from the measurement campaign were used to evaluate the performance analysis. It also focuses on various parameters, such as standard deviation, path loss exponent (PLE), accuracy, simplicity, and stability of the models. The FI and CI models produce comparable results for both antenna polarizations and clearly fit with the measured path loss. The PLE, with the highest value of 3.33 at 38 GHz (V–H), is much higher in the NLOS scenario with V–H polarization due to the signal degradation along the path from the transmitter (Tx) to the receiver (Rx). This is because there is no direct LOS between the Tx and Rx antennas. The Rx only relies on signal diffractions and reflections from obstacles as it transmits through the path from the Tx antenna.

Furthermore, this research evaluates the third order CI PLM as well as the improved version of the well-known CI and FI path loss models at frequency bands of 28 and 38 GHz in the same measurement environment. One of the key findings is that the improved versions of these models typically perform better in terms of consistency than the standard models thereby justifying their high accuracy level. The third order CI PLM and the improved versions of the CI as well as the FI demonstrate a significant improvement for various antenna polarizations. The mean prediction error (MPE) and standard deviation error (SDE) also show how precisely and accurately the improved models predict the path loss. Additionally, the improved models provide the reasonable responsiveness and uniformity of the parameters with the change in the antenna polarization and lower the shadow fading's standard deviation in LOS as well as NLOS situations. The results confirm that the modified versions of CI and FI models predict path loss better in an enclosed environment for 5G networks.

In addition, the analysis of a path loss prediction model based on squared root distance (SRD) measurement for wireless services in enclosed spaces was also performed in this work. The CI free space reference distance model as well as the FI model is employed to evaluate and assess this model. This research also contains an

improved CI as well as FI method to assess the consistency of the squared root distance model utilizing two main error benchmarks: MPE and SDE. The main results indicate that the squared root distance model, which perfectly aligns the measurement data, offers good precision for predictions in the two bandwidths studied. Besides that, when contrasted with the conventional CI and FI models, the squared root distance path loss models have outstanding mean prediction error and standard deviation error. Ultimately, this analysis showed that the standard deviation of shadow fading can be substantially lowered in LOS as well as NLOS, suggesting greater accuracy in estimating path loss.

Having seen the need to achieve a further improvement in the performance of the existing CI model, this study proposed an improved CI model which was evaluated at frequencies of 28 and 38 GHz. It outperforms the conventional CI model. The research results indicate that the proposed enhance model delivers a better output when compared to the existing single frequency path loss model characteristics of the enclosed environment used. The findings also indicate that the upgraded model raises stability and sensitivity in the NLOS scenarios (which usually has high level of signal degradation), indicating a higher degree of path loss prediction accuracy. The path loss measurements and model analysis presented here will be useful in designing 5G wireless communication systems for indoor environments, particularly for power budget calculations. These path loss models were improved by changing existing parameters, resulting in considerable improvements for various antenna polarizations, particularly in the path loss exponent and shadow fading standard deviation. Understanding that these two parameters are critical for minimizing path loss in wireless communication systems. The Rohde and Schwarz SMB 100A radio signal generator, a Rohde and Schwarz FSIQ 40 signal analyzer, two broadband horn antennas, and MATLAB software were used for measurement and model analysis.

Table of Contents

List of Figures

List of Tables

List of Acronyms

2-D	Two-Dimensional
3-D	Three Dimensional
3GPP	3rd Generation Partnership Project
5G	Fifth Generation
6G	Sixth Generation
ABG	Alpha-Beta-Gamma
A/V	Audio/Video
ACMA	Aperture Coupled Micro Strip Antenna
AoA	Angle of Arrival
AOBG	Alternate Offer Bargaining Game
AP	Access Point
APDP	Average Power Delay Profile
BLE	Bluetooth Low Energy
BMW-SS	Beam Widened via Multi-RF-chain Sub-array
BSs	Base Stations
CDF	Cumulative Distribution Function
CI	Close-In
FB	Frequency Band
FI	Floating Intercept
D2D	Device-to-Device
DS	Delay Spread
FCC	Federal Communication Commission
FSPLE	Free Space Path Loss Exponent
Gbps	Giga bit per seconds
GRIN	Gradient-Index Novel
HDTV	High Definition Television
HPBW	Half Power Beam Width
IOTs	Internet of Things
KED	Knife Edge Diffraction
LSF	Large Scales Fading
LOS	Line of Sight
LTE	Long Term Evolution
MATLAB	Matrix Laboratory
MIMO	Multiple-Input Multiple-Output
mmWave	Millimeter Wave
MPC	Multi-Path Component
NLOS	Non-Line of Sight
NoC	Networks-on-Chip

PAA	Phase Array Antenna
PDR	Pedestrian Dead-Reckoning
PL	Path Loss
PLE	Path Loss Exponent
PLM	Path Loss Model
PSD	Power Spectra Density
PSO	Particle Swarm Optimization
RDA	Rotated Directional Antenna
RMa	Rural Macro Cell
RMS	Root-Mean-Square
RoF	Radio over Fiber
RT	Ray Tracing
SBR	Shooting and Bouncing Ray
SFSD	Shadow Fading Standard Deviation
SNR	Signal to Noise Ratio
SRD	Square Root Distance
SSF	Small Scale Fading
TD	Tree Dictionary
UHDV	Ultra-High Definition Video
UMa	Urban Macro Cellular
UMi	Urban Micro Cellular
UR-SP	Uniform Random Single-Path
USB	Universal Serial Bus
UVA	Uniform Virtual Array
UWB	Ultra- wideband
V-H	Vertical to Horizontal
VNA	Vector Network Analyzer
V-Omni	Vertical to Omnidirectional
V-V	Vertical to Vertical
WARP	Wireless Open Access Research Platform
WLAN	Wireless Local Area Network
WS	Wireless Signal

Chapter 1

Introduction

1.1 Introduction

Wireless communication refers to the transmission of information via channels without physical interaction. Its usage has evolved considerably rapidly over the last two decades. Innovations in wireless network technologies have already significantly assisted our everyday lives, fueling the need for advanced mobile devices such as laptops, smart phones, tablets, and so on. The popularity of the smart phones has fueled the exponential growth of mobile telephone services. Nevertheless, rapidly rising in the usage of several smart phones has led to an enormous rise in the wireless connectivity, posing a huge task to the mobile communication functionalities [1] as shown in Figure 1.1 [2].

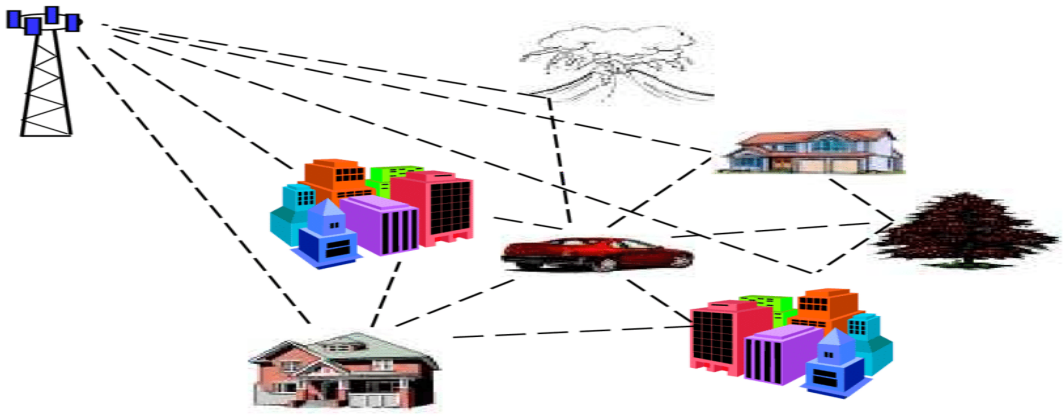

Figure 1.1: A typical mobile radio propagation environment [2].

The utilization of millimeter wave (mmWave) spectra bands is the most recent advancement in the wireless networking. The mmWave technology has several advantages in the wireless communication systems such as high capacity, high data rate, large bandwidth etc. Meanwhile, increasing mobile throughput has prompted the development of a variety of other technologies to the mobile radio networks. One popular initiative for the fifth generation (5G) involves the utilization of previously underutilized mmWave range [3]. When compared to radio systems which operate at frequency range below 6 GHz, the mmWave frequency bands provides much larger bandwidth which allows a greater number of wireless devices and applications. Potential uses include the internet backbone as well as elements that constitute connectivity [4] or access links. Recent research has shown that the broad practical applicability of the external access points in mmWave spectral range requires the path loss (PL) assessments [5]. The standout feature of the mmWave communication network is its capability to fulfill the specifications for the 5G network in the present as well as in the future. Despite having a bandwidth of approximately 250 GHz, mmWaves have a frequency range of 30 to 300 GHz. The mmWaves have a higher level of loss as compared to the microwaves. It motivates the implementations of several antennas which significantly contribute to improve the gains as well as offset the loss. A radio wave band with a wide range of bandwidths exists between 3Hz and 0.3 THz. As the frequency is increased, the wavelength of these waves decreases. The wavelength range of mmWaves is 1-100 mm. The International Telecommunication Union (ITU)

recommended its use because of the abundance of unlicensed bandwidths ready to be utilized in upcoming network systems [6]. Aside from the substantial increase in carrier frequency, which enables greater network speed as well as capacity, there are a number of additional advantages of using mmWave signals. The small wavelengths cause the reduction in the antenna dimensions which enables the use of the high gain and positional steerable antennas, potentially leading to novel spatial processing technologies such as massive MIMO and spatial signal processing [7]-[8]. MmWave communications have a relatively high PL when compared to the traditional bandwidths in the 700 MHz to 2.6 GHz frequency range. As cell communication range shrinks, collaborative configurations like node mobility, conventional intrusion detection, transmitters, and heterogeneous networks become more beneficial. In every communication network, a number of interconnected components (reflectors and/or scatters) are accessible between the Tx and Rx antennas. As a result, additional versions of the Tx signal are obtained at the Rx antenna, impacting the channel capacity performance [6]. PL in communication is thus one of the most important factors to consider when designing the wireless systems. Besides that, 5G network implementation is completely reliant on accurate PL link characterization as well as forecasting in order to increase coverage and accomplish the faster transmission speeds guaranteed by 5G technologies [9]-[10].

External signals invading from macrocells as well as microcells usually provide interior broadcasting coverage in the initial stages of wireless services. Indoor base stations or switches and routers, such as pico base stations (PBSs) as well as femto gateways provide the most of indoor radio coverage because of the growing number of broadband wireless services. As a matter of fact, interior broadcast coverage must be reconsidered from a fresh perspective. PL is the loss or degradation that an electromagnetic signal (or wave) experiences as it travels from sender to receiver. Because of PL, the signal's received power level is multiple orders of magnitude lower than the broadcast power [11].

Due to the complexities of the signal propagation environment and the various transmission techniques, real time PL is usually a mix of average path loss, Large Scale Fading (LSF), and Small Scale Fading (SSF). The average PL is deterministic, whilst large scale fading (also referred as shadow fading) and small scale fading are statistically defined. Path loss models (PLMs) are channel models that investigate the relationship between mean PL and Tx-Rx separation intervals. LSF models and SSF models deal with the large scale fading and the small scale fading, respectively. Despite the fact that the basic transmission principle in enclosed areas is similar to those in open areas, interior radio communication has the following essential specifications:

i. The reflections, scattering, as well as refractions are possible in interior radio wave propagation because of the wide variety of obstacles including furniture, wall surfaces etc. As a result, radio propagation mechanisms such as ray-optical methods, which are unlikely to be affected by the quantity of reflections and refractions, are beneficial.
ii. The size of the interior scenarios is usually smaller compared to the external scenarios. Wireless channel methods can allow for a considerably higher computation complexity per spatial unit in order to obtain a greater precision valuation.
iii. In comparison to outdoor spaces, indoor surroundings are typically occupied by slow-moving items as well as mobile users. As a result, in enclosed spaces, the Doppler shift is relatively insignificant [12].

The following are the four most common radio propagation modeling techniques for enclosed environments:

- Empirical models: Typically, these models come from channel field measurements at designated points. They are obtained by matching the measured data to a certain simplistic mathematical equation as well as gaussian distribution. As a matter of fact, empirical models tend to be simple to set up and have a reduced computation complexity. Despite the fact that empirical models are derived only from a few representative spots, they maintain several overall quality variables while disregarding the transmitting surroundings. For a various transmission situation, empirical models have a moderate level of precision. Among the widely used empirical models for enclosed spaces are the one-slope model, floor and wall factor models, COST231 model, as well as degradation rate model.
- Stochastic models: These are commonly used to model the non-periodic elements of wireless connections, such as radio bandwidth fading metrics. Stochastic models require little understanding of the transmission environment. In radio propagation channels, there are two kinds of fading: LSF and SSF. LSF describes signal quality fluctuations over long distances [4]. In contrast, SSF is distinguished by regular variations in received power over incredibly short intervals (typically, only few wavelengths). Stochastic models are commonly used to depict LSF and SSF. For example, LSF is commonly modeled as Log-normal fading, whilst SSF is popularly modeled as Rayleigh, Rice, or Nakagami-m fading, among many others.
- Deterministic models: These calculations represent the actual propagation of radiowaves. Deterministic theories are based on Maxwell's equations, which explain the motion of magnetic waves while accounting for particular transmission conditions. As a result, they are typically very precise. Deterministic models are also known as site-specific models since they involve the specific network environments. Deterministic models produce deterministic predictions, which indicate that no regardless of how frequently you operated it, the prediction values remain constant unless anything alters in the experiments conducted. Despite their high accuracy, parameters of the model have an increased computational load. Furthermore, the accuracy of simulations is highly dependent on the authenticity of the technology infrastructure used in simulation studies. The two most common deterministic transmission models are ray-optical models as well as Finite-Difference Time-Domain (FDTD) models [4].
- Semi-deterministic models: These are models that combine stochastic as well as deterministic or empirical elements. As a result, semi-deterministic models profit from deterministic as well as stochastic or empirical models. Semi-deterministic models, for example, involve less computational effort and load than deterministic models but have better accuracy than stochastic or empirical models. Among the semi-deterministic models that exist are the Dominant Path Model, the Motif Model, as well as the Geometry-based Stochastic Channel Models (GSCMs) [4].

1.2 Problem Statement

The path loss exponent (PLE) is used to evaluate the performance of a communication system in wireless channel propagation. It has been found that impediments, including walls, furniture, and people, can cause propagation loss in mmWave technology. The development of a good PL prediction model for these bands still depends on detailed characterization, analysis, and modeling in these frequency bands, despite the fact that the

research in this field is ongoing. Different PLM concepts have been proposed by researchers for PL analysis, particularly in indoor environments [13]–[21]. This study, which was carried out in both LOS and NLOS measurement data scenarios in an indoor corridor environment, assesses CI and FI PL prediction models for the frequencies 28 GHz and 38 GHz. A PL model which provides the solution to the perennial problem of signal degradation along the path of communication of wireless signals when travelling from the transmitter to the receiver is also proposed.

1.3 Research Aim and Objectives

The aim of the thesis is to investigate various precise path loss prediction models that can be utilized for 5G wireless indoors networks. The objectives utilized to achieve this aim are to:

i. Survey mmWave propagation in indoor environment undertaking for both LOS and NLOS scenarios as well as the comparison of path loss performance analysis of the three commonly used models: CI free space reference model, FI, and ABG models.

ii. Examine the large-scale path loss models for an indoor corridor environment at frequencies of 28 and 38 GHz in an indoor corridor with both LOS and NLOS scenarios using V–V and V–H antenna polarizations.

iii. Evaluate the performance analysis of the single-frequency CI, FI, free space large-scale PLMs and measured data from the measurement campaign.

iv. Evaluate the third order CI as well as the improved versions of the CI and FI PLMs at frequency bands of 28 and 38 GHz.

v. Analyze the square root distance (SRD) measurement-based path loss prediction model for enclosed environments which is assumed to vary with the square root of the distance between the transmitters (Tx) and receiver (Rx).

vi. Analyze the proposed path loss model which improves the CI PL prediction model by taking into account the influence of the difference in Tx and Rx heights.

1.4 Research Motivation and Contributions

It is indisputably necessary to mobilize mmWave for mobile phones in order to realize the full potency of 5G for improved mobile broadband. To date, we have seen numerous 5G mmWave smartphone disclosures, as well as numerous global telecom providers promoting mmWave in their channels, with the United States taking the lead with live commercial channels [13]. We expect mobile operators favoring mmWave service implementations in urban areas that require additional network capacity to accommodate rising mobile data requirement and gradually expanding their mmWave presence to smaller towns. It is also worth noting that these 5G mmWave communication systems will at first concentrate on offering macro outdoor coverage, with indoor implementations for interior coverage likely to follow [13]. With majority of mobile network traffic emanating or ending indoors, bringing mmWave services to the enclosed environments presents a huge opportunity for smartphone network operators. We are already witnessing 5G mmWave deployments for fixed wireless

connections. Potential deployment scenarios in numerous dense urban cities, such as how a dense urban city with an established outdoor access networks can re-use sites for 5G mmWave implementation, have been already examined [13].

Since mmWave does not transmit well outdoors to inside, it is advantageous to implement mmWave inside as well, given that the same mmWave frequency band can be used in indoors with the coordination with the exterior operation. This advantage expands mobile operators' options for offering private indoor mmWave network infrastructure as well as expanding mmWave indoors as part of their wireless connections [13]. 5G mmWave can enhance customer experiences to greater levels by introducing multi-Gigabit bandwidth, ultra-low response time, and practically unlimited capabilities to a wide range of gadgets such as mobile phones, tablet devices, XR (extended reality) headphones, and always-connected laptops, for enhancing the existing indoor Wi-Fi services [13].

The prime motive for using mm-wave frequency band is its ability of immensely high speed and low response times owing to the excessive channel capacity, empowering services with very flexible requirements such as mobile cognition, centimeter-level destination, and mega video and audio broadcasting [14]. Nonetheless, PLMs are important to better understand the attenuation of propagating signals and help researchers and standards organizations to create effective predictive models for the network infrastructure models. This has benefited in the development of communication channels such as mmWave technology, which is widely employed in 5G wireless systems. Most standard bodies demonstrate single frequency PLMs in either the CI free space reference distance or FI form [15]-[16].

Comprehensive measurement campaign evaluation [17]–[20] has revealed that high-frequency communication systems encounter transmission mechanism constraints when particularly in comparison to the sub-6 GHz band. Few studies have attempted to analyze the inner nature of the mm-wave medium, i.e. what transmission procedures actually generate such channel characteristics [21]-[24]. However, there are some significant aspects related to the improvement of PLMs in enclosed environments, particularly at frequency bands of 28 and 38 GHz; have yet to be entirely dealt with. This was completely addressed in this thesis.

This thesis contribution is as follows:

a) Comprehensive review of millimeter wave's propagation observations in the outdoor, interior office, and corridor for various frequencies to single frequency path loss models CI and FI, as well as the multi-frequency path loss model ABG. It was observed that because the CI and FI path loss models are simple and these models function well practically for all the examined frequency bands.

b) Analysis of large-scale path loss models in an indoor corridor environment at 28 and 38 GHz frequency bands with two different antenna polarizations, in both LOS and NLOS scenarios using CI and FI PL prediction models.

c) Performance analysis of CI and FI path loss model at 28 and 38 GHz to determine the behavior of the shadow fading standard deviation and path loss exponent in an enclosed environment.

d) Evaluation of the third order CI as well as the improved versions of CI and FI PLMs at frequency bands of 28 and 38 GHz using the MPE and SDE.

e) Assessment of the square root distance measurement-based model using the CI free space reference distance model as well as the FI model and also determine the degree of predictability of the squared root distance model using two major error metrics: MPE and SDE.

f) Proposing the improved path loss model which improves which takes into account the difference in Tx and Rx heights to produce the improved results for the shadow fading standard deviation and the path loss exponent values at 28 and 38 GHz frequency in an enclosed environment.

1.5 Scope of the Research Work

The scopes of the research work are:

i. Thorough review of literatures on the existing path loss models in order to determine efficient path loss models to overcome the challenge of path loss in millimeter wave propagation.
ii. Analysis of large-scale path loss models for an indoor corridor environment at frequencies of 28 and 38 GHz. The measurement environment consists of an indoor corridor with both LOS and NLOS scenarios using V–V and V–H antenna polarizations.
iii. The use single-frequency CI, FI, free space large-scale PLMs and measured data from the measurement campaign were used to evaluate the performance analysis.
iv. Proposing an improved CI model for enhanced prediction performances with less error prediction, reduced path loss exponent and a better performance of the shadow fading standard deviation in comparison with the conventional CI model.

1.6 Organization of the Thesis

The following is the thesis structure:

Chapter 1 introduces the introduction to path loss in millimeter wave propagation, the research goal and objectives, research contributions, and organization of the thesis.

Chapter 2 discusses the survey of indoor environment undertaking for both LOS and NLOS scenarios as well as the comparison of path loss performance analysis of the three commonly used models: CI free space reference model, FI, and Alpha-Beta-Gamma (ABG) models at some selected frequencies. The review looked at how to determine the efficient path loss models which is a major challenge in millimeter wave propagation. This chapter also focuses on the measurement work done in millimeter wave research in interior environments. The analysis of path loss and shadow fading in different frequency bands are presented. Another purpose of this chapter is to get a thorough understanding of the best path loss model, especially for interior situations, and to improve it in future research to provide a better line of fit and simplicity among the three fundamental path loss models: CI, ABG, and FI. In both LOS and NLOS scenarios, the study found that the CI free space reference model and the FI path loss model are the best path loss models for the indoor millimeter wave propagation.

Chapter 3 examines the large-scale path loss models for an indoor corridor environment at frequencies of 28 and 38 GHz. The measurement environment consists of an indoor corridor with both LOS and NLOS scenarios using V–V and V–H antenna polarizations. The single-frequency CI, FI, free space large-scale path loss models and measured data from the measurement campaign were used to evaluate the performance analysis. This

chapter also focuses on various parameters, such as standard deviation, PLE, accuracy, simplicity, and stability of the models. The analysis focuses on the peculiarity of the effect of the wall proximity on the path loss parameters as well as comparisons with the parameters in some of the reviewed literature studies.

Chapter 4 describes the analysis of the third order CI as well as the improved versions of the CI and FI path loss models at frequency bands of 28 and 38 GHz. One of the key findings of this study is that the enhanced versions of these models typically perform better in terms of consistency than the standard models thereby justifying their high accuracy level. The improved versions of the CI as well as the FI demonstrate a significant improvement for various antenna polarizations. The MPE and SDE also show how precisely and accurately the improved models predict the path loss. Additionally, the improved models provide the reasonable responsiveness and uniformity of the parameters with the change in the antenna polarization and lower the shadow fading's standard deviation in LOS as well as NLOS situations. The results confirm that the modified versions of CI and FI models predict path loss better in an enclosed environment for 5G networks.

Chapter 5 presents the analysis of the path loss prediction model based on the SRD for wireless services in enclosed spaces. The CI free space reference distance model as well as the FI model is employed to evaluate and assess this model. This research also contains an improved CI as well as FI method to assess the consistency of the squared root distance model utilizing two main error benchmarks: MPE and SDE. The main results indicate that the squared root distance model, which perfectly aligns the measurement data, offers good precision for predictions in the two bandwidths studied. Besides that, when contrasted with the conventional CI and FI models, the squared root distance path loss models have outstanding mean prediction error and standard deviation error. Ultimately, this analysis showed that the standard deviation of shadow fading can be substantially lowered in LOS as well as NLOS, suggesting greater accuracy in estimating PL.

Chapter 6 also presents the improved CI model whose results deliver a better output when compared to the existing single frequency path loss model characteristics for the enclosed environment. The findings also indicate that the upgraded model raises stability and sensitivity in the NLOS scenarios indicating a higher degree of path loss prediction accuracy.

Finally, conclusion and future work are given in Chapter 7.

1.7 Chapter Summary

This chapter discusses the introduction of path loss in wireless communication and the use of millimeter wave spectra bands, which is the most recent advancement in the wireless networking. It also explores the path loss models used in both enclosed and open environments, research problems, contributions, as well as the thesis organization. Recognizing that reliable signal propagation loss assessment is critical in the planning and development of the modern wireless communication networks. This thesis presents the improved CI path loss model by modifying existing parameters, resulting in significant improvements for various antenna polarizations, particularly the path loss exponent and shadow fading standard deviation being acquainted with the importance of these two parameters in minimizing path loss in wireless communication systems.

Chapter 2

Literature Review and Fundamentals of Millimeter Wave Propagation

This chapter focuses on the survey as well as the fundamentals of millimeter wave propagation in indoor and outdoor environments. It also undertakes a thorough understanding of the best path loss model, especially for interior situations, and to improve it in future research to provide a better line of fit and simplicity among the three fundamental path loss models: CI, ABG, and FI. In both LOS and NLOS scenarios, the study found that the CI free space reference model and the FI path loss models are the best path loss models for indoor millimeter wave propagation.

2.1 Introduction

In recent years, the rate of increase in wireless data traffic per subscriber has been above 50% per year, and due to the continued use of video and internet of things (IOTs) it is predicted to continue to rise over the next ten years [25]. It has also been predicted that by 2030, mobile data traffic will be increased by a factor of 5000 [25]. This anticipated rise in traffic may, however, be managed by increasing link capacity, spectrum availability, and significant small-cell densification [25]. To meet this demand, the wireless industry will need to shift to fifth-generation cellular technology which will use mmWave frequencies to provide unprecedented spectrum and multi-Gigabit-per-second (Gbps) data speeds to mobile devices [26].

Furthermore, as gigabit Ethernet and desktop connections have become inexpensive for server connections, the communication sector made a disclosure in 2007 of the empty 10 GB for usage [27]- [29]. In addition, gigabit Ethernet became the standard for servers, requiring systems to be ordered with gigabit network interface cards on a regular basis [29]. Over the time, the cost of wireless gigabit lines has about equaled the cost of wireless, which provides superior output in older wireless applications as well as other feasible uses at gigabit speeds. Wireless communications have become increasingly relevant in the business world, particularly in Universal Serial Bus (USB) 2.0, gigabit rates, and long-range connectivity, with the significant applications in high-quality multi-media, phone, and data services [29].

Previous wireless local area network (WLAN) speeds were just 54 Mb/s with IEEE 802.1 and achieved 150-300 Mb/s in some applications. However, when it comes to higher access speeds from rich media content, even 500Mb/s is insufficient. In the near future, home Audio/Video (A/V) networks will require Gb/s data speeds to help deliver uncompressed high-definition video at resolutions of up to 1920-1080 progressive scan, with latencies ranging from 5 to 15 milliseconds [29]-[30]. In addition, the technical requirements for the high-speed wireless systems must consider the following factors:

(a) The requirement for higher data rates will continue to grow as the demand for multimedia networks grows.

(b) The demand for shared resources has increased as a result of data streaming for both personal and mobile devices.

Although numerous approaches have been adopted, including IEEE 802.1, IEEE 802.16 WiMax, and Ultra-wideband (UWB). However, the effectiveness of wireless communications has not been sufficient to meet the expectations placed on them, particularly in 5G networks [31]. A better way to tackle these challenges is to make proper use of frequencies that are not employed in millimeter waves but have a lot of application potential. Despite the fact that millimeter wave technology has been in use for some time. With the advent of process technology, this technique has begun to garner a lot of traction among academics and businesses.

Even though the IEEE 802.11n standard will improve the reliability of wireless communications, the data rate will remain modest (even below 1Gbps) [29], [31], [32]. Millimeter wave technology has emerged as a critical field of research that has aided in the advancement of 5G wireless communications in broadband, with applications in ultrahigh and high definition technology [33]. Millimeter wave technology operates in the electromagnetic spectrum between 30 GHz and 300 GHz, with wavelength ranging from 10 mm to 1 mm [34]. This accessible spectrum at these frequencies is more than 200 times larger than all of the present cellular network allocations [35]. This technology is characterized by a huge quantity of idle bandwidth that can enhance the data rate available to end users, allowing it to meet the two major requirements for 5G Networks: ultra-high peak throughput (20 Gbps) and average user experience rate (50-100 Mbps) [36]. The generality of millimeter wave frequency ranges is found between microwaves and infrared waves in the electromagnetic spectrum regions that lie between 30 GHz (10 millimeters) and 300 GHz (1 millimeter) as shown in Figure 2.1 and Figure 2.2 [37], [38]. As shown in Figure 2.3, the 4G cellular networks has served as a cornerstone for 5G networks, as small cells, wideband data, and WiFi rely on servers at network edges to enable the adoption of lower latency applications in new scenarios [25].

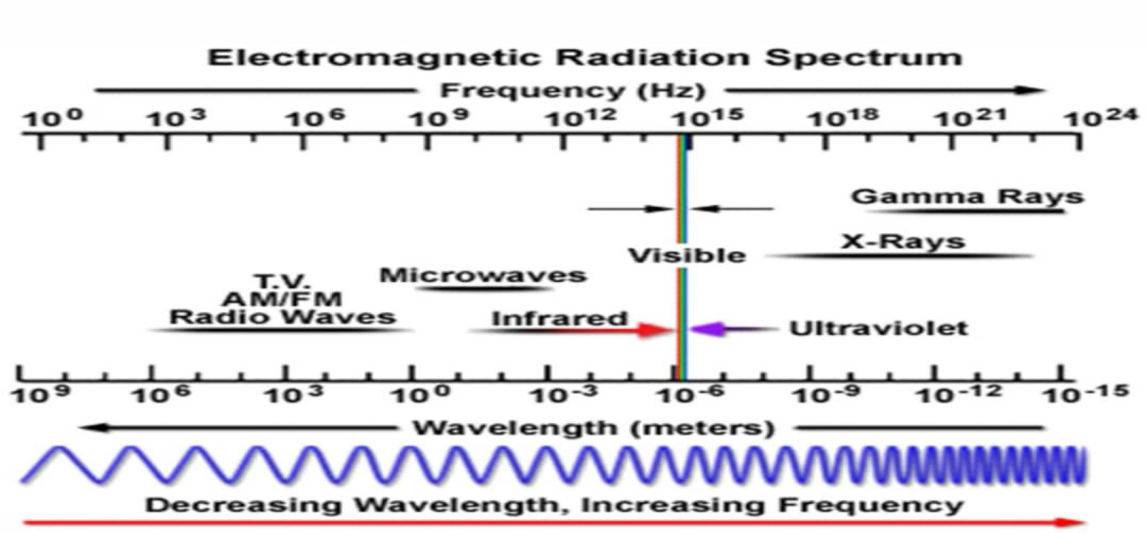

Figure. 2.1 Electromagnetic frequency spectrum [37].

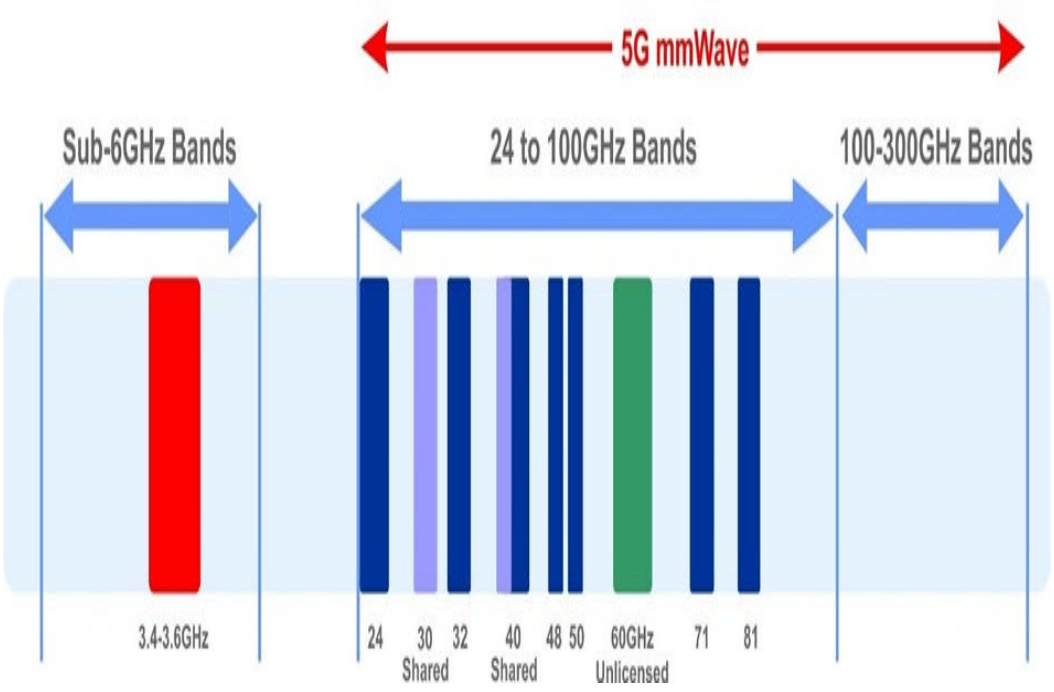

Figure. 2.2 ITU 5G frequency bands [38].

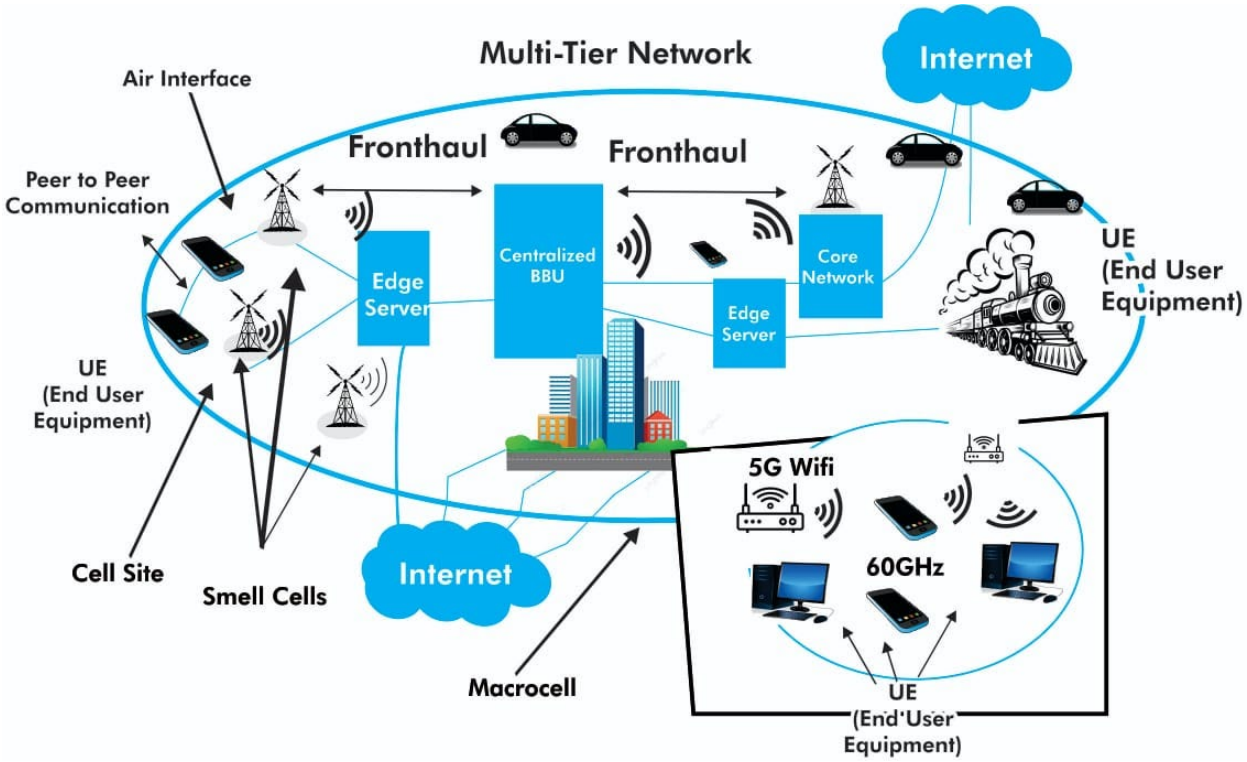

Figure. 2.3 Evolving mobile networks from 4G toward 5G multitier architecture [25].

The 5G millimeter wave wireless channel bandwidths will be substantially more efficient than the current 4G LTE 20 MHz cellular channels. Even though diffraction and material penetration will cause an increase in attenuation at millimeter wave frequencies compared to today's 4G microwave frequencies, boosting the relevance of LOS propagation, reflection, and scattering. The usage of accurate propagation models is critical

for the development of new mm wave signaling protocols e.g. air interfaces, as it is required for the proper operation of new millimeter-band 5G systems. The corresponding path loss models must be set up for link budget evaluation and signal strength proposal in the process of generating reliable models for 5G systems and determining standard performance measurements, with the addition of directional and beam forming antenna arrays and co-channel interference, which statistical models cannot adequately assess [36].

The path loss is a measure of the degeneration of the propagated signals over a distance range in both LOS and NLOS scenarios. The path loss exponent is a key indicator of any communication system's performance in wireless channel propagation. Wireless system design, planning, and simulation were all part of the model application. Different path loss model ideas have been proposed by numerous scholars for investigation, notably in indoor environments [6], [39]. Path loss models are used in a variety of applications, the most important of which include power budget calculations, modulation, cellular coverage/interference forecasts, and the design of coding schemes [40]. The data from the various measurements and models used in this work will also aid researchers in the standardization of 5G millimeter wave channel models, particularly in the link budget estimates described previously.

Although the main goal is to find an acceptable model with the best line of fit and the simplest application for path loss model estimate in both LOS and NLOS scenarios. However, this research will continue to work in the future to improve the FI and CI models which are user-friendly in a wide frequency range in order to achieve a higher level of accuracy while maintaining high energy efficiency, allowing for very robust and stable transmission capacity in both LOS and NLOS. Excessive path loss particularly in NLOS will be corrected by the use of high gain antennas, which has been one of the key flaws in previous works [40]-[45].

The reason for this study stems from the fact that channel modeling in 5G millimeter wave propagation in an indoor environment is a current research area in which variations in capacity have been observed as a result of different models being used. As a result, existing models must be validated and improved for future millimeter wave propagation in order to aid link design and to enable engineers and researchers in budget estimates for good wireless networks in the 5G wireless network propagation in an indoor environment. The findings of this chapter will aid design engineers and researchers in calculating budgets for the high performing 5G wireless networks and even the anticipated 6G network in an indoor environment. Another purpose of this work is to gain a comprehensive understanding of the best path loss model, particularly for indoor environments, and to improve on it in future research to provide a better line of fit and simplicity among the three basic path loss models: CI, ABG, and FI.

The rest of the chapter is organized as follows: Sections 2.2 and 2.3 cover fundamental characteristics of mm waves and review of literatures on mm waves, respectively. The path loss in mm wave propagation is explained in section 2.4. The overview of the accuracy and viability of models of propagation for outdoor as well as indoor environments in LOS and NLOS is reviewed in section 2.5, while section 2.6 discusses findings on path loss propagation in different antenna polarizations using the CI, FI, and ABG models. Finally, section 2.7 presents the chapter summary.

2.2. Fundamental Characteristics of mmWaves

Heavy path loss, increased bandwidth, reduced wavelength, increased penetration loss, and wavelengths in the millimeter range characterize millimeter wave communication. These characteristics are addressed below [44]:

2.2.1. Abundant Bandwidth

At the moment, the overall bandwidth available for the mobile networks is insufficient to meet the high data demand of devices; in fact the available bandwidth is less than 780 MHz for 2G, 3G and 4G networks. The biggest advantage of the millimeter communication over the microwave communication is the large bandwidth, which allows communication at high frequencies and provides the large bandwidth for wireless systems [46].

2.2.2 Short Wavelength

Because the mm wave signal has a short wavelength on the order of millimeters, it is necessary to communicate it via MIMO technology, and it is also appropriate for cramming a high number of half-wavelength spaced antennas into a small space. The combination of mm Wave with massive MIMO technology may considerably improve wireless access and throughput performance [46].

2.2.3. Propagation Loss

There are two types of propagation loss: path loss and penetration loss. According to the Friis transmission expression for the assumption of LOS, the free space path loss is proportional to the square of the carrier frequency. Because microwave frequencies start at 26.5 GHz, there is a larger propagation loss than in the microwave band. For example, at 60 GHz, the propagation loss is 28 dB higher than at 2.4 GHz. This has been a key drawback of mm wave, but with the introduction of D2D communications, a high gain directional antenna may compensate for the loss, improving network capacity and enhancing security against eavesdropping and jamming. There is a larger penetration loss in NLOS circumstances, making it harder for mm wave nodes put outdoors to cover indoor spaces. Signals/propagation may suffer a large penetration loss in the case of indoor users with outdoor base stations (BSs), lowering data throughput, spectrum efficiency and energy efficiency. As a result, it's unavoidable to separate outside and indoor scenarios [46]-[47].

2.3. Literature Review on mmWave Propagation

Salous et al. [26] pointed out that there is unallocated spectrum in the millimeter wave bands, prohibiting the full use of huge antenna arrays for high-speed data transfers. Despite the fact that gigabit data transmission in these bands necessitates accurate channel modeling, the shadowing effect and the need for adaptive beam formation in areas with significant mobility persist. As a result, it was suggested that in addition to end channel sounders, detailed measurements for full radio characterization should include angular spread and delay time in the characterization of multipath made-ups. The lack of channel models, on the other hand, must be addressed in order to provide the inputs to the standards organizations.

Hajj et al. [48] emphasized the relevance of millimeter bands as a proven solution for high-data-rate transmission, particularly in indoor environments. However, millimeter wave propagation technology has been reported to suffer from propagation loss of 25 dB to 30 dB due to the impediments such as walls, furniture, and human blocking. Another study used a frequency domain and a vector network analyzer (VNA) to investigate

millimeter wave propagation at 60 GHz in an indoor environment. The results suggest that an access point (AP) can be placed in the center of the network to reduce shadowing caused by the human impediments. It employs a high frequency for a problem that could have been solved with a frequency lower than 60 GHz. In [49], millimeter wave measurements were performed with the goal of determining the influence of atmospheric variables on transmission. The difference between the theoretical rain-induced signal attenuation and the practically recorded signal attenuation during rainfall was studied. The idea of rain forecasting and monitoring in real time was founded. As a result, the dynamic rain-aware link adaptation method was developed to allow the system to fit the modulation and coding scheme to rain intensity levels, resulting in improved performance of fixed modulation and coding schemes. The results demonstrate that the rain-induced signal is unpredictable in both practical and theoretical settings, ranging from 1.5 dB to 4.5 dB, due to attenuation caused by changes in weather conditions. This had the disadvantage of not allowing different linkages to be compared.

Gade et al. [50] discovered that on-chip wireless links function better than standard Networks –on- Chip (NoC) for millimeter wave systems. On-chip wireless channel characteristics, as well as antenna implementation with near field and multipath propagation effects, were used in the study. The near field/transition region, where the propagation in the on-chip wireless channel takes place, makes the channel more difficult. It was also discovered that directional antennas are less impacted by the channel time dispersion, despite the fact that this is accompanied by higher losses, as compared to the omnidirectional antennas. The on-chip wireless channel provides the information on the characteristics of wireless communications and aids in the design of circuits for improving the performance.

The performance of millimeter waves for indoor communication at multiple bands between 28 GHz and 73 GHz was thoroughly examined for LOS and NLOS conditions considering the effects of various building and frequency sensitive materials. The link between separation distances and the duo of receive power and the delay spread was predicted to be inverse. By increasing the antenna's directivity, the separation distance can be increased. The system has also been able to solve the problem of bandwidth in electronic devices which is allowing the growth of the low-cost infrastructure for broadband mobile devices. The main limitation of this approach is that it tends to fail as separation distance and the communication capacity increase [51]-[53].

Chittimoju and Yalavarthi [54] provided a thorough assessment of millimeter wave communications, including some of the benefits and uses. They demonstrated that millimeter wave encourages larger bandwidth while also increasing speed up to 10 Gbps. Some of the benefits include the utilization of the compact components, less interference, and high security. The range is limited in the LoS, which is one of the uncovered key flaws. In [55], authors suggested a novel technique, termed as Q learn-based system that incorporates edge computing function in an adjustable power and angle sub-6 GHz user equipment to tackle the capacity and efficiency problems in millimeter wave propagation. The end result shows that the user equipment using this scheme was able to achieve excellent energy efficiency which allows a very strong and steady transmission capacity. Further research by Maltsev et al. [56] focuses on the benefits, drawbacks, and common applications of millimeter wave propagation for various 5G communication bands. Millimeter wave was determined to be critical in the deployment of 5G, and it is believed that significant improvements in radio and network would be developed to aid in the deployment of the impending 6G.

Using ray tracing (RT) simulations and directed measurements, Fuschini et al [57] investigated the narrowband and wideband properties of an in-room 70 GHz wireless channel. Reflection is the most pronounced mode of propagation; however, scattering is still present and appears more than when the frequencies are below 6 GHz. When comparing a more detailed environment to a less detailed environment, if both are exposed to the same sources of error, a faster rate of calculation was seen, but this did not translate to greater simulation accuracy.

Further research work included compiling a broad analysis of 5G network approaches in millimeter wave wireless communication systems, as well as bringing together important millimeter wave propagation models from the past to the present. It also emphasizes the significance of developing diverse models based on RT and measurement procedures, not only for current use but also for future uses in academia and industry. Knowing full well that millimeter wave is still in the research era, notably in the application for 5G propagation [25], the data acquired on shadowing and path loss will aid in the predicted improvement. In [47], authors examine the main issues with millimeter wave propagation such as low beam width, high penetration loss, and strong route loss. It also discusses the differences between the analytical modeling and RT methods for channel modeling. After the measurement, data processing and analysis of the measurement results such as channel gain, scatterer identification, RMS delay spread and average power delay profile (APDP) were given. When taking measurements in varied settings, the usage of a MIMO channel with a wide frequency spectrum is essential.

The shooting and bouncing ray (SBR) method was validated by Wang et al. [58]. At a millimeter wave band frequency of 60 GHz and a decimeter band frequency of 2.4 GHz, the propagation parameters such as path loss, RMS delay speed, and so on were given. The results demonstrate that millimeter waves have a lesser coverage area than the lower frequencies due to high attenuation. Its main benefit is that it will be an effective way for deploying 5G networks. Further research into millimeter wave propagation at 60 GHz reveals that the multipath effect is more pronounced in indoor NLOS environments due to the reflection effect on the received power being greater than the diffraction effect on the received power. One of the flaws in this technique is that it is only helpful for short-distance communication. Also, because it will be used in a corridor, atmospheric absorption and wall roughness should be taken into account [59]. This study [60] highlights some of the characteristics of millimeter wave propagation, laying the groundwork for the creation of outdoor communication networks. This method used the SBR approach to simulate the environment at a frequency of 73 GHz in both LOS and NLOS circumstances. To verify the validity of the SBR approach, the measured results were compared with the simulated route loss data. In both LOS and NLOS conditions, the power angle and power delay profiles were scrutinized as propagation aspects.

Elmezughi et al. [41] reported propagation measurements at 14 GHz, 18 GHz, and 22 GHz frequency bands in an indoor environment. Two path loss prediction models and the analysis of communication scenarios for both NLOS and LOS were presented. The LOS analysis shows that the CI and FI models function nearly identically after execution at all frequencies. With the frequencies increasing along the LOS range, the PLE in the CI model rose tremendously. It rises from 1.37 to 1.66 for the 14 GHz and 22 GHz frequency bands, respectively; however, the LOS values do not match those of the FSPLE. Due to the environmental influences, it was discovered that path loss models exhibit symmetrical characteristics about 180° AoA. The models, on the other hand, perform better at 30°, 330°, and 180° AoA. The findings also demonstrated that CI and FI models

may be employed reliably in both LOS and NLOS corridor scenarios. The main flaw that has to be addressed is the adoption of a higher-gain antenna to decrease extra path losses to the absolute minimum. In addition, as a follow-up to the above-mentioned result, the effect of transmitting antenna heights on these models' parameters was studied in [42]. Elmezughi and Afullo [43] have recently updated this work, delivering an efficient improvement for both the CI and FI path loss models. The major findings show that for both LOS and NLOS communication scenarios, the modified models beat the standard models. Furthermore, the proposed models have substantially superior stability and sensitivity than standard models, especially in the NLOS condition. By combining these enhanced models with the LOS probability models described in [46], a generic and accurate model for indoor corridor environments may be obtained.

2.4. Path Loss in mm Wave Propagation

Path loss is a phenomenon that occurs when a transmitting signal is attenuated as a function of the distance traveled as well as the propagation channel characteristics. It also refers to the loss or attenuation that a propagating electromagnetic signal (or wave) experiences as it travels from the transmitter to the receiver. As a result, the received power is lower than the broadcast power level. However, it is influenced by a number of elements, including antenna gains, operating frequency, transmitted power, and the distance between transmitter and receiver. The most common way to express path loss is in decibel (dB) [61]. Since, the distance between the transmitter and receiver is no longer linear; path loss in wireless propagation is mostly a function of a logarithm factor. The power density PD_{rad} of an isotropic antenna, that has sphere radius R, with a transmitted power P_t and power gain G_t, is given by equation (2.1) [62]:

The path gain $G_p(\lambda, d)$ is given by equation (2.2) [49]:

$$PD_{rad} = \frac{P_t G_t}{4\pi R^2} \tag{2.1}$$

$$G_p(\lambda, d) = \left(\frac{\lambda}{4\pi d}\right)^2 \tag{2.2}$$

Where d , λ, c, f and $4\pi d^2$ are the sphere radius, the carrier wavelength, the speed of light in the vacuum, the carrier frequency, and the sphere area, respectively.

In the free space, the fall of signal strength is proportional to the square of the distance, also power path loss within a distance in meters is also proportional to d^2. In radio propagation, path loss is usually expressed with the channel attenuation which is the path gain inverse. The expression for the path loss (L_p) in decibel form is given in equation (2.3) [49]:

$$L_p = L_o + 20log_{10}(d) \tag{2.3}$$

Where L_o is the path loss in the first distance in meters and it is given by [49]:

$$L_o = 20log_{10}\left(\frac{4\pi}{\lambda}\right) \tag{2.4}$$

Equation (2.4) implies that the coefficient of path loss in free space is characterized by a component L_o that is fixed and its rate goes up as there is increase in the frequency and also another component causing attenuation of 20 dβ/decade of the distance [61]-[62].

2.4.1 Path Loss Propagation Models

In the last 20 years, there has been substantial research into various propagation channels that could be used for interior channels. While some have concentrated on both outdoor and indoor office environments, others have moved their focus to exclusively indoor office environments [63]-[69]. Wang et al. proposed model descriptions using probability distributions and their reliance on the parameters in his research on an empirical path-loss model for wireless channels in indoor short-range office environment. The model was able to depict appreciable variable values of route loss at different frequencies, while also resulting in a simpler model that simplifies radio propagation in difficult situations. However, because this study was conducted in an office setting, it is necessary to evaluate this unique prediction path loss model in a commercial setting with more obstacles [63].

Further study has revealed that most propagation models that work at frequencies less than 6 GHz are inapplicable when considering route loss models for millimeter wave frequency bands which are generally above 6 GHz. Majed et al. presented channel models that can operate in interior circumstances at frequency ranges of 4.5 GHz, 28 GHz, and 38 GHz in order to find a solution. Both LOS and NLOS measurements were taken in an inside office environment, with the transmitting and receiving antennas set at a distance of 23 meters. The goal of the research was to compare the new large-scale generic path loss models with the existing path loss models for omnidirectional and directional as well as multi-frequency and single-frequency. The results of the investigation show that when the large scale path loss model is modeled with one parameter PLE and related to the transmitted power, it tends to perform better [70]. Shadowing and attenuation, which were explored in [71], are another set of properties common to an indoor environment. Wireless open access research platform (WARP) equipment was used to model route loss and shadowing. As a result, the propagation path loss value is in line with those measured in the literature, with an exponent of 4 and a standard variation of 6.4 dB.

In millimeter wave propagation, the direct exchange of information between two near distance devices in the absence of a base station, known as device to device (D2D) communication, has various advantages such as energy efficiency, better data throughput and shorter latency [72]-[73]. The effect of path loss on D2D communication is unique and unequalled. Modeling a method that will result in a significant reduction in attenuation is required. In [70], a strategy was developed that uses mode assignment by reuse, cellular mode dedication based on a tradeoff of path loss attenuation and D2D user range. This scheme's analysis is compared with the other existing schemes such as the alternate offer bargaining game (AOBG) theory based algorithm and the heuristic algorithm. The main benefit of the proposed approach is that D2D users' SINR threshold is supported to a certain extent. The practicality of this technology is demonstrated by the fact that it is extremely useful in circumstances where path loss attenuation is a concern in both indoor and outdoor contexts. Another measurement work was conducted in two different locations in the United States of America (USA) by MacCartney Jr et al. to check the path loss models for 5G millimeter wave propagation channels in Urban Microcells using the best of sliding correlator channel sounder at 28 GHz and 38 GHz. Using directional antennas of varied heights as well as the gains, this experiment investigates multiple microcellular conditions.

The linear regression fits were used to create the path loss models. The path loss spanned a distance that is dependent on the power received, according to the measurements. When compared to the existing path loss models, the suggested model performs better in terms of lowering shadow factors by several decibels and provides a better fit to empirical data while permitting only a minor path loss [16].

Naruke et al. proposed an indoor localization method based on path loss – distance relationship using handset sensor data. The range between the Bluetooth Low Energy (BLE) transmitter and the smartphone was computed using this proposed model, which first used the relationship between distance and path loss, and then used the Pedestrian Dead-Reckoning (PDR) fixed on the mobile phone's accelerometer. When the proposed scheme is compared with the existing schemes, the results reveal a significant improvement in the distance error [74].

Al-Saman et al. conducted a comprehensive assessment for millimeter wave propagation models as well as measurements in indoor environments. Time dispersion and path loss were identified to be the key indoor wireless channels in terms of millimeter wave propagation. Although the path loss coefficient increases as the frequency increases, the exponent is only affected by the structure and kind of environment, not by the frequency [52]. Considering the various research articles in the frequency range of 28 GHz to 100 GHz, the overall observation is that the CI and FI models are the best for both LOS and NLOS channel propagation in millimeter wave bands especially in an interior environment. This achievement in the deployment of millimeter wave propagation for both 5G and 6G networks with negligible propagation loss [75] is an important advance forward. There is a general classification of models that require minimal site or path details and count hindrances or obstructions as a component of the distance dependent loss, whereas site-specific models assess the loss due to each hindrance separately. These models are taken into account by placing the measured variables into a generic phrase. There are four major path loss propagation models, CI, FI, CIF, and ABG, which are frequently used: two of them are single frequency models, while the other two are multi-frequency models [76]-[80].

The usage of models in propagation path loss can be used to reflect the effects of path loss on the signal at the receiving end on a wide scale. It is a useful tool for calculating signal attenuation and declining as it travels from the transmitter to the receiver, taking into account propagation distance and other factors. The models differ in that some specify the topographical profile for easy signal analysis, while others just use the carrier frequency and distance to determine their target [81]-[82]. The CI, CIF, and ABG path loss models are stochastic in nature. These models capture the phenomenon of large-scale propagation over a given distance and can work at all appropriate frequencies in the given environment. The CI and CIF models are found to be equivalent to the standard forms of 3GPP path loss models i.e. the FI and ABG models. Only the floating constant and the free space constant, which are dependent on propagation frequency and observance of the free space reference distance of 1m, are relevant in this case [83]-[87].

2.4.1.1 CI Free Space Path Loss Model

This is a model whose basic premise is based on the anchor point and is dependent on the frequency in free space. The model parameter includes the free space path loss (FSPL), which is also dependent on the carrier propagating signal frequency (f in GHz). The distance between the transmitter and receiver (*d* in meters) as well

as a specified reference distance (d_o) are both crucial. Another CI model parameter, PLE (n) [81], [87]-[89], is determined in dB. The path loss for CI model ($PL^{CI}(d)$) is given by equation (2.5):

$$PL^{CI}(d)[dB] = FSPL(f, d_o)[dB] + 10.n.\log\left(\frac{d}{d_o}\right) + X_{\sigma SF}^{CI} \quad \text{for } d \geq d_o \tag{2.5}$$

Where $X_{\sigma SF}^{CI}$ and σ are zero mean gaussian random variable and the standard deviation in dB, respectively. The $FSPL$ (in dB) is given by equation (2.6):

$$FSPL(f, d_o)[dB] = 10log_{10}\left(\frac{4\pi d_o}{\lambda}\right)^2 \tag{2.6}$$

2.4.1.2 FI Path Loss Model

This model is built around two primary components i.e. the line slope and the floating intercept. For path loss values [52], [82], [84], [87], the FI model is good at obtaining optimal least error fit. The path loss expression for the FI model is given by equation (2.7):

$$PL^{FI}(d)[dB] = \propto + 10.\beta\, log_{10}(d) + X_{\sigma SF}^{FI} \tag{2.7}$$

This model adopts $\propto$ as the floating intercept in dB and also the slope of the line be β (not as in PLE). The $\propto$ and β are the two parameters adopted by this FI model to make it different from the CI model. The variable $X_{\sigma SF}^{FI}$ is the zero Gaussian shadow fading (in dB) over the mean path loss on a specified distance.

2.4.1.3 ABG Path Loss Model

Another type of multi-frequency model approach is the ABG model. The reference distance and the reference frequency of the ABG model are 1 m and 1 GHz, respectively. The path loss dependency on distance coefficient and the path loss dependency on the frequency coefficient are α and γ, respectively. The offset path loss, the distance between transmitter and receiver, and the carrier frequency are β, d, and f, respectively [88]- [89]. Equation (2.8) gives the expression for the path loss (in dB) for the ABG model.

$$P_L^{ABG}(f, d)[dB] = \alpha.10\log\left(\frac{d}{d_o}\right) + \beta + 10.\gamma.\log\left(\frac{f}{1GHz}\right) + X_\sigma^{ABG} \tag{2.8}$$

When $d_o = 1m$. The ABG path loss model for $d_o = 1m$ is given in equation (2.9).

$$P_L^{ABG}(f, d)[dB] = \alpha.10\log(d) + \beta + 10.\gamma.\log(f) + X_\sigma^{ABG} \tag{2.9}$$

2.5. Accuracy and Viability of Propagation Models for Indoor and Outdoor Environments

The accuracy and feasibility of various models are highly dependent on the propagation scenario and the frequency spectrum that is taken into account. Various proposed models by the researchers have a unique application that has a long way to go in terms of distance and frequency of application in order to improve delay time output and PLE performance. An experiment on ultra-wideband propagation was carried out at New York University in a typical indoor office environment [88]. The results of the experiment were used to calculate the statistics of large-scale route loss for current and future applications. The measurements were conducted in an

enclosed structure with LOS and NLOS conditions using directional horn antennas at 28 and 73 GHz. During the investigation, it was discovered that basic CI and FI models may accurately represent large scale path loss (with distance and frequency) in millimeter wave indoor wireless channels while only employing one or two functions that are related to the transmitted power [61].

Maccarthney et al. presented some omnidirectional propagation data recorded at frequencies of 28 GHz, 38 GHz, and 73 GHz in New York Downtown city to validate the accuracy and validity of the CI path loss model. The paper's main goal is to give data for wave propagation research and comparison when working on similar measurements [62]. Sun et al used two primary large scale route loss models in their work on propagation path loss models, CI and ABG, for 5G urban micro and macro-cellular scenarios. Data was collected from around 20 measurement operations with frequency bands spanning from 2 GHz to 73.5 GHz over a distance of 5 m to 1429 m. According to the examination of the results, the simulation accuracy of the CI model is superior to the ABG model [84]. The former provides more consistent and acceptable performance across all frequencies and distance ranges investigated during the trial, whereas the latter does not. To reach a higher level of accuracy, only minor changes to the CI model, which is user-friendly over a wide frequency range, are required [90]- [93].

The ABG model was compared to the three most common large scale path loss models i.e. close in free reference distance model (CI), close in model with frequency-weighted path loss exponent (CIF), and ABG in a range of data sets with distances ranging from 4 m to 1238 m and frequencies ranging from 2 GHz to 73 GHz. Urban microcells, shopping malls, and an indoor office environment were the scenarios [84]. The CI (two parameters considered) and the CIF (three parameters considered) models have better goodness of fit and more stable behavior of the components, whereas the ABG model (four parameters considered) under predicts and over predicts path losses when it is close to the transmitter and when it is far from the transmitter, respectively. This discovery remains true across all distances and frequencies studied. The CI model was shown to be suitable for the outdoor application, whilst the CIF model was found to be the best for inside modeling [64], [94].

Haneda et al. used both present and past measurements on channel propagation in the frequency band up to 100 GHz in their work on indoor 5G 3GPP-like channel models for office and shopping mall environments. It was discovered that there is an increase in penetration loss as a result of increase in frequency changes the material's properties. According to the UMi and Uma models [65], the indoor channels have a higher dependency on the frequency as compared to the outdoor channels.

Measurements were performed at 28 GHz and 38 GHz in three cities: New York, Austin, and Texas, as part of an empirically-based large scale propagation route loss model for 5G cellular network planning in millimeter wave band. In the course of performing path loss simulations with a random selection of antenna pointing angles, it was discovered that when the best direction of the antenna is pointed at both the mobile and the base station, there is a significant increase in the portion of coverage. This reduces the interference and the number of 5G base stations [67]. The analysis of Rural Macrocell path loss models for millimeter wave wireless communications, which is part of a larger research project, provides a full understanding of the current 3GPP, RMa LOS, and NLOS path loss models in the frequency range of 0.5 GHz to 100 GHz. In a rural location with good weather, directional antennas were used for a real-time measurement campaign employing the CI and CIH model components. The finding brings into question the use of current 3GPP RMa path loss models for

frequencies above 6 GHz. The observed data verifies the CIH model's correctness, dependability, and frequency dependency even beyond the first meter of propagation distance [67].

The characteristics of propagation channels in the frequency bands of 6.5 GHz, 10.5 GHz, 15 GHz, 19 GHz, 28 GHz, and 38 GHz in an indoor scenario were investigated further with a measurement campaign spanning 4,000 power delay profiles using a horn directional antenna as a receiver and an omnidirectional antenna in the transmitting section. The frequency attenuation model, which considers both the distance and the frequency, has been presented as a novel path loss model. This also aids in the estimation of the XPD component of close in reference distance using XPD (CIX) and ABG with XPD (ABGX) path loss models, which do not require the use of the minimal mean square error approach. The RMS delay spread and dispersion factor values of this model illustrate its simplicity, lower path loss exponents, and good RMS delay spread and dispersion factor values [68].

Al-Samman et al. examined the features of millimeter wave 5G channels in order to figure out the components of path loss and time dispersion in an outdoor situation in their work on path loss and RMS delay spread model for 5G channel at 19 GHz [69]. When using the horn-horn as well as the horn-omni antennas in a line of sight condition, the path loss model generated from the observed data shows a drop in the PLE, which is due to the summing up of the multipath component parameters in the LOS environment. However, the values of the PLE and free space path loss in the two situations are identical in the NLOS scenario. The results of this experiment show that when using horn-horn and horn-omni antenna applications in both LOS and NLOS situations, the mean values of the delay spread drop dramatically, indicating that the influence of delay spread on the directional horn antenna at the transmitting side is minimal [69].

The FI model and the CI model were used to conduct measurement campaigns in an interior environment in both LOS and NLOS cellular systems at a frequency of 40 GHz in order to access the functionality of 5G wireless propagation and the route loss exponent at this frequency band. The two models are compared to the ones used during the measuring campaign. The results of this experiment reveal that the CI and FI models have similar values for the PLE and slope line in both the LOS and NLOS. This is strong evidence that the CI and FI models are the best large-scale path loss models for indoor application in a 5G propagation system at the 40 GHz frequency band [70]. Work was done on the 10 GHz, 20 GHz, and 26 GHz frequency bands in the measurement of diffraction as well as the prediction models of signal strengths in environments with corners, irregular objects, and pillars in both indoor and outdoor scenarios using a continuous wave channel sounder with similar antenna pairs that are a directional horn type at the receiving and transmitter sections [71].

Khatun et al. took the research on the comparison of the path loss model in both outdoor and interior environments in both LOS and NLOS scenarios to the next level. They carried out their survey at the Boise Airport and Boise State University [72]. At a frequency band of 60 GHz, a detailed research was carried out using the techniques of CI reference and FI path loss models with a high gain directional antenna. Although there was a correlation between the final result and the measurement campaign results [72], stochastically and statistically analyzing it revealed that the weather condition at the Boise airport was responsible for the higher value of PLE associated with the outdoor scenario when compared to the indoor scenarios.

Due to the obvious signal propagation disparity, the majority of the propagation models now in use for any frequency band below 6 GHz are not acceptable for path loss modeling of millimeter wave propagation, and of course any frequency band above 6 GHz. The measurement was performed in an indoor situation in the frequency bands of 4.5 GHz, 28 GHz, and 38 GHz for LOS and NLOS in order to construct a model that can sufficiently work in these bands together [70]. The research was carried out at Universiti Teknologi Malaysia (UTM Malaysia). In directional and Omni directional antenna applications, path loss analysis of single and multi-frequency signals was performed. It was deduced that modeling path loss on a large scale with respect to distance over distance is easier to do using a less complex model approach with the adoption of only one PLE parameter (n) that is dependent on the transmitted power, rather than using a model that is not transmitted power dependent and may require more parameters, making the modeling complex [70].

Another indoor laboratory measurement scenario was carried out for LOS and NLOS propagation at a frequency of 2.4 GHz, and a route loss with spatial variability was proposed. This proposed model was built on the foundation of FI and log-distance models. It uses a combination of coherent and non-coherent power gains to reduce the percentage path loss exponent and the cumulative distribution function (CDF). As a result, the average route loss value in four coherent signals for a LOS scenario decreases path loss by 89.4 percent, compared to the strategy of employing the NCC scenario, which reduces path loss by only 55.98 percent [16]. The characteristics of millimeter-wave channels in the Urban Microcell Environment were discussed in [62]. In the transmitter and reception sections; a vertically polarized omnidirectional antenna is used based on the SBR Method. The performance of the SBR technique was further validated by analyzing the LOS and NLOS in the vertical and horizontal directions and justifying the performance with both measured and simulated data. As a result, certain characteristics of millimeter wave channel in UMi provide a good background for propagation, but only in outdoor circumstances.

Furthermore, Wang et al. studied the 60 GHz millimeter-wave propagation characteristics in indoor environment. Efforts were made to thoroughly examine the workability and performance of the SBR/IM method on the basis of accuracy, reliability, and ease of use, as well as a simulation of the important components of channel propagation such as RMS delay spread and path loss. At a frequency of 60 GHz, the RMS delay spread has a very low value and a rise in the coherent bandwidth, but there is a tendency for anti-interference at 2.4 GHz [58]. In the empirical research of millimeter wave in an indoor context, the dual slope model was used. The measurement was performed in a completely blocked location to a location with deep fading, and the performance was compared to the single slope path loss model, which is the most prevalent in both LOS and NLOS scenarios utilizing omni directional antennas. The results reveal that the suggested dual slope model fits the values of the measurement campaigns fairly well, but with certain shadow variables [74].

Schilcher et al. In [87], authors provided a stretching out tool box of stochastic geometry based model and proof of the theorem that yields the expression of the functional of the result in their work on interference functional in Poisson networks. This finding was put to use in wireless networks. Also, authors computed the joint outage probability of some transmissions, which would be utilized as a template for any path loss models. The efforts of numerous international groups to model channels for both licensed and unlicensed applications are described here, along with early results and key concepts of 5G networks that were presented in [88]- [89].

Over the frequency range of 0.5-100 GHz, various standardization bodies' simulations of various propagation parameters and channel models, including LOS probabilities, large-scale path loss, and building penetration loss, is compared. Yang and associates developed a geometry-based multipath model to characterize the rapidly changing properties of high-speed trains communicating in the millimeter wave frequency region. A validated RT simulator was used to create this model [90]. Because each dominant multipath lifetime has a defined geometry factor, which is drawn out inside separate local Wide-Sense Stationary (WSS) regions and monitored to determine its "birth and death" positions, the dominant multipath component in this approach. By comparing the Doppler and delay spreads of the channel being modeled with the channel of the simulated RT, the model's notion is proven. In a comparable model, the overall result of this work provides a good channel model for the overall design procedures. However, when utilizing the large antenna arrays to increase power gain, one of the primary issues in millimeter wave propagation is the beam direction of the domain angles of both transmitting and receiving antennas. The codebook design was a two-step process that used sub-array and deactivation approaches to solve the problem. The BMW-SS codebook was found to have the advantages of flatter and more active beams, resulting in improved power system performance and models [91]-[93].

Wu et al. [94] used a rotated directional antenna (RDA) method in conjunction with the uniform virtual array (UVA) method to analyze the three-dimensional channel of the frequency band, which takes into account both the azimuth and co-elevation domains for modeling of mm Wave channel for indoor office situations at a frequency band of 60 GHz. Using the UVA on SAGE algorithm as well as the K-means algorithm, the results of both LOS and NLOS in roughly 6 instances were analyzed. Despite being located in a limited direction distance, the angles of departure of the azimuth differ. This is strongly linked to the height difference of the antennas. It was also revealed that in either the cluster or global level, the faster rate of spread of the angle of azimuth is on the high side when compared to the elevation angle. In the mm wave band, Qu and Zhe [95] proposed a design technique for a high-gain wide-angle antenna. It utilized a novel gradient-index (GRIN) lens and a phase array antenna (PAA) coupled to a high-directivity aperture coupled microstrip antenna (ACMA). Particle swarm optimization (PSO) was first employed in conjunction with a quasi-two-dimensional (2-D) model, and excitation coefficients for beam steering were later derived using the PSO algorithm. Although the antenna is to be manufactured using three-dimensional (3-D) printing, measurements conducted using the antenna demonstrate a good agreement with the simulated findings. The research in [96] revealed the introduction of the eventual deployment of E-band spectrum for broadband propagation. The capacity to minimize interference among neighboring broadband BSs and a visible overlap of their coverage areas were identified to be the key advantages of E-band that necessitate its wide implementation in broadband. The main disadvantage of this strategy is its inability to guarantee good network coverage, especially when some mobile users do not have access to LOS links in the BSs closest to them. This research also suggests the solution to this problem by deploying a hybrid EMB and 4G system in order to provide a decent balance of data and coverage.

In their work channel estimation and hybrid beam forming for reconfigurable intelligent surfaces assisted THz communications, Nin et al. proposed a three-phase approach to bringing about distinct groups of measurements employing a cooperative channel method via beam training. A pair of innovative codebooks was also created to make the 3-tree search necessary in the beam generating procedure as simple as possible. A tree dictionary (TD) technique was combined with a phase shifter deactivation (PSD) approach in the application of

wide-beam designs in the codebook. A twin closed form propagation technique was also developed to improve the overall efficiency of the spectrum, despite its modest complexity [97].

The analysis of these path loss models reveals that there is a need to develop a model that is an improvement over the basic models, such as CI, FI, and ABG, that is simple but performs better in terms of path loss of the transmitted signal from the transmitter to the receiver as shown in Table 2.1 and Table 2.2. The CI free space reference model and the FI path loss models were found to be the best appropriate path loss models for indoor millimeter wave propagation in both LOS and NLOS scenarios in the study. Future research will concentrate on how to improve the appropriate model with the best line of fit and the simplest application for path loss model estimation in both LOS and NLOS scenarios in an indoor environment.

Table 2.1. Comparison of general works on millimeter wave propagation.

Ref	Frequency (GHz)	Scenario	Environment	Area of Focus/Methodology	Important results
[25]	0.5-100	LOS and NLOS	Indoor and Outdoor	Rappaport et al. did a thorough investigation of the fundamental propagation modelling techniques for the 5G networks in millimetre wave wireless communication systems.	The data gathered on shadowing and path loss will help with the improvement expected knowing fully well that millimetre wave is still in the research era especially in the use for 5G propagation.
[41]	14, 18 and 22	LOS and NLOS	Indoor	The measurements for two different path loss models at frequencies 14 GHz, 18 GHz and 22 GHz in an indoor situation for LOS and NLOS communication scenarios.	Analysis in the LOS indicates that CI and FI models are similar in execution at all frequencies used. In the CI model, a notable increment of the PLE was observed with the increase in frequency.
[48]	60	NLOS and LOS	Indoor	Analysis for the deployment of wireless high-speed local and personal area networks (WLANs/WPANs)	The millimetre wave propagation was observed to be characterised with propagation loss due to obstructions like walls, furniture and human blockage, to the level of between 25-30 dB.
[49]	23, 25, 28, and 38	LOS	Outdoor	Dynamic rain-aware link adaptation scheme to allow the system to fit the modulation and coding scheme for rain intensity levels	Result shows that the improbability lies between the theoretical and practical signal induced with rain in the range 1.5-4.5 dB, which was attenuation due to unstable conditions of the weather.
[50]	55-65	NLOS	Outdoor	On-chip wireless channel characteristics in conjunction with antenna implementation with near field and multipath propagation effects	It shows that the near field/ transition region is where the propagation in the on-chip wireless channel is located thus making the channel complicated. It was also observed on antennas that the directional antennas are less affected by channel time dispersion, however, there are higher losses. The characteristics are reversed for omnidirectional antennas.
[51-53]	28 and 73	NLOS and	Indoor	Analysis of millimetre wave propagation at different	This implies that a rise in the path loss brings about a corresponding

		LOS		frequency bands	increase in the separation distance as a result of issues associated with the directivity of the antenna. Also, the scheme has been able to surmount the problem of bandwidth in electronic devices and opens the room for the development of low-cost infrastructure demand for the broadband mobile devices.
[55]	73	LOS and NLOS	Outdoor	Proposed a new technique known as Q learn-based scheme which encompasses edge computing function in an adjustable power and angle, which uses sub-6 GHz user equipment (UE)	The result from this investigation indicates that the user equipment with this scheme was able to achieve high energy efficiency and thus creating a room for a very robust and stable capacity in transmission.
[56]	60	NLOS and LOS	Outdoor and Indoor	Made us to realize that there is unallocated spectrum in the millimetre wave bands which is not making the full opportunity of the use of large antenna arrays for high speed data rates to be achievable.	It was discovered that millimetre wave communication has played a vital role in the deployment of 5G and it is expected that the fundamental improvement in radio and network will be made to help in the deployment of the upcoming 6G.
[57]	6 and 70	LOS and NLOS	Indoor	Fuschini et al [57] studied the narrowband and wideband features of in-room 70 GHz wireless channel using Ray Tracing (RT) simulations and making the measurement to be directional.	Observations show that reflection is the most pronounced mode of propagation, scattering is still present and it appears more than when the frequencies are below 6 GHz.
[58]	2.4 and 60	LOS	Indoor	Wang et al. validated the eligibility of the SBR modelling method. The SBR method makes use of some propagation parameters such as path loss, RMS delay speed etc.	The results show that strong attenuation leads to smaller coverage area for millimetre waves than lower frequencies.
[59]	60	LOS and NLOS	Indoor	Verification of multipath effects in an indoor environment	This investigation shows that the multipath effect is more pronounced in indoor NLOS surroundings because the reflection effect on the received power is more as compared to the diffraction effect.
[60]	73	LOS and NLOS	Indoor	The work uses simulated surroundings at a frequency of 73 GHz in LOS as well as NLOS situations using SBR method.	The measured results are put in comparison with the simulated results of path loss to be able to authenticate the correctness of the SBR method. The profiles of the power angle as well as the power delay were critically examined.

Table 2.2. Evaluation of the relevant works on path loss models for millimeter wave propagation.

Ref	Frequency (GHz)	Environment	Scenario	Methodologies	Model	Important Reasons
[16]	2.4	Indoor	LOS and NLOS	A laboratory measurement for indoor scenario was conducted for LOS and NLOS propagation at a frequency of 2.4 GHz for proposing a path loss with the spatial diversity.	FI and log-distance models	Results show that the average path loss value in four coherent signals for a LOS scenario brings about a path loss reduction of 89.4% in comparison to the technique of using NCC scenario which only reduces the path loss by 55.98%.
[58]	60	Indoor	NLOS and LOS	Efforts were made to properly scrutinize the workability and the performance of the SBR/IM method on the basis of accuracy, reliability and the ease of use. The simulation of the important components of the channel propagation such as RMS delay spread and the path loss was carried out.	SBR/IM method	It was inferred that the RMS delay spread has a very low value and a rise in the coherent bandwidth at a frequency of 60 GHz, but at 2.4 GHz, there is a tendency for anti-interference.
[60]	2-73	Urban micro cell	LOS and NLOS	The analysis of millimetre-wave channel characteristics in urban microcell environment based on the SBR method adopts a vertically polarized antenna which is omnidirectional in nature in the transmitter and the receiver section.	SBR technique	The results of this method indicate that some of the features of the millimetre wave channel in UMi is a good background for propagation but only in the outdoor scenarios.
[61].	28 and 73	Indoor	LOS and NLOS	An experiment on ultra-wide band propagation with the statistics of the large scale path loss for present as well as future use was conducted by adopting directional horn antennas.	CI and FI	It was observed during analysis that simple CI and FI models can be used to model large scale path loss (with distance and frequency) in millimetre wave indoor wireless channels with the correctness intact while using one or two functions that have a connection with the transmitted power.
[64]	2 -73.5	Indoor	LOS and NLOS	Data were obtained from about 20 measurement campaigns for frequency bands 2 GHz and 73.5 GHz over a path of distances starting at 5 m and stopping at 1429 m.	CI and ABG	Observation of the analysis of the result shows that the simulation accuracy of the CI model is better than the ABG model even though it is a three parameter model. The former offers more stable and acceptable performance in all the frequencies and the range of distance considered in the course of the experiment which is not so in

						the latter.
[65]	2-73	Urban micro cell, shopping malls and indoor office	LOS and NLOS	The analogy of three most common models of path loss that is CI, CIF and ABG models was done in the range of data sets of distance ranging from 4 m to 1238 m and frequency of 2 to 73 GHz.	CI, CIF and ABG	It was concluded that for outdoor use, the CI model is more preferable but in the case of indoor modelling, the CIF is the better model.
[67]	0.5-100		LOS and NLOS	A study of rural macrocell path loss models for millimetre wave wireless communications gives a comprehensive understanding of the present 3GPP, RMa LOS as well as NLOS scenarios of models of path loss in range of frequencies of 0.5 GHz to 100 GHz. The use of directional antennas was adopted for real-time measurement campaign in a rural area	CI and CIH	The observation queries continued application of the present 3GPP RMa path loss models for frequencies above 6 GHz. The result of the measured data validates the accuracy, reliability and frequency dependence of the CIH model even beyond the first meter distance of propagation.
[68]	6.5, 10.5, 15, 19, 28 and 38	Indoor	LOS and NLOS	Characteristics analysis of millimetre wave channels in the frequency bands of 6.5 GHz, 10.5 GHz, 15 GHz, 19 GHz, 28 GHz and 38 GHz in an indoor scenario was done with measurement campaign taken across 4,000 power delay profiles using horn directional antenna in the receiver and an omnidirectional antenna in the transmitting section.	Path loss models, known as frequency attenuation model ABGX, CIX as well as ABG with XPD were proposed.	The results of this model show its simplicity, less path loss exponents, better RMS delay spread and good dispersion factor values.
[69]	19	Outdoor	LOS and NLOS	Examination of the features of millimetre wave 5G channels in order to find out the components of path loss together with dispersion of time for an outdoor scenario was carried out.	Free space path loss model	This experiment deduced that there is a very great drop in the mean values of the delay spread in both LOS and NLOS situations when adopting the use of horn-horn as well as Horn-Omni antenna applications. It indicates that the influence of the delay spread is minimal to the directional horn antenna at the transmitting side.
[70]	40	Indoor	LOS and NLO	Measurements were conducted in order to access the functionality	CI and FI Models	Results of this experiment show that in both the LOS as well as NLOS the FI together with CI

			S	of 5G wireless propagation and the path loss exponent.		models have similar values for the PLE and slope line. This is a very strong indication that the FI together with the CI model have the best performance for indoor use at the frequency band of 40 GHz in a 5G propagation system.
[71]	10, 20, and 26	Indoor and Outdoor	LOS and NLOS	The measurement of the diffraction as well as the prediction models of the signal strengths in environments where there are corners, irregular objects, and pillars in both indoor and outdoor scenarios were conducted. The continuous wave channel sounder with similar antenna pairs that is a directional horn type at the receiving as well as at the transmitter section were used.	The KED was the reference model.	Observation shows that the KED fits accurately with the indoor scenarios as well as with the rounded corners in the outdoor situations. However, there is a notice of the increase in diffraction as a result of rise in frequency in the outdoor scenarios, but less in indoor environments.
[74]	27.5	Indoor	NLOS and LOS	The measurement took place in an environment that is totally blocked for a deep fading. The model of dual slope, which takes into account this deep fading, was adopted. The performance of the model was compared with the single slope path loss model which is the most common in both LOS and NLOS scenarios using omni directional antennas.	Dual slope model	Results show that the proposed dual slope model has a very good fitting with the values of the measurement campaigns but with a little shadow factor.
[77]	28-73	Indoor	NLOS and LOS	Capacity analysis of non-orthogonal multiple access with mm wave massive MIMO systems	Uniform random single-path (UR-SP) model	Observations show that there is an improvement in the capacity when compared with the present LTE systems. Other results indicate the improvement and compromise between energy usage and the capacity advancement which can also be an advantage in the mm wave propagation.

2.6. Findings on Path Loss Propagation in Different Antenna Polarizations Using the CI, FI, and ABG Models

Observations in [41], [43], as shown in Table 2.3 and Table 2.4, demonstrate that the PLE increases in a logarithmic fashion, when the frequency of operations increases. Because of diffractions, reflections, and wave

guiding, constructive interference occurs at the receiving end. In a LOS indoor setting, the PLE for the CI path loss model at 14 GHz, 18 GHz, and 22 GHz is less than the theoretical free space path loss exponent FSPLE of 2. At frequencies 14 GHz, 18 GHz, and 22 GHz, the values of the floating intercept parameter are 55.44, 57.45, and 61.03, respectively, which are almost identical to the predicted PLE in the FI path loss model. When compared to the LOS, high values of path loss are observed in the NLOS environment. It is also worth noting that the maximum PLE is recorded in the 18 GHz frequency as opposed to 14 GHz and 22 GHz frequencies, indicating that reflections off the building's structural routes are more problematic at 18 GHz.

The parameters tested in [68] were in the frequency ranges of 6.5 GHz, 10.5 GHz, 15 GHz, 19 GHz, 28 GHz, and 38 GHz, with two antenna configurations of cross polarization (V-H) and co-polarization (V-V). The PLE value for the frequency bands under consideration with the two antenna configurations i.e. V-V (1,1,1.4,0.6,0.9, and 0.8) and V-H (1.3,1.2,1.9,1.4,1.8, and 1.1) for 6.5 GHz, 10.5 GHz, 15 GHz, 19 GHz, 28 GHz, and 38 GHz correspondingly is less than the theoretical standard value of 2. This demonstrates that the MPCs of the internal corridor's walls combine to generate a waveguide. The values of $\propto$, deviate from the space path loss for the V-V polarization in the case of the FI path loss model parameters, showing that this channel has not been physically described properly by the FI. The V-V measurement and the combined polarization measurements of both the V-H and V-V have identical values in the ABG multi-frequency path loss model. In [70], the research indicates that the PLE obtained in the NLOS environment for the CI path loss is higher than the FSPLE, indicating that the received signals are produced by diffraction and reflection processes. In the LOS, the PLE (n) values are less than the FSPLE (=2). The received power will go off at a distance rate of 18 dB and 29 dB per decade for LOS and NLOS environments, respectively. For the FI path loss model, the same result is obtained for the PLE in both the NLOS and LOS settings. These are summarized in Table 2.3 and Table 2.4.

The path loss model in [70] uses the CI model for directed and omnidirectional paths in the LOS and NLOS settings at frequency ranges of 4.5,28, and 38 GHz. The antenna's polarizations were V-V and V-H. The PLE values determined from V-V polarization in the LOS are 0.7, 0.92, and 2.229 at frequencies of 4.5, 28, and 38 GHz, respectively. Because their PLE was significantly less than the FSPLE (of 2) in the V-V antenna polarization, the effect of constructive interference was more noticeable at 4.5 GHz and 28 GHz frequencies. In the V-H polarization, on the other hand, the PLE values obtained are higher than those obtained in the V-V polarization. There is strong evidence of depolarization in the PLE values for both LOS and NLOS settings in the NLOS environment at frequencies of 28 GHz and 38 GHz. The result of the FI path loss model in the LOS was compared to the theoretical FSPLE values of 45.5 dB, 61.4 dB, and 64 dB, as well as the FI path loss model values of 41.4 dB, 60.1 dB, and 82.5 dB in the V-V polarization at 1 m reference distance for the frequencies 4.5 GHz, 28 GHz, and 38 GHz, respectively. In the theoretical FSPLE, the V-Omni path loss LOS values are 45.5 dB, 61.4 dB, and 64 dB, whereas the FI path loss values are 71.09 dB, 68.23 dB, and 83.79 dB. The NLOS scenario demonstrates that the FI values are independent of frequency. Although, it demonstrates that the FI path loss model is highly sensitive. Only two antenna polarizations, V-V and V-Omni, are present in the ABG path loss model. When compared with the LOS scenario, the $\propto$ in the NLOS case study has a greater value.

Results in the LOS scenario for the frequencies 26 GHz, 32 GHz, and 39 GHz in [81] show that horn antenna configurations create higher path loss values when compared to the omnidirectional antenna configurations. Despite the fact that none of the path loss values were close to the theoretical FSPLE value of 2, the influence of

reflections in the walls and structures of the buildings, which function as a wave guide in the signal propagation, was confirmed in Table 2.3 and Table 2.4.

In [84], the LOS PLE demonstrates that their CI path loss models have values of 1.1 at 28 GHz and 1,3 at 73 GHz, implying that there is constructive interference, as seen in practically all other indoor millimeter wave propagation measurements, which is caused by diffractions, reflections, and wave guiding. It has a PLE of 2.7 at 28 GHz and 3.2 at 73 GHz in the NLOS environment, showing considerable attenuation at 73 GHz, although there is a reduction of attenuation in the FI model for both LOS and NLOS circumstances. The CI model's simplicity and correctness were further validated by the fact that just one parameter is necessary. The analysis and observation of various existing models for millimeter wave for the indoor office environments are presented in Table 2.5 and Table 2.6. This further collaborates with the simplicity of the CI and FI models, but the CI model provides better accuracy.

Table 2.3. Comparison of parameters for single frequency CI, FI and multi-frequency ABG path loss models for millimeter wave in indoor environments for LOS scenarios at different frequencies.

Ref	Frequency (GHz)	Environment	Scenario	Polarization	Distance range (m)	Model	PLE (α)	β (dB)	σ (dB)	γ
[41], [43]	15	LOS	Indoor Corridor	V-H	1.00-40.00	CI	1.90	—	2.40	—
						FI	63.50	1.10	2.90	—
						ABG	—	—	—	—
[41], [43]	14	LOS	Indoor Corridor	V-V	2.00-24.00	CI	1.37	—	2.19	—
						FI	55.41	1.37	2.19	—
[41], [43]	18	LOS	Indoor Corridor	V-V	2.00-24.00	CI	1.58	—	1.53	—
						FI	57.48	1.59	1.53	—
[68]	22	LOS	Indoor Corridor	V-V	2.00-24.00	CI	1.66	—	1.31	—
						FI	61.04	1.50	1.12	—
[68]	6.5	LOS	Indoor Corridor	V-V	1.00-40.00	CI	1.00	—	3.10	—
						FI	40.70	1.00	3.10	—
						ABG	1.10	15.70	3.20	3.10
[68]	6.5	LOS	Indoor Corridor	V-H	1.00-40.00	CI	1.30	—	2.30	—
						FI	44.30	1.10	2.20	—
						ABG	—	—	—	—
[68]	10.5	LOS	Indoor Corridor	V-V	1.00-40.00	CI	1.00	—	2.50	—
						FI	45.40	1.30	2.30	—
						ABG	1.10	15.70	3.20	3.10
[68]	10.5	LOS	Indoor Corridor	V-H	1.00-40.00	CI	1.20	—	2.00	—
						FI	48.50	1.40	2.00	—
						ABG	—	—	—	—
[68]	15	LOS	Indoor Corridor	V-V	1.00-40.00	CI	1.40	—	2.80	—
						FI	51.90	1.40	2.80	—
						ABG	1.10	15.70	3.20	3.10
[68]	19	LOS	Indoor Corridor	V-V	1.00-40.00	CI	0.60	—	2.20	—
						FI	56.60	0.90	2.10	—
						ABG	1.10	15.70	3.20	3.10

[68]	19	LOS	Indoor Corridor	V-H	1.00-40.00	CI	1.40	—	3.00	—
						FI	63.30	1.10	2.80	—
						ABG	—	—	—	—
[68]	28	LOS	Indoor Corridor	V-V	1.00-40.00	CI	0.90	—	2.10	—
						FI	58.70	1.20	2.00	—
						ABG	1.10	15.70	3.20	3.10
[68]	28	LOS	Indoor Corridor	V-H	1.00-40.00	CI	1.80	—	3.80	—
						FI	69.10	1.10	3.10	—
						ABG	—	—	—	—
[68]	38	LOS	Indoor Corridor	V-V	1.00-40.00	CI	0.80	—	2.30	—
						FI	67.90	0.90	2.30	—
						ABG	1.10	15.70	3.20	3.10
[68]	38	LOS	Indoor Corridor	V-H	1.00-40.00	CI	1.10	—	2.70	—
						FI	70.00	1.00	2.70	—
						ABG	—	—	—	—
[69]	40	LOS	Indoor Corridor	V-V	2.00-2.70	CI	1.80	—	4.70	—
[70]	4.5	LOS	Indoor Office	V-V	1.00-22.70	CI	0.70	—	3.14	—
						FI	41.45	1.32	1.79	—
						ABG	0.43	1.56	0.24	4.83
[70]	4.5	LOS	Indoor Office	V-H	1.00-22.70	CI	1.13	—	2.63	—
[70]	4.5	LOS	Indoor Office	V-Omni	1.00-22.70	CI	2.31	—	6.64	—
						FI	71.0	0.88	1.79	—
						ABG	0.90	35.77	0.19	3.02
[70]	28	LOS	Indoor Office	V-V	1.00-22.70	CI	0.92	—	2.18	—
						FI	60.10	1.06	2.15	—
						ABG	0.43	1.56	0.24	4.83
[70]	28	LOS	Indoor Office	V-H	1.00-22.70	CI	3.87	—	7.83	—
[70]	28	LOS	Indoor Office	V-Omni	1.00-22.70	CI	2.49	—	4.38	—
						FI	68.23	1.77	3.97	—
						ABG	0.90	35.77	0.19	3.02
[70]	38	LOS	Indoor Office	V-V	1.00-22.70	CI	2.29	—	5.6	—
						FI	82.53	0.33	2.57	—
						ABG	0.43	1.56	0.24	4.83
[70]	38	LOS	Indoor Office	V-H	1.00-22.70	CI	4.81	—	12.67	—
[70]	38	LOS	Indoor Office	V-Omni	1.00-22.70	CI	3.25	—	5.27	—
						FI	83.79	1.12	2.04	—
						ABG	0.90	35.77	0.19	3.02
						FI	61.04	1.50	1.12	—
[80]	26	LOS	Indoor office (Horn Antenna)	V-V	1.00-50.00	CI	1.46	—	4.94	—
						FI	62.12	1.36	4.94	—
						ABG	30.51	1.32	4.81	2.25
[80]	32	LOS	Indoor office (Horn Antenna)	V-V	1.00-50.00	CI	1.35	—	4.54	—
						FI	65.84	1.13	4.94	—
						ABG	30.51	1.32	4.81	2.25
[80]	39	LOS	Indoor office (Horn Antenna)	V-V	1.00-50.00	CI	1.53	—	4.55	—
						FI	63.19	1.61	4.54	—
						ABG	30.51	1.32	4.81	2.25
[80]	26	LOS	Indoor office	V-V	1.00-50.00	CI	1.34	—	4.49	—
						FI	64.78	1.05	4.43	—

			(Omni Antenna)			ABG	54.50	1.14	4.41	0.66
[80]	32	LOS	Indoor office (Omni Antenna)	V-V	1.00-50.00	CI	1.35	—	4.30	—
						FI	63.50	1.29	4.30	—
						ABG	54.50	1.14	4.41	0.66
[80]	39	LOS	Indoor office (Omni Antenna)	V-V	1.00-50.00	CI	1.14	—	4.25	—
						FI	65.86	1.03	4.24	—
						ABG	54.50	1.14	4.41	0.66
[84]	28	LOS	Indoor Office	V-V	4.10-21.30	CI	1.10	—	1.80	—
						FI	1.20	60.40	1.80	—
[84]	73	LOS	Indoor Office	V-V	4.10-21.30	CI	1.30	—	2.40	—
						FI	0.50	77.90	1.40	—
[84]	73.5	LOS	Indoor Office	V-V	4.10-21.30	CI	1.20	—	2.30	—
						ABG	0.90	26.80	1.80	2.60

Table 2.4. Comparison of parameters for single frequency CI, FI and multi-frequency ABG path loss models for millimeter wave in indoor environments for NLOS scenarios at different frequencies.

Ref	Frequency (GHz)	Environment	Scenario	Polarization	Distance Range (m)	Model	PLE (α)	β (dB)	σ (dB)	γ
[41], [43]	14	NLOS	Indoor Corridor	V-V	2.00-24.00	CI	2.07	—	5.98	—
						FI	67.27	1.01	3.69	—
[41], [43]	18	NLOS	Indoor Corridor	V-V	2.00-24.00	CI	2.38	—	6.87	—
						FI	71.02	1.17	4.32	—
[41], [43]	22	NLOS	Indoor Corridor	V-V	2.00-24.00	CI	2.26	—	6.86	—
						FI	73.24	1.01	4.07	—
[69]	40	NLOS	Indoor Corridor	V-V	2.00-2.70	CI	2.90	—	9.00	—
[70]	4.5	NLOS	Indoor Office	V-V	1.00-22.70	CI	2.26	—	4.56	—
						FI	16.22	4.85	3.91	—
[70]	4.5	NLOS	Indoor Office	V-Omni	1.00-22.70	CI	3.69	—	2.89	—
						FI	40.48	4.55	2.84	—
[70]	4.5	NLOS	Indoor Office	V-H	1.00-22.70	CI	1.97	—	6.00	—
[70]	28	NLOS	Indoor Office	V-V	1.00-22.70	CI	3.21	—	4.48	—
						FI	50.31	4.13	4.39	—
[70]	28	NLOS	Indoor Office	V-Omni	1.00-22.70	CI	3.85	—	4.85	—
						FI	37.45	5.83	4.50	—
[70]	28	NLOS	Indoor Office	V-H	1.00-22.70	CI	4.65	—	3.57	—
						FI	43.63	6.12	3.31	—
[70]	38	NLOS	Indoor Office	V-V	1.00-22.70	CI	4.38	—	4.14	—
						FI	87.91	2.40	3.73	—
[70]	38	NLOS	Indoor Office	V-Omni	1.00-22.70	CI	4.54	—	2.62	—
						FI	71.06	3.96	2.57	—
[70]	38	NLOS	Indoor Office	V-H	1.00-22.70	CI	5.28	—	4.09	—
						FI	43.63	6.12	3.31	—
						FI	73.24	1.01	4.07	—
[84]	28	NLOS	Indoor Office	V-V	4.1-21.3	CI	2.70	—	9.60	—
						FI	3.50	51.30	9.30	—
[84]	73	NLOS	Indoor Office	V-V	4.1-21.3	CI	3.20	—	11.30	—

						FI	2.70	76.30	11.20	—
[84]	73.5	NLOS	Indoor Office	V-V	4.1-21.3	CI	2.90	—	10.90	—
						ABG	3.10	1.30	10.30	3.80

Table 2.5. Evaluation and observation of usage of various existing models for millimeter wave propagation.

Ref	Frequency (GHz)	Environment	Model	Observation
[52]	28 and 73	Indoor office	CI and FI	Simple CI models can be used in indoor wireless channels with the correctness even when using one or two functions that has a connection with the transmitted power.
[62]	28, 38 and 73	Indoor and outdoor	CI	It only provides data for future research.
[63]	73.5	Urban micro and macro cellular	CI and ABG	Simulation shows the accuracy of the CI model to be better than the ABG model as it offers a more stable and acceptable performance with greater level of accuracy.
[64]	2 to 73	Urban microcell and macro cell	CI, CIX and ABG	CI and CIF models show a better goodness of fit and more stable behavior of the components unlike the ABG. Inferring that CI is good for outdoor use.
[65]	1 to 100	Indoor office and shopping mall	3GPP	There is more dependency on the value of the frequency in the indoor environments as compared to the outdoor environments.
[71]	10, 20, and 26	Indoor and outdoor	KED model	It shows that the KED model fits accurately with the indoor environment as well as rounded corners in outdoor scenarios.
[73]	40	Indoor	CI and FI	Analysis of the CI and FI models shows that they have similar values for the PLE and slop line.

Table 2.6. Comparison of various propagation models in millimeter wave for the indoor office environments.

Ref	Frequency (GHz)	Environment	Scenario	Models	Result	Observation
[69]	6.5, 10.5, 15, 19, 28 and 38	Indoor	NLOS and LOS	Frequency attenuation model CIX, ABG and ABGX	The results indicate that the value of the path loss exponents for the models adopted is lesser compared to the value when the model is in a free space, which is applicable for all the frequencies. The values were within 0.1 to 1.4.	This new proposed model shows its simplicity, lesser path loss exponent and has a god RMS delay spread and dispersion factor value.
[70]	4.5, 28 and 38	Indoor office	NLOS and LOS	New improved model	It shows that there is a better result of path loss when modelled with one parameter.	The result should be modelled with more than one parameter to actually know the stability at multiple frequencies.
[76]	Varying frequency	Indoor and outdoor	NLOS and LOS	A scheme that adopts	It uses D2D communication with good values of SINR.	The major advantage of this model is that it

				mode assignment by reuse		helps in a situation when there is problem of path loss attenuation in both indoor and outdoor environment.
[78]	Varying frequency	Indoor	LOS and NLOS	Indoor localization approach	There is a major improvement in the environment at different distances when compared to the existing schemes.	It only considers the distance and path loss. Frequency is another major factor that needs to be considered.
[85]	Varying frequencies	Indoor short office range	NLOS and LOS	Empirical path loss models	It shows appreciable varying values of path loss at different frequencies which also shows less complexity.	There is a need to test this novel prediction path loss, model in a commercial environment where more obstructions will take place.

2.7. Chapter Summary

This chapter compares millimeter wave's propagation observations in the outdoor, interior office, and corridor for various frequencies to single frequency route loss models from CI and FI, as well as the multi-frequency path loss model from ABG. Because the CI and FI route loss models are simple, they function similarly practically for all the examined frequency bands. Their PLE values are in line with the measured values for the LOS environment. In a similar vein, the NLOS performance is not awful; nevertheless, a higher gain antenna should be used to compensate for the significant path loss. Almost all of the models PLE values are less than the FSPLE of 2, owing to the multipath components being added together as a result of reflections and wave guiding along the walls of the interior environment, whether it's an office or a corridor. In the LOS context, the conventional 1 m reference distance also allows for simple calculations, a better degree of precision and good prediction of measured path loss. The sole need for this to work in an NLOS environment is that there are no barriers in the first meter of propagation. According to the multi-frequency ABG route loss model, the value of the frequency slope value (γ) at all frequency bands in both LOS and NLOS environments does not convert to a realistic amount of attenuation as frequency increases. Although all three models perform well, the model with the smallest amount of parameters is the best to utilize for simplicity and convenience of use. This is shown in Table 2.5 and Table 2.6. The theory and performance of various path loss models, including ABG, CI, and FI, as well as some other modified models derived from the three fundamental path loss models: ABG, CI, and FI for 5G networks have been presented in detail. The study looked at measurement situations in both LOS and NLOS for both indoor and outdoor environments at the frequencies of 0.5 GHz, 2 GHz, 2.4 GHz, 6.5 GHz, 10 GHz, 10.5 GHz, 15 GHz, 14 GHz, 18 GHz, 19 GHz, 20 GHz, 22 GHz, 26 GHz, 28 GHz, 38 GHz, 40 GHz, 60 GHz, and 73 GHz. To illustrate the process, the results of each article were quickly described in each instance. Despite the fact that some studies employ identical frequencies but distinct path loss models, others

use a modified version of the path loss models used in previous research but with better performance and simplicity than before. It was revealed that increasing the frequency does not result in an increase in the path loss exponent, but rather has an effect on the environment. The chapter concluded that the CI free space reference models and the FI path loss models are the most appropriate path loss models for indoor millimeter wave propagation in both LOS and NLOS scenarios. However, since each indoor environment investigated in the literature are made of different building designs, the improved models for both CI and FI path loss models with better performance in path loss exponent, shadow fading and other path loss parameters for the specific building designs in the propagation of millimeter wave for 5G networks in an enclosed environment should be developed.

Chapter 3

Path Loss Measurements and Model Analysis in an Indoor Corridor Environment at 28 GHz and 38 GHz

This chapter focuses on the effects of the wall proximity on the path loss parameters as well as comparisons with the parameters in some of the reviewed literature studies. The FI and CI models produce comparable results for both antenna polarizations and clearly fit with the measured path loss. The path loss measurements and model analysis presented in this chapter are useful in designing 5G wireless communication systems for indoor environments, particularly for power budget calculations.

3.1 Introduction

High data rate wireless communications are essential, and a number of solutions have been presented to address this issue. The requirements for greater capacity, high dependability, data rates, and quality for a number of applications have been met by a variety of current wireless communication systems, notwithstanding this. The most solid answer to this issue is millimeter wave propagation. It is referred to as centimeter wave (cm-wave) or mmWave spectra. 5G technology has drawn interest since it can provide data rates of many gigabits per second (Gbps) [98] - [99]. The lower band has been used in many wireless systems, whilst the majority of the upper portion of the spectrum is not used (but may be used) for 5G technology. Potential commercial uses, such as automobile radars and high-data-rate systems, have been made possible due to the rising demand for inexpensive circuitry and better data transfer rates in these bands [100] – [102]. Achieving complete transparency and rate convergence between wireless and wired links, mmWave, and terahertz (THz) bands, which are the new wireless communication technology frontiers, could lead to seamless interconnections between ultra-high speed wired networks (fiber optic links) and personal wireless devices (laptops).

Millimeter wave technology operates in the electromagnetic range between 30 and 300 GHz, with wavelengths ranging from 10 to 1 mm [30], [34], [103]-[106]. A detailed diagram of the millimeter wave spectrum is shown in Figure 3.1. The available spectrum at the presented frequencies is more than 200 times larger than all of the present cellular network allocations [103]. This technology is characterized by a large quantity of idle bandwidth that can improve the data rate available to end users, allowing it to meet the two primary requirements for 5G networks: ultra-high peak throughput (20 Gbps) and the average user experience rate (50–100 Mbps) [105]. Since gigabit Ethernet and desktop connections have become inexpensive for server connections, in 2007, the communication sector disclosed the unoccupied 10 Gb for usage [105]-[106]. In addition, gigabit Ethernet became the standard for servers, requiring systems to be ordered with gigabit network interface cards on a regular basis [106]. Over time, the cost of wireless gigabit lines has equaled the cost of wireless. This provides superior output in older wireless applications as well as other feasible uses at gigabit speeds. Wireless communications have become increasingly relevant in the business world, particularly in Universal Serial Bus (USB) 2.0, gigabit speeds, and extended range services [106].

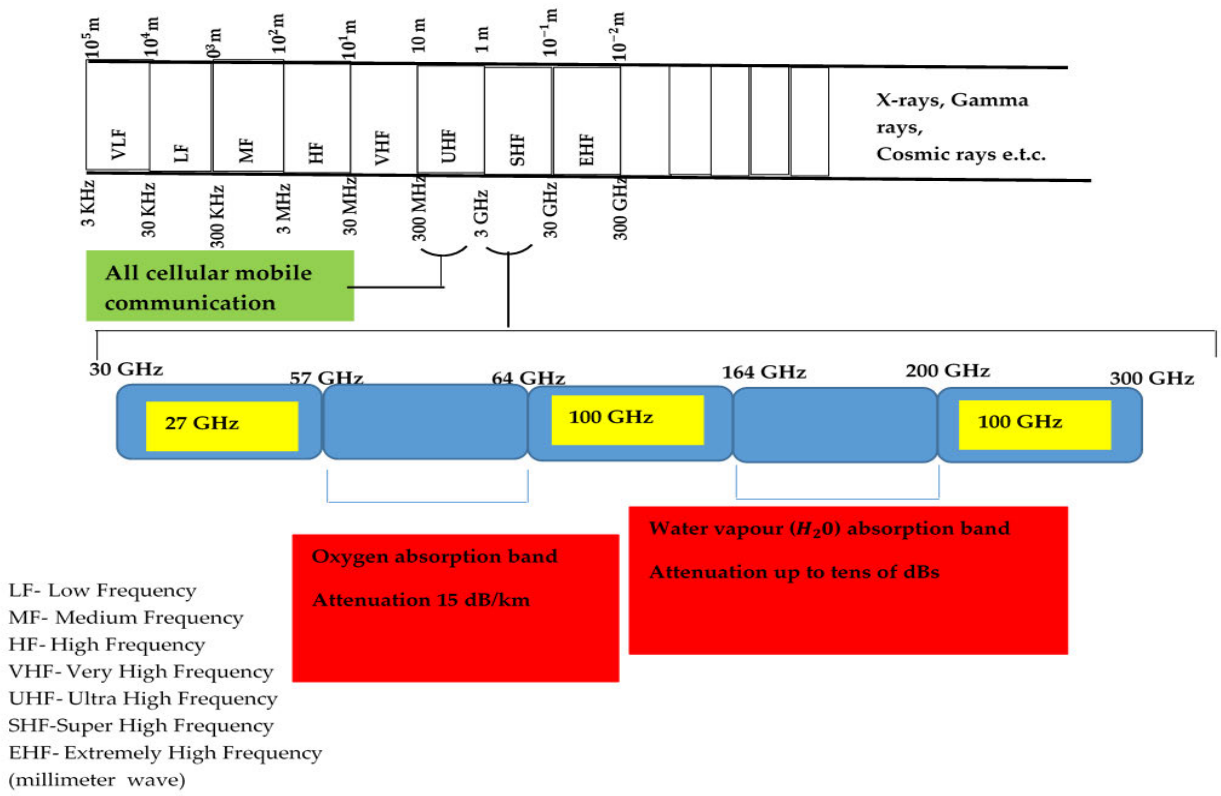

Figure 3.1. Millimeter wave spectrum [107].

Previous WLAN speeds were just 54 Mb/s, with IEEE 802.11n applications reaching 150–300 Mb/s. However, when it comes to accessing rich media information, even 500 Mb/s is insufficient. In the near future, home A/V (audio/video) networks will need Gb/s data rates to deliver uncompressed high-definition video at resolutions of up to 1920–1080 progressive scans, with latencies ranging from 5 to 15 ms [30], [106]. In addition, the technical requirements for high-speed wireless systems must take into account the following factors:

1. The requirement for higher data rates will continue to grow as the demand for multimedia networks grow.
2. The demand for shared resources has increased as a result of data streaming for both personal and mobile devices.

Although numerous technologies have been used, such as IEEE 802.11n, IEEE 802.16 (WiMax), and UWB, their efficiencies have not been sufficient to meet the demands placed on wireless communications, particularly in 5G networks [30]. A better way to tackle these challenges is to make proper use of frequencies that are not employed in millimeter waves but have application potential. These frequencies are shown in Figure 3.1. Despite the fact that millimeter wave technology has been in use for some time, with the advent of process technology, this technique has begun to receive widespread acceptance among academics and industries.

After building a communication channel that spans the capacity and dependability of data rates, the path loss exponent is one major metric that a good communication channel depends on [98], [101], [108]-[109]. Path loss is a measure of the degeneration of the propagated signals over a distance range in both LOS and NLOS scenarios. The path loss exponent is used to evaluate the performance of a communication system in wireless

channel propagation. It has been found that impediments, including walls, furniture, and people, can cause propagation loss in millimeter wave technology. The development of a good path loss prediction model for these bands still depends on detailed characterization, analysis, and modeling in these frequency bands, despite the fact that research in this field is ongoing. Wireless system design, planning, and simulation were all part of the model application. Different path loss model concepts have been proposed by various academics for examination, particularly in indoor environments [6], [39]-[43], [110]. The most important use of path loss models will be in [40], where calculations of power budgets, modulations, forecasts of cellular coverage/interferences, and the design of coding schemes are all highly critical.

This research which offers LOS and NLOS measurement data scenarios in an indoor corridor environment assesses CI and FI path loss prediction models for frequency ranges of 28 and 38 GHz. The measuring campaign took place on the 5th floor of the Discipline of Electrical, Electronic, and Computer Engineering Department building at the University of KwaZulu-Natal's Howard Campus in Durban, South Africa. In the NLOS scenario, the evaluation included propagation characteristics for both FI and CI free space path loss models. Oyie and Afullo [33] worked on the same channel settings of 14 and 22 GHz using the Rohde & Schwarz SMF 100A for signal generation at the Tx, Rohde & Schwarz FSIQ signal analyzer at the Rx, and two directional pyramidal horn antennas. Previous work of [40] did not consider the behaviors of the model parameters when two antenna polarizations were used but dwelled only on one antenna polarization, which was the V–V antenna polarization in an indoor environment. However, to fill this gap, this chapter evaluated the measurement analysis of the existing CI together with the FI path loss models in terms of the antenna polarizations using measured data from the measurement campaign. The measurement campaign was conducted at frequency bands of 28 and 38 GHz using the Rhode and Schwarz SMB 100A radio signal generator to generate continuous wave (CW) signals, which were then delivered across a wireless medium to the Rhode and Schwarz FSIQ 40 signal analyzer of a frequency range of 100 kHz to 40 GHz with the use of broadband horn antennas at both the transmitter and receiver ends. The accuracy, simplicity, and stability of the parameters of the models were evaluated in both LOS and NLOS scenarios.

This work established an appropriate antenna polarization mode with the lowest path loss when transmitting power from the transmitter to the receiver in both LOS and NLOS communication scenarios. It will also be a good indication for developmental initiatives for future wireless communication research on specific building design prediction path loss models for brick and concrete walls (since the indoor corridor is made of dry concrete and bricks). The rest of the chapter is organized as follows: Section 3.2 reviews the literature studies and works on millimeter waves. Details of the environment used for the measurement campaign and various path loss models are discussed in Section 3.3. The results and the comprehensive discussion of the results are presented in Section 3.4. The chapter summary is presented in Section 3.5.

3.2. Review of Relevant Works

The review related to propagation path loss, wide bandwidth, narrow wavelength, and high penetration that characterize millimeter wave communication is given as follows:

(a) Abundant bandwidth: At the moment, the overall bandwidth available for a mobile network is insufficient to meet the increased data demands of devices for 2G, 3G, and 4G networks. The most significant advantage of

millimeter communication over classical communication is the increased bandwidth, which allows the transmission at very high frequencies up to few hundreds GHz [110].

(b) Short wavelength: Because mmWave signals have wavelengths in the order of millimeters, they must be communicated using MIMO, and they are particularly well suited to packing a large number of half-wavelength-spaced antennas into tiny spaces. The combination of mmWave with massive MIMO can considerably improve the wireless access and throughput performance [45].

(c) Propagation loss: Path loss and penetration loss are two different types of propagation losses. Under the assumption of the LOS, the free space route loss is proportional to the square of the carrier frequency, according to the Friis trans-mission formula. Because microwave frequencies start at 26.5 GHz, there is more propagation loss than in the microwave band. For example, at 60 GHz, it is 28 dB higher than at 2.4 GHz. This has been a key drawback of mmWave, but with the introduction of device to device (D2D) communications, a high-gain directional antenna may compensate for the loss, improving network capacity and enhancing security against eavesdropping and jamming. The increased penetration loss in NLOS set-tings makes it difficult for mmWave nodes placed outdoors to reach indoor spaces. Signals/propagation may suffer from large penetration losses in the case of indoor users with outdoor base stations (BSs), lowering data throughput, spectrum efficiency, and energy efficiency. The separation of outside and indoor scenarios is, therefore, unavoidable [46]-[47].

According to Salous et al. [26], there are unallocated spectra in millimeter wave bands, preventing the full use of massive antenna arrays for high-speed data transfers. Although gigabit data transmissions in these bands necessitate accurate channel modeling, the shad-owing effect and the necessity for adaptive beam formations in areas with significant mobility persist. As a result, it was suggested that in addition to end-channel sounders, detailed measurements for full radio characterization should include angular spread and delay time in the evaluation of multipath make-ups. However, in order to provide in-put to standard organizations, the lack of channel models must be addressed. El Hajj et al. [48] emphasized the relevance of millimeter bands as a proven solution for high data rate transmissions, particularly in indoor environments. However, millimeter wave propagation technology has been reported to suffer from propagation loss of 25 to 30 dB due to impediments, such as walls, furniture, and human blocking. Another study used a frequency domain and a vector network analyzer (VNA) to investigate millimeter wave propagation at 60 GHz in an indoor environment. The results suggest that an access point (AP) can be placed in the center of the network to reduce shadowing caused by human impediments. It has a high frequency that could be solved with a frequency lower than 60 GHz.

As mentioned in [49], millimeter wave measurements were made in China with the goal of determining the influences of atmospheric variables on transmission. There was a difference between the theoretical rain-induced signal attenuation and the practically recorded signal attenuation during the rainfall. It was founded on the idea of rain fore- casting and monitoring in real-time. As a result, the dynamic rain-aware link adaptation method was developed to allow the system to fit the modulation and coding scheme to rain intensity levels, the production efficiency of fixed modulation, and coding schemes. The results reveal that the rain-induced signal is unpredictable in both practical and theoretical situations, with attenuation due to variations in weather conditions ranging from 1.5 to 4.5 dB. The drawback was that the different links were not compared. Gade et al. [50] discovered that on-chip wireless links function better than a standard NoC in additional millimeter wave

research. The on-chip wireless channel characteristics were combined with antenna implementation and near-field multipath propagation effects. The near-field/transition region is where the propagation in the on-chip wireless channel takes place, making the channel more difficult. On antennas, it was also discovered that directional kinds are less impacted by channel time dispersion, despite higher losses, and that omnidirectional antennas obtained a reserve. The on-chip wireless channel provides information on the characteristics of wireless communications and aids in the design of circuits for improved performance.

The performances of millimeter wave for indoor communication at different bands between 28 and 73 GHz were carefully examined for LOS and NLOS conditions, taking into account the effects of different buildings and frequency-sensitive materials. The links between separation distances and the received power and delay spread were inversed. As a result of the concerns with the antenna's directivity, a rise in path loss causes a commensurate increase in separation distance. The system was also able to solve the problem of bandwidth in electronic devices, allowing for the growth of low-cost infrastructure demand for broadband mobile devices. The main disadvantage of this strategy is that it tends to fail as distance and communication capabilities grow [51]–[53]. Chittimoju and Yalavarthi [54] conducted a complete assessment of millimeter wave communications, including some of the benefits and uses. They demonstrated that millimeter waves encourage larger band-widths while increasing the speed to 10 Gbps. Some of the benefits observed include the utilization of compact components, less interference, and increased security. The range is limited in the line of sight, which was one of the key flaws uncovered. The authors in [55] introduced a novel technique termed the Q learn-based system, which incorporates the edge computing function in adjustable power and angle sub-6 GHz user equipment to tackle capacity and efficiency problems in millimeter wave propagation. The results suggest that the user's equipment (using this method) was able to achieve great energy efficiency, allowing for a very strong and steady transmission capacity.

Maltsev et al. [56] concentrated on the merits, limitations, and common applications of millimeter wave communications in several bands. Millimeter wave was determined to be critical in the deployment of 5G, and it is believed that significant improvements in radio and networks could be developed to aid in the deployment of 6G. Fuschini et al. [57], using ray tracing (RT) simulations and directed measurements, investigated the narrowband and wideband properties of an in-room 70 GHz wireless channel. Reflection is the most pronounced mode of propagation; however, scattering is still present and appears more than when the frequencies are below 6 GHz, according to the observations. When comparing a more detailed environment to a less detailed environment, if both were exposed to the same error sources, a faster rate of calculation was seen, but this did not translate to greater simulation accuracy.

In [48], the authors reviewed the results of observations taken in two indoor locations at a transmission frequency of 60 GHz. The responses of three distinct types of antennas to power loss factors were verified using a VNA. The results revealed that big aperture antennas had greater guided wave effects than those with narrow apertures, resulting in a more accurate path loss model for the latter. The measurements also showed that positioning an omnidirectional antenna in the access point (AP) in the center of the meeting room provided better radiation than placing it in a corner because the shadowing effect produced by human obstruction was reduced. These findings will aid in the deployment of new wireless local and personal area networks. Further research work included compiling a comprehensive overview of 5G network approaches in millimeter wave

wireless communication systems, as well as bringing together essential millimeter wave propagation models from the past to the present. It also emphasized the significance of developing diverse models based on ray tracing and measuring procedures for current and future uses in academia and industries. As millimeter wave is still in the research era, especially in the application for 5G propagation [25], the data acquired on shadowing and path loss will aid in the predicted improvement. The major issues with millimeter wave propagation, such as limited beam width, high penetration loss, and strong path loss, were highlighted in [47]. The authors also discussed the differences between analytical modeling and ray tracing approaches for channel modeling. After the measurements, data processing and analysis of the measurement results were given, including channel gain, scatterer identification, RMS delay spread, and average power delay profile (APDP). When taking measurements in varied settings, however, the usage of a MIMO channel with a wide frequency spectrum is essential.

Elmezughi et al. [41] discussed the frequency measurements in 14, 18, and 22 GHz frequency bands in an indoor environment. The authors of [41] also presented two path loss prediction models and communication scenario analyses for both NLOS and LOS. The LOS analysis showed that the CI and FI models functioned nearly identically after execution at all frequencies. With the frequencies increasing along the LOS range, the PLE increased significantly in the CI model. It rose from 1.37 to 1.66 for the 14 and 22 GHz frequency bands, respectively; however, the LOS values did not match those of the FSPLE. Due to environmental considerations, the path loss models had symmetrical features at around 180 AoA. The models, on the other hand, performed better at 30, 330, and 180 AoA. The findings also demonstrated that CI and FI models may be employed reliably in both LOS and NLOS corridor scenarios. The main flaw that needs to be addressed is the adoption of a higher gain antenna to decrease additional path losses to the absolute minimum. In addition, as an extension to the above-mentioned conclusion, the effects of transmitting antenna heights on these parameters were explored in [42]. Elmezughi and Afullo [43] recently updated this work, delivering efficient improvements for both the CI and FI path loss models. The major findings showed that, for both LOS and NLOS communication scenarios, the enhanced models beat the standard models. Furthermore, the proposed models have substantially superior stability and sensitivity than standard models, especially in the NLOS condition. By combining these enhanced models with the LOS probability models provided in [46], a generic and accurate model for indoor corridor environments may be obtained. Despite the research on these frequency bands, thorough characterization, analysis, and modeling in these bands remain crucial. This study used the MMSE approach to analyze large-scale path loss models in the 28–38 GHz frequency spectrum in order to reduce the complexities and errors in LOS and NLOS scenarios.

Path loss is a phenomenon that occurs when a transmitter's signal is attenuated in the communication channel as a function of the distance traveled as well as the propagation channel characteristics. Path loss (or path attenuation) is the decrease in the power density of an electromagnetic wave as it travels through space. Path loss can be caused by a variety of factors, including natural radio wave expansion, diffraction path loss caused by obstruction, and absorption path loss due to the presence of a form of media that is not transparent to electromagnetic waves. It is crucial to remember that even when a path is lost, the transmitted signal may still travel along other paths to its destination; this process is known as multipath. Since these waves or transmitted data travel along different paths, the wave may reconvene at the destination point, resulting in significantly

different received signals [111]. It also refers to the loss or attenuation that a propagating electromagnetic signal (or wave) experiences as it travels from the transmitter to the receiver. As a result, the received power is lower than the broadcast power level. Antenna gains, operational frequency, transmission power, and the range of separation between the transmitter and receiver are all elements to consider. The most common way to express path loss is in decibels (dB) [61]. Because the dependency of the distance between the transmitter and the receiver distance on the path loss is no longer linear, the path loss in wireless propagation is mostly a function of a logarithm factor. However, in LOS environments signal attenuation over distance closely follows Friis' free space path loss equation, propagating signals attenuated according to the square power law [61], [63].

In the last 20 years, there has been substantial research into various propagation channels that could be used for indoor channels. While some have concentrated on both outdoor and indoor office spaces, others have concentrated solely on interior office environments [62], [64]-[69]. Wang et al. produced model descriptions with probability distributions; they relied on the parameters in research on an empirical path loss model for wireless channels in indoor short-range office environments. The model depicted appreciable variable values of route losses at different frequencies and produced a simpler model that simplified radio propagation in difficult situations. However, because this study was conducted in an office setting, it was necessary to evaluate this innovative prediction path loss model in a commercial setting with more obstacles [112].

Further research has revealed that most propagation models that work at frequencies less than 6 GHz are inapplicable when considering route loss models for millimeter wave frequency bands (which are generally above 6 GHz). Majed et al. constructed channel models that could operate in indoor circumstances at frequency ranges of 4.5, 28, and 38 GHz in order to find a solution. Both LOS and NLOS measurements were taken in an inside office environment with the transmitting and receiving antennas separated by 23 m. The purpose of the study was to compare the new large-scale generic path loss models to existing path loss models, omnidirectionally and directionally, as well as multi-frequency and single-frequency path loss models. The investigation shows that when modeled with one parameter PLE and associated with transmitted power, the large-scale route loss model has a propensity to perform better [70]. Shadowing and attenuation, which were explored in [70], are another set of properties common to indoor environments. Wireless open-access research platform (WARP) equipment was used to model path loss and shadowing. As a result, the propagation path loss value was consistent with measurements in the literature, with an exponent of 4 and a standard variation of 6.4 dB.

In millimeter wave propagation, the direct exchange of information between two near-distance devices in the absence of a base station (known as D2D communication) has various advantages, including energy efficiency, increased data throughput, and shorter latency [52], [113]. The effect of path loss on this D2D communication, however, is unique and unsurpassed. Modeling a method that will result in a significant reduction in attenuation is required. The authors in [114] proposed a strategy that uses mode assignment by reuse as well as cellular mode dedication based on a tradeoff of path loss attenuation and ranges between D2D users. This scheme's analysis was compared to other existing schemes, such as the alternate offer bargaining game theory algorithm (AOBG) and the heuristic algorithm. The main benefit of the proposed approach is that the D2D user's SINR threshold is supported to a certain extent. The practicality of this technology is demonstrated by the fact that it is extremely useful in situations where path loss attenuation is a concern in both indoor and outdoor contexts.

Another measurement work was conducted in two different locations in the USA by MacCartney. Jr. et al. to check the path loss models for 5G millimeter wave propagation channels in urban microcells using the best of the sliding correlator channel sounder at two frequency bands (28 and 38 GHz). Using directional antennas of varying heights and gains, this experiment investigated multiple microcellular conditions. The linear regression fits were used to create the path loss models. The path loss spanned a distance that depended on the power received, according to the measurements. When compared to existing path loss models, the suggested model performed better in terms of lowering shadow factors by several decibels and providing a better fit to empirical data while permitting only a minor path loss [16].

Naruke et al. proposed an indoor localization method based on the path loss—distance relationship using handset sensor data. This proposed model computed the range between the Bluetooth low energy (BLE) transmitter and the smartphone by first using the distance and path loss relationship and then using pedestrian dead-reckoning (PDR) fixed on the mobile phone's accelerometer. When compared to previous methods, the results revealed a significant improvement in the distance error [74]. Al-Saman et al. conducted a comprehensive investigation in which the investigated mmWave propagation models as well as measurements in indoor environments. Time dispersion and path loss were identified as the key indoor wireless channels in terms of millimeter wave propagation. Although the path loss coefficient grew as the frequency increased, the exponent was only affected by the structure and kind of environment, not by the frequency. The overall observation is that CI and FI models are the best for both LOS and NLOS channel propagations in millimeter wave bands, especially in indoor environments, based on multiple applications of different research articles regarding frequency ranges of 28 to 100 GHz. This development represents a significant step forward in the deployment of millimeter wave propagation for both 5G and 6G networks with low propagation losses [39]. To the best of our knowledge, there is no other analysis that covers the peculiarity of the effect of the proximity of walls on path loss parameters. To fill this research gap, one of the main goals of this work was to find an acceptable model with the best line of fit and the simplest application for the path loss model estimation in both LOS and NLOS scenarios. The well-known single-frequency CI and FI path loss models for V–V and V–H antenna polarizations were used to examine the channel characterization. The work also shows that the multipath components added up favorably due to wave-guiding and reflections in the inside corridor environments. Another contribution from this investigation is that the proximity of the walls, the materials of the walls, the floor, and other irregular elements, such as wooden doors, concrete, and elevator doors along the corridor, all have effects on radio wave propagation (indoors).

3.3. Path Loss Measurements and Models

This section presents the details of the environment used for the measurement campaign and the propagation models.

3.3.1. Measurement Setup

The setups used for the measurement, the measurement scenario, and the channel sounder are shown in Figure 3.2. The measurements were carried out at the Howard College Campus of the University of KwaZulu-Natal on the 5th floor of the Department of Electrical, Electronic, and Computer Engineering. The

measurements were conducted at frequencies of 28 and 38 GHz with a transmitting antenna height of 1.6 m and receiving antenna height of 2.3 m. There was a total of 13 measured points for the both LOS and NLOS scenarios. Although a reference distance of 1 m was observed, subsequent measurements were done from 2 m points with increments of 2 m each until reaching 24 m. The measurements for Tx and Rx combinations included two antenna polarization combinations, i.e., V–V and V–H. For the LOS, the bore sight alignments of the two antennas were used. Whereas, in the NLOS scenario, the received power was determined when the transmitting antenna was rotated to make sure there was an obstruction resulting in no clear optical path between the Tx and Rx antennas. At this point, there was no aligning bore sight between the two antennas.

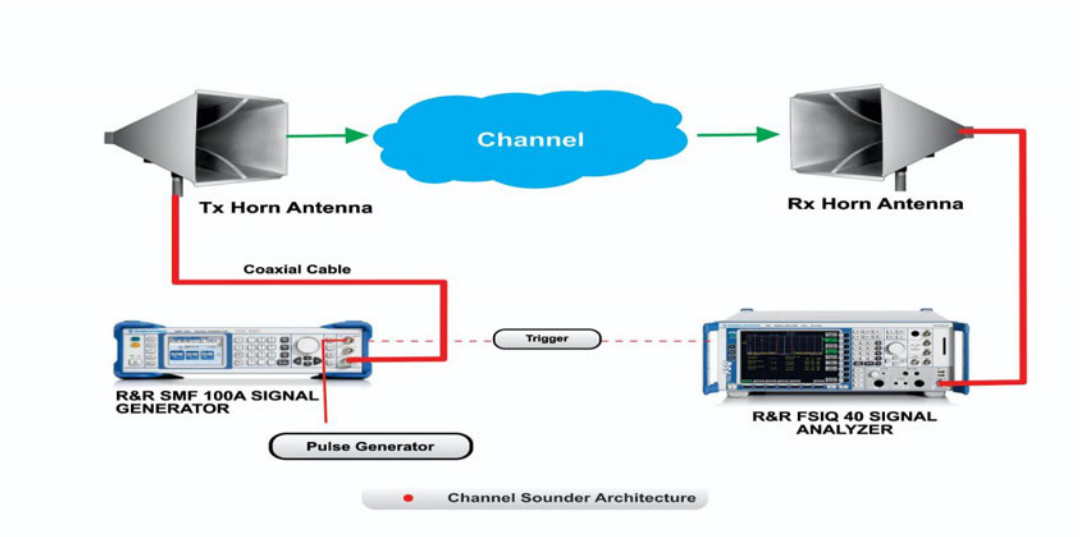

Figure 3.2. The architecture of the channel sounder.

The complete description of the channel sounder, as well as the measurement setup, is provided. On the transmitting end, the Rhode and Schwarz SMB 100A radio signal generator was used to generate CW signals, which then radiated across a wireless medium. This signal generator has a frequency range of 100 kHz to 40 GHz. A Rhode and Schwarz FSIQ 40 signal analyzer was used at the receiver end to receive the continuous wave signal from the SMB 100A signal generator. The frequency range of this FSIQ 40 signal analyzer is 20 to 40 GHz with a maximum bandwidth of 120 MHz. Two identical LB-180400-KF broadband horn antennas with frequency ranges of 18 to 40 GHz were used in this setup for transmitting and receiving radio signals. They had a nominal gain of 15 dBi, a low VSWR of 1.5:1, and a uniform gain across the frequency ranges, resulting in efficient performances and directionality. The antennas were also linearly polarized and could handle 10 W continuously and 20 W peak output. In the elevation plane, the half-power beam width (HPBW) had a minimum of 21 degrees and a maxi-mum of 42 degrees, whereas, in the H-plane, it was a minimum of 17 degrees and a maximum of 45 degrees. The measurements were conducted at the height of 1.6 m for the transmitting antenna and 2.3 m for the receiving antenna above the floor for both LOS and NLOS situations. Figures 3.3–3.6 present the transmitter setup, receiver setup, and indoor corridor environment. Table 3.1 lists the channel sounder's parameter settings.

Figure 3.3. The indoor corridor environment.

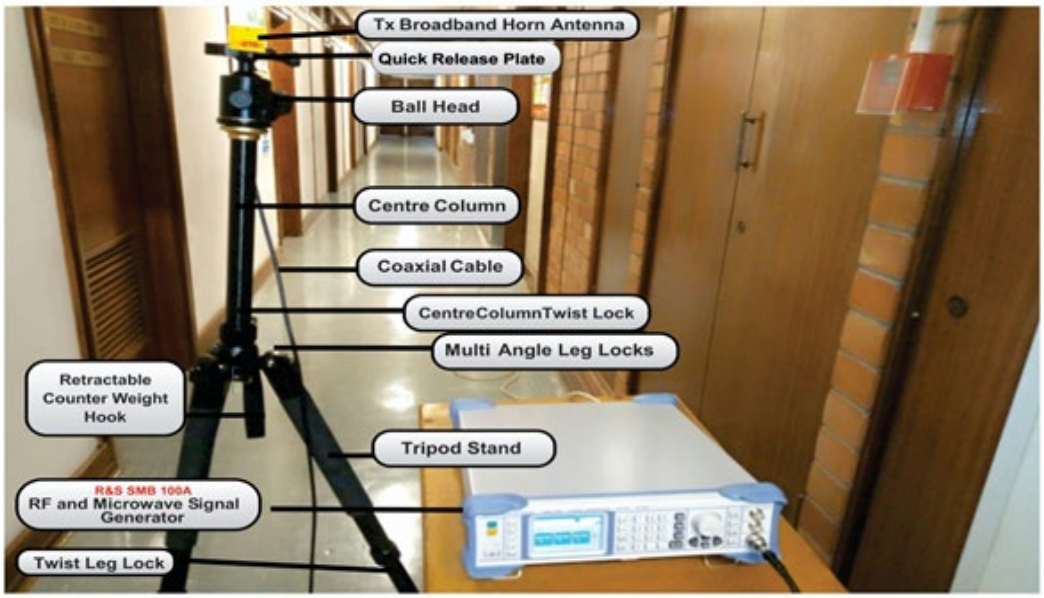

Figure 3.4. The transmitter setup.

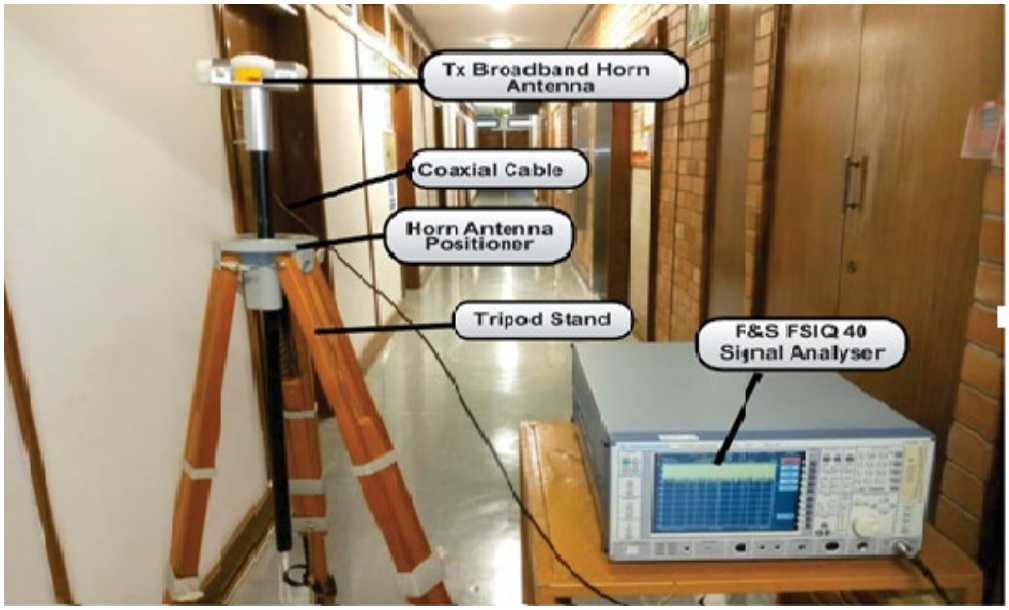

Figure 3.5. The receiver setup.

Figure 3.6. The setup of the transmitter and the receiver in the indoor corridor environment.

Table 3.1. Parameter specifications of the channel sounder for the experiment.

Parameters	Configuration/Value	Unit
Centre frequency	28, 38	GHz
Bandwidth	100	MHz
Transmission signal	Continuous wave	
Tx and Rx Antennas	Broadband horn antenna	
Tx Antenna power	10	dBm
Tx Antenna height	1.6	m
Rx Antenna height	2.3	m
Tx and Rx antenna gain at 28 GHz	15	dBi
Tx and Rx antenna gain at 38 GHz	17	dBi

Tx and Rx antenna polarization	Vertical/horizontal	
Antenna size L × W × H	71 × 32 × 28.6	mm^3
Antenna weight	0.08	Kg

The measuring campaigns took place on the 5th floor of the Electrical, Electronic, and Computer Engineering Department at the University of KwaZulu-Natal in Durban, South Africa. The length, height, and width of the indoor corridor are 30, 2.63, and 1.4 m, respectively. The corridor is made up of dry concrete brick walls, a square tiled floor, an elevator, and wooden office doors. The floor plan is shown in Figure 3.7. The indoor corridor was used for both the LOS and NLOS scenarios of the campaign.

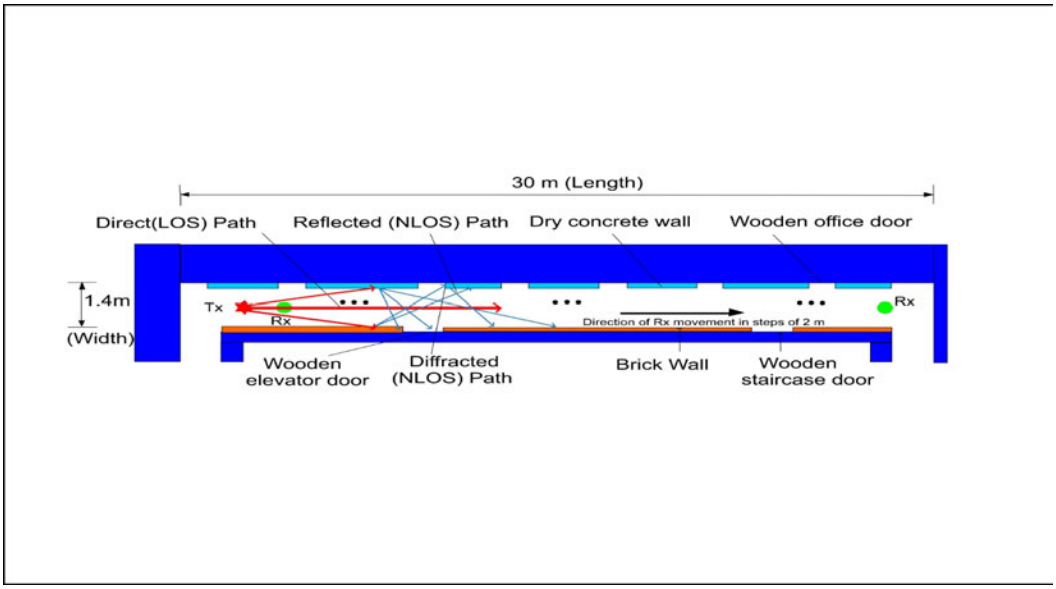

Figure 3.7. Floor plan of the indoor corridor environment.

The transmission of a continuous wave signal between the two broadband horn antennas used in the transmitting and receiving ends had antenna heights of 1.6 m at the transmitting antenna stand and 2.3 m at the receiver's end. Both polarizations were placed in the vertical and horizontal directions; the center frequencies used were 28 and 38 GHz. For the V–V polarization, the Tx and Rx broadband horn antennas were vertically polarized. On the other hand, the Tx antenna for the V–H was vertically polarized, while the Rx antenna was horizontally polarized. The transmitting antenna was placed at one end of the corridor, and the receiver antenna was moved away from the transmitter by 2 m until it reached a distance of 24 m. Meanwhile, specialists in this field proposed a reference distance of 1 m between the transmitter and receiver. With a reference distance d_o = 1 m., the number of Tx–Rx separation distances was 13. When both antennas were aligned on the bore sight with no obstacles in the transmitting signal path between them, the LOS scenario was evaluated. However, in the NLOS, the received power was determined when the transmitting antenna was rotated to make sure that there was an obstruction resulting in no clear optical path between the Tx and Rx antennas. At this point, there was no aligning bore sight between the two antennas. The floor layout and the inside corridor are depicted in detail in Figures 3.3 and 3.7, respectively.

It is worth noting that during the campaign, measuring cautions were observed in order to acquire accurate measurements. During the campaign, all doors were closed and human movement along the inside corridor was prohibited. In addition, all objects in the corridor were eliminated. The path loss was calculated using Equation (3.1), having considered the transmitted power P_t, received power P_r, gain of the transmitting antenna G_t as well

as the gain of the receiving antenna G_r. The path loss equation (all parameters in dB) is as follows, as computed in [43]:

$$P_L = P_t - P_r + G_r + G_t \tag{3.1}$$

3.3.2. Path Loss Propagation Models

There is a general classification of models that requires minimal site or path details and that counts hindrances or obstructions as components of the distance-dependent losses, whereas site-specific models assess the losses due to each hindrance separately. These models are taken into account by placing the measured variables into a generic phrase. Approximately four major path loss propagation models are frequently used: two are single-frequency models, while the other two are multi-frequency models. CI, FI, CIF, and ABG models are used in various studies [12], [16], [71], [73], [75]- [76], [78], [92], [115]-[125].

Models in propagation path loss can be used to reflect the effects of path loss on the signal at the receiving end on a wide scale. It is a useful tool for calculating signal attenuation as it travels from the transmitter to the receiver, taking into account the propagation distance and other factors. The models differ in that some specify the topographical profile for easy signal analysis, while others just use the carrier frequency and distance to determine their targets [82], [124]. The CI, CIF, and ABG path loss models are stochastic in nature, yet they capture the phenomenon of large-scale propagation across a given distance, keeping in mind that they can work at all appropriate frequencies in a given environment. The CI and CIF models are found to be equivalent to the standard forms of 3GPP path loss models (the FI and ABG models). Only the floating constant and the free space constant, which are dependent on propagation frequency and observance of the free space reference distance of 1 m [63], [84]-[88], are relevant in this case.

3.3.2.1 The CI Free Space Reference Distance Path Loss Prediction Model

This is a model that has its primary principle on the anchor point and depends on the frequency in the free-space. The FSPL is present in the model parameter, which also depends on the frequency of the carrier propagating signal (f in GHz). The distance between the transmitter and the receiver (d in meters), as well as the chosen reference distance (d_o), are also important factors. The CI model has one parameter to be calculated in dB, i.e., PLE (n) [64], [88], [124]. The equation for the model is shown in (3.2).
The reference distance of the CI model is 1 m, given by [63], [88]:

$$P_L^{CI}(d)[dB] = FSPL(f, d_o)[dB] + 10.n.\log\left(\frac{d}{d_o}\right) + X_{\sigma SF}^{CI} \tag{3.2}$$

For $d \geq d_o$, where $d_o = 1m$
Where $X_{\sigma SF}^{CI}$ is a zero mean gaussian random variable with a standard deviation σ in *dB*

$$FSPL(f, d_o)\,[dB] = 10log_{10}\left(\frac{4\pi d_o}{\lambda}\right) \tag{3.3}$$

To determine the CI path loss model, the PLE *n* is found using the MMSE approach, which commiserates with the data measured by adopting a physical anchor location that represents the free space power transmitted from the antenna at the transmitter out to the reference distance d_o of the CI . The reference distance $d_o\ of\ 1m$ is

utilized in the mmWave CI model, which was proposed as a standard in [61] and [88]. Far-field radiation patterns (Fraunhofer distances) from high-gain directional antennas may be greater than 1 m from the antenna, but the CI path loss model may simply be converted to a 1 m reference distance by assuming that the far field begins at 1 m (even if it does not).

$$FSPL(f, d_o)[dB] = 10log_{10}\left(\frac{4\pi f d_o}{c}\right)^2 \tag{3.4}$$

$$FSPL(f, 1m)[dB] = 10log_{10}\left(\frac{4\pi f}{c}\right)^2 \tag{3.5}$$

Where c represents the speed of light.

From (3.1), the shadow-fading random variable is

$$X_{\sigma SF}^{CI} = PL^{CI}(d)[dB] - FSPL(f, 1m)[dB] - 10.n.\log(d) \tag{3.6}$$

Let $A = PL^{CI}(d)[dB] - FSPL(f, 1m)[dB]$ *and* D= $10.n.\log(d)$

Therefore,

$$X_{\sigma SF}^{CI} = A - nD \tag{3.7}$$

Then, the standard deviation of the random variable $X_{\sigma SF}^{CI}$ *is*

$$\sigma^{CI} = \sqrt{\sum \frac{X_{\sigma}^{CI^2}}{N}} = \sqrt{\sum \frac{(A-nD)^2}{N}} \tag{3.8}$$

Where N represents the number of measured path loss points.

In order to obtain the PLE at the optimum value and σ^{CI}, the partial differential of the numerator of equation (3.8), with respect to the value of PLE, is equal to zero. Then,

$$\frac{\partial[\sum(A-nD)^2]}{\partial n} = 0 \tag{3.9}$$

$$\sum 2D\ (nD - A) = 0 \tag{3.10}$$

$$2\sum D\ (nD - A) = 2(n\sum D^2 - \sum DA) = 0 \tag{3.11}$$

Therefore, from Equation (3.11), $n = \frac{\sum DA}{\sum D^2}$

The minimum shadow fading (SF) standard deviation for the CI model is

$$\sigma_{min}^{CI} = \sqrt{\frac{\sum(A - D\frac{\sum DA}{\sum D^2})^2}{N}} \tag{3.12}$$

The closed-form solution value was processed through MATLAB, *n*, and can be expressed using a matrix formation:

$$n = A^T(D^T D)^{-1}D \tag{3.13}$$

$$\sigma_{min}^{CI} = \sqrt{\frac{\sum(A - A^T(D^T D)^{-1}D)^2}{N}} \tag{3.14}$$

3.3.2.2. The FI Free Space Reference Distance Path Loss Prediction Model

This model relies on two major integral parts, i.e., the line slope, as well as the floating intercept. The FI model is good at achieving the optimal minimum error fit for the path loss values, [61], [88]. It can be expressed by Equation (3.15):

The equation of this path loss model is [61]:

$$PL^{FI}(d)[dB] = \propto + 10.\beta\, log_{10}(d) + X_{\sigma SF}^{FI} \tag{3.15}$$

This model adopts $\propto$ as the floating intercept in dB, and the slope of the line is β (not as in PLE). Moreover, $\propto$ and β were the two parameters adopted by this FI model to make it different from the CI model. The zero-Gaussian shadow fading (in dB) variable over the mean path loss on a specified distance was $X_{\sigma SF}^{FI}$. The best fit, such as the CI model, entailed solving $\propto$ and β and minimizing σ; the closed-form optimized solutions are provided below. It is worth noting that the FI model requires two model parameters, whereas the CI model only requires one.

Let $B = PL^{FI}(d)[dB]$, and $D = 10.log_{10}(d)$

Then, Equation (3.15) becomes,

$$B = \propto + \beta\, D + X_{\sigma SF}^{FI}. \tag{3.16}$$

$$X_{\sigma SF}^{FI} = B - \propto - \beta\, D \tag{3.17}$$

Then the standard deviation of the random variable is X_{σ}^{FI}

$$\sigma^{FI} = \sqrt{\frac{\sum X_{\sigma}^{FI^2}}{N}} = \sqrt{\frac{\sum (B - \propto - \beta\, D)^2}{N}} \tag{3.18}$$

If we want to minimize $\sum (B - \propto - \beta\, D)^2$,

It implies that its partial derivate should be zero with respect to β and $\propto$; that is,

$$\frac{\partial[\sum (B - \propto - BD)^2]}{\partial \propto} = \sum 2(\propto + \beta D - B) \tag{3.19}$$

$$2(N \propto + \beta \sum D - \sum B) = 0 \tag{3.20}$$

$$N \propto + \beta \sum D - \sum B = 0 \tag{3.21}$$

$$\frac{\partial[\sum (B - \propto - BD)^2]}{\partial \beta} = \sum 2D(\propto + \beta D - B) \tag{3.22}$$

$$2(\propto \sum D + \beta \sum D^2 - \sum DB) = 0 \tag{3.23}$$

$$\propto \sum D + \beta \sum D^2 - \sum DB = 0 \tag{3.24}$$

Now, combining equations (3.21) and (3.24),

$$\propto = \frac{\sum D \sum DB - \sum D^2 \sum B}{(\sum D)^2 - N \sum D^2} \tag{3.25}$$

$$\beta = \frac{\sum D \sum B - N \sum DB}{(\sum D)^2 - N \sum D^2} \tag{3.26}$$

The minimum shadow-fading standard deviation can be obtained by substituting $\propto$ and β in Equation (3.18), with (3.25) and (3.26), respectively [39]:

Then, the minimum SF standard deviation is now:

$$\beta = (D - \overline{D})^T (D - \overline{D})^T (D - \overline{D})^{-1} (B - \bar{B}) \tag{3.27}$$

$$\propto = \left(B - \overline{\beta D}\right) \tag{3.28}$$

Column vectors B and D have mean values of $\bar{B}$ and $\overline{D}$, respectively.

3.4. Results and Discussion

This section details the discussion of results in the LOS and NLOS analyses of path loss models as well as the performance assessments of the model's variables. The Rohde & Schwarz FSIQ 40 signal analyzer was used to capture the LOS and NLOS data, which were coupled to a broadband horn antenna. The data were analyzed in order to propose viable large-scale path loss prediction models using the minimum mean square error (MMSE) method, which fits the measured data in an indoor corridor environment at 28 and 38 GHz frequencies in two different antenna polarizations.

3.4.1 LOS Measurement Evaluation Study Results and Discussion

This experiment examined two frequency bands (28 and 38 GHz) at two antenna polarizations, revealing the findings and allowing for a comparison with the other propagation models. Figures 3.8 and 3.9 present the measured data and FPSL curves, illustrating the CI and FI models for the 28 GHz frequencies at V–V polarization and V–H polarization, respectively. The CI and FI path loss model curves overlapped with each other and accurately fit the real measured data in both antenna polarizations. They still closely matched the V–H polarization than the V–V. When the experiment was run using 28 GHz V–V antenna polarization, the PLE value was 2.254. However, when the experiment was run using a V–H antenna polarization, the PLE value increased to 2.979, indicating that the signal degraded more in the V–H polarization than in the V–V mode. Moreover, the values of α for the V–V and V–H were 58.8294 and 59.9354, respectively. Nevertheless, the value of β^{FI} rose from 2.154 to 3.05. It was observed that the value of σ^{FI} declined from 1.7431 (for V–V) to 1.3008 (for V–H).

When transitioning from the V–V to the V–H antenna polarizations in the 38 GHz frequency band, there was an increase of 0.4186 in the path loss exponent. This shows that while changing antenna polarizations at a 38 GHz frequency, signal degradation occurred. The curves are shown in Figures 3.10 and 3.11. When contrast to the 28 GHz frequency, the PLEs for both antenna polarizations were significantly larger at 38 GHz. This is because increased scattering and penetration losses were generated by an increase in the signal attenuations at higher frequencies. The various irregular materials, such as bricks, concrete, and other building materials (e.g., wooden doors and elevator doors), produce interference and may potentially impact the outcome. The standard deviation for shadow fading σ^{CI} for the V–V antenna polarization was 3.1874; nevertheless, it climbed slightly to 4.1001 for the V–H antenna polarization. This demonstrates that there are many signal fluctuations in both situations. Additionally, α^{FI} has a 1.6439 increase from the V–V to the V–H. While β^{FI} goes from 3.1461 to 3.6625, the σ^{FI} min value rises from V–V to V–H by 0.8016.

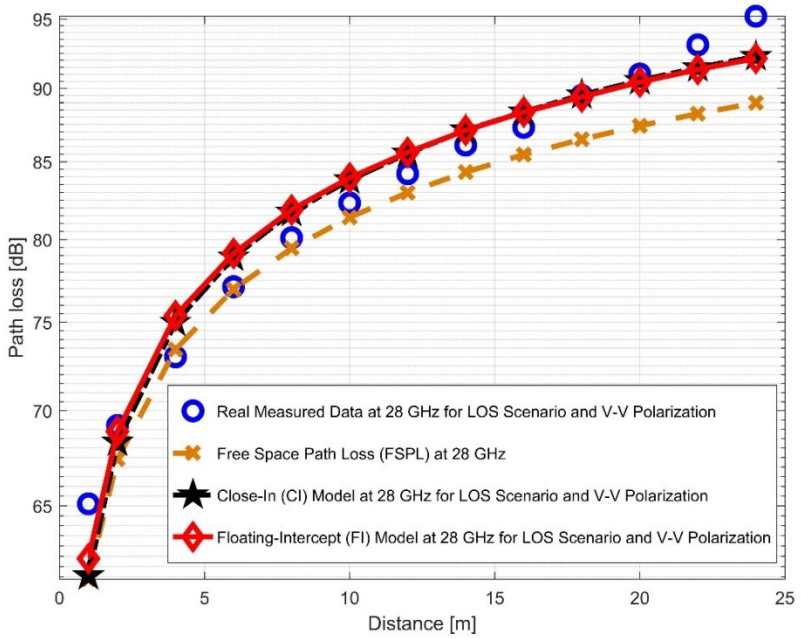

Figure 3.8. Path loss versus distance at 28 GHz for the LOS scenario and V–V polarization.

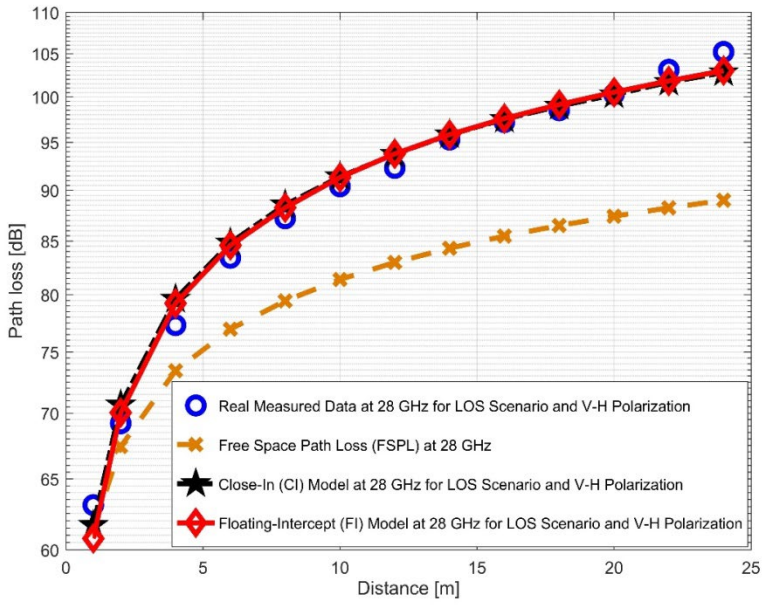

Figure 3.9. Path loss versus distance at 28 GHz for the LOS scenario and V–H polarization.

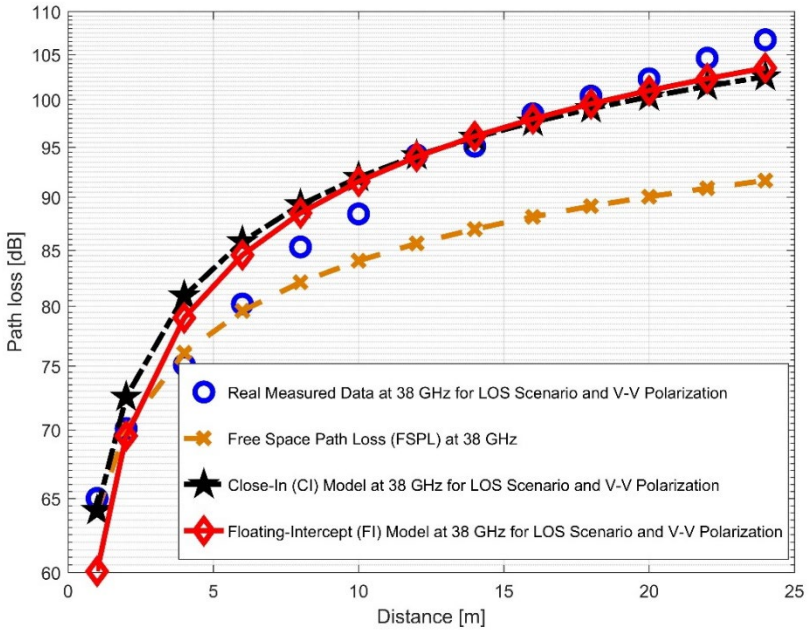

Figure 3.10. Path loss versus distance at 38 GHz for the LOS scenario and V–V polarization.

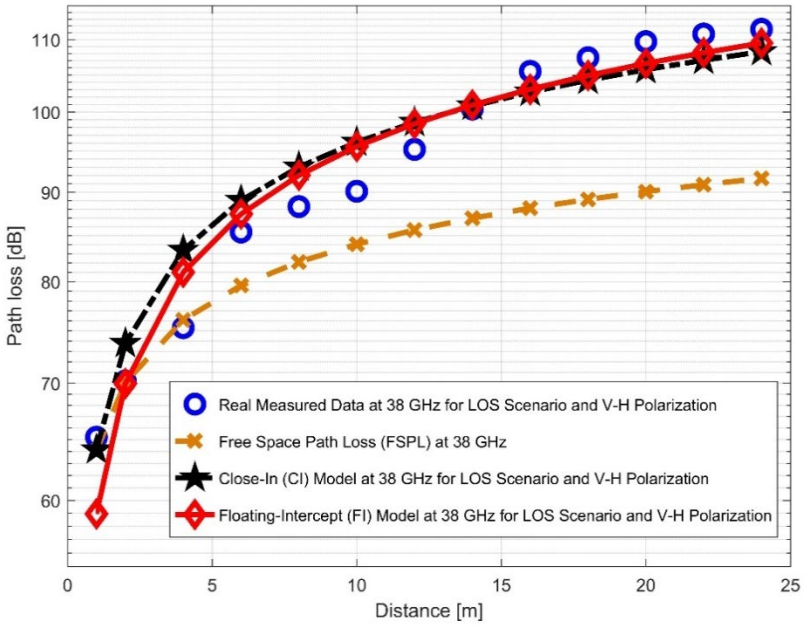

Figure 3.11. Path loss versus distance at 38 GHz for the LOS scenario and V–H polarization.

Figures 3.12 and 3.13 compare the path loss for LOS CI at 28 and 38 GHz for the two antenna polarizations. It is observed that path loss is more pronounced at 38 GHz than at 28 GHz for the V–V polarization. This indicates that higher frequencies are subject to the numerous propagation effects and path losses. The correlations between the path loss values in FI (in Figures 3.14 and 3.15) are very close to V–H, but have larger differences in the V–V polarization (similar to the CI case). This means that in the LOS scenario, both CI and FI behave similarly. Table 3.2 presents the LOS parameters of the CI and FI path loss models.

Table 3.2. The LOS comparative study results at 28 and 38 GHz frequencies.

28 GHz LOS Communication Scenario		
	V-V polarization	V-H polarization
PLE (n)	2.2254	2.9790
σ_{min}^{CI} [dB]	1.7718	1.3425
α_{FI} [dB]	58.8294	59.9354
β_{FI}	2.1537	3.0540
σ_{min}^{FI} [dB]	1.7431	1.3008
38 GHz LOS Communication Scenario		
	V-V polarization	V-H polarization
PLE (n)	2.7801	3.1978
σ_{min}^{CI} [dB]	3.1874	4.1001
α_{FI} [dB]	60.5444	62.1883
β_{FI}	3.1461	3.6625
σ_{min}^{FI} [dB]	2.7439	3.5455

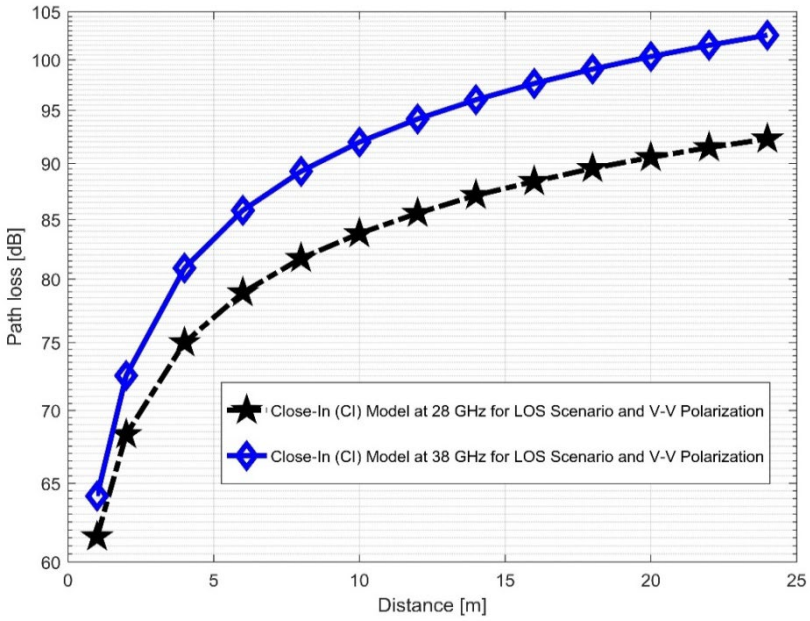

Figure 3.12. CI path loss versus distance at 28 and 38 GHz for the LOS scenario and V–V polarization.

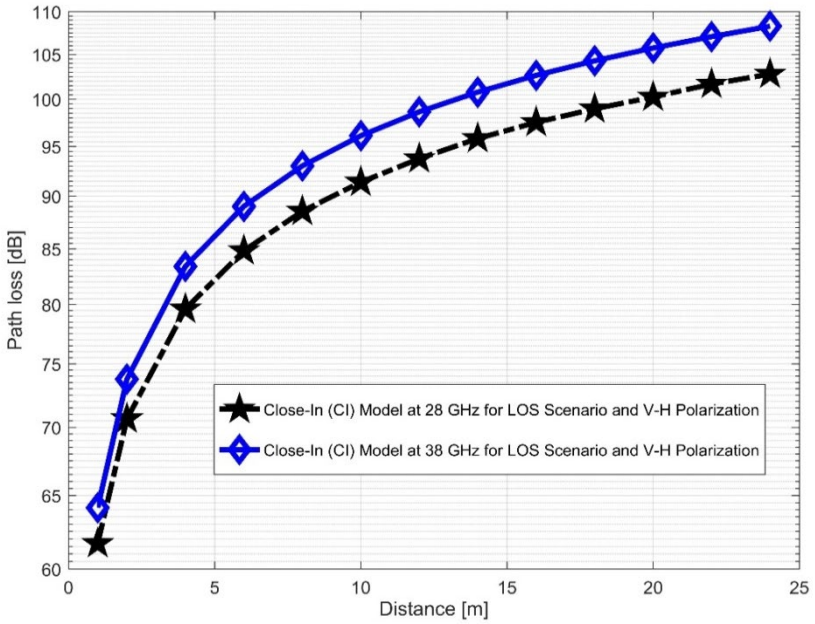

Figure 3.13. CI path loss versus distance at 28 and 38 GHz for the LOS scenario and V–H polarization.

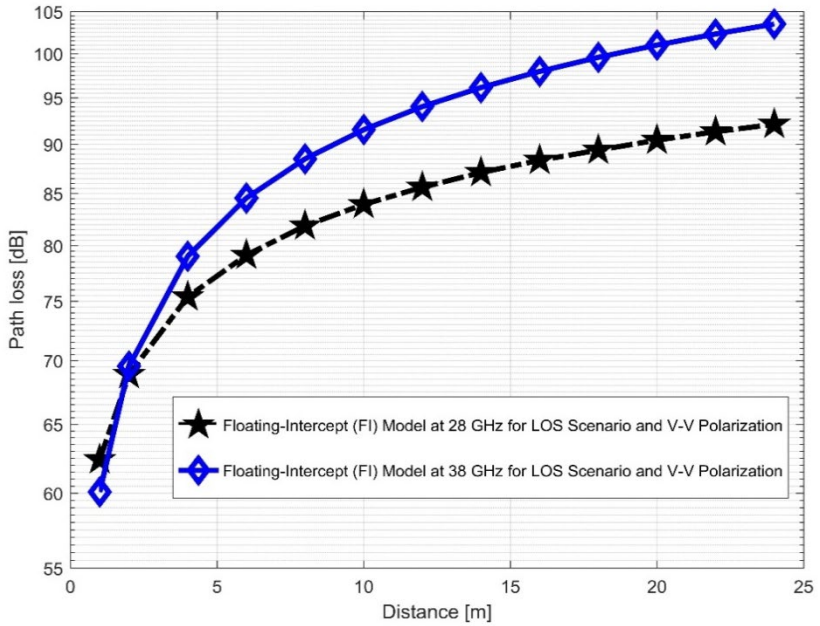

Figure 3.14. FI path loss versus distance at 28 and 38 GHz for the LOS scenario and V–V polarization.

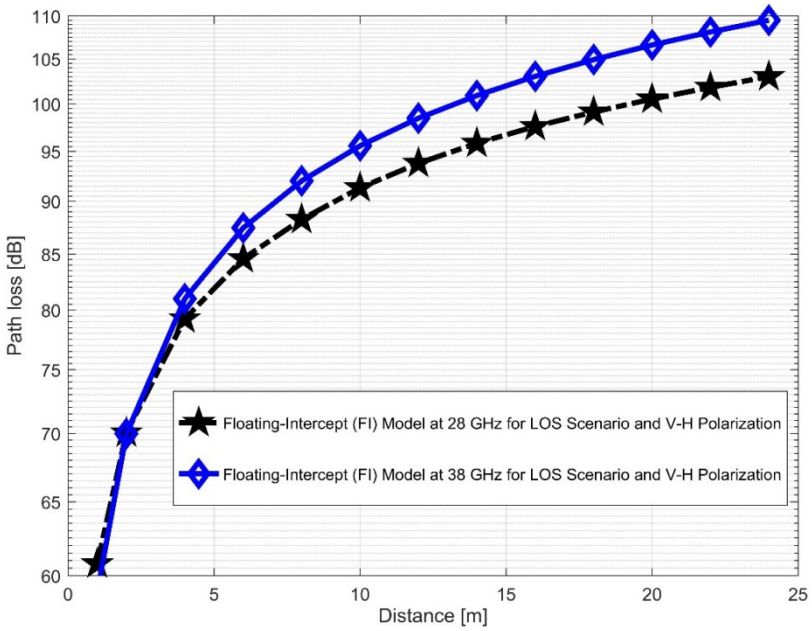

Figure 3.15. FI path loss versus distance at 28 and 38 GHz for the LOS scenario and V–H polarization.

3.4.2 NLOS Measurement Evaluation: Study Results and Discussion

The CI and FI models for both V–V and V–H antenna polarizations were evaluated using NLOS measurements. It is clear that, compared to the 28 GHz frequency band, the reflection from the corridor's walls—made of dry concrete and bricks—is more difficult when the values of the PLE in both the V–V and V–H are maximum at 38 GHz. Plots for the measured values, CI, FI, and FSPL models for the V–V and V–H in the 38 GHz and 28 GHz frequency bands are shown in Figures 3.16 and 3.17, respectively.

The PLEs of the 28 GHz in V–V and V–H antenna polarizations differ, with the PLE for the V–H polarization increasing by about 0.445. The standard deviation of 0.78 decibels was approximately the same for both polarizations. The PLE in the 38 GHz situation was 2.8207 in the V–V polarization, increased by 0.6475 in the V–H polarization, and a notable increase was observed in the value of the standard deviation, which rose from 1.6283 to 2.9396 dB. The changes in the PLE and standard deviation were caused by changes in the antenna polarization due to different wave guiding effects, diffraction, and reflections at the two antenna polarizations, culminating in constructive interference of the multiple signal components that reached the receiver in both cases.

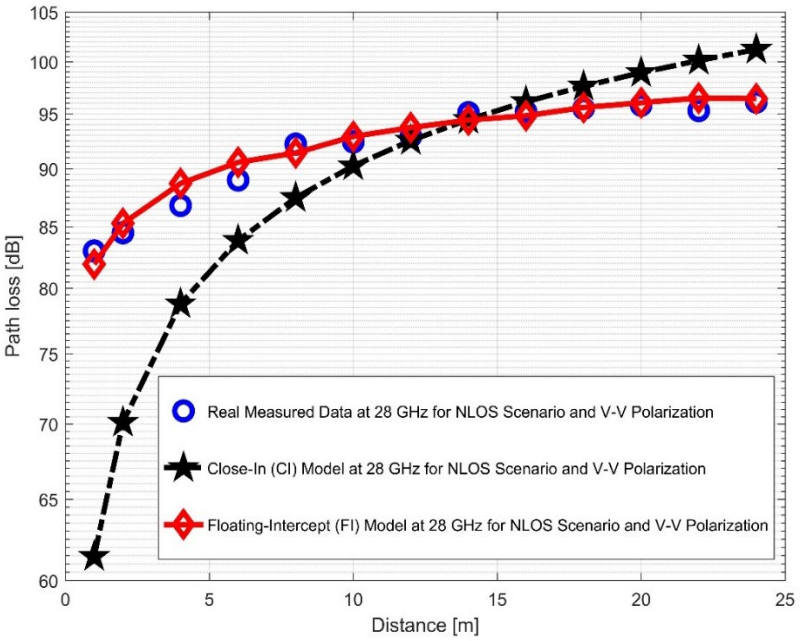

Figure 3.16. Path loss versus distance at 28 GHz for the NLOS scenario and V–V polarization.

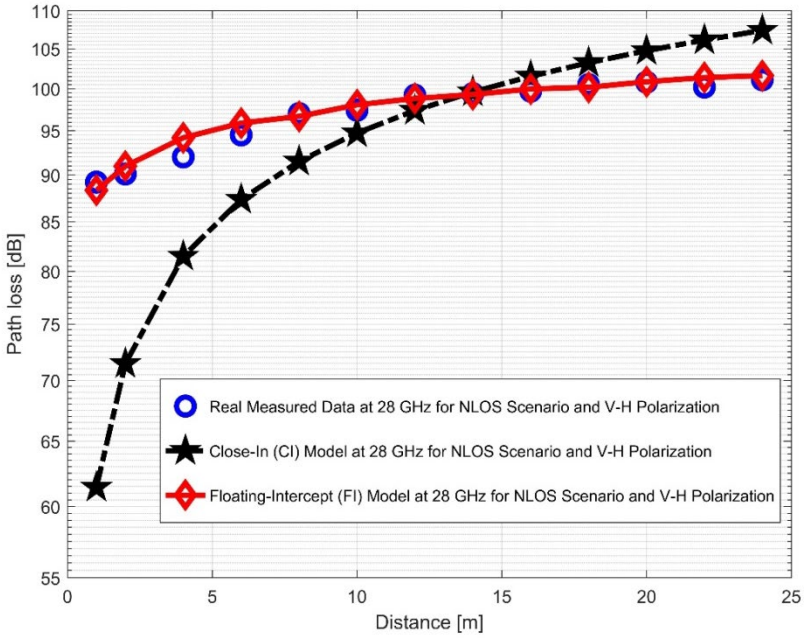

Figure 3.17. Path loss versus distance at 28 GHz for the NLOS scenario and V–H polarization.

When considering the 38 GHz frequency, the higher value of PLE and standard deviation indicated that there was a low wavelength and a higher path loss at a higher frequency. Figures 3.18 and 3.19 display the plots for both V–V and V–H antenna polarizations. The floating intercept values (β) at 28 GHz were 1.0558 and 0.9722, which were approximately the same in V–V and V–H. However, at 38 GHz, the floating intercept value rose to 2.7254 in V–V polarization and 3.3064 in V–H polarization.

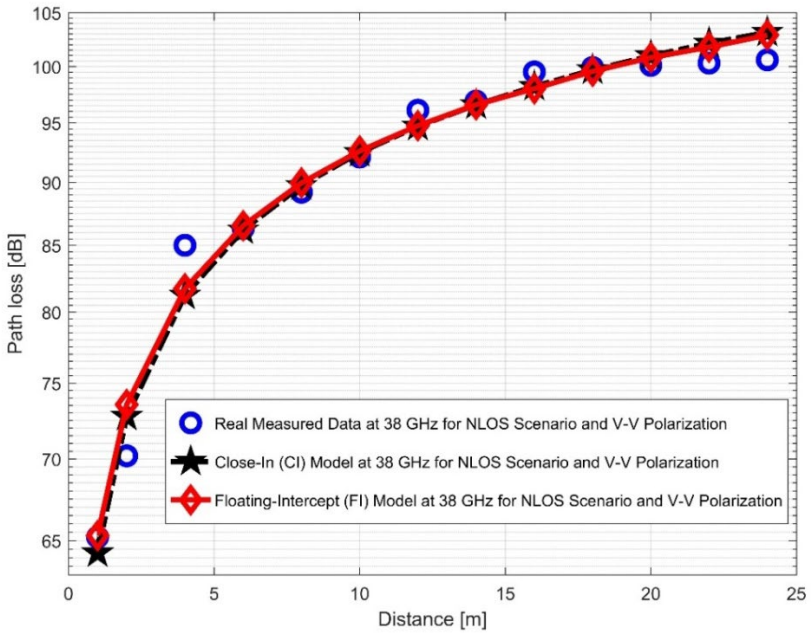

Figure 3.18. Path loss versus distance at 38 GHz for the NLOS scenario and V–V polarization.

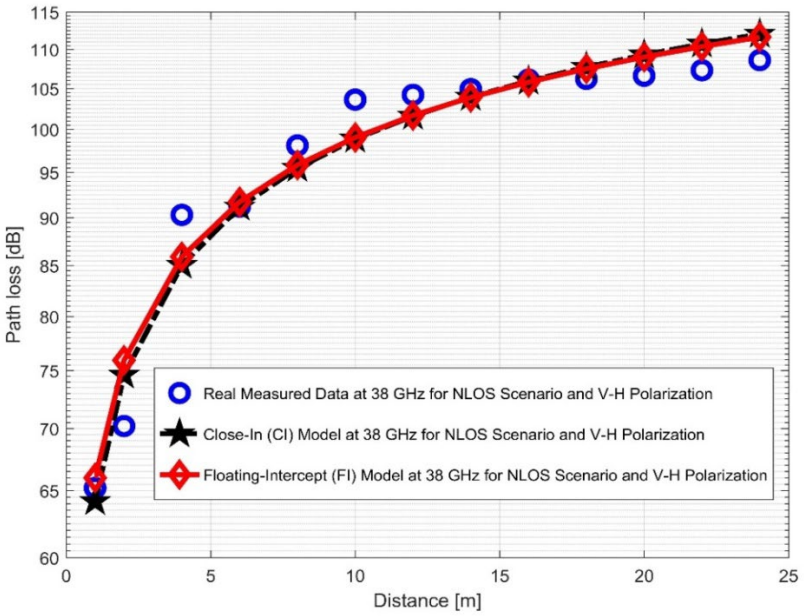

Figure 3.19. Path loss versus distance at 38 GHz for the NLOS scenario and V–H polarization.

Furthermore, the values of σ_{min}^{CI} in the 28 GHz frequency band had a sharp increase in both polarizations when compared to the value in the LOS scenario. The value was 8.1287 for V–V and 10.4790 for V–H, while the 38 GHz values increased slightly from 1.6822 for V–V to 3.0257 for V–H. This indicates that the signal performance in the NLOS was better in the 38 GHz frequency band when compared to the 28 GHz in both polarizations (although the contrast occurred for the LOS situations). The rate of increase in penetration losses at 28 GHz was higher in the NLOS than 38 GHz. A similar behavior occurred in the experimental analysis by [69, 77]. This behavior is seen in the plotting of the path losses shown in Figures 3.16 and 3.17 for 28 GHz, and in

Figures 3.18 and 3.19 for 38 GHz. The behaviors of the curves (of CI path losses for 28 and 38 GHz in the NLOS for V–V antenna polarization) in Figure 3.20 is strikingly similar. This demonstrates that the path loss follows nearly the same patterns at both frequencies, albeit with a higher value at 38 GHz. However, in the case of V–H polarizations, as seen in Figure 3.21, it almost follows the same pattern as the V–V situation, but with a slight difference in the value of the path loss in the frequency bands. This still justifies the fact that the path loss is greater at higher frequencies. Figure 3.20 demonstrates improved sensitivity. The path loss in the 38 GHz band was higher in the FI cases of Figure 3.22, as expected. However, there was a case where the value was similar when the distance between the Tx and the Rx was 10 m. Figure 3.23 depicts the same situation, but with a higher path loss value for the two frequencies. At a distance of 10 m, the path loss values also coincided. Tables 3.3 and 3.4 display the parameters of the CI and FI path loss models for both polarizations for the NLOS and LOS, respectively. Figures 3.20–3.23 show comparisons of the CI and FI plots for the 28 and 38 GHz frequency bands.

Table 3.3. The NLOS comparative study results in 28 and 38 GHz frequencies.

28 GHz NLOS Communication Scenario		
	V-V polarization	V-H polarization
PLE (n)	2.8815	3.3303
σ_{min}^{CI} [dB]	8.1287	10.4790
α_{FI} [dB]	81.8470	87.8146
β_{FI}	1.0558	0.9722
σ_{min}^{FI} [dB]	0.7872	0.7796
38 GHz NLOS Communication Scenario		
	V-V polarization	V-H polarization
PLE (n)	2.8207	3.4682
σ_{min}^{CI} [dB]	1.6822	3.0257
α_{FI} [dB]	65.1057	65.8500
β_{FI}	2.7254	3.3064
σ_{min}^{FI} [dB]	1.6283	2.9396

Table 3.4. Single-frequency CI and FI path loss model parameters for all measured frequencies in the indoor channels.

LOS						
Frequency (GHz)	Polarization	CI		FI		
		PLE (n)	$\boldsymbol{\sigma}^{\mathrm{CI}}$ [dB]	$\boldsymbol{\alpha}^{\mathrm{FI}}$ [dB]	$\boldsymbol{\beta}^{\mathrm{FI}}$	$\boldsymbol{\sigma}^{\mathrm{FI\ min}}$ [dB]
28	V-V	2.2254	1.7718	58.8294	2.1537	1.7431
	V-H	2.9790	1.3425	59.9354	3.0540	1.3008
38	V-V	2.7801	3.1874	60.5444	3.1461	2.7439
	V-H	3.1978	4.1001	62.1883	3.6625	3.5455
NLOS						
28	V-V	2.8815	8.1287	81.8470	1.0558	0.7872
	V-H	3.3303	10.4790	87.8146	0.9722	0.7796
38	V-V	2.8207	1.6822	65.1057	2.7254	1.6283
	V-H	3.4682	3.0257	65.8500	3.3064	2.9396

Taking a look at the overall measurement results in the LOS and NLOS, both models clearly fit the measured path losses and produce comparable results in both antenna polarizations. The PLE was also much higher in the V–H polarization of the NLOS scenarios due to signal degradation along the path from Tx to Rx. At 38 GHz,

the highest value was 3.33 for V–H. This demonstrates that reflections from dry concrete and bricks become more difficult at this frequency when compared to other frequencies. This was due to the lack of direct bore sight between the Tx and Rx antennas. The Rx (as it transmits through the path from the Tx antenna) only relies on signal diffractions and reflections from obstacles. Furthermore, the values of σ_{min}^{CI} and α_{FI} increase to a peak at 28 GHz, rather than 38 GHz, in the NLOS scenario. This demonstrates that both antenna polarizations have better signal performances at 38 GHz. The slope of the path loss curve was roughly the same as the PLE values in both LOS and NLOS situations. This means they behaved similar in this environment. In the NLOS scenario, the minimum standard deviation values were much higher. This is due to the richness of the reflections and diffractions, which allowed for constructive inference of the multiple signal components reached on the Rx side, particularly in the 38 GHz V–V polarization. The NLOS scenario's general behavior, which was characterized by a higher path loss, was caused by the diffraction effect, which disrupted signal transmissions. Because the Tx and Rx are not in the bore sight, obstructions between them tend to interfere with the signal transmission. Some obstacles reflect signals at specific frequencies, while others simply absorb and garble them. However, in either case, they degrade the signals, especially when the power budget is limited. The electrical properties of the material causing the obstruction also have significant impacts on the signal. Some are excellent conductors, while others are excellent insulators.

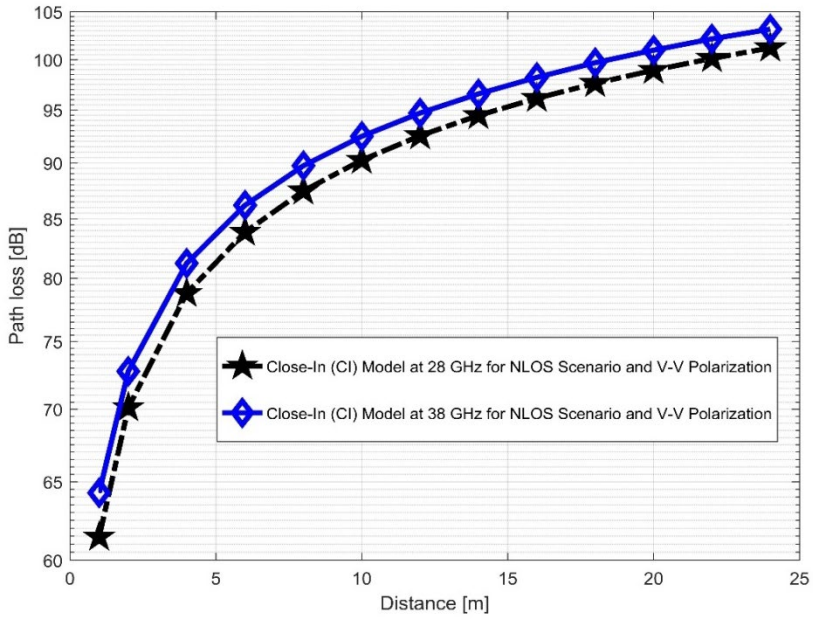

Figure 3.20. CI path loss versus distance at 28 and 38 GHz for the NLOS scenario and V–V polarization.

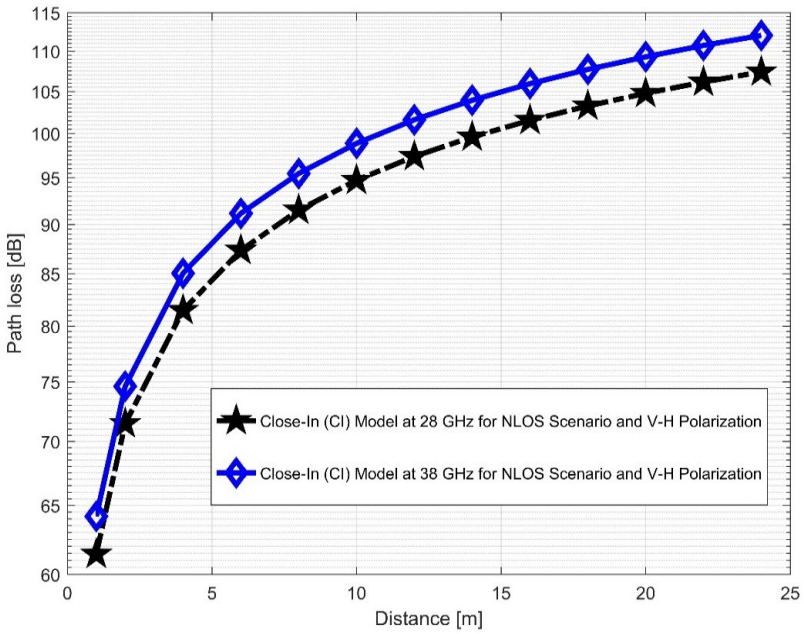

Figure 3.21. CI path loss versus distance at 28 and 38 GHz for the NLOS scenario and V–H polarization.

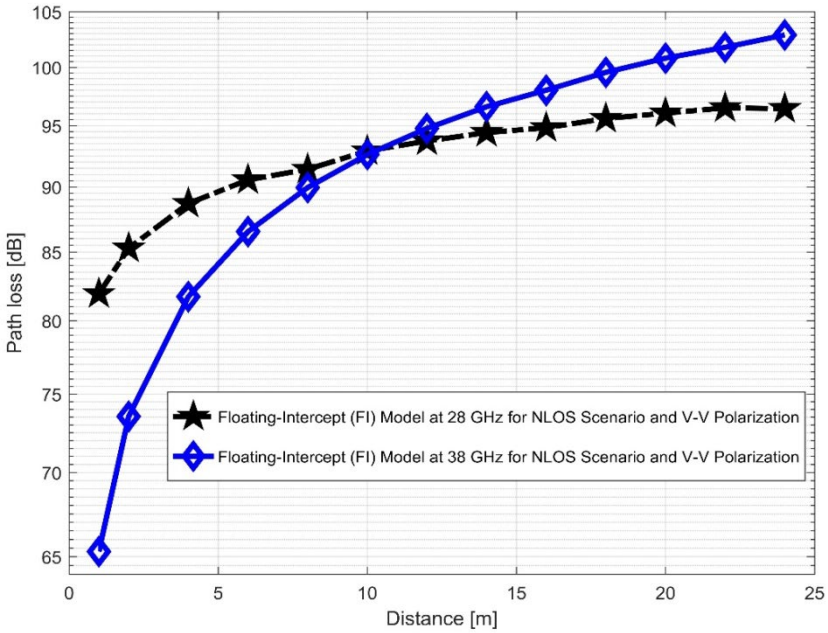

Figure 3.22. FI path loss versus distance at 28 and 38 GHz for the NLOS scenario and V–V polarization.

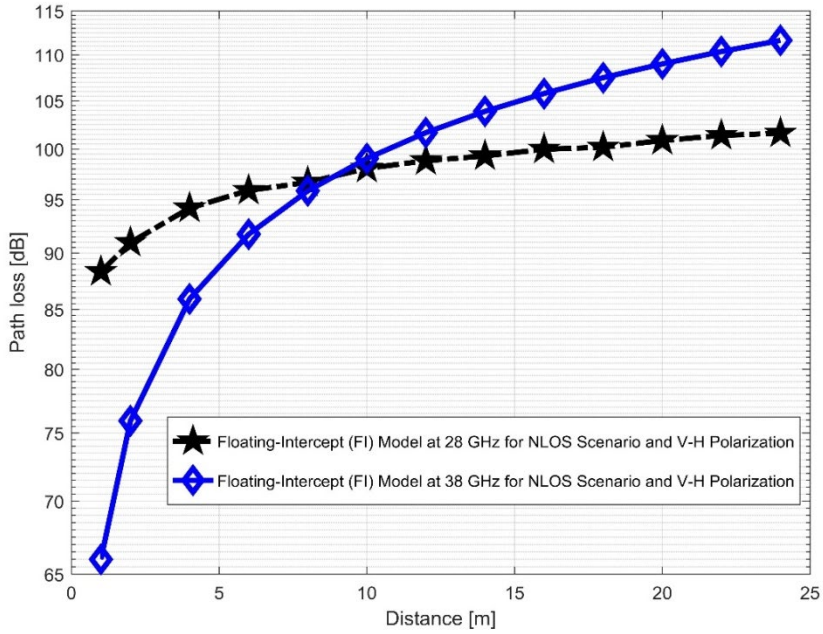

Figure 3.23. FI path loss versus distance at 28 and 38 GHz for the NLOS scenario and V–H polarization.

3.4.3 Comparison of the Obtained Propagation Parameters with the Other Indoor mmWave Outcomes

The propagation variable values are listed in Table 3.5. This is due to the fact that the work was conducted under a variety of LOS and NLOS conditions. Due to the accumulation of many path components, the lower range of PLE in this work under the LOS scenario was 2.23 at 28 GHz V–V. In the 73 GHz frequency range for V–H antenna polarization, the authors of [39] found the greatest PLE for an indoor environment with the measuring campaign conducted in a sizable open hall. The maximum upper value of PLE=3.47 in this investigation, however, was recorded at 38 GHz for V–H polarization. Practically all of the PLE values for the LOS in this study had FSPL exponents higher than 2.

Table 3.5. Comparison of indoor channels at mmWave frequency ranges for single-frequency path loss model parameters.

Ref	Dist. (m)	Freq. Range GHz	Pol.	Envi.	Dimen. (m^3)	Materials Make	Sce.	*PLE (n)*	σ^{CI} [dB]	α^{FI} [dB]	β^{FI}	σ^{FImin} [dB]
[61]	4.1–21.3	28–73	V–V V–H	Indoor office	39.3 × 2.7 × 45.9	Cubicle partitions, doors, dry walls, elevator	LOS	3.5	1.8–8.6	60.4–101.1	0.5–1.6	1.6–15.8
[68]	1–40	6.5–38	V–V V–H	Indoor corridor	2.8 × 2.4 × 40	Plywood, glass doors, concrete walls, glass, and gypsum board.	LOS	0.6–1.9	1.31–2.8	40.7–70	0.9–1.4	1.12–3.1
[84]	4.1–21.3	28–73.5	V–V	Indoor office	39.3 × 2.7 × 45.9	Desks, chairs, cubicle partitions, doors, dry walls, elevator	LOS	1.1–1.3	1.8–2.4	60.4–77.9	0.5–1.2	1.8–2.3
[113]	1–22.7	4.5–38	V–V V–H	Indoor office	21 x 2.7 × 30	Concrete walls and gypsum board	LOS	1.13–3.87	2.18–5.6	41.45–83.79	0.33–1.77	1.12–3.97
[122]	1–50	26–39	V–V	Indoor office	2.41 × 2.89 × 40	Wooden doors, light concrete walls, a false ceiling of gypsum	LOS	1.14–1.53	4.25–4.94	62.12–65.86	1.03–1.61	4.24–4.94
[125]	14–50	26–38	V–V	Indoor Library	14 × 7 x 52	Non-tinted glass and printed hardboard frames	LOS	1.96–3.24	3.78–6.30	52.63–100.71	0.95–4.18	3.99–7.86
This Work	2–24	28–38	V–V V–H	Indoor Corridor	2.63 × 1.4 × 30	Dry concretes and bricks, staircase, elevator, and office wooden doors	LOS	2.23–3.47	1.34–4.10	58.82–62.19	2.15–3.66	1.30–3.55
[61]	4.1–21.3	28–73	V–V V–H	Indoor office	39.3 × 2.7 × 45.9	Cubicle partitions, doors, dry walls, elevator	NLOS	4.4- 6.4	10.9–15.9	81.6–120.5	1.3–2.6	8.0–11.3
[84]	4.1–21.3	28–73.5	V–V	Indoor office	39.3 × 2.7 × 45.9	Cubicle partitions, doors, dry walls,	NLOS	2.7–3.2	9.6–11.3	51.3–76.3	2.7–3.5	9.30–11.2

						elevator						
[113]	1–22.7	4.5–38	V–V V–H	Indoor office	21 x 2.7 × 30	Concrete walls and gypsum board	NLOS	1.97–5.28	2.62–6.0	16.22–87.91	2.4–6.12	2.57–4.5
[125]	51–113	26–38	V–V	Indoor Library			NLOS	2.36–3.1893	3.78–8.87	52.63–100.7	0.96–4.18	3.7–7.86
This Work	2–24	28–38	V–V V–H	Indoor Corridor	2.63 × 1.4 × 30	Dry concretes and bricks, staircase, elevator, and office wooden doors	NLOS	2.82–3.46	1.68–10.48	65.11–87.82	0.97–3.31	0.78–2.94

Table abbreviations: Ref = Reference, Dist. = Distance Range, Freq. range = Frequency range, Pol. = Polarization, Envi. = Environment, Sce. = Scenario. Dim = Dimension.

In the FI model, the frequency-dependent α^{FI} had a value of 58.83 dB for V–V that varied slightly with the FSPL at 1 m for 28 GHz, which was 61.4 dB. In the V–H, however, the value was 59.94. At 1 m, the FSPL at 38 GHz was 64 dB. However, the V–V value obtained in this study was 60.54 and the V–H value was 62.19. The lowest range in the literature [61] was at a frequency of 6.5 GHz (in an indoor corridor environment, with a value of 40.7) and the highest was at 73 GHz, with a value of 101.1, as recorded in [61]. At 4.5 GHz for V–V polarization, the slope value $\boldsymbol{\beta}^{FI}$ had the lowest value of 2.16; however, the lowest value of our experiment was 2.16 for 28 GHz V–V polarization. The values of $\boldsymbol{\sigma}^{CI}$ and $\boldsymbol{\sigma}^{FI\ min}$ in both the lower and higher ranges were also consistent with the mean values in all of the literature studies taken into consideration. The highest value of β^{FI} was in [125] for a frequency of 28 GHz.

The lowest range of the PLE value, which was 1.97 at 4.5 GHz frequency V–V [113], was lower in the NLOS scenario than our 2.384 estimate. Our PLE's greatest value, 3.47, was less than the number in the highest range, 73 GHz [61]. These findings demonstrate that our study remains consistent with previous studies in the literature. The rise in signal degradation, particularly with a higher frequency, is a clear NLOS indicator. Depolarization occurs as a result of this. The range value for the α^{FI} model ranges from 16.22 at 4.5 GHz to 120.5 at 73 GHz [61], with 16.22 being the lowest number and 120.5 being the highest. Our work's lowest value of α^{FI} is 65.11 at 38 GHz for V–V polarization, but it rises to 87.81 at 28 GHz for V–H polarization, which is still within the acceptable range for the works we took into consideration. The values in our work, however, fell within the range of the value β^{FI} (documented in both upper ranges) [113]. The values of additional parameters, such as σ^{CI} and $\sigma^{FI\ min}$, were congruent with those reported in the literature, after carefully contrasting the path loss parameters from the work with those from the literature. The majority of the work's ranges were consistent; however, a key result was that these parameters differed based on the indoor environment. This is because different indoor settings in the literature were constructed from various materials, which caused the multipath components to vary and, thus, impacted the received signals. Different building materials and obstacles have varying penetration losses, dispersions, and fading. It is possible that some situations could experience signal

attenuation because of air concentration, which can also be the reason for the various path loss propagation parameters.

The comparison results show that almost all of the path loss parameters in our work are within the range of the works considered in the literature. The main accomplishment of our work is the better analysis, which resulted in superior results in the PLE and standard deviation values. These two factors are critical when assisting engineers and researchers in budget calculations in 5G wireless network propagations in indoor environments.

This chapter's main goal was to examine single-frequency path loss models in an indoor environment at frequencies of 28 and 38 GHz. A thorough comparison of the path loss parameters was also performed to compare the values of the parameters with those in the literature. Although the ranges were consistent with the majority of the work, one major finding was that these parameters varied depending on the indoor environment. This is due to the fact that various indoor environments in the literature were made of different materials, causing the multipath components to differ and, thus, affecting the received signals. Each obstacle and building material had different penetration losses, scattering, and fading. However, more measurements in these frequency bands considering the losses of building materials and obstructions in each indoor environment will be required in the future. This will aid in the conception of a building structure-specific model.

3.5. Chapter Summary

This chapter presented the results of an analysis of path loss models in an indoor corridor environment at 28 and 38 GHz frequency bands with two different antenna polarizations in both LOS and NLOS scenarios. For both the frequency bands, measurements were taken using a channel sounder based on a Rohde & Schwarz SMB 100A radio frequency signal generator as the transmitter and a Rohde & Schwarz FSIQ 40 signal analyzer as the receiver. In this environment, two vertically polarized high-gain directional broadband horn antennas for both vertical-to-vertical and vertical-to-horizontal polarizations were adopted, analyzed, and contrasted for LOS and NLOS communication scenarios. The single-frequency CI and single-frequency FI path loss models were used in this investigation. The measurement evaluations in an indoor corridor environment at 28 and 38 GHz frequency bands were the focus of this work. The LOS study results showed that when changing the antenna polarization from V–V to V–H at 28 GHz, the path loss values increased, but only slightly at 38 GHz, indicating that signal degradation was not too noticeable when changing the antenna polarization at 38 GHz. However, in the NLOS scenario, the PLE was higher at 38 GHz when compared to 28 GHz for both antenna polarizations. This was due to greater dispersion and penetration losses at higher frequencies. The minimum standard deviation values for CI and FI were quite near to one another for 28 GHz at both antenna polarizations. However, the minimum standard deviation for the 38 GHz frequency increased from 2.7 in the V–V polarization to 3.59 in the V–H polarization. The V–V antenna polarizations had better accuracy and path loss efficiencies than the V–H polarizations in both scenarios and frequencies, according to the results in both antenna polarizations. The proximity of the walls, the materials used for the walls, the floor, and other irregular items, such as wooden doors, concretes, and elevator doors along the hallway, all have an impact on how radio waves propagate indoors. Both of the employed models (CI and FI) had good overall performances. In order to achieve a better outcome, it will be a good idea to develop an improved CI–FI model. Moreover, the high reflection rate

of power and penetration losses in millimeter wave propagation will require researchers to devise path loss models that are unique to each building's structure in the future.

Chapter 4

Performance Analysis of Improved Path Loss Models for Millimeter-Wave Wireless Networks at 28 and 38 GHz

The analysis of improved PL models for different antenna polarizations for LOS and NLOS is presented in this chapter. The results confirm that the modified versions of CI and FI models predict path loss with better accuracy in an enclosed environment for 5G networks.

4.1 Introduction

In the last few years, there has been a tremendous amount of change in the field of telecommunications. There is a need for general improvement of today's mobile communication system in order to meet future expectations and challenges [126], [127]. 5G mobile networks are widely expected to address some important issues, including higher data rates, widespread device connectivity, larger capacity, low cost and dependability [126]-[131]. However, the anticipated increase in traffic may be accommodated by increasing link capacity, opening up more spectrums, and massively increasing the density of tiny cells [25].

In order for the wireless industry to meet the demands associated with 5G networks, there is a need for the mmWave FB. This will help in developing previously untapped FB as well as multi-Gbps data rates for mobile devices. MmWave technology is required because FB ranges below 6 GHz lack the bandwidth capacity required for 5G wireless systems to achieve maximum data transmission rates of multiple Gbps [41], [132]. The majority of the mmWave FB bands are located between microwave and infrared waves, as shown in Figure 4.1 [133].

Furthermore, the business world has recognized the value of wireless communication, particularly for gigabit speeds, longer range connectivity, and high-quality multi-media, voice, as well as data services, [26], [28]- [29], [41], [126], [134]. Because these bands have the potential for the implementation of 5G wireless networks and meeting future demands, there has been an increase in recent years in research into the mmWave FB (30-300 GHz) [130]. In the mmWave FB, massive contiguous blocks of raw bandwidth are available, allowing for increased data flow for various multimedia services. The upper centimeter wave (cm wave) bands of the licensed spectrum will remain accessible to 5G technology [33], [41], [88], [126], [135]- [138].

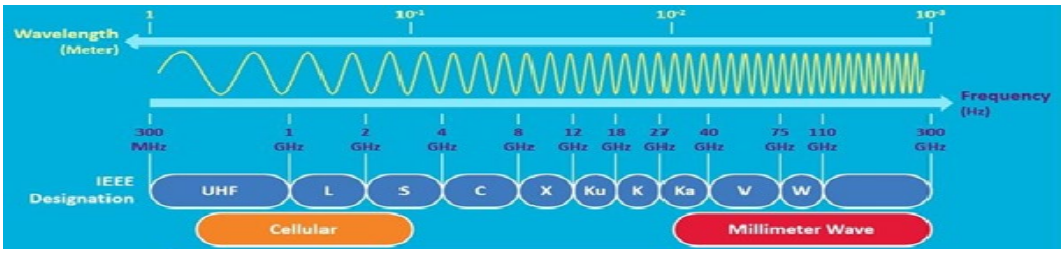

Figure 4.1. MmWave frequency spectrum band [133].

The abundance of untapped spectrum benefits mmWave bands. Along with the wider bandwidth, running at a higher FB, comes the following benefits: intrinsic beam forming improves wireless signal (WS) strength and spectral efficiency because (i) antennas can achieve stronger directivity at higher FBs, and (ii) smaller beams allow for greater node mobility. Despite these advantages, the applicability of these bands must be determined by classification of WS transmission behavior. MmWave bands exhibit distinct electromagnetic propagation with varying reflection and diffraction characteristics. They also have higher absorption losses [139]-[141]. The cell radius for mmWave bands, on the other hand, is significantly smaller (a few hundred meters), because the environment in which the WS travels has a significant effect on its ability to spread. Furthermore, the penetration loss in solid materials has a significant impact on the mmWave frequency spectrum. It is critical to accurately understand and characterize the behaviors of the mmWave FBs in a variety of indoor and outdoor locations and scenarios in order to accurately analyze performance and ensure the safe deployment of 5G cellular systems [16], [33], [41], [142]-[145].

Numerous studies have been conducted on this topic in order to make predictions about the behavior of a wireless channel using models based on theories. When a communication system transmits and receives the WSs, the signal strength decreases as it travels over the wireless communication channel. PL is an important factor that must be predicted accurately for proper system design and link budget evaluation. Furthermore, it generates radio channel parameters that have been empirically averaged across both space and time. To accurately explain the attenuations in WS levels, researchers must develop more precise PL simulation models that can successfully fit real quantitative measurements obtained under various interior and outdoor conditions over a wide FB. Because of the high responsiveness of the WSs at these radio frequencies to the transmission procedures in the signal propagation process, conventional models are unable to serve as precise models for the SHF, mmWave, and far above FBs [34], [43], [146] - [147].

The measurement of this study was done in LOS as well as NLOS scenarios at 28 and 38 GHz FBs in order to evaluate CI and FI PLMs in an interior passage. The measurement was done on the fifth (5th) floor of the Electrical, Electronic and Computer Engineering (EECE) Department of UKZN in Durban, South Africa. Despite the fact that Elmeguzi and Afullo [43] proposed this improved version of CI and FI PLMs, these models perform well in terms of precision of matching measured data obtained during measurement settings at FBs of 14, 18, and 22 GHz for V-V antenna polarization. However, this model has not been validated in higher FBs or with different antenna polarizations. To the best of our knowledge, there is a gap in the literature that justifies the accuracy and stability of these proposed models by [43] in the modeling and characterization of single frequency PLM that consider two antenna polarizations. The work aims to test the accuracy, stability, and sensitivity of these models by using measured parameters collected in an enclosed corridor. Furthermore, in this chapter, the upgraded version of the standard CI model based on the third (3rd) order log-distance was also analyzed. The shadow fading standard deviation (SFSD), which is the foundation for high precision PL prediction in both LOS and NLOS scenarios, is also examined. Despite this extensive study by [43], it was discovered that at the same antenna height (for 14, 18 and 22 GHz) for both the transmitter and the receiver, there was a noticeable decrease in path loss exponent and a slight increase in shadow fading standard deviation for the NLOS scenario, but when the antenna heights are not of the same height, the two major metrics (path loss exponent and shadow fading standard deviation) increase. Nevertheless, as the frequency increases, the

effect of the antenna height difference has little effect on the value of the path loss exponent and the standard deviation of shadow fading. When using two different antenna heights, several authors in [16], [26], [33], [41]-[42], [62]-[65], [88], [131]-[132], [136], [139], [144], [146], [148], have adopted the use of higher values of antenna heights at the transmitting end of the measurement set up. However, in this study the analysis of the path loss prediction models for the higher height of the antenna at the receiving end is presented. The analysis of V-V and V-H antenna polarizations is also presented in this study. The following are the remaining sections of the chapter: The related works are presented in Section 4.2, while the measurement campaign details and large-scale PLMs are presented in Section 4.3. Section 4.4 contains the results and discussion, while Section 4.5 presents the chapter summary.

4.2. Related Works

The mmWave spectrum's ability to produce high throughput in the Gbps spectrum, which is required for 5G systems, has been demonstrated. However, the environment in which the WS is transmitted has a significant effect on mmWave propagation. Furthermore, penetration loss through solid objects has a significant impact on WSs in the mmWave frequency range [142], [145]. The propagation scenarios as well as the FB considered have a significant impact on the accuracy of these models. Many models proposed by researchers to improve delay time, output, and PLE performance have a distinct application that still has a long way to go in terms of distance and frequency of application [42], [148]. An experiment on ultra-wideband propagation was carried out at New York University in an enclosed office setting. The statistics of large-scale PL were calculated using the experiment's findings in both existing and upcoming applications. The tests were carried out in an enclosed structure under LOS and NLOS conditions using directional antennas at FBs of 28 and 73 GHz. The experiment revealed that simple CI and FI models can accurately predict PL in mmWave indoor wireless channels on a large scale (with distance and frequency) using only one or two functions related to transmitted power [62]. Maccarthney et al. presented some omnidirectional propagation data captured in New York Downtown metropolis [62] to ensure the accuracy and effectiveness of the CI PLM.

Sun et al. investigated propagation PLMs for 5G urban micro and macro-cellular situations using the CI and ABG as large scale PLMs. Data were collected over the course of about 20 measurement procedures that ranged in distance from 5 to 1429 m and used FBs ranging from 2 to 73.5 GHz. An examination of the research findings reveals that the CI model's simulation accuracy performs better than the ABG model. In comparison to the latter, the former provides more consistent and tolerable performance across all FBs and distance ranges investigated during the study. To improve accuracy, the CI model, which is simple to use over a wide FB, must simply be modified [63]. The close in model with frequency-weighted PLE, the close in model with free reference distance, and the ABG were compared in a variety of data sets with distances ranging from 4 to 1238 m and FBs ranging from 2 to 73 GHz. Urban microcells, malls, and an indoor work environment were among the scenarios. While the ABG model (four parameters considered) under-predicts path losses near the Tx and over-predicts PLs far from the Tx, the CI (2 variables considered) and CIF (3 variables considered) models have better goodness of fit and more stable component behavior. This discovery holds true across all distances and FBs investigated [64].

In their study on indoor 5G 3rd Generation Partnership Project (3GPP) like channel models for workplace and commercial settings, Haneda et al. used both current and historical measurements of channel propagation

for FBs up to 100 GHz. It was discovered that as frequency increased, so did penetration loss. According to the UMi and Uma models [65], the indoor channels are more frequency dependent than the outside channels.

At 28 and 38 GHz, measurements were taken in New York, Austin, and Texas as part of an empirically-based large scale propagation PL modeling for 5G mobile systems scheduling in the mmWave band. The portion of coverage increased significantly when the antenna was aimed in the optimal direction towards both the mobile and the base station. As a result, there are fewer 5G base stations, and interference is reduced [66]. The Rural Macrocell PLMs for mmWave wireless network analysis, which is part of a larger research project, provides a thorough understanding of the existing 3GPP, RMa LOS, and NLOS PLMs in the FBs of 0.5 to 100 GHz. In a rural location with good weather, directional HA were used for a real-time measurement campaign using the CI and CIH model components. Even beyond the first meter of propagation distance, the observed data confirms the CIH model's correctness, dependability, and frequency dependency [66].

The characteristics of propagation channels in the FBs of 6.5, 10.5, 15, 19, 28, and 38 GHz were further investigated in an indoor setting using a measurement campaign spanning 4,000 power delay profiles and employing a directional HA as a Rx and an omnidirectional antenna as a Tx section. The frequency attenuation model is a novel PLM that takes both distance and FB into account. RMS delay spread and dispersion factor values for this model demonstrate its simplicity, lower PLEs, and good RMS delay spread and dispersion factor values [67].

The majority of propagation models currently in use for any FB below 6 GHz are not suitable for mmWave PL modeling, nor are they suitable for any FB above 6 GHz. This is due to the obvious disparity in WS propagation. A measurement campaign was conducted indoors at UTM Malaysia. PL analysis of single and multi-frequency signals was performed in applications utilizing omnidirectional and directional antennas. It was discovered that using a less complex model approach with only one PLE parameter (n) that is dependent on transmitted power makes modeling PL on a large scale with respect to distance easier [70]. In contrast, using a model that is not dependent on transmitted power may necessitate more variables, making the modeling complex. The examination of these PLMs demonstrates the need to develop a model that is more effective than the fundamental models, such as the CI, FI, and ABG, at reducing PL of the propagated SIG from the Tx to the Rx [70].

In [43], Elmezughi and Afullo proposed an improved model for improving the accuracy of CI and FI model standards. This enhanced model was used for FBs 14, 18, and 22 GHz taking into account wave-guiding effects, which are most common in enclosed indoor spaces like hallways, as well as propagation processes like reflections and diffractions. Because they are appropriate, specific PLMs, such as the ABG, CI, and FI models, have recently received the most attention in research aimed at describing and modeling the wireless channel [43]. In these research studies: [61], [63], [65]- [67], [84], [146], [149] - [152], more sophisticated models based on a wide range of other precepts can be discovered.

In addition, tests for 28 GHz reflection and penetration loss were performed in buildings in various areas of New York City [84]. The results show that a three-wall office complex has a significant absorption loss of 45.1 dB. Furthermore, whereas exterior tinted glass had absorption loss of 40.1 dB, interior non-tinted glass had an absorption loss of 3.9 dB. The authors of [153] performed a measurement in a lab using 28 and 82 GHz FB, as

well as an anechoic chamber, to determine the qualities of the link in the mmWave bands. Hindia et al. measured an established channel model inside an outdoor area for single and multi-frequency models, as well as proposing a novel model [154]. The authors of [61], [84], and [155] conducted measurements at 28 and 73 GHz in an interior office using omnidirectional and directional HAs. Measurements and simulations were carried out at FBs of 28, 38, and 73 GHz in order to assess and estimate a number of parameters as well as classify the transmission channel in CI and ABG PLMs [156]-[157].

Zwick et al. measured several wideband link statistics at 60 GHz using heterodyne and channel bandwidth of 500 MHz. They used omnidirectional antennas for close-quarters distances in a number of apartments and combined the measured data (for an overall bandwidth of 5 GHz) [158].

4.3 Measurement Campaign and Environment

The measurement setup is given in Figure 4.2. The Rohde and Schwarz (R&S) 100A SMB radio WS generator was used to provide a CW signal to the transmitting antenna. The receiving system of the set-up has a signal analyzer (R &B FSIQ 40) of a FB range up to 40 GHz. The signal analyzer was connected to a Rx HA system. The two HAs were used with the FB range of 18 to 40 GHz. Figure 4.2 provides the detailed explanation for the arrangement. The measurement process involves the LOS as well as the NLOS scenario in V-V and V-H polarizations. The indoor hallway is 30 meters long, 2.63 meters in height and 1.4 meters wide. The Rx HA was shifted away from the Tx by 2 meters at the distance until it reached a distance of 24 meters, while the Tx HA was positioned at one end of the walkway. The LOS situation was assessed with both HA matched on bore sight and no obstructions in their path of the Tx WS. However, in the NLOS there was no alignment between the Tx and Rx HAs. In the meantime, experts in this field recommend a reference distance of 1m between the Tx and the Rx. The number of Tx - Rx separation distances is 13 with a reference distance d_o=1. The channel sounder's specifications are listed in Table 4.1. The detail images for the measurement campaign and the floor plan of the indoor hallway are provided in Figures 4.3, 4.4, 4.5, 4.6 and 4.7. The PL (in dB) is calculated using equation (4.1) [43]:

$$P_L = P_t - P_r + G_r + G_t \tag{4.1}$$

Where P_t, P_r, G_t , and G_r are the transmitted power, the received power, the gain of Tx HA and the gain of Rx HA, respectively.

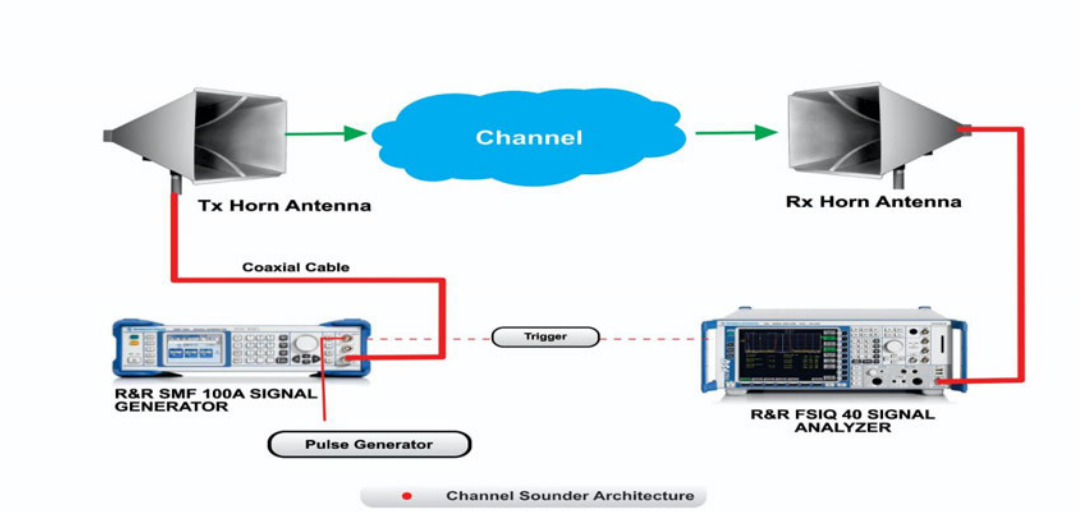

Figure 4.2. The channel sounder's architecture.

Figure 4.3. The indoor corridor environment.

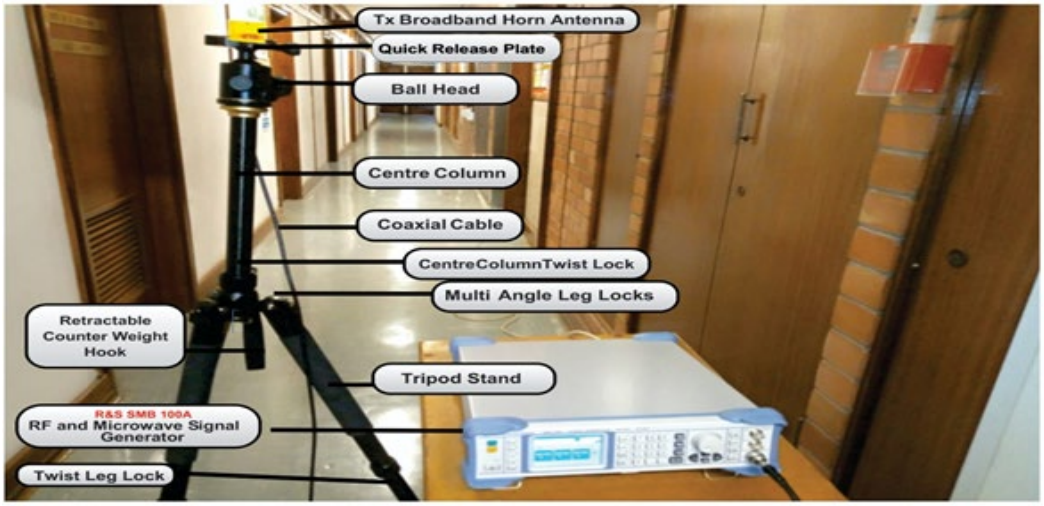

Figure 4.4. The Tx setup.

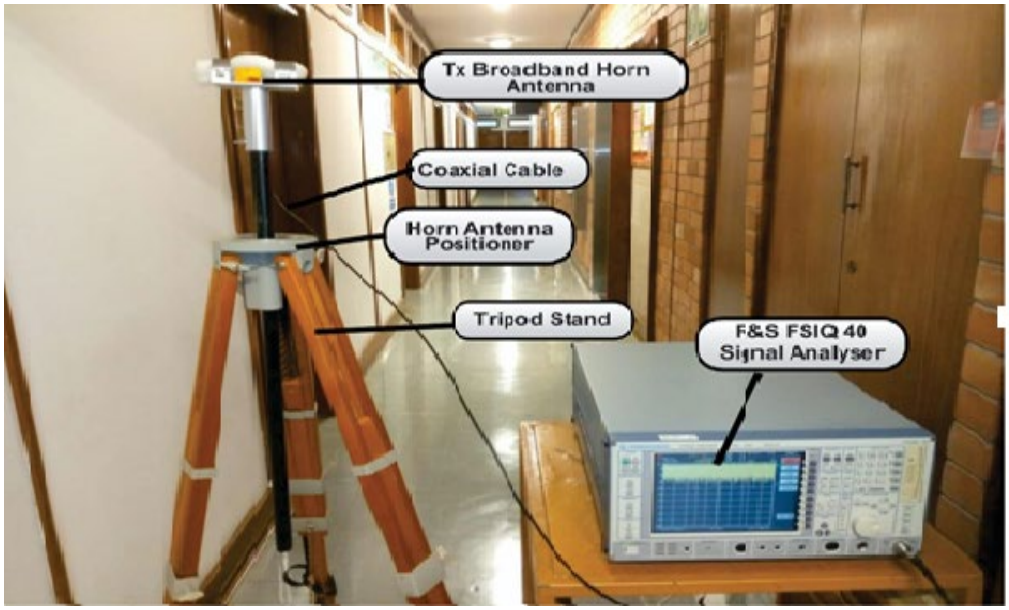

Figure 4.5. The Rx setup.

Figure 4.6. The setup of the Tx and the Rx in the indoor corridor environment.

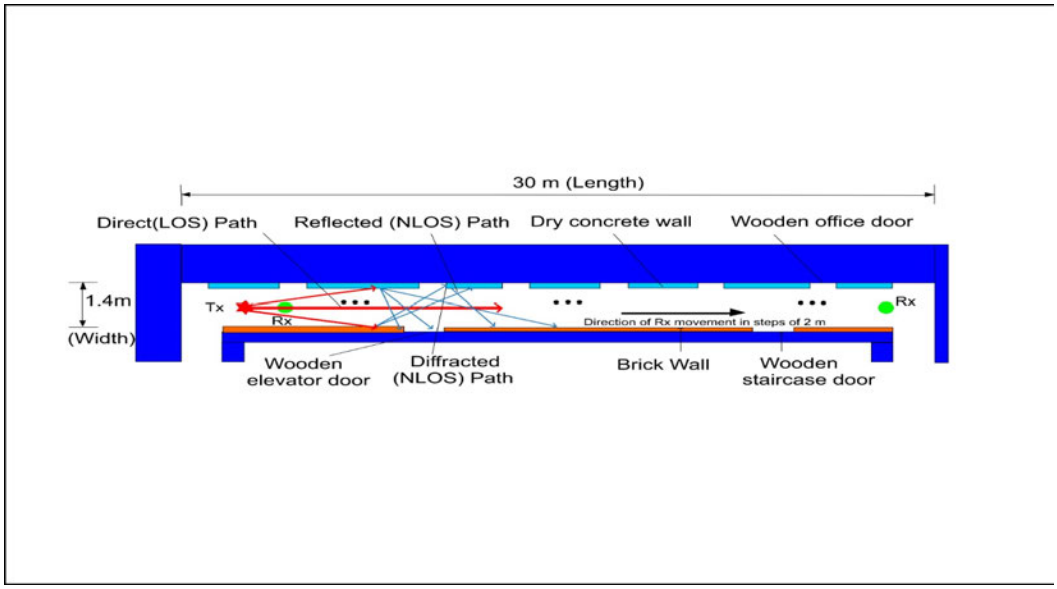

Figure 4.7. Measurement environment floor plan.

Table 4.1. Parameter specifications of the channel sounder for the experiment.

Parameter	Value/Type	Unit
Centre frequency	28, 38	GHz
Transmission bandwidth	100	MHz
Transmission signal	CW	-
Tx and Rx Has	Broadband HA	-
Tx HA power	10	dBm
Tx HA height	1.6	m
Rx HA height	2.3	m
Tx and Rx HA gain at 28 GHz	15	dBi
Tx and Rx HA gain at 38 GHz	17	dBi
Tx and Rx HA polarization	V/ H	-
HA dimension (L x W x H)	71 x 32 x 28.6	mm^3
HA weight	0.08	Kg

4.3.1 Large Scale PL Prediction Models

Friis' equation [43], [69], [159]-[160] can be used to derive all PL prediction models in general as given below:

$$FSPL(f,d)[dB] = 10log_{10}\left(\frac{4\pi fd}{c}\right)^2 \quad (4.2)$$

Where d, c and f are the separation distance between the Tx and the Rx, speed of light in the space and the frequency of the WS, respectively. Equation (4.2) demonstrates that the PL is dependent on the FB and the distance between the Tx and the Rx. The PL formulas are more easily understood on the logarithmic scale. This can be expressed in equation (4.3) as follows [43]:

$$FSPL(f,d)[dB] = 32.4 + 20log_{10}(f) + 20log_{10}(d) \quad (4.3)$$

The operating frequency in equation (4.3) is represented by f (in GHz), and f using the expression $10log_{10}\left(\frac{4\pi\times10^9}{c}\right)^2$, the value of 32.4 was obtained. The term $20log_{10}(f)$ is a constant term which is common to the single frequency CI and FI PLMs. Each model has a different representation of this parameter. Let us call

this variable as k_1. The PL in free space changes as a square of the Tx-Rx distance and is represented by the expression $20log_{10}(d)$ which, on a logarithmic scale, is mainly twice the distance. Nevertheless, this number will vary greatly, primarily due to the nature of the medium used to transmit and receive data. It will generally be simpler to designate it as k_2. The PL in terms of k_1 and k_2 is represented by equation (4.4) [43].

$$PL(d)[dB] = k_1 + k_2 \times 10log_{10}(d) \quad (4.4)$$

Where k_2 is a unitless coefficient and k_1 is expressed in decibels. The above equation makes it evident that the WS's power reduces by $\frac{1}{d^{k_2}}$. Therefore, a higher value of k_2 will lead to an increased reliance between the PL and the distance separating the Tx and Rx. According to equation (4.1), the SIG strength power at the Rx side is primarily influenced by the P_t, PL, G_r and G_t, as shown in equation (4.5) [43]:

$$P_r(d)[dBm] = P_t - PL(d) + G_r + G_t \quad (4.5)$$

4.3.3.1 CI Free Space Reference Distance PL Prediction Model

The expression of the CI PLM is shown in the equation (4.6) [61]:

$$P_L^{CI}(d)[dB] = FSPL(f, d_o)[dB] + 10.n.\log\left(\frac{d}{d_o}\right) + X_{\sigma SF}^{CI} \quad (4.6)$$

Where X_σ^{CI}, d_o, f and n are the gaussian random variable with zero mean, the reference distance, the frequency of operation and the PLE, respectively. The standard deviation is expressed in decibels (dB). Shadow fading is characterized by widespread changes in PL values caused by obstacles and other random propagation factors [43], [73].

At a reference distance of $d_o = 1\ m$, the $FSPL$ is expressed in equation (4.7) as follows [43]:

$$FSPL(f, 1m)[dB] = 10log_{10}\left(\frac{4\pi f}{c}\right)^2 \quad (4.7)$$

Keep in mind that the only significant parameter that needs to be optimized for the CI model is the $PLE\ (n)$. This unitless variable indicates how the path loss model is affected by the Tx-Rx gap distance. This model is based on a physical anchor that detects PL close to the transmitting antenna. The transmission frequency found in the FSPL term clearly has a significant impact on the CI model [71], [146]. The CI model's parameter is enhanced using the MMSE technique. By lowering the SF standard deviation, we can apply this method to minimize the errors while accurately fitting with the measured data.

4.3.3.2 CI PL Prediction Model with Improvements

The CI model's equation can be modified by adding an independent component to make the PL prediction more precise and sensitive to the propagation conditions. Two variables in the modified model are dependent on the separation between the Tx and the Rx. The equation (4.8) indicates that the PLE concept is presented in the two variables (n_1 and n_2) [43]:

$$P_L^{Imp.CI}(d)[dB] = FSPL(f, d_o)[dB] + 10n_1\, log_{10}(d) + 10n_2(log_{10}(d))^2 + X_{\sigma SF}^{Imp.CI} \quad d > 1m \quad (4.8)$$

Where n_1 and n_2 are the PLE's first order and second order, respectively. With this CI improvement, it will be easier to suit the actual measured data obtained from the measuring campaigns. The n_1 and n_2 will

noticeably fluctuate depending on the environment in which the signal travels. Let's assume that these parameters have a closed form [43] with $A = FSPL\ (f, d_o), B = PL^{Imp.CI}, D = 10log_{10}(d)$ and $E = 10(log_{10}(d)\ )^2$. Then SF can be written in equation (4.9) as:

$$X_{\sigma SF}^{Imp.CI} = B - A - n_1 D - \ n_2 E \tag{4.9}$$

The experimental data can be used to calculate the SF standard deviation (Imp. CI) as expressed in equation (4.10):

$$\sigma^{Imp.CI} = \sqrt{\sum \frac{(X_{\sigma}^{Imp.CI})^2}{N}} \tag{4.10}$$

Where N denotes the number of Tx-Rx separation distances. We must now distinguish the numerator of equation (4.10), with regard to both n_1 and n_2, and set the result equal to zero to obtain the parameters' ideal values, which will result in the following standard deviation as expressed in equations (4.11) and (4.12) [43]:

$$\frac{\partial}{\partial n_1}\ (\sum (B - A - n_1 D - \ n_2 E)^2) \tag{4.11}$$

$$\frac{\partial}{\partial n_2} (\sum (B - A - n_1 D - \ n_2 E)^2) \tag{4.12}$$

The two previous equations have been differentiated and simplified, leaving us with two linear equations that can be written as:

$$\sum D_{n1}^2 + \sum (DE)_{n2}\ = \sum (BD) - A \sum D \tag{4.13}$$

$$\sum (DE)_{n1} + \sum E_{n2}^2\ = \sum (BE) - A \sum E \tag{4.14}$$

The equations (4.13) and (4.14) can be stated easily in the form of matrix as expressed in equation (4.15) as follows:

$$\begin{bmatrix} \sum D^2 & \sum (DE) \\ \sum (DE) & \sum E^2 \end{bmatrix} \begin{bmatrix} n_1 \\ n_2 \end{bmatrix} = \begin{bmatrix} \sum (BD) & -A \sum D \\ \sum (BE) & -A \sum E \end{bmatrix} \tag{4.15}$$

Finally, the earlier matrix can be used to determine the closed-form of n_1 and n_2.

4.3.3.3 FI Path Loss Prediction Model

The two parameters of the FI model are the path loss line slope β and the intercept ∝, as shown in equation (4.16), [61], [126]:

$$PL^{FI}(d)[dB] = \propto + 10\beta\, log_{10}(d) + X_{\sigma SF}^{FI} \tag{4.16}$$

Where $PL^{FI}(d)$ depicts the PL in dB, and X_{σ}^{FI} represents the gaussian random variable with a zero mean. The models perform equally well overall in estimating the PL, despite there being a desire for one model over the other depending on the operating FB, environment, and transmitting circumstances of the mobile communication system [41], [43], [71]-[72].

4.3.3.4 FI PL Prediction Model with Improvements

Using the same approach as in the enhanced CI model to add a new variable, the FI model can be improved. This is expressed in equation (4.17) [43]:

$$PL^{Imp.FI}(d)[dB] = \propto + 10\beta_1\, log_{10}(d)\ + 10\beta_2\, log_{10}(d)^2 + X_{\sigma SF}^{Imp.FI} d > 1m \tag{4.17}$$

This model is dependent upon the three parameters i.e. $\propto, \beta_1$, and β_2. Using the MMSE process and the identical derivation as for the enhanced CI model, the solution matrix for all these variables is given in equation (4.18) [43]:

$$\begin{bmatrix} N & \sum D & \sum E \\ \sum D & \sum D^2 & \sum(DE) \\ \sum E & \sum(DE) & \sum E^2 \end{bmatrix} \begin{bmatrix} \propto \\ \beta_1 \\ \beta_2 \end{bmatrix} = \begin{bmatrix} \sum B \\ \sum(BD) \\ \sum(BE) \end{bmatrix} \quad (4.18)$$

Where $B = PL^{Imp.CI}, D = 10log_{10}(d)$ and $E = 10(log_{10}(d))^2$. Using the prior matrix, the variables' closed-forms are found. We used actual measurement results of path loss conducted in an enclosed environment to validate the suggested models in equations (4.18) and (4.17) [43].

4.3.3.5 Third Order CI Path Loss Model

For better accuracy in the forecasting of any feasible transmission effects, a three-variable distance dependent CI PLM referred to as 3rd order CI PLM is considered. The 3rd order PLE depends upon three variables that rely on the Tx-Rx log range and both its squared as well as the cubic values to improve the shadow fading standard deviation which is an important metric for the path loss improvement. It is crucial to understand that having more variables will increase precision.

The 3rd order CI PLM currently incorporates more transmission effects, thus the growth on the model will be less than the progression on the regular CI as well as 2nd order CI. Additionally, adding more variables will make the model more complex and the designers of communication systems won't take it into account because more than three variables will be needed. The expression for the 3rd order CI PLM is given by [44]:

$$PL^{log^3 CI}(d) = FSPL + 10k_1 log_{10}\left[\frac{d}{d_o}\right] + 10k_2\left[log_{10}(\frac{d}{d_o})\right]^2 + 10k_3\left[log_{10}(\frac{d}{d_o})\right]^3 + X_\sigma^{log^3 CI} \quad (4.19)$$

The 3rd order CI model's prediction of the typical PL value in dB at a particular Tx-Rx gap (in m) is shown in Eq. (4.19) by $\boldsymbol{PL^{log^3 CI}(d)}$. The variables $\boldsymbol{k_1, k_2, k_3}$ regulate the dependency on the log distance driven by 1, 2, and 3, respectively. Through the use of the MMSE concept, the values of the three variables are computed by supplying the measured data.

4.4. Results and Discussion

The specifics of the study's findings were covered in this section. The presentation is separated into four segments, which illustrates the improved and third models with the existing ones at 28 as well as 38 GHz. For both V-H and V-V polarizations, consideration was given to both LOS and NLOS situations.

4.4.1 Performance Analysis of Standard CI and Improved CI Models

The path loss analysis for well-known CI model, improved version of the CI model and measurements is plotted at the two FBs in Figures 4.8 (a) and (b) as well as Figure 4.9 (a) and (b). The figures unequivocally demonstrate that the measured PL for the LOS situation is satisfactorily fit by the two models (the improved CI as well as the conventional CI). When antenna polarization is changed, the improved model, which is based on the Table 4.2 parameters, archives the lower values of the SFSD at both FBs. The reduction of the SFSD for the

28 GHz V-V, 28 GHz V-H, 38 GHz V-V, and 38 GHz V-H FBs are 0.3748 dB, 0.6232 dB, 2.372 dB, and 2.5306 dB, respectively. It should be noted that the standard deviation value decreases as the frequency increases. This was due to an increase in propagation effects and PL. The PLE values increase with the frequency, despite being higher in the V-H polarization. Two more parameters are added to the improved model. These variables are denoted by n_1 and n_2. It is evident that n_1 in both polarizations is greater than n_2 for the 28 GHz FB. The decrease in n_2 was balanced by an increase in n_1 to make the model follow all of the observed PL as well as WS effects. At 38 GHz, there is a different situation where n_1 values are greater than n_2 values. This suggests that the increased PL occurs at higher FBs due to more pronounced propagation effects and WS degeneration. There is a high level of fitting of the improved model to the measured data in Figure 4.8 (a) and (b) as well as Figure 4.9 (a) and (b). This shows that the improved model can predict the PL very well.

Both the Tx as well as the Rx HAs been not physically aligned or in line of sight in the NLOS scenario. Only the effects of the corridor environment; diffraction, reflection, and wave guiding, allow WSs to pass from the Tx to the Rx. In contrast to the LOS scenario, PLE values are thus overwhelmingly high. These values are still better compared to the outdoor scenarios with a maximum rate of WS fluctuations. With the CI model, the PLE values are 2.8815 for V-V at 28 GHz band and 3.3303 for V-H at 28 GHz band. Other values of PLE are 2.8207 for V-V at 38 GHz band, 3.4682 for V-V at 38 GHz band and 3.4682 for V-H at 38 GHz band.

The improved version of the CI model responded positively to adjustments in SF standard deviation values in the NLOS scenario. The reduction in the SF standard deviation is 1.6132 dB (at 28 GHz V-V), 2.0917 dB (at 28 GHz V-H), 0.1697 dB (at 38 GHz V-V), and 0.5992 dB (at 38 GHz V-H), respectively. With the exception of 28 GHz, this had a higher value for the SFSD for the CI PLM, indicating that 28 GHz is more sensitive to the effects of wireless links than the other FBs under study. Table 4.3 presents the specific parameters.

Regardless of the polarization, n_1 values are high in both FBs, whereas n_2 values are consistently negative. The model can take into account all potential WS effects in addition to the measured PL because the negative values of n_2 balance out the increase in n_1 values. Figure 4.10 (a) and (b), as well as Figure 4.11 (a) and (b) show how the improved model's curves differed from those of the current CI model, showing a notable improvement and increased accuracy in PL forecasting. The CI model's shadow fading standard deviation increases as a result of the NLOS scenario. PL prediction in NLOS situation is therefore less precise than in LOS scenario. The proposed model nevertheless resulted in a SFSD reduction of 0.1697 dB, as shown in Table 4.3, and offers an appealing decrease in standard deviation. Tables 4.4 and 4.5 present various parameters for the standard FI and improved FI models. The behavior of the path loss in Figure 4.10 (a) and (b) as well as in Figure 4.11 (a) and (b) is understandably not similar with the LOS scenario. The reason was the higher PL experienced in this situation. Nevertheless, the improve model's performance in the curves (Figures 4.10 (a) and (b), Figure 4.11 (a) and (b)) shows that the improved model is capable of estimating the PL values with respect to the distance accurately.

Table 4.2. Parameters for the standard CI and improved CI models.

Parameters	V-V polarization (28 GHz)	V-H polarization (28 GHz)	V-V polarization (38 GHz)	V-H polarization (38 GHz)
PLE (n)	2.2254	2.9790	2.7801	3.1978
σ_{min}^{CI} [dB]	1.7718	1.3425	3.1874	4.1001

$n_1^{Imp.\ CI}$	1.6058	2.3345	1.0281	1.0442
$n_2^{Imp.\ CI}$	0.5273	0.5485	1.4909	1.8328
$\sigma_{min}^{Imp.\ CI}$ [dB]	1.3970	0.7193	0.8154	1.5695

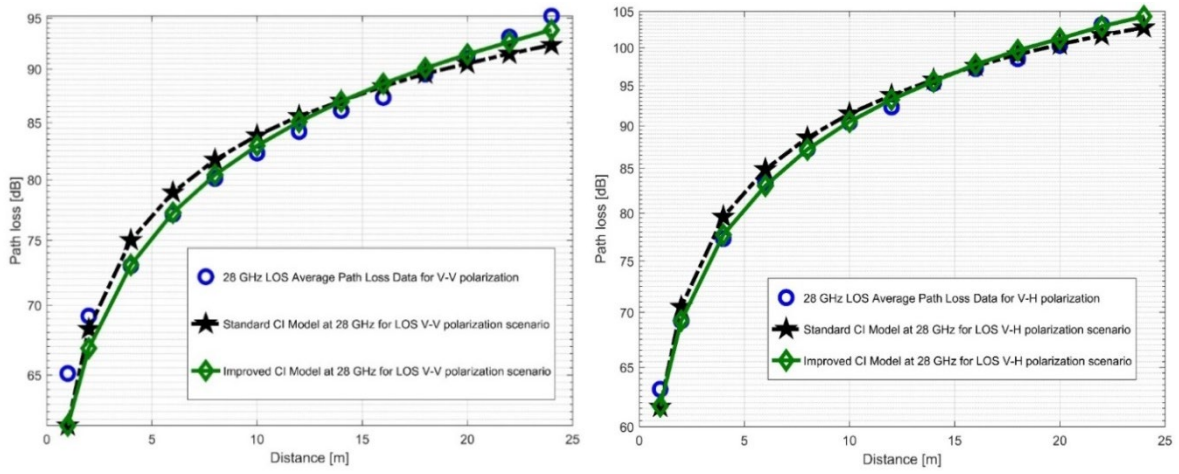

(a) (b)

Figure 4.8. PL versus (vs) distance at 28 GHz for the LOS scenario at (a) V-V polarization, (b) V-H polarization.

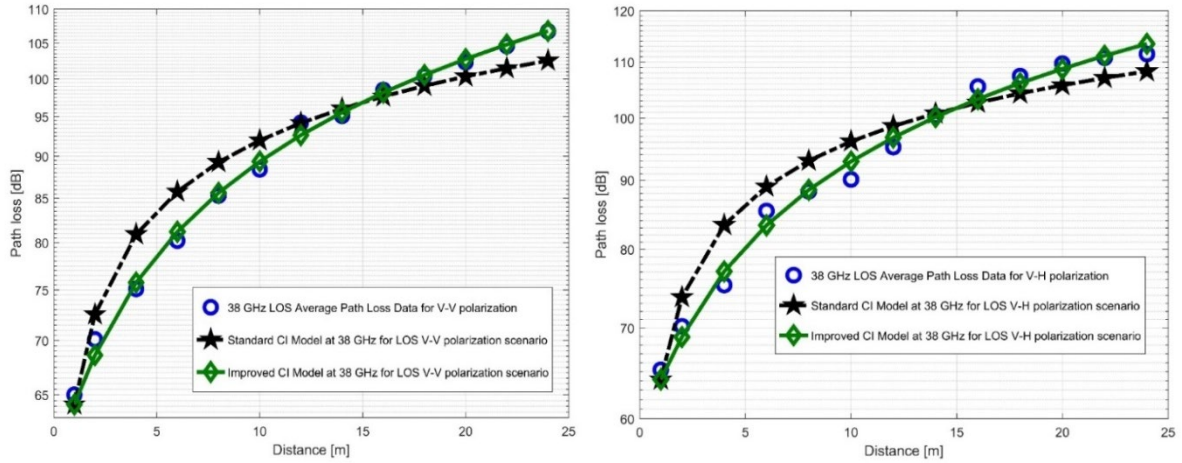

(a) (b)

Figure 4.9. PL vs distance at 38 GHz for the LOS scenario at (a) V-V polarization, (b) V-H polarization.

Table 4.3. Parameters for the standard CI and improved CI models for the NLOS scenario.

Parameters	V-V polarization (28 GHz)	V-H polarization (28 GHz)	V-V polarization (38 GHz)	V-H polarization (38 GHz)
PLE (n) (28 GHz)	2.8815	3.3303	2.8207	3.4682
σ_{min}^{CI} [dB]	8.1287	10.4790	1.6822	3.0257
$n_1^{Imp.\ CI}$	5.6450	6.9020	3.2393	4.4959
$n_2^{Imp.\ CI}$	-2.3517	-3.0396	-0.3562	-0.8746
$\sigma_{min}^{Imp.\ CI}$ [dB]	6.5155	8.3873	1.5125	2.4265

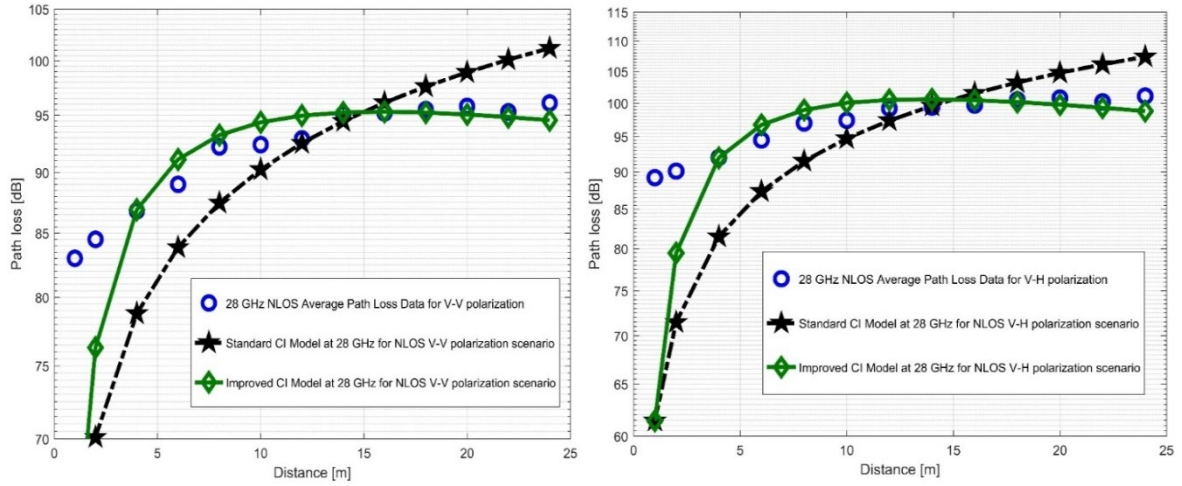

(a) (b)

Figure 4.10. PL vs distance at 28 GHz for the NLOS scenario at (a) V-V polarization, (b) V-H polarization.

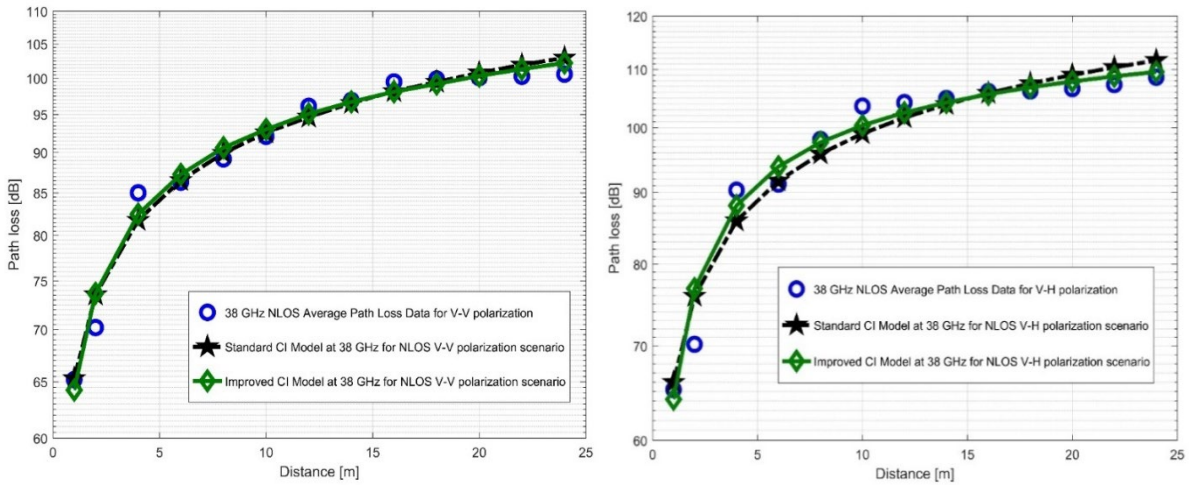

(a) (b)

Figure 4.11. PL vs distance at 38 GHz for the NLOS scenario at (a) V-V polarization, (b) V-H polarization.

4.4.2 Performance Analysis of Standard FI and Improved FI Models

The values of MPE and SDE for 28 and 38 GHz at both antenna polarizations for the LOS situation are given in Table 4.6. The MPE and SDE values for each parameter in the standard CI, improved CI, standard FI and improved FI models are also compared. The result in Figures 4.12 (a) and (b) as well as Figure 4.13 (a) and (b) demonstrate that the improved FI model outperform the standard FI PLM at both 28 and 38 GHz in the LOS scenario. Figures 4.14 and 4.15 present the PL versus distance for NLOS. It can be observed that the improved FI performs better at the V-H polarizations at the 28 GHz FB with a performance of 0.6249 dB. In a similar vein, the V-H antenna polarization exhibits a good error performance in the improved FI model with a 0.5805 dB error performance. The improved CI model for V-V polarization gives 1.9294 dB which is noted for the MPE's best performance at the 38 GHz FB. The improved FI model provides an increase in the PE value for both polarizations, but not quite to the same extent as of the improved CI model.

The MPE is model predictability metric. The level of prediction accuracy is determined by its reduction. In the LOS scenario, the improved CI model predicts the PL with greater precision for both polarizations and FBs. The NLOS scenario reveals a comparable situation, but the PE is significantly higher than in LOS due to the higher PLE values. In the improved models for CI and FI, it is observed that the SDE values for the FBs of 28 GHz and 38 GHz decrease. This is shown in Table 4.6. However, it is found that as propagation frequency increases, the SDE's value reduces. For both polarizations, the best improvement of SDE is at 38 GHz. For improved CI and FI models, the values are: 1.3785 dB for V-V, 2.3192 dB for V-H, 1.2059 dB for V-V and 0. 9437 dB for V-H. It is worth mentioned that the MPE and SDE values are high in the NLOS scenario. The fact that the Tx as well as Rx HAs been not located in a straight line of sight was the main reason for this. The MPE and SDE values, however, are within a tolerable range at both 28 and 38 GHz. The values of the MPE as well as the SDE for the NLOS situation are listed in Table 4.7.

Table 4.4. Parameters for the standard FI and improved FI models for the LOS scenario.

Parameters	V-V polarization (28 GHz)	V-H polarization (28 GHz)	V-V polarization (38 GHz)	V-H polarization (38 GHz)
α_{FI} [dB]	58.8294	59.9354	60.5444	62.1883
β_{FI}	2.1537	3.0540	3.1461	3.6625
σ_{min}^{FI} [dB]	1.7431	1.3008	2.7439	3.5455
$\alpha_{Imp.\ FI}$ [dB]	65.3730	65.3464	62.9705	65.5702
$\beta_1^{Imp.\ FI}$	0.6415	1.9692	0.7265	0.7364
$\beta_2^{Imp.\ FI}$	1.0301	0.7390	1.6482	1.9932
$\sigma_{min}^{Imp.\ FI}$ [dB]	0.5418	0.5285	0.7090	1.5148

Table 4.5. Parameters for the standard FI and improved FI models for the NLOS SCE.

Parameter	V-V polarization (28 GHz)	V-H polarization (28 GHz)	V-V polarization (38 GHz)	V-H polarization (38 GHz)
α_{FI} [dB]	81.8470	87.8146	65.1057	65.8500
β_{FI}	1.0558	0.9722	2.7254	3.3064
σ_{min}^{FI} [dB]	0.7872	0.7796	1.6283	2.9396
$\alpha_{Imp.\ FI}$ [dB]	82.4265	88.5524	63.8704	62.2893
$\beta_1^{Imp.\ FI}$	0.7967	0.6423	3.2778	4.8987
$\beta_2^{Imp.\ FI}$	0.1765	0.2247	-0.3763	-1.0846
$\sigma_{min}^{Imp.\ FI}$ [dB]	0.7342	0.6908	1.5116	2.3661

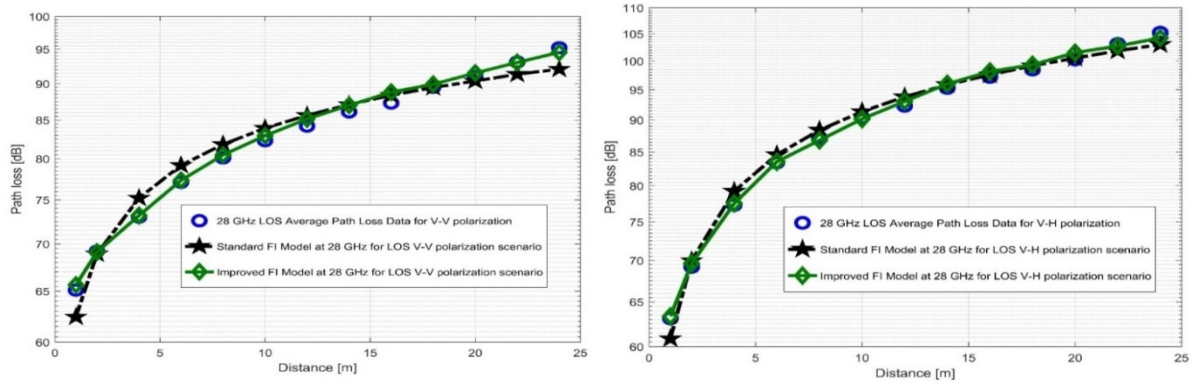

(a) (b)

Figure 4.12. PL vs distance at 28 GHz for the LOS scenario at (a) V-V polarization, (b) V-H polarization.

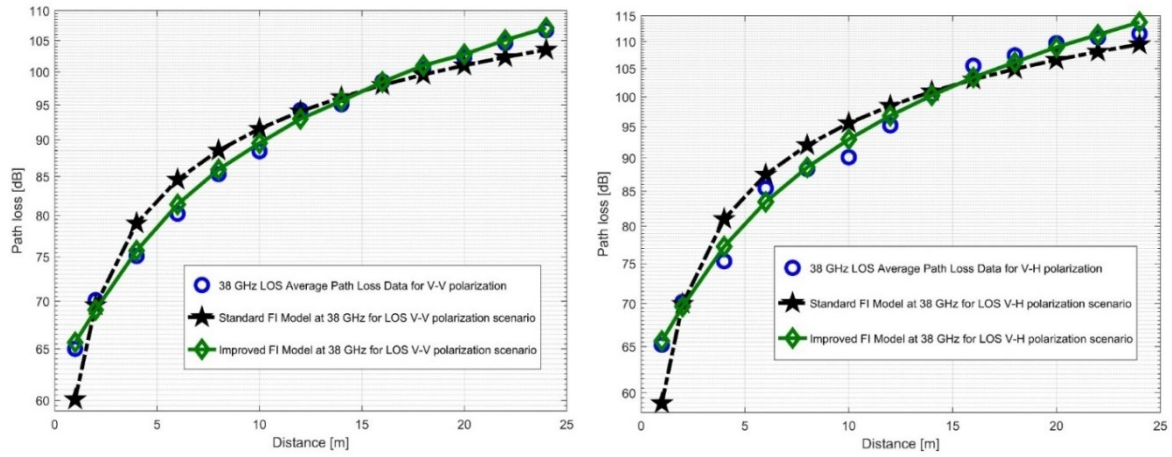

(a) (b)

Figure 4.13. PL vs distance at 38 GHz for the LOS scenario at (a) V-V polarization, (b) V-H polarization.

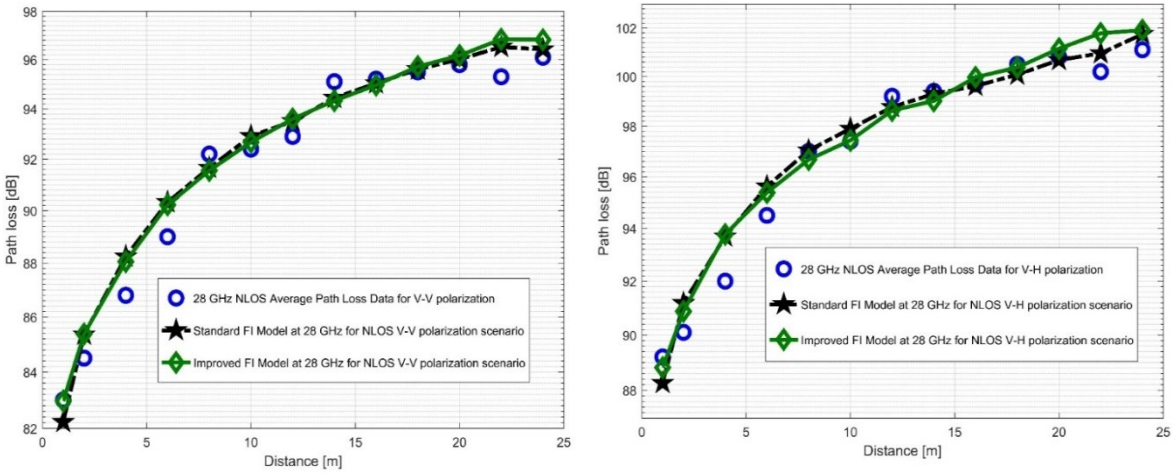

(a) (b)

Figure 4.14 PL vs distance at 28 GHz for the NLOS scenario at (a) V-V polarization, (b) V-H polarization.

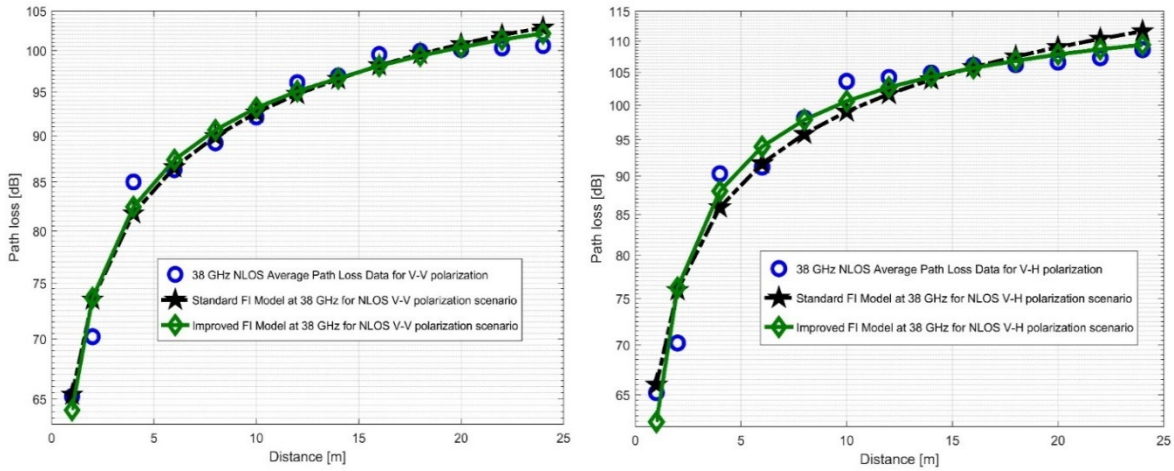

(a) (b)

Figure 4.15. PL vs distance at 38 GHz for the NLOS scenario at (a) V-V polarization, (b) V-H polarization.

4.4.3 MPE and SDE Performance of the Improved Models

The FBs below 6 GHz have up until recently been considered for mobile systems due to their ability to support wide area scope and their simplicity of passage through structures. On the other hand, the cell radius for mm Wave bands is much smaller, as the environment within which the WS travels have a major impact on the WS's ability to spread. Additionally, the mm wave frequency spectrum is greatly impacted by the penetration loss in solid materials. In order to accurately analyze performance and ensure the safe deployment of 5G cellular systems, it is crucial to accurately understand and characterize the behavioral patterns of the mmWave FBs at different interior as well as outdoor locations [16], [33], [41], [126], [142]-[145].

MPE and SDE are additional metrics used to assess the model's efficacy. These two indicators contrast the exact receive data provided during the measurement campaign with the predicted amplitude of the WS provided by the models [161]. According to the following equations, the prediction error (PE) is the difference between the measured and predicted Rx powers which is dependent on the separation of the Tx-Rx. This is expressed in equation (4.20) as computed by [64]:

$$PE(d)[dB] = P_r^M\,(d)[dBm] - P_r^P\,(d)[dBm] \tag{4.20}$$

Where $\boldsymbol{PE(d)}$ represents the decibel value of the prediction error. The predicted value of the received power in dBm is $\boldsymbol{P_r^M\,(d)}$, and the power measured at the receiver is $\boldsymbol{P_r^P\,(d)}$. The expression for $\boldsymbol{P_r^P\,(d)}$ is explained further in equation (4.21):

$$P_r^P\,(d)[dBm] = P_t - P_L^P\,(d)[dB] + G_r + G_t \tag{4.21}$$

The transmitter power is P_t while the gains of the transmitting and receiving HAs are $G_r\ and\ G_t$, respectively. The models' PL is predicted by $P_L^P\,(d)$. SDE, represented by equation (4.22), is a measurement of how far the errors deviate from the MPE value [161]:

$$SDE\ [dB] = \sqrt{\frac{1}{N}\sum_{i=1}^{N}(PE_i - MPE)^2} \tag{4.22}$$

N is the total average PL values were recorded.

The values of MPE and SDE for 28 and 38 GHz at both antenna polarizations for the LOS situation are given in Table 4.6. The MPE and SDE values for each parameter in the standard CI, improved CI, standard FI and improved FI models are also compared. Figures 4.14 (a) and (b) demonstrate that the improved CI performs better at the V-H polarizations at the 28 GHz FB with a performance of 0.6249 dB. In a similar vein, the V-H antenna polarization exhibits a good error performance in the improved FI model with a 0.5805 dB error performance. The improved CI model for V-V polarization gives 1.9294 dB which is noted for the MPE's best performance at the 38 GHz FB. The improved FI model provides an increase in the PE value for both polarizations, but not quite to the same extent as of the improved CI model.

The MPE is model predictability metric. The level of prediction accuracy is determined by its reduction. In the LOS scenario, the improved CI model predicts the PL with greater precision for both polarizations and FBs. The NLOS scenario reveals a comparable situation, but the PE is significantly higher than in LOS due to the higher PLE values. In the improved models for CI and FI, it is observed that the SDE values for the FBs of 28

GHz and 38 GHz decrease. This is shown in Table 4.6. However, it is found that as propagation frequency increases, the SDE's value reduces. For both polarizations, the best improvement of SDE is at 38 GHz. For improved CI and FI models, the values are: 1.3785 dB for V-V, 2.3192 dB for V-H, 1.2059 dB for V-V and 0. 9437 dB for V-H. It is worth mentioned that the MPE and SDE values are high in the NLOS scenario. The fact that the Tx as well as Rx HAs been not located in a straight line of sight was the main reason for this. The MPE and SDE values, however, are within a tolerable range at both 28 and 38 GHz. The values of the MPE as well as the SDE for the NLOS situation are listed in Table 4.7.

Table 4.6. MPE and SDE parameters for the LOS situation

	MPE [dB]				SDE [dB]			
Polarization	V-V		V-H		V-V		V-H	
Frequency [GHz]	28	38	28	38	28	38	28	38
Standard CI model	1.5211	2.6632	1.1936	3.6772	0.9044	1.8002	0.7028	1.8593
Improved CI model	0.9884	0.7338	0.5687	1.3580	0.8996	0.4217	0.4791	0.7787
Standard FI model	1.5108	2.2633	1.1306	3.0731	0.8566	1.5534	0.6679	1.7711
Improved FI model	0.5037	0.7528	0.5501	1.2607	0.4011	0.3475	0.4097	0.8274

Table 4.7. MPE and SDE parameters for the NLOS situation

	MPE [dB]				SDE [dB]			
Polarization	V-V		V-H		V-V		V-H	
Frequency (GHz)	28	38	28	38	28	38	28	38
Standard CI model	5.6233	1.2904	7.3110	2.5307	5.8432	1.0629	7.4866	1.6403
Improved CI model	3.1018	1.2504	4.0887	1.7985	5.7089	0.8550	7.3067	1.6433
Standard FI model	0.6920	1.2390	0.6325	2.4524	0.5226	1.0647	0.5811	1.6277
Improved FI model	0.7390	1.2163	0.5962	1.8123	0.3806	0.8568	0.4627	1.5247

4.4.4 Performance Analysis of Standard CI and Third Order CI Models

This part comprises information on the results of the comparative analysis performed for the third order CI model comparison with the conventional CI model. The main criterion is the best fit of the PL forecasts as measured by MMSE. The outcomes for LOS as well as NLOS situations circumstances for V-V as well as V-H polarizations are shown. The typical CI PLM measured data, as well as 3rd order CI PLMs are compared in Figures 4.16, 4.17, 4.18, and 4.19. Table 4.8 demonstrates that the 3rd order CI PLM performs better in both polarizations and in both communication scenarios. As the model's order rise, the value of the shadow fading standard deviation dropped precipitously. However, this reduction varies from antenna polarization to antenna polarization and from frequency to frequency. At FB of 28 GHz for the two antenna polarizations the conventional CI PLM's shadow fading standard deviation in LOS scenario are 1.7718 and 1.3425, respectively. When the 3rd order CI PLM is applied, it results in 1.1173 and 0.6809. The PLE has also been seen to deteriorate to 2.2254 for V-V and 2.9790 for V-H at 28 GHz. However, because the power depreciation was larger than 2

dB per decade in the V-H polarization more degradation is obvious. However, it is less than 1 dB/decade in the V-V.

In the 38 GHz FB, a comparable phenomenon takes place. In this sense, the shadow fading standard deviation for both polarizations is markedly reduced by the 3rd order PLM. The existing CI shadow fading standard deviation was decreased from 3.1874 to 0.7983 in the V-V and from 4.1001 to 1.5679 in the V-H. Despite the fact that the V-V and V-H polarizations gave results that were similar in decrement, the power loss in this region exceeds 2.5 dB/decade in both situations. In the NLOS situation, the 28 GHz FB at both HA polarizations degrades its power more than the 38 GHz FB. This demonstrates that the WS efficiency in the NLOS is improved in this interior setting at the 38 GHz FB. At 38 GHz, the CI model in the 3rd order lowered the standard shadow fading of the standard CI model significantly for V-H. This shows that the improvement is better in comparison to the V-V polarization. In almost all the scenario looked at, the 3rd order CI PLM provided the better match with the observed data. Furthermore, MPE as well as SDE are additional metrics used to assess the PLM's effectiveness. The MPE as well as the SDE values for the 3rd order CI PLM are shown in Table 4.9 to have better error performance in the LOS scenario. This drop shows that the 3rd order CI model predicts propagation effects quite accurately. Since these metrics (MPE and SDE) evaluate the effectiveness of the projected received WS strength of the models. The MPE and SDE formulae as computed by [44] are shown in equations (4.20) and (4.22).

Also, in the NLOS scenario the predictability by MPE and SDE, as shown in Table 4.9, indicate a good error prediction representation but not as conspicuous as in the LOS situation. The PLMs are more fit to the measured data in LOS scenario than the NLOS, as evidenced by the lower values of the MPE that occur in the LOS. When the third order CI model was used in the LOS scenario for both the 28 and 38 GHz frequency bands, the shadow fading standard deviation improved significantly when compared to the standard CI model. Although the improvement is more pronounced at 28 GHz for the NLOS situation due to signal fluctuations. However, at 38 GHz, the same pattern of improvement was observed as in the LOS. It is also worth noting that the V-V antenna polarization outperforms the V-H antenna polarization due to the latter's polarization difference.

Table 4.8. Parameters for the Third Order CI in the LOS and NLOS Scenario

28 GHz LOS communication scenario			28 GHz NLOS communication scenario	
	V-V polarization	V-H polarization	V-V polarization	V-H polarization
PLE (n)	2.2254	2.9790	2.8815	3.3303
σ_{min}^{CI} [dB]	1.7718	1.3425	8.1287	10.4790
k_1	2.9720	2.7120	8.9497	11.3454
k_2	-2.2854	-0.2286	-9.1556	-12.1877
k_3	1.3644	0.3770	3.3005	4.4377
$\sigma^{log^3 CI}$	1.1173	0.6809	6.1916	7.9313
38 GHz LOS communication scenario			38 GHz NLOS communication scenario	
	V-V polarization	V-H polarization	V-V polarization	V-H polarization
PLE (n)	2.7801	3.1978	2.8207	3.4682
σ_{min}^{CI} [dB]	3.1874	4.1001	1.6822	3.0257
k_1	1.2984	1.1600	2.2289	1.8082

k_2	0.9345	1.5942	1.7241	4.6542
k_3	0.2699	0.1157	-1.0091	-2.6842
$\sigma^{log^3 CI}$	0.7983	1.5679	1.3794	1.7791

Table 4.9. Third Order CI model MPE and SDE Parameters for LOS and NLOS Scenario

MPE [dB]					SDE [dB]			
Polarization	V-V		V-H		V-V		V-H	
Frequency [GHz]	28	38	28	38	28	38	28	38
LOS scenario	0.6418	0.7283	0.5071	1.3533	0.8655	0.3112	0.4344	0.7752
NLOS scenario	2.7817	1.0784	4.4935	1.3801	5.5114	0.8413	7.1047	1.1367

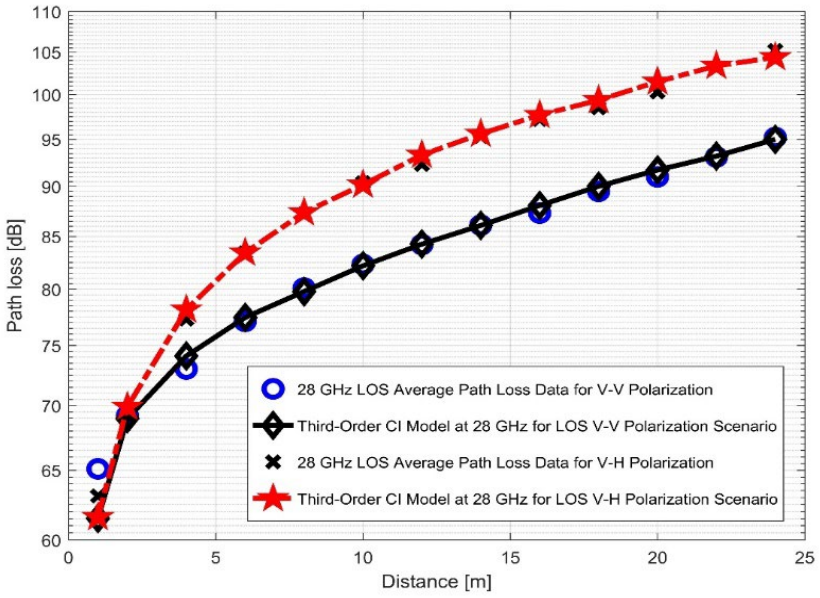

Figure 4.16. PL versus distance at 28 GHz LOS

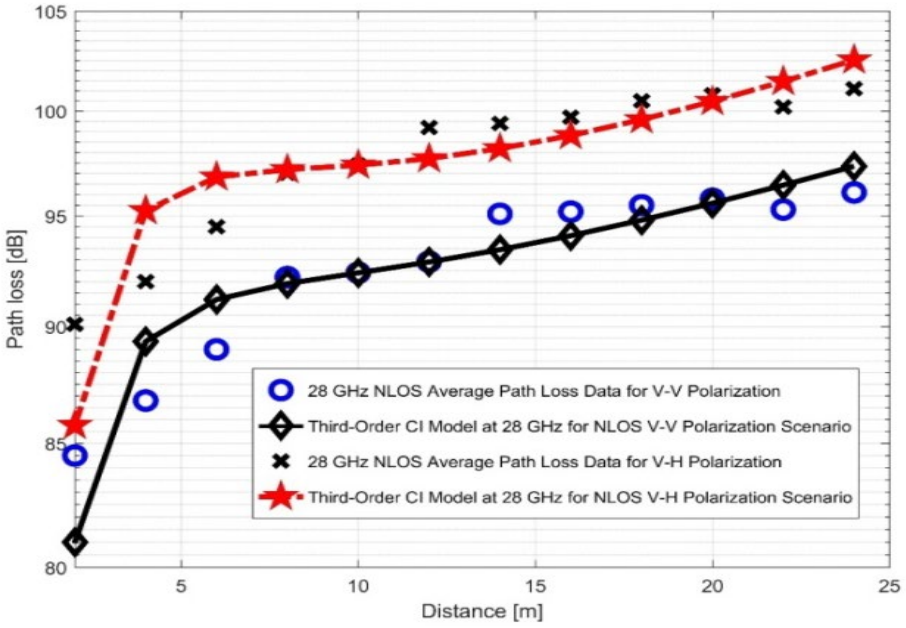

Figure 4.17. PL versus distance at 28 GHz NLOS

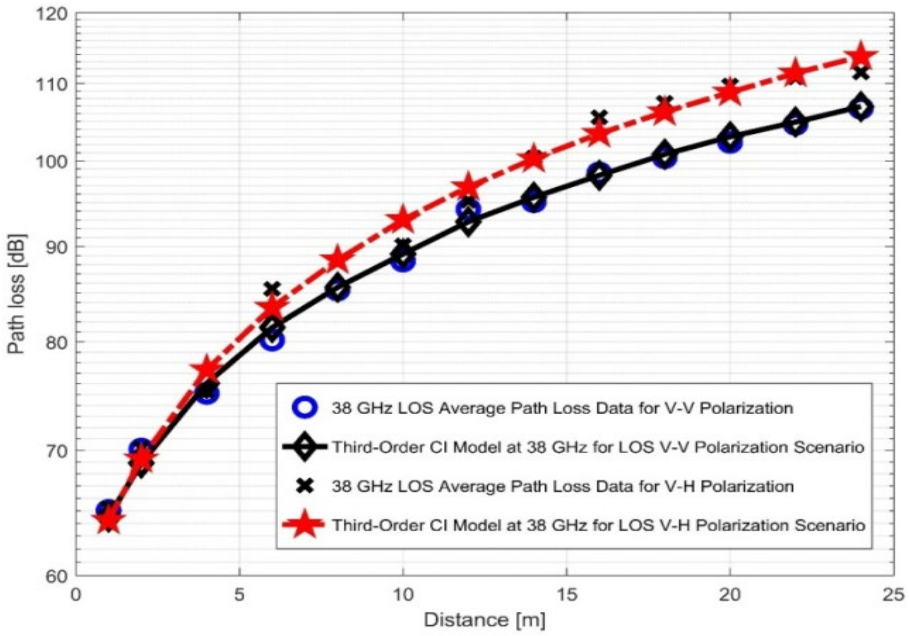

Figure 4.18. PL versus distance at 38 GHz LOS

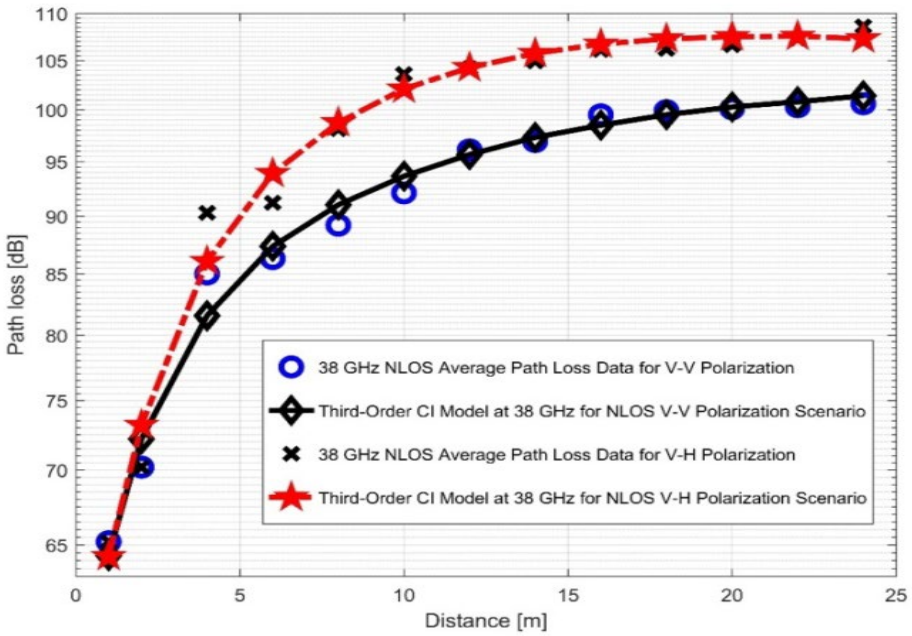

Figure 4.19. PL versus distance at 38 GHz NLOS

4.5. Chapter Summary

In this chapter, the analysis of the improved versions of the CI and FI PLMs as well as the third order CI PLM at 28 GHz and 38 GHz has been presented. The MPE and SDE are also used to check for the efficiency of the improved PLMs. To collect the data for the study a measurement campaign was carried out at FBs of 28 and 38GHz. The R&S SMB 100A radio WS generator was used to generate CW signal and that was supplied over a transmission media to the signal analyzer using broadband Tx and Rx HAs. The analysis also focused on the LOS and NLOS scenarios at V-H as well as V-V polarizations. One of the key findings of this work is that the improved PLMs typically perform better in terms of consistency as compared to the current standard models thereby justifying their high accuracy level. The third order, the improved CI as well as the FI PLMs showed a significant percentage improvement even at higher FBs and for various antenna polarizations. The MPE and SDE used in percentage error also show how precisely and accurately the improved models predict the PL. In addition, the MPE and SDE used in percentage error also corroborate how precisely and accurately the 3rd order CI PLMs predicts the PL. After verifying the precision of the improved CI as well as FI models used in this study, the findings also demonstrated that these models' fundamental use is suitable for LOS and NLOS indoor environments and for various antenna polarizations at millimeter wave frequencies. Also, noteworthy is the fact that the design engineers and researchers will benefit from the values of MPE and SDE in order to make accurate computation of the system design which covers all surroundings as well as connectivity scenarios. The improvement of current PLM parameters should be the main focus of future work, especially for outdoor areas like big shopping malls and cities.

Chapter 5

Path Loss Analysis using Squared Root Distance based Model in the 28 and 38 GHz Frequency Bands

The measurements and analysis of the squared root distance path loss model are presented in this chapter. The analysis showed that the standard deviation of shadow fading can be substantially lowered in LOS as well as NLOS, suggesting greater accuracy in estimating path loss using SRD based model.

5.1 Introduction

Due to the exponential rise in mobile data usage, and the desire for faster connection speeds, the contradiction involving reduced spectrum as well as higher capacity has emerged as a critical issue. Conventional wireless network FBs, i.e., those less than 6 GHz, are experiencing a spectrum crunch as a result of rapidly increasing cellular data speeds and widespread data access requests. Wireless data networks can be enhanced to increase the likelihood that they will be able to accommodate the anticipated accelerated growth in mobile traffic levels as well as users' increasing demand for faster data speeds [48], [48], [126], [148]. 5G wireless communications are being developed as a result of technological advancements [162]-[165] as well as the mmWave frequency band spectrum allocations [42]. These technologies can help with the current spectrum shortage. The 5G mobile communication systems will bring about a significant shift in application and user perspectives [41], [130], [166]. However, for the 5G system to minimize physical constraints and fully utilize capacity of the system, sophisticated signal processing methods and new frequency space are needed [68], [166]-[168]. Mobile operators all over the world are introducing 5G services, but path loss must be assessed in order for wireless communication operators to plan their networks for the target coverage area [169]. Numerous PLMs for wireless propagations have been investigated in the past [42], [48], [68], [130], [162]-[167]. The authors of [170] investigated the relationship between path loss and terrain data by presenting in-depth driving test sensor readings of wave propagation in a college community. PL modeling for 5G networks has been accomplished through channel measurements in urban and suburban in [171].

Researchers in [172] compared 5G PL approaches using measured data as well as evaluating the models' validity across various environments. Sun et al. compared the ABG and CI PLMs with FB ranging from 2 GHz to 73 GHz using measured data as well as ray-tracing methods [64]. The researchers discovered that the CI model produced less error in prediction [64]. As way of enhancing the ABG model, authors in [173] proposed a weighted ABG model that appropriately integrated or combined various available datasets and produced improved outcomes in terms of prediction accuracy. The weighted ABG model has been shown to produce better prediction error results, with standard deviations ranging from 1.2 to 12.5 dB [173]. Authors proposed probabilistic models for predicting mmWave PL in [146]. Based on measurements taking at FBs of 28 and 73 GHz, the authors of [146] developed a hybrid PLM that was a weighted combination of LOS and NLOS signal attenuation.

The propagation channel characteristics in the FBs of 6.5, 10.5, 15, 19, 28, and 38 GHz were investigated further in an indoor setting using a measurement campaign spanning 4,000 power delay profiles and employing a directional HA as Rx and an omnidirectional antenna as a Tx section. The frequency attenuation model is a novel PLM that considers both distance and FB. This model's RMS delay spread and dispersion factor values show its simplicity, lower PLEs, and good RMS delay spread and dispersion factor values [48]. The large percentage of propagation models currently in use for any FB below 6 GHz are not appropriate for mmWave PL modeling, nor are they appropriate for any FB above 6 GHz. This is due to the noticeable difference in WS propagation. An indoor measurement campaign was carried out at UTM Malaysia. In applications utilizing omnidirectional and directional antennas, PL analysis of single and multi-frequency signals was performed. It was discovered that modeling PL on a large scale with respect to distance is easier when using a less complex model approach with only one PLE parameter (n) that is dependent on transmitted power [70]. Using a model that is not dependent on transmitted power, on the other hand, may necessitate more variables, making the modeling complex. The analysis of these PLMs demonstrates the need for the development of a model that is more effective than the fundamental models, such as the CI, FI, and ABG, at reducing the PL of the propagated signal from the Tx to the Rx [70].

Furthermore, tests for 28 GHz reflection and penetration loss were executed in buildings throughout New York City [84]. According to the findings, a three-wall office complex has a significant absorption loss of 45.1 dB. Furthermore, while exterior tinted glass had a loss of absorption of 40.1 dB, interior non-tinted glass had a loss of absorption of 3.9 dB. The authors of [153] measured the quality of the link in the mmWave bands in a lab using 28 and 82 GHz FB as well as an anechoic chamber.

Hindia et al. measured a proven channel model for both single and multi-frequency models inside an outdoor area, as well as proposing a novel model [154]. The authors of [61], [84], and [155] used omnidirectional and directional HAs to measure at 28 and 73 GHz in an interior office. At FBs of 28, 38, and 73 GHz, measurements and simulations were performed to assess and estimate a number of parameters as well as classify the transmission channel in CI and ABG PLMs [156]-[157]. In many ways, the interior surroundings differ greatly from the outdoor surroundings. Indoor PLMs must therefore account for various indoor layouts, building materials, office equipment types and counts, worker movements, the density of nearby smart devices, and so on. In addition to the usual fading and PL caused by range, obstruction, shadowing, reflection, refraction, scattering, and penetration, dispersion has an effect on the characteristics of the received signal [174].

Having considered many research literatures, it has been discovered that PL modeling is critical when designing a wireless communication network. PL prediction models can be obtained deterministically, stochastically, or empirically through measurement campaigns that collect actual data [5], [39]. The most commonly used path loss modeling is measurement-based, as evidenced by its high prediction accuracy and reliability, [18], [144], [126], [175]-[176]. Extensive measurement campaigns have been conducted globally in various outdoor as well as indoor environments using various communication techniques, including LOS, NLOS, and other scenarios, in order to provide accurate propagation models for each specific frequency band and communication environment. For mmWave and sub-THz propagation, several measurement-based PLMs have been used. However, because of their outstanding precision and simplicity, the conventional CI and FI PLMs are the most commonly used among the various models [5], [18], [39], [144], [174]-[178].

A SRD measurement based PL prediction model for enclosed environments which is an expanded work from [179] is analyzed in this paper at higher frequencies. The model differs from conventional CI and FI models in that the PL (in dB) is assumed to vary with the square root of the separation between the Tx and Rx, measured in meters. Because shifting to higher FBs results in more sensitive propagation signals, the motivation for the evaluation of this PLM is the increased possibility of improving the PLM equation to achieve much greater accuracy in prediction and sensitivity to wireless channel effects. The squared root distance PLM is evaluated and validated by comparing it to the FSPLM, the CI PLM, as well as the FI PLM at two selected FBs of 28, and 38 GHz using polarizations of the antennas at V-H as well as V-V. The data for this study were collected in an enclosed environment on the fifth floor of the Department of EECE at the UKZN's Howard College Campus in Durban, South Africa. The remainder of the chapter is structured as follows: The measurement campaign and the PLMs are covered in section 5.2 and section 5.3, respectively. Section 5.4 presents the results and discussions, while the chapter summary is presented in section 5.5.

5.2 Measurement Campaign and Environment

This section explains the measurement setup including the Tx and Rx in a typical indoor corridor environment. The channel sounder was cautiously calibrated prior to the start of the measurements to ensure accurate data collection. Furthermore, we affirmed that there were no interfering signals in the corridor. The wireless propagation channel, as previously stated, is an enclosed interior corridor. This corridor is 30 m in length, 1.4 m in width, and 2.63 m in height. This corridor, as it typically exists, is made primarily of bricks and dry concrete, with wooden doors to entrance offices on one side and a staircase and elevator on the other. The Rohde and Schwarz SMB 100A Signal Generator was used in the Tx section, and the Rohde and Schwarz FSIQ 40 Signal Analyzer was used in the Rx section. Images of the Tx and Rx units used in measurement campaigns are shown in Figures 5.1, 5.2, 5.3, 5.4, and 5.5. The parameter setup as well as equipment set-up are shown in Table 5.1. During the campaign, the Tx HA was positioned at one end of the passage, while the Rx HA shifted away from the Tx in 2 m increments up to the opposite end. When both antennas were aligned toward each other for LOS, the Rx received wireless signals at each Tx-Rx separation distance. However, there was no alignment in the NLOS between the Tx and Rx HAs. The center FBs used for CW signal transmission between two broadband HAs adopted in both the Tx and Rx ends, with HA heights of 1.6 m for the Tx HA and 2.3 m for the Rx HA. The Rx HA was placed 24 meters away from the Tx by starting at one end of the hallway and the samples were taken at every 2 meters. The reference distance ($d_o = 1m$) is taken as 1m. Figures 5.2 and 5.6 show a comprehensive view of the floor plan and the interior passage. Thus, the path loss was calculated using equation (5.1) [40]:

$$P_L = P_t - P_r + G_r + G_t \tag{5.1}$$

Where Tx power = P_t, Rx power = P_r, the gain of Tx antenna = G_t and the gain of Rx antenna =G_r.

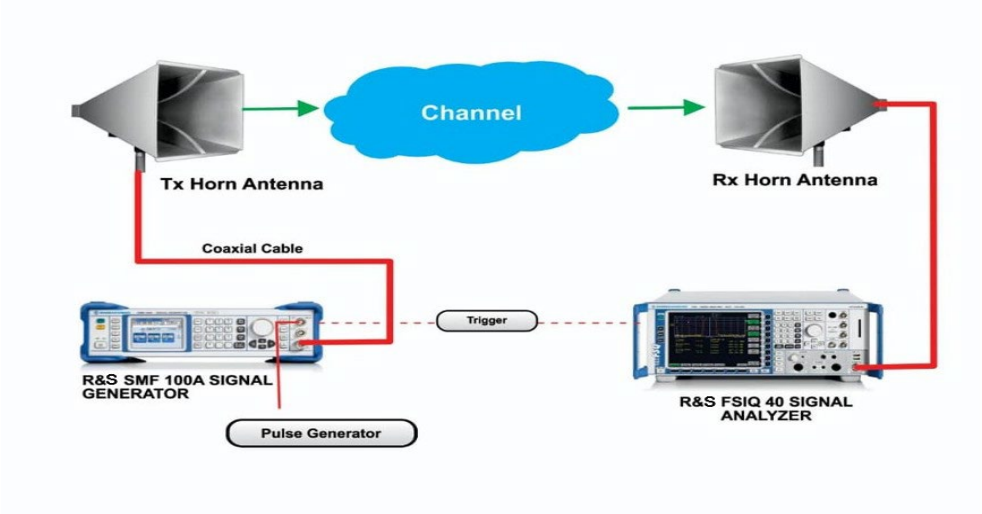

Figure 5.1. Building blocks of the channel settings.

Figure 5.2. The interior corridor

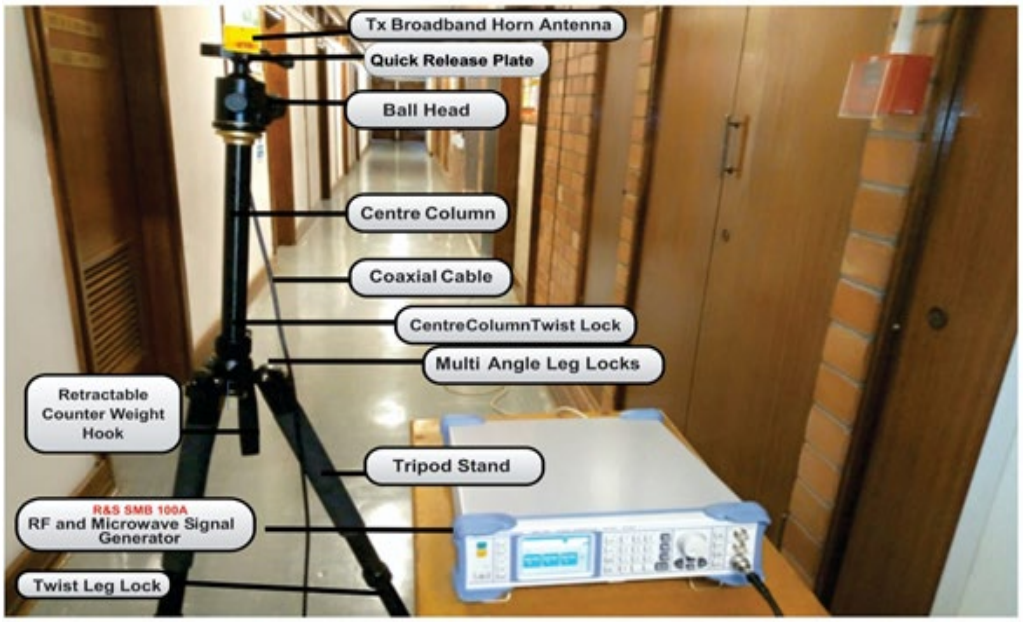

Figure 5.3. Setup for Tx

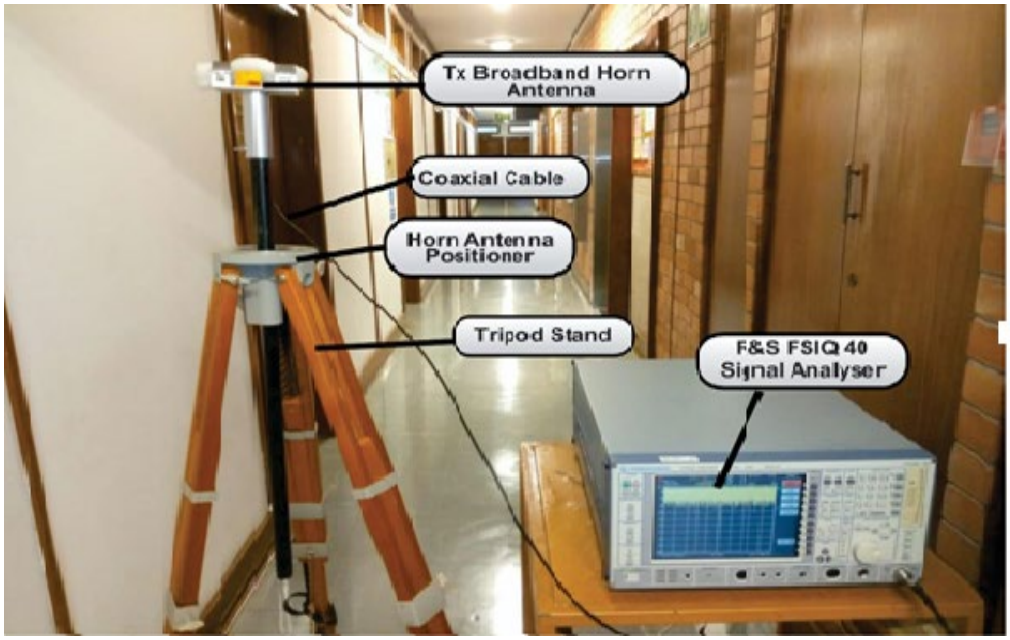

Figure 5.4. Setup for Rx

Figure 5.5. The configuration of the Tx and Rx in the indoor passage

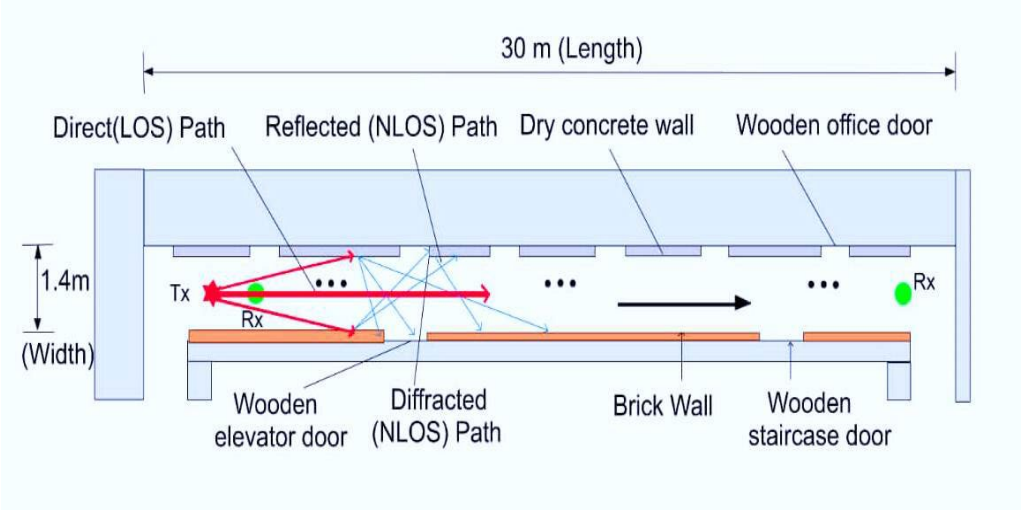

Figure 5.6. A floor plan for the indoor passage

5.3 Large-Scale PLM Analysis

Large-scale PLMs predict the losses in the transmission signal with the increase in distance. They foretell the attenuation of WS that travels through space and time. They are crucial in the development of innovative communication systems that are more effective. They are also useful tool for calculating how much the wireless signal will be weaken and decayed as it travels from Tx to Rx while taking transmission distance and other factors into account. In this paper, we analyze a squared root distance PLM that was used in an interior passage while accounting for the most common propagation paths.

Table 5.1. Equipment set-up parameters′ description for the experiment

Parameters	Configuration/Value	Unit
Centre FBs	28, 38	GHz
Transmission bandwidth	100	MHz
Transmission signal	CW	
Tx and Rx HAs	Broadband HA	
Power of Tx HA	10	dBm
Height of Tx HA	1.6	m
Height of Rx HA	2.3	m
Gain of Tx and Rx HA at 28 GHz	15	dBi
Gain of Tx and Rx HA at 38 GHz	17	dBi
Polarizations of Tx and Rx HA	V/ H	
Dimension of HA (L x W x H)	71 x 32 x 28.6	mm^3
Weight of HA	0.08	Kg

5.3.1 The SRD PLM

This proposed PLM by [179] differs from the conventional CI and FI PLMs in that it is assumed that the PL varies with the square root of the separation between the Tx and Rx. Because shifting to higher FBs results in more sensitive propagation signals, the motivation analyzing this model is the increased possibility of improving the PLM equation to achieve much greater accuracy in prediction and sensitivity to wireless channel effects.

The squared root distance model for predicting PL is given in equation (5.2) as computed by [179]:

$$PL(d)[dB] = A + B\sqrt{d} + X_\sigma \tag{5.2}$$

Where PL$(d)[dB]$ represents the predicted path loss value in decibels (dB) expressed as a function of the separation between the Tx and Rx antennas. The two major parameters of the squared root distance PLM are A and B, where A denotes the PL value right next to the Tx antenna and B regulates the path loss's dependence on $\sqrt{d}$. The operating frequency of the propagating signal, the characteristics of the wireless medium in terms of its dimensions, and propagation techniques like reflections, diffractions, and wave-guiding effects are the variables that affect the parameters A and B. To represent the effects of shadow fading, $X\sigma$, and σ represent the Gaussian random variable with a zero mean, and the SD, respectively.

The best-fit values for the parameters: A, B and σ are provided by adopting the technique of MMSE. The goal is to minimize prediction error while having the squared root distance model match the actual measured path loss. Thus, the SD σ can be described as follows as computed by [39]:

$$\sigma = \sqrt{\frac{\sum X_\sigma^2}{N}} = \sqrt{\frac{\sum (PL(d)[dB] - A - B\sqrt{d})^2}{N}} \tag{5.3}$$

N is the total number of PL recorded. The parameters of the squared root distance model must meet the requirements listed below based on the content of eq. (5.3) as computed by [179]:

$$\frac{\partial}{\partial A}((PL(d)[dB] - A - B\sqrt{d})^2 = 0 \tag{5.4}$$

$$\frac{\partial}{\partial B}((PL(d)[dB] - A - B\sqrt{d})^2 = 0 \tag{5.5}$$

The two previous equations can be simplified as [179]):

$$NA + \sum \sqrt{d}\ \ B = \sum PL(d)[dB] \tag{5.6}$$

$$\sum \sqrt{d}\ \ A + \sum d\ \ B = \sum (PL(d)[dB] \times \sqrt{d}) \tag{5.7}$$

Following the provision of the matrix forms of equations (5.6) and (5.7), the parameters A and B can be described in their closed-form [179]:

$$\begin{bmatrix} N & \sum \sqrt{d} \\ \sum \sqrt{d} & \sum d \end{bmatrix} \begin{bmatrix} A \\ B \end{bmatrix} = \begin{bmatrix} \sum PL(d)[dB] \\ \sum (PL(d)[dB] \times \sqrt{d}) \end{bmatrix} \tag{5.8}$$

$$A = \frac{(\sum d) \times (\sum PL(d)[dB] - (\sum \sqrt{d}) \times (\sum (PL(d)[dB] \times \sqrt{d}))}{N \sum d - (\sum \sqrt{d})^2} \tag{5.9}$$

$$B = \frac{-(\sum d) \times (\sum PL(d)[dB] + N(\sum (PL(d)[dB] \times \sqrt{d}))}{N \sum d - (\sum \sqrt{d})^2} \tag{5.10}$$

After substituting the values for the parameters, Eq. (5.3) can be employed to calculate the value of the SD (σ) of the shadow fading.

5.3.2 CI PLM

The expression of writing the CI PLM is shown in the equation (11) as computed by, [10], [13], [126]:

$$P_L^{CI}(d)[dB] = FSPL(f, d_o)[dB] + 10.n.\log\left(\frac{d}{d_o}\right) + X_{\sigma SF}^{CI} \tag{5.11}$$

Where the gaussian random variable which has zero mean is X_σ^{CI} , d_o is the reference distance, f is the frequency of operation, and the PLE is n, [43], [126]. At a reference distance of d_o = 1 m, its *FSPL in dB* is expressed in equation (5.12) as follows [126], [130]:

$$FSPL(f, 1m)[dB] = 10log_{10}\left(\frac{4\pi f}{c}\right)^2 \tag{5.12}$$

Keep in mind that the only significant parameter that needs to be optimized for the CI model is the PLE (n). This unitless parameter indicates how the PLM is affected by the Tx-Rx gap distance. For this concept, actual positioning is required to demonstrate PL close to the Tx antenna. The transmission frequency found in the FSPL term clearly has a significant impact on the CI PLM. The parameter of the CI model is improved using the MMSE technique (i.e., the PLE). We can use this method to obtain the fewest errors while accurately fitting the measured data by lowering the SFSD [40].

5.3.3 FI PLM

The two parameters of the FI model, which is a linear equation, are the PL line slope β and the intercept ∝, respectively, as shown in equation (5.13) computed by [126], [130]:

$$PL^{FI}(d)[dB] = \propto + 10\beta\, log_{10}(d) + X_{\sigma SF}^{FI} \tag{5.13}$$

Where $PL^{FI}(d)$ depicts the PL in dB, and X_{σ}^{FI} represents the zero mean value of the gaussian random variable with a zero mean. The FI PLM's parameters are different from those of the CI PLM, which is an important distinction to make [126], [130], [167].

5.4 Discussion of Results

This section discusses the results and study's findings. The presentation is divided into two parts, the first of which compares the squared root distance based-model parameters with the existing CI and FI models at FBs of 28 as well as 38 GHz. Consideration was given to LOS as well as NLOS scenarios for the two antenna polarizations. The second sub-section describes the predictability (in terms of MPE and SDE) of the squared root distance model in comparison with the existing CI and FI PLMs, as well as an improved version of CI and FI PLMs.

5.4.1 Squared Root Distance Model Comparison with CI and FI Models

Figures 5.7 and 5.8 show the variation of measured PL values, the FSPLM, the squared root distance model, and the standard CI and the FI PLMs with the distance between the antennas for the two antenna polarizations at 28 GHz. The figures show that all of the models are above the FSPL model's curve. This is understandable given that the path loss at this frequency exceeds the FSPL due to increased signal attenuations at high frequencies, resulting in a rise in path loss. It is also worth noting that Figures 5.7 and 5.8 show that the squared root distance models′ curves have higher prediction accuracy and precision than the existing CI and FI PLMs, as well as improved versions of the CI and FI PLMs. The parameters of the squared root distance model that provide the best-fit prediction at 28 GHz FB were $A = 52.3240, B = 7.3941\ and\ \sigma = 0.4757$ and $A = 54.3988, B = 10.2694\ and\ \sigma = 1.5982$ for the V-V and V-H antenna polarizations, respectively as shown in Table 5.2. The very small sigma values demonstrate the accuracy and sensitivity of the SRD models to the transmission mechanism inside these indoor corridor environments. The parameter values in the V-H polarizations were higher as compared to the values in V-V polarizations due to the shift in antenna polarizations, which causes a slight increase in path loss. Figures 5.9 and 5.10 depict the variation of measurement data and models' data with the distance between the antennas at frequency 38 GHz for LOS. The figures show that the models follow the measured data, resulting in high prediction accuracy. The curves are steeper than the FSPL due to high frequencies. For the squared root distance model, Table 5.3 presents the PLMs' parameter at 38 GHz V-V as well as V-H polarizations which are $A = 55.9571, B = 10.8279$ and $\sigma = 0.8253$, and $A = 58.4551, B = 12.6235$ and $\sigma = 1.6164$, respectively. There was a clear notice of high stability of the model as the values have slight changes when frequency changes from 28 GHz to 38 GHz. The numerical increase of $A, B,$ and σ are 3.6331 dB, 3.4338 dB, 0.3496 dB and 4.0593 dB, 2.3541 dB, 0.0182 dB for the V-V and V-H polarizations, respectively. This demonstrates that more precision is required for mmWave propagation at higher frequencies in order to have an accurate and efficient PL of the propagating signals.

Figures 5.11 and 5.12 depict the variation of average actual observed PL values, the FSPLM, the standard CI and FI models, the squared root distance model, and improved versions of the CI and FI PLMs with the distance between the antennas at 28 GHz for NLOS. The graphs show that the PL for all of the models are above the FSPLM's curve. This is reasonable given that there is increase in signal attenuations due to non-bore sight

between the antennas. Despite the high PL observed in this scenario, the squared root distance models' curves exhibit higher predictive accuracy and precision than the current CI and FI models, as illustrated in Figures 5.11 and 5.12. This is because all of the curves in the models are close to the measurement data sets. The squared root distance model shows the finest prediction at 28 GHz for NLOS situation with the parameters $A = 80.3789, B = 3.5141,$ and $\sigma = 1.0464,$ and $A = 86.4113, B = 3.2516,$ and $\sigma = 0.9281$ for the V-V and V-H antenna polarizations, respectively as presented in Table 5.4.

However, in the NLOS scenario, the signal effectiveness at 38 GHz FB is superior in both antenna polarizations despite the fact that the opposite occurred in LOS situations. This was also observed during the study's performance analysis in [126]. The performance of the SRD model for NLOS, which produces a good match between all of the curves and the measured data values, is shown in Figures 5.13 and 5.14. The parameters of SRD model at 38 GHz for NLOS situation are $A = 62.027, B = 8.8539,$ and $\sigma = 3.3895,$ and $A = 62.7455, B = 10.5468,$ and $\sigma = 5.2621$ for V-V and V-H polarizations, respectively, as shown in Table 5.5. This demonstrates that the SRD model accurately predicts as compared to the standard CI and FI PLMs in the same environment. The high standard deviation is due to the fact that the Rx signal powers are primarily due to reflection and diffraction effects.

5.4.2 Comparison of the Squared Root Distance Model to Existing and Improved CI and FI Models Based on MPE and SDE Parameters

The PLM's efficacy is assessed by analyzing the prediction error of the SRD model using real measurement data and using the MPE as well as the SDE as additional metrics. The squared root distance model's MPE and SDE values are compared with the standard CI and FI models, and its performance was further validated by contrasting it with the improved CI and FI models proposed in [43]. The details of the improved CI and FI models proposed in [43] are given in Equations (5.17) and (5.18). The PE is defined as the difference between the measured and predicted Rx powers and is expressed in equation (5.14) [161].

$$PE(d)[dB] = P_r^M\ (d)[dBm] - P_r^P\ (d)[dBm] \tag{5.14}$$

Where $\boldsymbol{PE(d)}$, $\boldsymbol{P_r^M\ (d)}$ and $\boldsymbol{P_r^P\ (d)}$ are the prediction error in dB, the predicted value of the received power in dBm, and the power measured at the receiver, respectively.
The expression for $\boldsymbol{P_r^P\ (d)}$ is explained further in equation (5.15):

$$P_r^P\ (d)[dBm] = P_t - P_L^P\ (d)[dB] + G_r + G_t \tag{5.15}$$

The Tx power is P_t while the antenna gains at the Tx and Rx are G_r and G_t , respectively. The models' PL is predicted by $P_L^P\ (d)$. The SDE, represented by equation (5.16), is defined as the deviation of error from the MPE value [161]:

$$SDE\ [dB] = \sqrt{\frac{1}{N}\sum_{i=1}^{N}(PE_i - MPE)^2} \tag{5.16}$$

where N is the total average recorded PL values.

The expressions for the improved version CI and FI models are shown in equations (5.17) and (5.18) [43]:

$$P_L^{Imp.CI}\ (d)[dB] = FSPL(f, d_o)[dB] + 10n_1\ log_{10}(d) + 10n_2(log_{10}(d)\ )^2 + X_{\sigma SF}^{Imp.CI}\ d > 1m \tag{5.17}$$

$$PL^{Imp.FI}(d)[dB] = \propto + 10\beta_1 \, log_{10}(d) \; + 10\beta_2 \, log_{10}(d)^2 + X_{\sigma SF}^{Imp.FI} \; d > 1m \tag{5.18}$$

Where n_1 and n_2 are the PLE's first and second orders in equation (5.17), and $\beta_1 \, and \, \beta_2$ are the slope intercepts parameters in equation (5.18).

Tables 5.6 and 5.7 show the MPE and SDE values for 28 as well as 38 GHz at both polarizations in LOS and NLOS situations. Because the MPE is model predictability metric, its reduction determines the level of prediction accuracy. When considering the V-V antenna polarization in the LOS scenario, the improved CI and FI models perform well, with error value improvements of 0.5327 dB and 1.0071 dB, respectively. However, the SRD PLM performs better in both situations, increasing its error betterment to 1.1341 dB in the 28 GHz FB and 1.9045 dB in the 38 GHz FB. The SRD model outperforms the other PLMs considered in the V-H polarization, with the exception of the 28 GHz FB, where the error of predictability did not have a superior response. The squared root distance model's MPE behavior is not stable in the NLOS scenario for both antenna polarizations. Because the Tx and Rx antennas weren't in line of sight, it is obvious that there were more signal fluctuations in the NLOS situation. The prediction error is greater at the 38 GHz frequency in NLOS, even greater than the cases recorded using the improved CI and FI model. Nonetheless, when the SRD model was used at the 28 GHz frequency for V-V and V-H, the degree of predictability increased significantly. At these two polarizations, the squared root distance model produces the error values. The error values for the V-V and V-H polarizations are 4.7187 dB and 6.506 dB, respectively. The results show that for the two polarizations at 28 GHz provided the best and most accurate degree of precision when predicting PL values. When considering the V-V antenna polarization in the LOS scenario, the SRD achieves the greatest level of improvement at 38 GHz. At 38 GHz V-V polarization, SDE has an error improvement of about 1.3264 dB. This is due to the change in antennas' polarization, which increased the PL and caused the decrease in SDE. The NLOS situation results in an excellent SDE error values at 28 GHz for both antenna polarizations. This demonstrates that the SRD PLM outperforms the improved versions of CI and FI. The SDE and MPE values shown in Tables 5.6 and 5.7 clearly demonstrate that the squared root distance model is more suitable to estimate the PL in the enclosed surroundings. Aside from the good performance of the MPE and SDE metrics, another major advantage of the squared root distance model is its simplicity. The squared root distance model is accurate and consistent, and therefore is simple to understand and utilize.

Table 5.2. Parameter comparisons for the 28 GHz LOS scenario

28 GHz LOS results			
Model	Parameters	V-V	V-H
CI	PLE (n)	2.2254	2.9790
	$\sigma_{\min}^{\mathrm{CI}}$ [dB]	1.7718	1.3425
FI	α_{FI} [dB]	58.8294	59.9354
	β_{FI}	2.1537	3.0540
	$\sigma_{\min}^{\mathrm{FI}}$ [dB]	1.7431	1.3008
SRD	A [dB]	52.3240	54.3988
	B	7.3941	10.2694
	$\sigma_{\min}$ [dB]	0.4757	1.5982

Table 5.3. Parameter comparisons for the 38 GHz LOS scenario

38 GHz LOS results			
Model	Parameters	V-V	V-H
CI	PLE (n)	2.7801	3.1978
	σ_{min}^{CI} [dB]	3.1874	4.1001
FI	α_{FI} [dB]	60.5444	62.1883
	β_{FI}	3.1461	3.6625
	σ_{min}^{FI} [dB]	2.7439	3.5455
SRD	A [dB]	55.9571	58.4581
	B	10.8279	12.6235
	$\sigma_{\min}$ [dB]	0.8253	1.6164

Table 5.4. Parameter comparisons for the 28 GHz NLOS scenario

28 GHz NLOS results			
Model	Parameters	V-V	V-H
CI	PLE (n)	2.8815	3.3303
	σ_{min}^{CI} [dB]	8.1287	10.4790
FI	α_{FI} [dB]	81.8470	87.8146
	β_{FI}	1.0558	0.9722
	σ_{min}^{FI} [dB]	0.7872	0.7796
SRD	A [dB]	80.3789	86.4113
	B	3.5141	3.2516
	$\sigma_{\min}$ [dB]	1.0464	0.9281

Table 5.5. Parameter comparisons for the 38 GHz NLOS scenario

38 GHz NLOS results			
Model	Parameters	V-V	V-H
CI	PLE (n)	2.8207	3.4682
	σ_{min}^{CI} [dB]	1.6822	3.0257
FI	α_{FI} [dB]	65.1057	65.8500
	β_{FI}	2.7254	3.3064
	σ_{min}^{FI} [dB]	1.6283	2.9396
SRD	A [dB]	62.0237	62.7455
	B	8.8539	10.5468
	$\sigma_{\min}$ [dB]	3.3895	5.2621

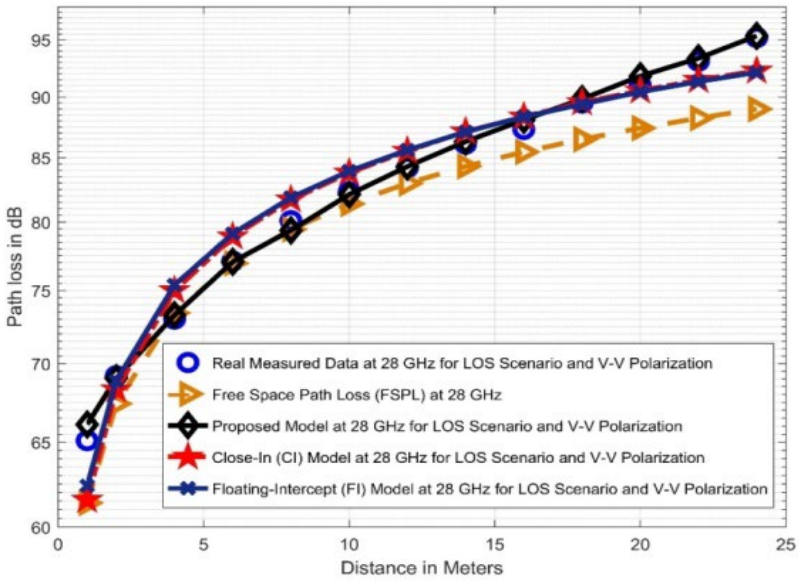

Figure 5.7. Squared root distance PL against distance for 28 GHz LOS at V-V polarization

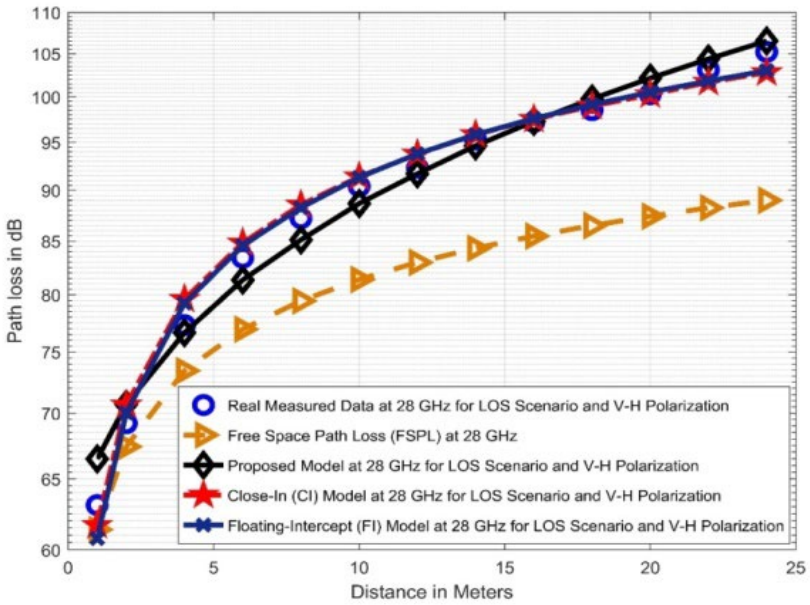

Figure 5.8. Squared root distance PL against distance for 28 GHz LOS at V-H polarization

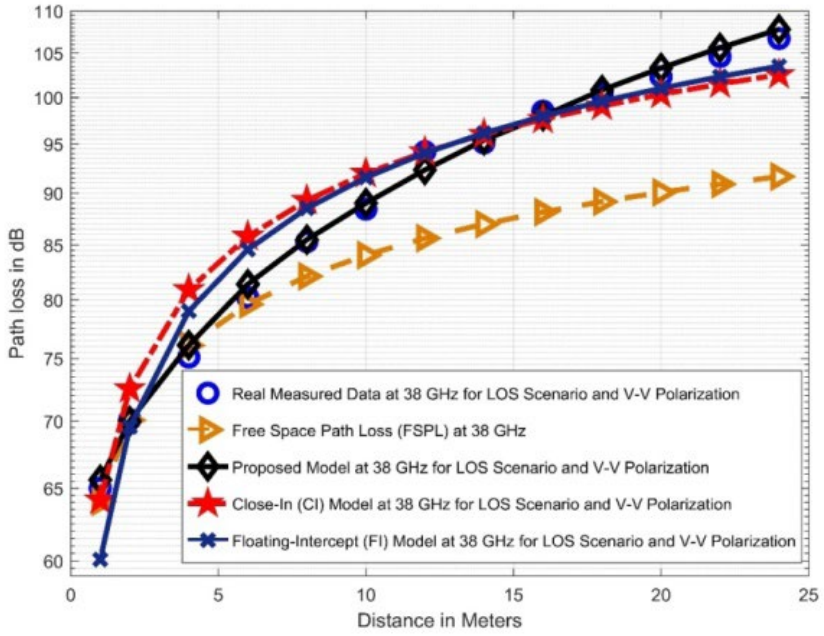

Figure 5.9. Squared root distance PL against distance for 38 GHz LOS at V-V polarization

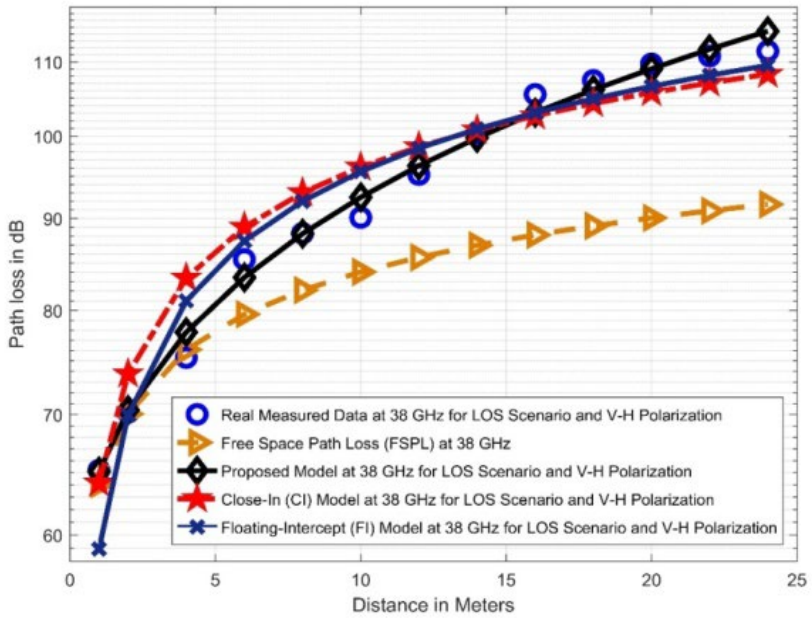

Figure 5.10. Squared root distance PL against distance for 38 GHz LOS at V-H polarization

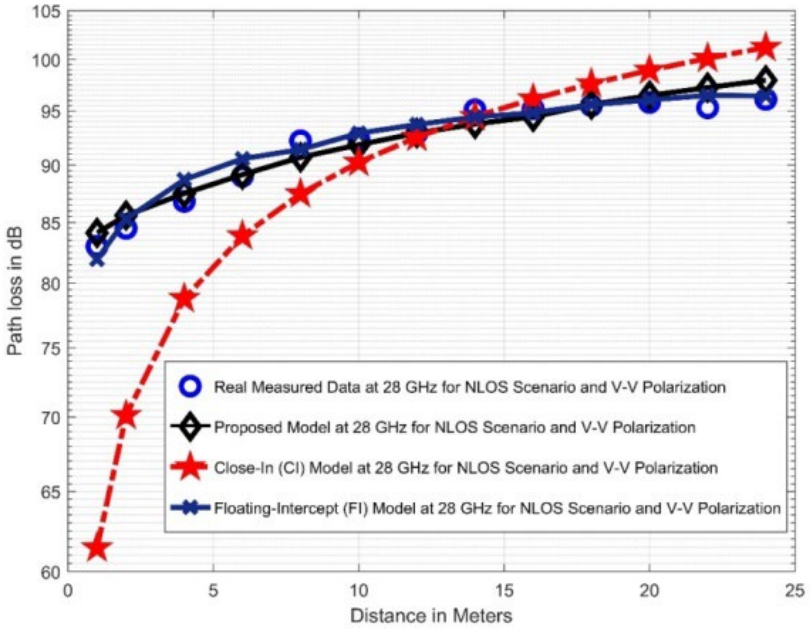

Figure 5.11. Squared root distance PL against distance for 28 GHz NLOS at V-V polarization

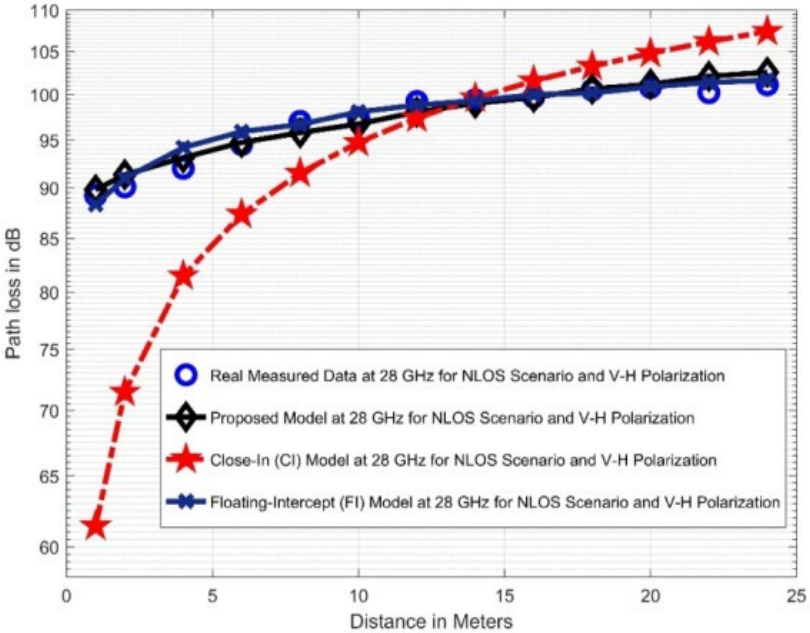

Figure 5.12. Squared root distance PL against distance for 28 GHz NLOS at V-H polarization

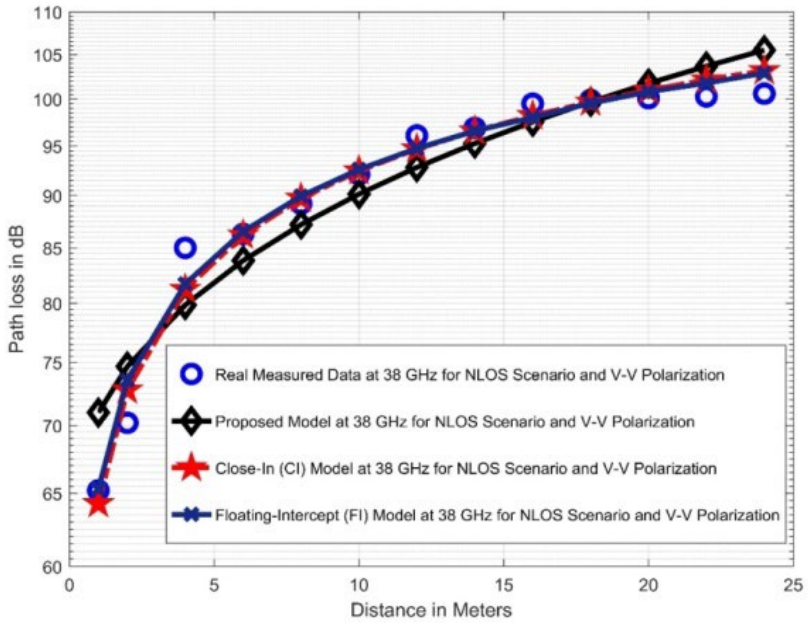

Figure 5.13. Squared root distance PL against distance for 38 GHz NLOS at V-V polarization

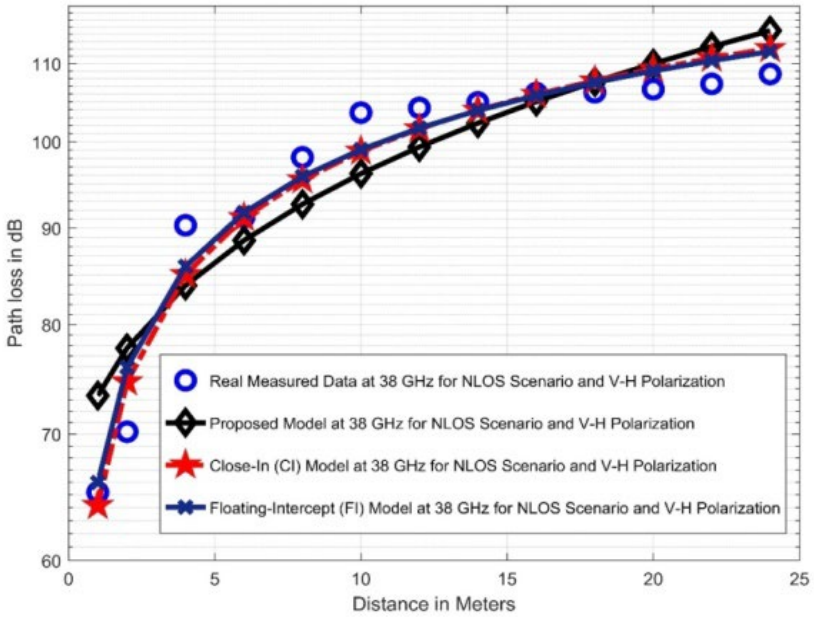

Figure 5.14. Squared root distance PL against distance for 38 GHz NLOS at V-H polarization

Table 5.6. The PLMs' MPE and SDE for the LOS Result at 28 and 38 GHz

	MPE [dB]				SDE [dB]			
Polarization	V-V		V-H		V-V		V-H	
Frequency [GHz]	28	38	28	38	28	38	28	38
Standard CI model	1.5211	2.6632	1.1936	3.6772	0.9044	1.8002	0.7028	1.8593
Improved CI model	0.9884	0.7338	0.5687	1.3580	0.8996	0.4217	0.4791	0.7787
Standard FI model	1.5108	2.2633	1.1306	3.0731	0.8566	1.5534	0.6679	1.7711
Improved FI model	0.5037	0.7528	0.5501	1.2607	0.4011	0.3475	0.4097	0.8274
Squared root distance model	0.3870	0.7587	1.4173	1.3236	0.3060	0.4738	0.8135	0.9582

Table 5.7. The PLMs' MPE and SDE for the NLOS Result at 28 and 38 GHz

	MPE [dB]				SDE [dB]			
Polarization	V-V		V-H		V-V		V-H	
Frequency [GHz]	28	38	28	38	28	38	28	38
Standard CI model	5.6233	1.2904	7.3110	2.5307	5.8432	1.0629	7.4866	1.6403
Improved CI model	3.1018	1.2504	4.0887	1.7985	5.7089	0.8550	7.3067	1.6433
Standard FI model	0.6920	1.2390	0.6325	2.4524	0.5226	1.0647	0.5811	1.6277
Improved FI model	0.7390	1.2163	0.5962	1.8123	0.3806	0.8568	0.4627	1.5247
Squared root distance model	0.9046	2.9861	0.8050	4.7454	0.6094	1.6028	0.5494	2.2730

5.5 Chapter Summary

The main accomplishment of this chapter was the comprehensive performance evaluation of a concise and precise indoor corridor SRD based PLM at higher FBs. In response to the high demand for precise PL prediction models, this chapter analyzed the square root distance model for predicting PL in enclosed environments such as corridors. The MMSE method was used to collect the measurement data from which the parameters of the model were derived. For this study, FBs of 28, as well as 38 GHz were used. In addition, two different antenna polarizations were considered. The model demonstrated its accuracy by maintaining low SF standard deviation values, particularly at LOS, where its maximum value was 1.6 dB. The concept of prediction error was also applied to evaluate the model. The model's MPE and SDE values were found to be within a reasonable range, demonstrating the accuracy of the squared root distance based scheme. Finally, this model can be easily improved in the future by adding a new parameter that makes the model more sensitive to the wireless channel's propagation characteristics for the outdoor environments.

Chapter 6

An Improved Path Loss Model for 5G Wireless Networks in an Enclosed Hallway

This chapter proposes an improved PLM in which the studies demonstrate that the improved propagation model works significantly better than the CI model, owing to its simple setup, precision, and accurate function. Ultimately, this work illustrates that the standard deviation of shadow fading can be significantly reduced in the NLOS scenario (since signal degradation is more in NLOS), implying greater accuracy in making predictions for path loss for wireless communication.

6.1 Introduction

In order to support the over 11 billion mobile linked devices brought about by the internet of things idea, the current development in the wireless communication system is necessitated for information sharing and pervasive wireless connectivity. More mobile devices are connected to the internet than the current capacity, so a larger network with greater encryption and capacity is required [126], [180]. The key barrier is bandwidth, which cannot keep up with the escalating rate of traffic demand by the 6 GHz frequency ranges [55], [130], [181]–[183].

Due to the vast amount of available spectrum, which can support the demands of high data rate and massive capacity, millimeter wave (mmWave) communication is now the best technology for 5G deployment. The frequency range of mmWaves is 3-300 GHz, and their wavelength range is 1-100mm. Due to the existence of unapproved bandwidths that are prepared for usage in next-generation networks and are particularly suitable for 5G networks, the World Radio Conference (WRC) has designated mmWave for 5G implementation. Despite these advantages, employing mmWaves has several disadvantages, such as a restricted beam width, high PL, and higher penetration loss. In particular, because it affects the PLE [52], [88], [147], [184] – [185], this calls for a full understanding of the propagation PLM to be used for 5G mmWave deployment.

Before deploying the full wireless system, it is imperative to examine the propagation path loss in the wireless media. The use of European Cooperation in Science and Technology (COST) and the 3GPP has been the primary method of propagation models from the first to the fifth generation. Studies show that radio system generations endure ten years. With a bandwidth of 40MHz and a singular focus on delivering calling services, the wireless systems initially arrived in 1974. With a 200 kHz bandwidth, the 2G of wireless communication was established in the 1980s by the 3GPP with the intention of offering speech services identical to 1G with the additional capacity of data service. Even though it was initially restricted to the 3GPP spectrum, the International Mobile Telecommunications (IMT) started creating a channel model for the 3G in 2000. Along with enhanced voice services, multimedia application technology is also introduced. The COST model is consequently adopted, followed by the 3GPP model. The fourth generation, or 4G, debuted in 2010 with a 20 MHz capacity increase while retaining the 3GPP advanced format and MIMO technology [40], [186]. The top

data rate for services in this generation is 150 megabits per second. The most recent rollout of 5G in early 2020 makes use of the IMT-2020/3GPP technology of channel models. The majority of nations worldwide are considering using the millimeter wave band to deliver 5G due to the available frequency bands, even if the majority of them still operate in the C band. Up to 20 Gbps of data rates could be offered by 5G [40], [186]–[190].

The 5G data rate has been steadily increasing, requiring more network capacity and improved energy efficiency. The characterization and modeling of channels has been driven by the numerous requirements of the 5G network such as security, traffic latency, reliability, and other major broadcast requirements in diverse applications for successful propagation. This has resulted in a notable improvement in channel performance. Path loss occurs when factors like reflection, refraction, diffraction, scattering, and other atmospheric issues affect the signals along the way. In order to address this issue, an appropriate model for propagation that can measure the PL must be developed, especially for 5G high frequencies. This will make it possible to create a solid system that takes antenna directions and arrays into account while performing link budget analysis and signal strength prediction. It is necessary to construct an accurate model that tends to fit propagation PL parameters in many applications, whether indoor or outdoor situations, because 5G satisfies the desire for huge data consumption in the mmWave band [191]. The importance of PL in mmWave channel transmission cannot be overemphasized in terms of implementation, design, assessment, as well as planning. It establishes the network coverage area, interference ratios, and data speeds. High-fidelity models are therefore necessary since the focal reference affects the wireless network's propagation channel's performance [33]. Various researchers have proposed and supported numerous PLMs, including quantitative and evidence based models based on linear regression quantification. Both indoor and outdoor contexts can be used to quantify PL, but the results are different. Interior route loss models will consider a number of factors, such as the furniture in the indoor office or corridor, indoor designs, construction materials, any smart devices present and human mobility in the surrounding area, among others. The parameters of the received signal are affected by the multipath fading, reflection, scattering, shadowing, PL due to distance, refraction, as well as penetration [33], [192]-[193].

In an indoor setting, mobile communication signals encounter obstructions on their passage from the Tx to the Rx, which increases the PL of the signal [194]. The height disparity between the Tx and Rx is another factor that affects path loss. The PL for the two potential 5G frequencies 28 GHz and 38 GHz is analyzed in this study. Barriers frequently have a greater impact on high-frequency signal transmissions. Radio waves travel differently in indoors depending on the distance between the walls, the materials used for the passage as well as other irregular objects that are placed along the hallway [195].

To the extent that we are aware, there is a limited study in the precise modeling and characterization of the single frequency PLMs that take the antenna height difference of the Tx as well as Rx into account at 28 and 38 GHz frequency bands. This work aims to fill the gap by developing an improved model that allows for easier design and performance evaluation for NLOS situations in indoor passageway surroundings at 28 and 38 GHz. The V-V as well as the V-H polarizations of the antenna were adopted for the measurement. This study proposes to improve the CI PL prediction model. Comprehensive modeling and characterization are essential components of a general model. The results show that the improved model outperforms the conventional CI model. The

research was conducted in an indoor corridor setting on the 5th floor of the building of the Department of EECE at the UKZN in Durban, South Africa.

To gain a good comparison of the existing and new large scale PLMs, a measurement process was done for the scenario in the NLOS for two different antenna polarizations i.e. V-V and V-H polarizations. To create a general model in the mmWave frequency ranges, extensive research and modeling are needed. In the previous study, extensive analysis of indoor corridor propagation for V-V as well as V-H antenna polarizations were performed for the 28 and 38 GHz FBs [126]. However, a novel improved PLM is proposed in this work. Nonetheless, in order to accurately evaluate the established and proposed large-scale PLMs, the process of data gathering by measurement was done for the NLOS, and the results of the propagation parameters are compared. The need to reduce the standard deviation and improve the path loss parameters of these models while maintaining simplicity motivates this work. The rest of the chapter is organized as follows: Section 6.2 encompasses the related works, whilst Section 6.3 discusses the measurement campaign details and large scale PLMs. Section 6.4 encapsulates the results and discussions, while Section 6.5 concludes the work.

6.2 Related Works

Traditional methods for PL forecast characterization are essentially stochastic, deterministic as well as empirical in nature. Site-specific and requiring appropriate knowledge of the propagation environments are requirements for deterministic route loss prediction models. These models, like the ray-tracing models, are frequently connected to 3-D map propagations. These deterministic models also have significant computing cost since they repeat calculations when the environment changes. The Hata model as well as the COST 231 model is two examples of empirical PLMs that are based on measurements and observations. Although these models are simpler to use, they take more time to implement because they call for comprehensive measurement processes in certain settings and network scenarios. Additionally, these models offer poorer prediction accuracy than deterministic models [195]-[198].

Channel modeling characterization for an enclosed surrounding at FBs of 4.5, 28, and 38 GHz is presented in the work of [70]. For 28 GHz as well as 38 GHz FBs, a novel PLM is proposed. Measurements for the interior LOS as well as NLOS situations were taken at every meter over range of 23 meters between the Tx and Rx antenna positions in order to compare the conventional PLMs with a new large-scale generic PLM. Conventional and suggested PLMs for single-frequency, multi-frequency, directional as well as Omni-directional PLMs, were used to examine the results. The outcome shows that the proposed PLM, which has only one variable and is physically centered to the Tx power, can model the large-scale PL over distance more accurately than the well-known models. Also, the absence of physical basis for the transmission signal, have more issues (involve additional parameters), and lack expectation when describing parameter values.

Al-Saman et al. carried out another examination of models in an interior environment for mmWave in terms of PL in 2021. Different PLMs, which include the CI PLM, the 3GPP and WINNER FI PLM, were presented and analyzed for the interior channels at different mmWave FBs. The PLM determines the rate of signal degradation along the propagation path for both LOS and NLOS channels at a specified distance [39]. Further researches on the traditional CI as well as the FI PLMs was adopted for both interior and outdoor airport

environments as a result of additional mmWave propagation research on a 73 GHz measurement campaign at Boise State University and the airport [3]. The study shows that although the PLEs of the CI and the free-space model are substantially similar, however, the FI PLM offers a superior match to the measured data. These data also show how distinctly different the inside airport environment is from other indoor settings due to its roomy and open layout. Additional mmWave propagation study by [143] presented measurement studies at the 30, 140, and 300 GHz FBs in the interior LOS surroundings. The performance of the single-frequency CI, CIF, and ABG PLMs was tested at these FBs. The results show that all four PLMs perform equally, but the PLM with the fewest parameters would be the best choice for simplicity. PL as well as small-scale fading on the corridor were looked into in [66], [199] utilizing antennas operating at 30 GHz. The improved model produced the exact PLE as the FI PLM while requiring less mathematical complexity [66]. In their latest work, Oladimeji.et.al 2023 in [166] analyzed the performance of the improved CI and FI models and observed a remarkable improvement for both the CI and FI PLMs at 28 GHz and 38 GHz. The key findings demonstrated that the improved PLMs outperform the conventional CI and FI PLMs for the LOS as well as NLOS network situations. Also, the stability and sensitivity of the suggested models are also noticeably better than those of the conventional models in both network scenarios.

6.3 PL Measurements and PLMs

Details about the setting for the measurement as well as the propagation PLMs are provided in this section.

6.3.1 Measurement Campaign and Environment

This section explains the measurement campaigns carried out as a wireless communication channel between both the Tx and Rx in a typical indoor passageway. The measurement setup was located in the EECE Departmental building at UKZN Durban, South Africa. The channel sounder was cautiously calibrated prior to the start of the measurements to ensure accurate data collection. Furthermore, we affirmed that there were no interfering signals in the corridor. The wireless propagation channel, as previously stated, is an enclosed interior corridor. This corridor measures 30 m in length, 1.4 m in width, and 2.63 m in height. This corridor is made primarily of bricks and dry concrete, with wooden doors to entrance offices on one side and a staircase and elevator on the other side. The Rohde and Schwarz SMB 100A Signal Generator was used as a Tx, and the Rohde and Schwarz FSIQ 40 Signal Analyzer was used as Rx. Images of the Tx and Rx units used in measurement campaigns are shown in Figures 6.1, 6.2, 6.3, 6.4, and 6.5. The parameter setup as well as equipment setup are shown in Table 6.1. During the campaign, the Tx HA was positioned at one end of the passage, while the Rx HA shifted away from the Tx in 2 m increments up to the opposite end. When both antennas were not aligned toward each other for NLOS. The center FBs used for CW signal transmission between two broadband HAs adopted in both the sending and Rx ends, with Tx HA height of 1.6 m and Rx HA height of 2.3 m, were 28 GHz and 38 GHz. At the Tx end, the antenna was placed for vertical polarization, while the Rx end was placed for vertical polarization and horizontal polarization for the V-V and V-H polarizations, respectively. Figures 6.2 and 6.6 show a comprehensive view of the floor plan and the interior passage. The path loss was calculated using equation (6.1) [130]:

$$P_L = P_t - P_r + G_r + G_t \tag{6.1}$$

Where P_t, P_r, G_t and G_r are the transmitted power, received power, the gain of the transmitting antenna and the gain of the receiving antenna, respectively.

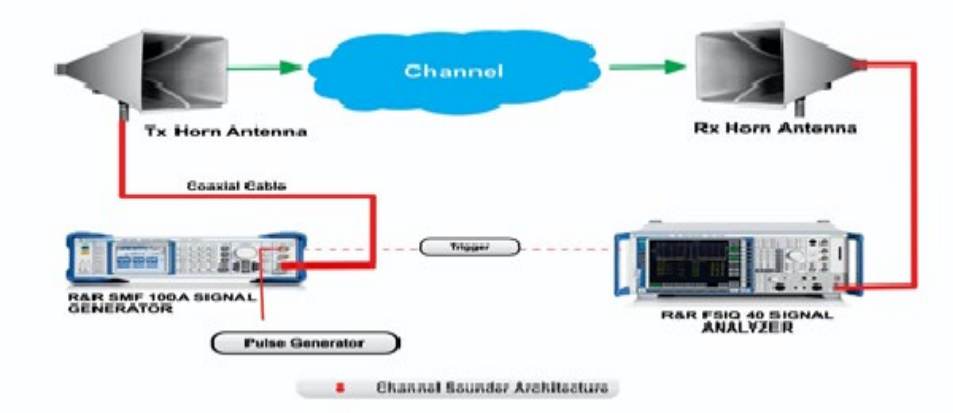

Figure 6.1. Building blocks of the channel settings.

Figure 6.2. The interior passage

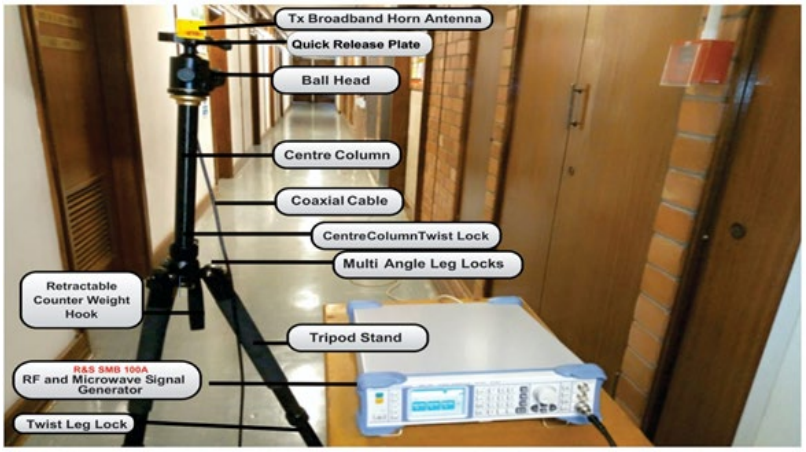

Figure 6.3. Setup for Tx.

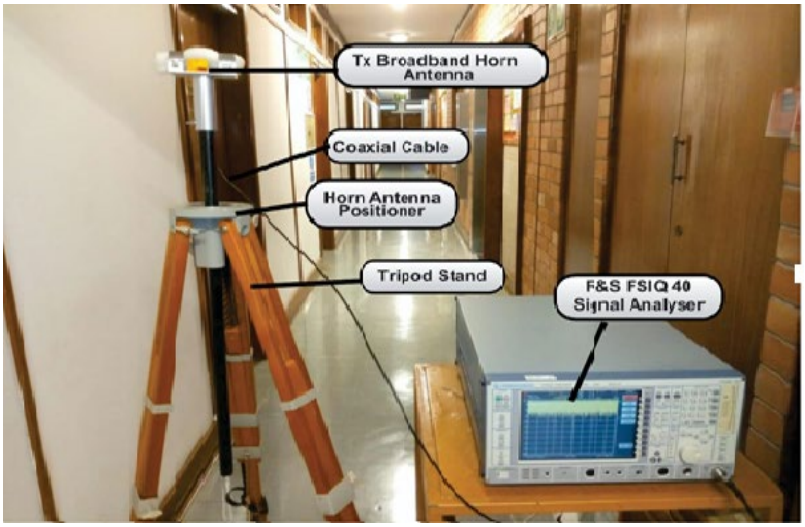

Figure 6.4. Setup for Rx.

Figure 6.5. The Tx and Rx configuration in the indoor passage

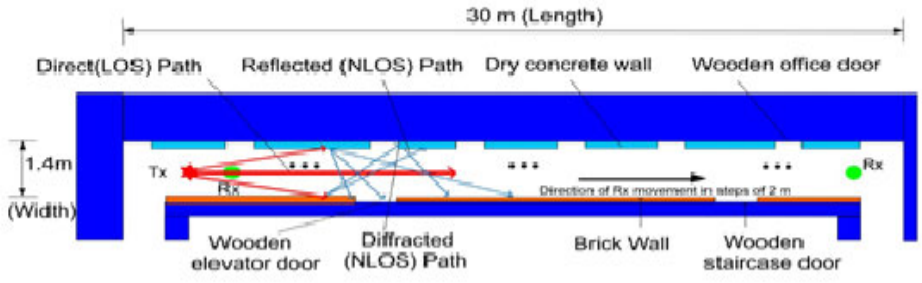

Figure 6.6. A floor plan for the indoor passage.

Table 6.1. Equipment setup parameters′ description for the experiment

Measuring equipment parameters	Configuration/Value	Unit
Centre FBs	28, 38	GHz
Transmission bandwidth	100	MHz
Transmission signal	CW	
Tx and Rx HAs	Broadband HA	
Power of Tx HA	10	dBm
Height of Tx HA	1.6	m
Height of Rx HA	2.3	m
Gain of Tx and Rx HA at 28 GHz	15	dBi
Gain of Tx and Rx HA at 38 GHz	17	dBi
Polarizations of Tx and Rx HA	V/ H	
Dimension of HA (L x W x H)	71 x 32 x 28.6	mm^3
Weight of HA	0.08	Kg

6.3.2 Path Loss in mmWave Propagation

PL is a process that happens when a Tx's signal weakens in the transmission channel due to the propagation channel's properties. The PL is often expressed in dB [39]. When used in wireless propagation, PL is dependent on many factors such as frequency, distance between the antennas, propagation channel properties etc.

6.3.3 Large Scale PL Prediction Model

Radio propagation in physical surroundings affects the quality of wireless communication systems due to the fading of the radio waves. Any wirelessly propagated signal from the transmitting antenna(s) of a communication system is subject to go under degradation over the distances as well as FBs, which is considered as fading (it may either be on a large scale or small scale). The air conditions and nearby physical objects also induce signal losses which results in multipath transmission since the Rx antenna (or antennas) primarily picks up the signal through reflections, diffractions, and scattering mechanisms [110], [160], [195]. Signal power fluctuation and increased signal power uncertainty are also caused by these multipath effects [160], [200]. The PL impacts on the communication signal at the Rx end. It's important to determine how much a signal will diminish and decay as it travels from the Tx to the Rx, taking propagation distance and other factors into account. Some PLMs specify the profile of the topographical to make signal analysis simpler, while others merely use the frequency of the carrier frequency as well as the distance to accomplish their objectives [63], [81]-[82], [84], [87].

6.3.3.1 CI PL Prediction Model

This PLM's fundamental principle is grounded in the point of anchor as well as the reliance on the frequency in empty space. Both the distance (in meters) between the Tx and Rx as well as the reference distance (d_o) are essential. The expression for the CI PLM can be seen in equation (6.2) as follows [126]:

$$P_L^{CI}(d)[dB] = FSPL(f, d_o)[dB] + 10.n.\log\left(\frac{d}{d_o}\right) + X_{\sigma SF}^{CI} \quad (6.2)$$

For $d \geq d_o$, where $d_o = 1m$

Where $X_{\sigma SF}^{CI}$ is a zero mean Gaussian random variable with the standard deviation σ.

$$FSPL(f, d_o)[dB] = 10log_{10}\left(\frac{4\pi d_o}{\lambda}\right)^2 \quad (6.3)$$

To calculate the CI PLM, PLE n is obtained by adopting the MMSE method which commiserates with the recorded measurements.

$$FSPL(f, d_o)[dB] = 10log_{10}\left(\frac{4\pi f d_o}{c}\right)^2 \tag{6.4}$$

$$FSPL(f, 1m)[dB] = 10log_{10}\left(\frac{4\pi f}{c}\right)^2 \tag{6.5}$$

Where c represents the speed of light.

6.3.3.2 Improved CI PL Prediction Model

The improved model includes the other parameters to improve the performance. The parameters of barriers inside the measuring environment were not considered by the existing single slope PLMs. However, the proposed model takes into account the close-in height and obstruction factors. The proposed improved CI-based PLM (PL^{CI-HO}) is expressed as:

$$PL^{CI-HO}(f, d, h) = PL(f, d_0) + 10n\log_{10}(d) + 10k_{CI}\log_{10}(h)^2 + X_\sigma^{CI-HO} \tag{6.6}$$

Where $PL(f, d_0) = 20\log_{10}(4\pi f d_0/c)$ is the FSPL, f is the carrier frequency which is assumed to be 28 GHz or 38 GHz in this study, d_0 is the reference distance which is taken to be 1 meter, n is the PLE of the environment, d is the distance between Tx and Rx, $h(= h_{R_x} - h_{T_x})$ is the difference in Tx height h_{T_x} and Rx height is h_{R_x}. It is assumed that h_{R_x} is larger than h_{T_x}, k_{CI} is the second PLE variable for CI and X_σ^{CI-HO} is shadow fading for CI which is presumed to be zero mean Gaussian distributed random samples with standard deviation σ. In terms of changing antenna heights as reported in the works of [42] and [161], the MSE curves show that the CI model parameters are sensitive. In addition, adjusting the antenna altitude alters the incidence angle of the transmitted signals on obstructions near the receiving antenna. Furthermore, in the work of [33], with the difference in Tx and Rx height during the experiment in the same surroundings used for this investigation, stronger constructive interferences as well as better wave guiding influence in the corridor were observed. Therefore, this approach will pave the way for optimized PL prediction models that take the altitude of the Tx and Rx antennas into consideration. As a result, greater accuracy is provided in predicting PL for the design process as well as for the link budget estimations.

The two parameters in equation (6.6) to be determined are n and k_{CI}. Assuming $A = PL^{CI-HO}(f, d, h) - PL(f, d_0)$, $B = 10\log_{10}(h)^2$, and $D = 10\log_{10}(d)$, then equation (6.2) can be expressed in terms of the shadow fading as:

$$X_\sigma^{CI-HO} = A - k_{CI}B - nD \tag{6.7}$$

The standard deviation of X_σ^{CI-HO} can be obtained using minimum mean squared error (MMSE) as:

$$\sigma^{CI-HO} = \sqrt{\frac{\sum(X_\sigma^{CI-HO})^2}{N}} \tag{6.8}$$

The representation of PL sample numbers is denoted by N. To minimize the error in σ^{CI-HO}, the partial derivative of $\sum(X_\sigma^{CI-HO})^2$ is taken with respect to n and k_{CI} and set the derivatives to zero as follows:

$$\frac{\partial \sum(A-k_{CI}B-nD)^2}{\partial n} = 0 \tag{6.9}$$

$$\frac{\partial \sum(A-k_{CI}B-nD)^2}{\partial k_{CI}} = 0 \tag{6.10}$$

Equations (6.9) and (6.10) are simplified into the following:

$$\sum B^2 k_{CI} + \sum(BD)n = \sum(AB) \tag{6.11}$$

$$\sum(BD)k_{CI} + \sum D^2 n = \sum(AD) \tag{6.12}$$

Equations (6.11) and (6.12) in the matrix for can be written as:

$$\begin{bmatrix} \sum B^2 & \sum(BD) \\ \sum(BD) & \sum D^2 \end{bmatrix} \begin{bmatrix} k_{CI} \\ n \end{bmatrix} = \begin{bmatrix} \sum(AB) \\ \sum(AD) \end{bmatrix} \tag{6.13}$$

Therefore, the improved close in parameters can be determined in closed form as:

$$\begin{bmatrix} k_{CI} \\ n \end{bmatrix} = \begin{bmatrix} \sum B^2 & \sum(BD) \\ \sum(BD) & \sum D^2 \end{bmatrix}^{-1} \begin{bmatrix} \sum(AB) \\ \sum(AD) \end{bmatrix} \tag{6.14}$$

6.4 Results and Discussion

This part discusses the improved model's performance results in the NLOS scenario. Figures 6.7, 6.8, 6.9, and 6.10 represent the variation of the measured path loss, CI, as well as proposed PLM for the two frequencies and two antenna polarizations in the NLOS scenario. There was clear evidence that both models appropriately match the measured path loss, despite the significant superiority of performance in the curves of the proposed improved CI PLM. The parameters in Table 6.2 show that the SFSD when using the proposed improved CI PLM has better values 6.7717 dB for 28 GHz for V-V, 9.173 dB for 28 GHz for V-H, 0.3959 dB for 38 GHz for V-V, and 1.2852 dB for 38 GHz for V-H. When the proposed improved PLM is used, the PLE, which is a major factor used in characterization of large scale impacts of the propagation channel, is improved substantially. The PLE values for the improved PLM are 1.69 for 28 GHz for V-V, 1.74 for 28 GHz for V-H, 0.4351 for 38 GHz for V-V) and 0.3036 for 38 GHz for V-H. The values of k_{CI} rise as the antenna polarization shifts from V-V to V-H at both FBs.

Figure 6.7 shows that the improvement in the prediction of path loss for the improved PLM from the distance greater than 12m, despite the fact that there is similarity in the V-H polarization as shown in Figure 6.8, but the level of improvement is still better for V-V polarization. However, when looking at Figures 6.9 and 6.10, the improved PLM provides better performance for the distance starting from less than 10m. Even though the Figures 6.7, 6.8, 6.9, and 6.10 show that the improved PLM provides better performance, the higher path loss is understandable at higher frequencies. Also looking at the SFSD, at the two frequencies, the betterment of the results is observed as the improved model minimizes the SFSD in the two FBs. Ultimately, the proposed improved CI model has been demonstrated to be suitable for the indoor environments.

Table 6.2: A comparison of the parameters of the Improved-CI & CI PLMs in NLOS.

Frequency		28 GHz		38 GHz	
Polarization		V-V	V-H	V-V	V-H
CI PLM	PLE (n)	2.8815	3.3303	2.8207	3.4682
	σ_{min}^{CI} [dB]	8.1287	10.4790	1.6822	3.0257
Proposed Improved Model	PLE (n)	1.1850	1.5879	2.3856	3.1646
	k_{CI}	8.1178	9.4686	2.1631	2.3922
	σ_{min}^{CI} [dB]	1.357	1.306	1.2863	1.7405

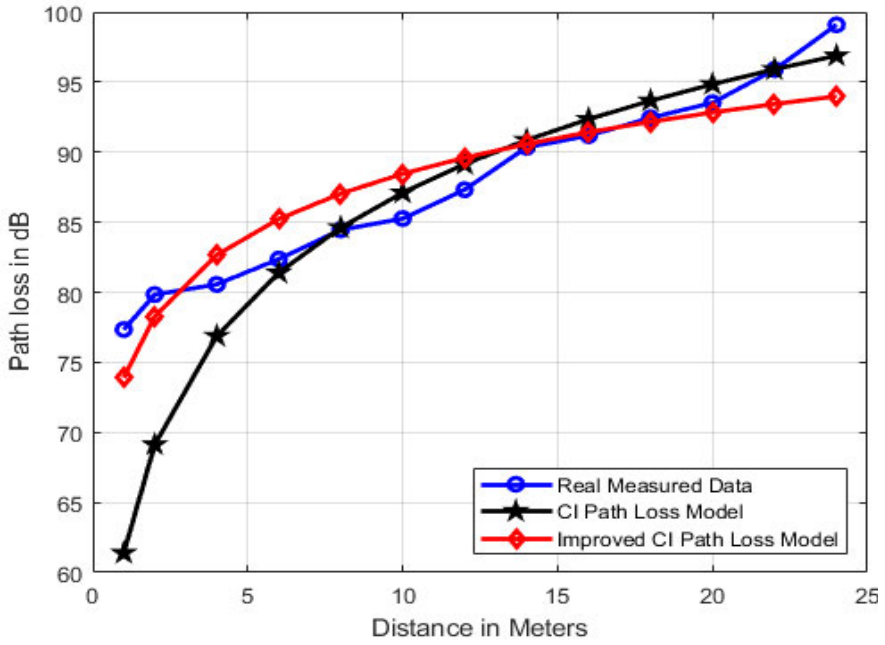

Figure 6.7. Improved-CI PL against distance for 28 GHz NLOS at V-V polarization

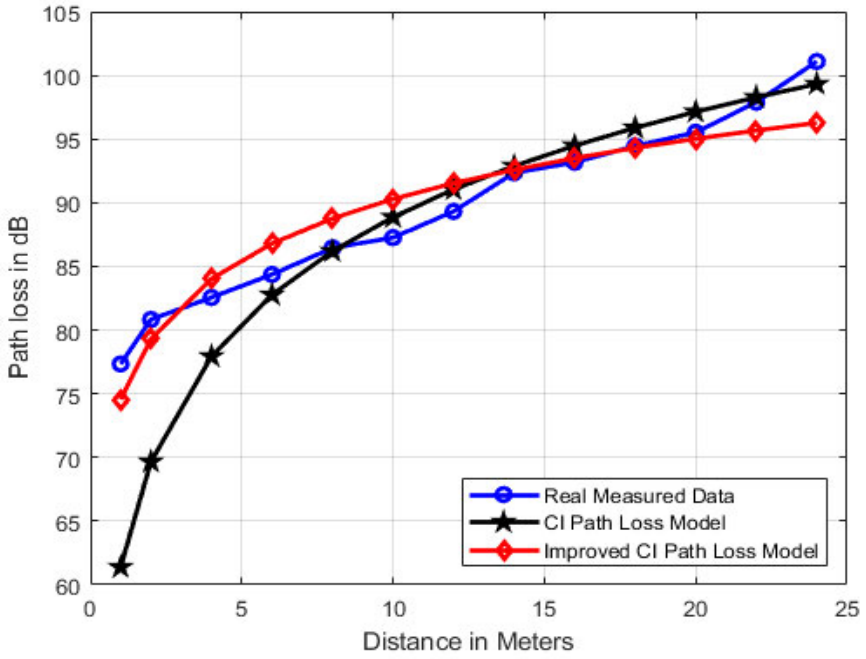

Figure 6.8. Improved-CI PL against distance for 28 GHz NLOS at V-H polarization

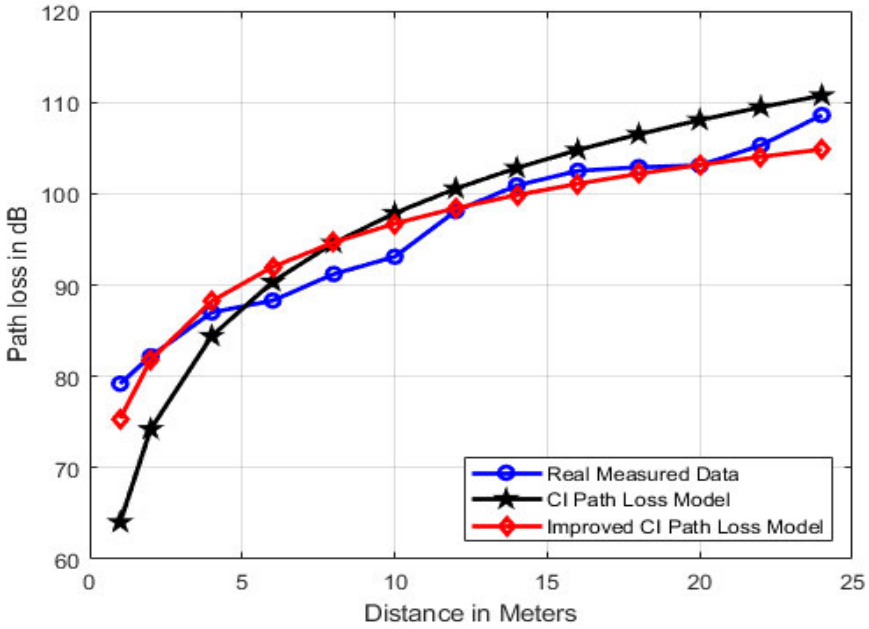

Figure 6.9. Improved-CI PL against distance for 38 GHz NLOS at V-V polarization

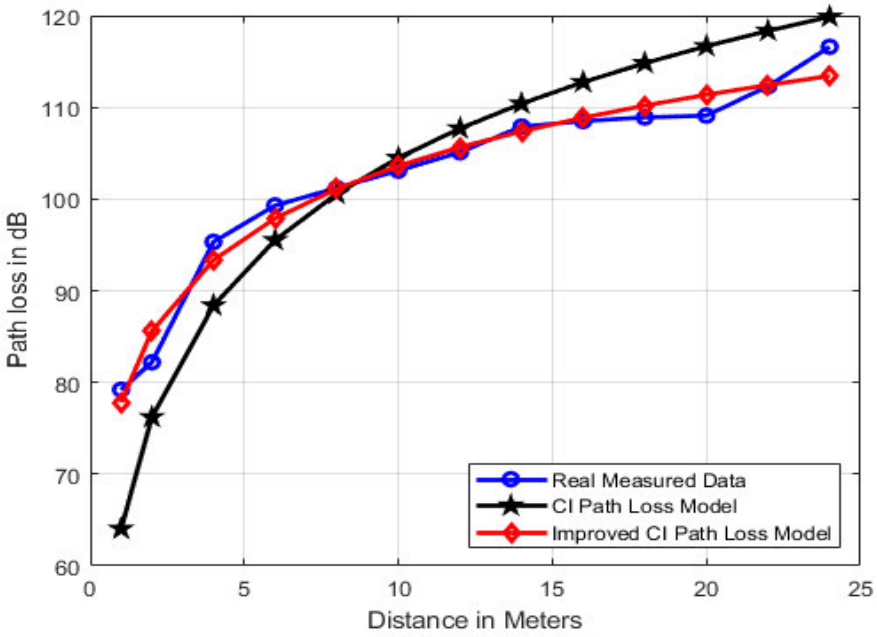

Figure 6.10. Improved-CI PL against distance for 38 GHz NLOS at V-H polarization

6.5 Chapter summary

An improved version of the CI PLM has been presented in this chapter. The model's performance was validated by using the CI PLM and the measured values. In a typical indoor corridor scenario, data was gathered for the two FBs, 28 and 38 GHz NLOS for the vertical to vertical and vertical to horizontal polarizations. The improved PLM outperforms when compared to the conventional CI PLM. The free space reference distance of 1 m was established in the CI path loss model because it enhances the stability of the model. The main achievement of this work has been that the improved CI PLM performs better than the standard CI PLM in a number of ways. The improved CI PLM provides prediction of PL with less error, reduction in the SF's standard deviation, and better sensitivity as well as consistency with antenna polarization variations, which make the model suitable for estimating the path loss at mmWave frequencies in enclosed indoor corridors.

Chapter 7

Conclusions and Recommendations

7.1 Conclusions

High data rate wireless communications are essential, and the mmWave technology plays a significant role to address this issue. The requirements for greater capacity, high dependability, data rates, and quality for a number of applications have been met by a variety of current wireless communication systems. The mmWave technology makes proper use of frequencies that are not employed but have potential applications. Despite the fact that millimeter wave technology has been in use for some time, with the advent of process technology, this technique has begun to receive widespread acceptance among academics and industries. However, after building a communication channel that spans the capacity and dependability of data rates, the path loss exponent is one major metric that a good communication channel depends on it. The development of a good path loss prediction model for these bands still depends on detailed characterization, analysis, and modeling in these frequency bands, despite the fact that research in this field is ongoing. Different path loss model concepts have been proposed by various academics, particularly in indoor environments. The most important use of path loss models which is applicable in the calculations of power budgets, modulations, forecasts of cellular coverage/interferences, and the design of coding schemes is highly critical. This research, which offers LOS and NLOS measurement data scenarios in an indoor corridor environment, assesses CI and FI path loss prediction models for frequency ranges of 28 and 38 GHz. It also utilizes various improvements of the CI and FI path loss prediction models which will be useful in designing 5G wireless communication systems for indoor environments, particularly for power budget calculations in wireless networks. The findings reported in chapters 2, 3, 4, 5, and 6 lead to the following conclusions.

In the chapter two, the literature review along with essential basics of mmWave propagation has been discussed. It also studies the comparison of path loss performance analysis of the three commonly used models: CI, FI, and ABG models. The review looked at how to determine the efficient path loss models which is a major challenge in millimeter wave propagation. The chapter also focused on the measurement work done in millimeter wave research in interior environments. The analysis of path loss and shadow fading in different frequency bands is presented. This work is helpful for the design engineers and researchers to calculate power budgets for a suitable 5G and even forecasted 6G wireless network in an inside environment. Another purpose of this chapter is a thorough understanding of the best path loss model, especially for interior situations, and to improve it in future research to provide a better line of fit and simplicity among the three fundamental path loss models: CI, ABG, and FI. In both LOS and NLOS scenarios, the study found that the CI free space reference model and the FI path loss models are suitable path loss models for indoor millimeter wave propagation.

In chapter three, the analysis of the large-scale path loss models for an indoor corridor environment at frequencies of 28 and 38 GHz has been presented. The measurement environment consists of an indoor corridor with both LOS and NLOS scenarios using V–V and V–H antenna polarizations. The single-frequency CI and FI free space large-scale path loss models and measured data from the measurement campaign were used to evaluate the performance analysis. The work also focused on various parameters, such as standard deviation, PLE, accuracy, simplicity, and stability of the models. The analysis focused on the peculiarity of the effect of

the wall proximity on the path loss parameters as well as comparisons with the parameters in some of the reviewed literature studies. The FI and CI models produced comparable results for both antenna polarizations and clearly fit with the measured path loss. The LOS study results showed that when changing the antenna polarization from V–V to V–H at 28 GHz, the path loss values increased, but only slightly at 38 GHz, indicating that signal degradation was not too noticeable when changing the antenna polarization at 38 GHz. However, in the NLOS scenario, the PLE was higher at 38 GHz when compared to 28 GHz for both antenna polarizations. This was due to greater dispersion and penetration losses at higher frequencies. The minimum standard deviation values for CI and FI were quite near to one another for 28 GHz at both antenna polarizations. However, the minimum standard deviation for the 38 GHz frequency increased from 2.7 in the V–V polarization to 3.59 in the V–H polarization. The V–V antenna polarizations had better accuracy and path loss efficiencies than the V–H polarizations in both scenarios and frequencies, according to the results in both antenna polarizations. The PLE is much higher in the NLOS scenario with V–H polarization due to the signal degradation along the path from the Tx to the Rx. This is because there is no direct LOS between the Tx and Rx antennas. The Rx only relies on signal diffractions and reflections from obstacles as it transmits through the path from the Tx antenna. The path loss measurements and model analysis presented here are useful in designing 5G wireless communication systems for indoor environments, particularly for power budget calculations.

The importance of the path loss in millimeter wave channel propagation cannot be taken for granted in terms of deployment, design, performance assessment, and planning. The path loss helps to determine the network's geographic coverage. Although many path loss models, including statistical and empirical models based on measurement and linear regression, have been proposed by various researchers, high fidelity is required to determine the performance of the wireless network's channel. The validation of the improved version of the well-known CI and FI path loss models at frequency bands of 28 and 38 GHz has been presented in chapter four. The measurement surroundings comprised of an enclosed passageway with V-H and V-V antenna polarizations. One of the key findings of this study is that the enhanced versions of these models typically perform better in terms of consistency than the standard models thereby justifying their high accuracy level. The third order as well as the improved versions of the CI and the FI models demonstrated a significant improvement for various antenna polarizations. The MPE and SDE also show how precisely and accurately the third order and the improved models predict the path loss. Additionally, the improved models provide the reasonable responsiveness and uniformity of the parameters with the change in the antenna polarization and lower the shadow fading's standard deviation in LOS as well as NLOS situations. The results confirm that the modified versions of CI and FI models predict path loss better in an enclosed environment for 5G networks. In addition, after verifying the precision of the improved CI as well as FI models used in this study, the findings also demonstrated that these models' fundamental use is suitable for LOS and NLOS indoor environments and for various antenna polarizations at millimeter wave frequencies. Also, noteworthy is the fact that the design engineers and researchers will benefit from the values of MPE and SDE in order to make accurate computation of the system design which covers all surroundings as well as connectivity scenarios.

Chapter five examines a path loss prediction model based on SRD measurement for wireless services in enclosed spaces. The CI free space reference distance model as well as the FI model is employed to evaluate and

assess this model. This research also contains an improved CI as well as FI method to assess the consistency of the SRD model utilizing two main error benchmarks: MPE and SDE. The chapter's main results indicate that the SRD model, which perfectly aligns the measurement data, offers good precision for predictions in the two frequencies. The model demonstrated its accuracy by maintaining low SF standard deviation values, particularly at LOS. The concept of prediction error was also applied to evaluate the model. The model's MPE and SDE values were found to be within a reasonable range, demonstrating the accuracy of the squared root distance measurement-based scheme. Besides that, when contrasted with the conventional CI and FI models, the squared root distance path loss models have better performance in terms of mean prediction error and standard deviation error. Ultimately, this analysis showed that the standard deviation of shadow fading can be substantially lowered in LOS as well as NLOS, suggesting greater accuracy in estimating path loss.

Given the disparity in signal transmission properties for both current bandwidths and mmWave radio frequencies, the present propagation models used for low frequency range up to few gigahertz are not suitable to be utilized for the PL modeling techniques as well as modulation schemes for the high frequency ranges such as mmWave spectra. As a result, rigorous research on link analysis as well as PL modeling are needed to create a broad and suitable transmission scheme with modeling variables that can handle a broad spectrum of mmWave frequency spectra. Chapter six presented an improved CI path loss model for an indoor space operating in the 28 and 38 GHz range bands. The results for the NLOS situations were collected every two meters over spacing of 24m separating the transmitting and receiving antenna locations to make a comparison the well-known and improved large-scale generic PLMs. The proposed model has the advantage of offering a broad form of model for PL prediction in mmWave propagation in addition to taking height difference into account. The precision of the model that the planning engineers will use to build wireless systems and determine the link budget has not much increased. This work demonstrates that the suggested model is more accurate for estimating the path loss at mmWave frequencies in enclosed indoor situations, including corridors. Finally, the results demonstrate that the improved propagation model works significantly better than the CI model, owing to its simple setup, precision, and accurate function.

7.2 Possible Future Prospects

AI enabled channel measurements as well as modeling techniques are just a few of the aspects where this research has opened up a scope of site investigations that will aid in the design of the channel interface budget analysis for future wireless connections. This study has also developed a good understanding of millimeter wave channel propagation, laying the groundwork for future work in the terahertz frequency spectrum to realize various applications aimed at wireless operations in 6G technology.

Furthermore, there is a need to use machine learning techniques in the prediction of propagation path loss for wireless communication. Also, there is also requirements of development of improved propagation models for outdoor environments, particularly in the current deployment of 5G networks as well as future generation wireless network planning**.**

References

[1] A. K. Jain, Acharya, R. S Jakhar, and T. Mishra, "Fifth Generation (5G) Wireless Technology Revolution in Telecommunication*", 2018 Second International Conference on Inventive Communication and Computational Technologies (ICICCT*), pp. 1867-1872, 2018.

[2] D. Liang , "Adaptive antenna systems for mobile broadband communications" *Texas Scholars work, The University of Texas* , Austin, USA, 2002.

[3] M. Khatun, C. Guo, L. Moro, D. Matolak, and H. *Mehrpouyan, "Millimeter-wave path loss at 73 GHz in indoor and outdoor airport environments", 2019 IEEE 90th Vehicular Technology Conference (VTC2019-Fall),* pp,1-5. 2019

[4] N. Hosseini, M. Khatun, C. Guo, K. Du, O. Ozdemir, D. Matolak, I. Guvenc, and H. Mehrpouyan, "Attenuation of several common building materials in millimeter-wave frequency bands: 28, 73 and 91GHz," *IEEE Antenna and Propagation Magazine*, vol. 63, pp. 40-50,2021.

[5] T. S. Rappaport, R. W. Heath Jr, R. C. Daniels, and J. N. Murdock, "Millimeter wave wireless Communications". *Englewood Cliffs,* NJ, USA: Prentice Hall, 2015.

[6] C.A. L. Diakhate: Propagation Channel Modeling at Centimeter–and–Millimeter–Wave Frequencies in 5G Urban Micro–cell Context. *A thesis submitted to Paris-Saclay University, Paris* in partial fulfilment for the degree of Philosophy in Information communication technology.

[7] F. Rusek, D. Persson, B. K. Lau, E. G. Larsson, T. L. Marzetta, O. Edfors, and F. Tufvesson, "Scaling up mimo: Opportunities and challenges with very large arrays*," IEEE Signal Processing Magazine*, vol. 30, pp. 40–60, 2013.

[8] M. Wen, B. Zheng, K. J. Kim, M. Di Renzo, T. A. Tsiftsis, K. Chen, and N. Al-Dhahir, "A survey on spatial modulation in emerging wireless systems: Research progresses and applications," *IEEE Journal on Selected Areas in Communications*, vol. 37, pp. 1-22, 2019.

[9] International Telecommunication Union, Guidelines for evaluation of radio interface technologies for IMT2020, 2017. https://www.itu.int/dms_pub/itu-r/opb/rep/R-REP-M.2412-2017-PDF-E.pdf

[10] D. P. He, B. Ai, K. Guan, L. H. Wang, Z. D. Zhong, T. Kurner, "The Design and Applications of High Performance Ray-Tracing Simulation Platform for 5G and Beyond Wireless Communications: A Tutorial," *IEEE Communications Surveys and Tutorials*, vol. 21, pp. 10-27, 2019.

[11] T.S. Rappaport. Wireless communications: principles and practice. Prentice Hall PTR New Jersey, 1996. 2, 4, 13, 17, 63

[12] H. Hashemi, "The indoor radio propagation channel". *In Proceedings of the IEEE,* Spokane, WA, USA, vol. 81; pp. 943–968, 1993.

[13] https://www.qualcomm.com/news/onq/2019/05/what-new-indoor-opportunities-will-5g-nr-mmwave-bring. Retrieved 10.02 am, December 1st 2022.

[14] L. Possenti, M. Barbiroli, E. M. Vitucci, F.Fuschini, M. Fosci, and V. Degli-Esposti, "A Study on mm-wave Propagation in and around Buildings", *arXiv:2210.06883v1* [eess.SP] pp. 1-10, 2022

[15] G. R. MacCartney, Jr., S. Deng, and T. S. Rappaport, "Indoor Office Plan Environment and Layout-Based MmWave Path Loss Models for 28 GHz and 73 GHz," *published in 2016 IEEE 83rd Vehicular Technology Conference Spring (VTC 2016-Spring),* pp. 1-6, 2016.

[16] G. R. MacCartney, J. Zhang, S. Nie, and T. S. Rappaport, “Path Loss Models for 5G Millimeter Wave Propagation Channels in Urban Microcells”, *2013 IEEE Global Communications Conference (GLOBECOM),* pp. 3948-3953, 2013,

[17] X. Zhang, G. Qiu, J. Zhang, L. Tian, P. Tang and T. Jiang, "Analysis of millimeter-wave channel characteristics based on channel measurements in indoor environments at 39 GHz", *in Proc. 11th Int. Conf. Wireless Commun. Signal Process. (WCSP)*, pp. 1-6, 2019.

[18] D. Chizhik, J. Du, R. Feick, M. Rodriguez, G. Castro and R. A. Valenzuela, "Path Loss and Directional Gain Measurements at 28 GHz for Non-Line-of-Sight Coverage of Indoors with Corridors,″ *IEEE Trans. Antennas Propag.,* vol. 68, pp. 4820-4830, 2020,

[19] K. Haneda, J. Jarvelainen, A. Karttunen, M. Kyro and J. Putkonen, "A statistical spatio-temporal radio channel model for large indoor environments at 60 and 70 GHz*″, IEEE Trans. Antennas Propag.,* vol. 63, pp. 2694-2704, 2015.

[20] K. Wangchuk, K. Umeki, T. Iwata, P. Hanpinitsak, M. Kim, K. Saito, et al., "Double directional millimeter wave propagation channel measurement and polarimetric cluster properties in outdoor urban pico-cell environment", *IEICE Trans. Commun.,* vol. E100.B, pp. 1133-1144, 2017.

[21] H. Ding et al., "Ray-tracing Based Channel Clustering and Analysis at 28 GHz in Conference Environment," *in Proc. 2020 14th European Conference on Antennas and Propagation (EuCAP)*, pp. 1-5, 2020.

[22] M. Kim, T. Iwata, K. Umeki, K. Wangchuk, J.-I. Takada and S. Sasaki, "Simulation based mm-wave channel model for outdoor open area access scenarios," *in Proc. 2016 URSI Asia-Pacific Radio Science Conference (URSI AP-RASC)*, pp. 1292-1295,2016.

[23] J. Järveläinen, K. Haneda and A. Karttunen, "Indoor Propagation Channel Simulations at 60 GHz Using Point Cloud Data," *IEEE Trans. Antennas Propag.,* vol. 64, pp. 4457-4467, 2016.

[24] I. Rodriguez et al., "Analysis of 38 GHz mmWave Propagation Characteristics of Urban Scenarios," *in Proc. 21th European Wireless Conference*, pp. 1-8, 2015.

[25] T. S. Rappaport, Y. Xing, G. R. MacCartney, Jr., A. F. Molisch, E. Mellios, J. Zhang, “Overview of Millimeter Wave Communications for Fifth-Generation (5G) Wireless Networks-with a focus on Propagation Models”, *IEEE Transactions on Antennas and Propagation*, vol. 65, pp. 6213-6230, 2017,

[26] S Salous, E.V Degli, F. Fuschini, D. Dupleich, R. Müller, R.S Thomä, K. Haneda, G. Molina, Jose-Maria, G.J. Pascual, D.P Gaillot,M. Nekovee, S. Hur, R. Müller, “Millimeter-Wave Propagation Characterization and Modelling towards 5G Systems”, *IEEE Antennas and Propagation Magazine*, vol. 58, pp. 115-127, 2016.

[27] http://www.eng.tau.ac.il/~dbl/mmw.htm. Retrieved 10th August 2021. 10.59am.

[28] J. Caruso, “Copper 10 gigabit ethernet NICs unveiled”, Network World, 2007.

[29] K. C. Huang and Z. Wang, “Millimeter Wave Communication Systems”, *Institute of Electrical and Electronics Engineers,* John Wiley & Sons, Inc. Piscataqay, New Jersey, 2011.

[30] W. I. Way, “Spectrally efficient parallel PHY for 100GbE MAN and WAN”, *IEEE Commun. Mag.*, vol. 45, pp. 20–23, 2007.

[31] K. C. Huang and Z. C. Wang, “Millimeter-Wave Circular Polarized Beam-Steering Antenna Array for Gigabit Wireless Communications”, *IEEE Trans. Antennas Propag.*, vol. 54, pp. 743–746, 2006.

[32] R. C. Qiu, H. Liu, and X. Shen, "Ultra-Wideband for Multiple Access Communications", *IEEE Commun. Mag.*, vol. 43, pp. 80–87, 2005.

[33] N. O. Oyie and T. J. O. Afullo, "Measurement and Analysis of Large Scale Path Loss Model at 14 and 22 GHz indoor Corridor", *IEEE Access*, vol. 4,pp. 1-12, 2018.

[34] N. A. Muhammad, P. Wang, Y. Li, B. Vucetic, "Analytical Model for Outdoor Millimeter Wave Channels Using Geometry-Based Stochastic Approach", *IEEE Transactions on Vehicular Technology,* vol. 66, pp. 912-926, 2016.

[35] M. R. Akdeniz, Y. Liu, M. K. Samimi, S. Sun, S. Rangan, T. S. Rappaport, E, Erkip, "Millimeter Wave Channel Modeling and Cellular Capacity Evaluation", *IEEE Journal on Selected Areas in Communications.* vol. 32, pp. 1164-1179, 2014.

[36] M Lecci, P Testolina, M Giordani, M Polese, T Ropitault, C Gentile, "Simplified Ray Tracing for the Millimeter Wave Channel: A Performance Evaluation", *A publication of National Institute of Technology (NIST), Information Theory and Applications Worksho*p (ITA), Gaithersburg, 2020.

[37] https://micro.magnet.fsu.edu/primer/lightandcolor/electromagintro.html/retrieved 1st August 2022, 9.05am

[38] https://www.accton.com/Technology-Brief/the-emergence-of-5g-mmwave/retrieved 1st August 2022, 9.05am

[39] A. Al-Saman, M. Cheffena, O. Elijah, Y. A. Al-Gumaei, S.K, AbdulRahim, T, Al-Hadhrami, "Survey of Millimeter-Wave Propagation Measurements and Models in Indoor Environments", *Electronics,* vol. 10, 1653, 2021.

[40] A. F. Molisch, "Wireless Communications", Second Edition, 2011 John Wiley & Sons, Ltd, *A John Wiley and Sons, Ltd., Publication,* ISBN 978-0-470-74187-0 (cloth) – ISBN 978-0-470-74186-3, 2011.

[41] M. K. Elmezughi, T. J. Afullo and N.O. Oyie, "Performance Study of Path Loss Models at 14, 18, and 22 in an Indoor Corridor Environment for Wireless Communications", *SAIEE Africa Research Journal*, vol. 112, pp. 32-45, 2021.

[42] M. K. Elmezughi, T. J. Afullo, and N. O. Oyie, "Investigating the Impact of Antenna Heights on Path Loss Models in an Indoor Corridor Environment", *icABCD 2020 Conf., IEEE*, pp. 1–7, 2020.

[43] M. K. Elmezughi and T. J. Afullo, "An Efficient Approach of Improving Path Loss Models for Future Mobile Networks in Enclosed Indoor Environments", *IEEE Access*, vol. 9, pp. 110332–110345, 2021.

[44] M. Elmezughi, and T. Afullo, "Investigations into the Effect of High-Ordering the Log-Distance Dependency of Path Loss Models for Indoor Wireless Channels" *International Journal on Communications Antenna and Propagation*, vol. 12, pp. 1-12, 2022.

[45] N. Faruk, I. Y. Abdulrasheed, N. T. Surajudeen-Bakinde, E. Adetiba, A. A. Oloyede, A. Abdulkarim, O.Sowande, A. H. Ifijeh, A. A. Atayero, "Large-Scale Radio Propagation Path Loss Measurements and Predictions in the VHF And UHF Bands", *Heliyon*, vol. 7, pp. 1-15, 2021.

[46] C. Seker, M. T. Guneser, and H. Arslan, "Millimeter-Wave Propagation Modeling and Characterization at 32 GHz in Indoor Office for 5G Networks", *The International Journal of RF and Microwave Computer-Aided Engineering,* vol.30, pp. 1-12, 2020.

[47] Z. Lin, X. Du, H. Chen, B. Ai, Z. Chen, and D. Wu, "Millimeter Wave Propagation Modelling and Measurements for 5G Mobile Network*", IEEE Wireless Communications,* vol. 26, pp. 72 - 77,2019.

[48] M. E. Hajj, G. Zaharia, G. E. Zein, H. Farhat and S. Sadek, "Millimeter-Wave Propagation Measurements at 60 GHz in Indoor Environments", *2019 International Symposium on Signals, Circuits and Systems (ISSCS)*, pp. 1-4, 2019.

[49] C. Han and S. Duan, "Impact of Atmospheric Parameters on the Propagated Signal Power of Millimeter-Wave Bands Based on Real Measurement Data", *IEEE Access*, vol. 7, pp. 113626 – 113641, 2019.

[50] S. H. Gade, S. S. Ram, S. Deb, "Millimeter Wave Wireless Interconnects in Deep Submicron Chips: Challenges and Opportunities", *Integration,* vol. 64, pp. 127-136, 2019.

[51] M. M. Abdulwahid, O. A. S. Al-Ani, M. F. Mosleh, and R. A. Abd-Alhmeed, "Investigation of Millimeter-Wave Indoor Propagation at Different Frequencies", *4th Scientific International Conference Najaf (SICN)*, pp 25-30, 2019.

[52] A. M. Al-Samman, M.H Azmi, Y.A Al-Gumaei, T Al-Hadhrami, T.Abd. Rahman, Y. Fazea, A. Al-Mqdashi, "Millimeter Wave Propagation Measurements and Characteristics for 5G System", *Applied Sciences,* vol. 10, pp. 1-17, 2020.

[53] J. Xiao, C. Zhao, X. Feng, X. Dong, J. Zuo, J.Ming , and Y. Zhou, "Review on the Millimeter-Wave Generation Techniques Based on Photon Assisted for the RoF Network System", *Advances in Condensed Matter Physics,* vol. 10, pp. 1-14, 2020.

[54] G. Chittimoju and U.D.Yalavarthi, "A Comprehensive Review on Millimeter Waves Applications and Antennas", *Journal of Physics:* Conference Series, vol. 1804, pp. 1-8, 2021

[55] J. Gui, X. Dai, and X. Deng, "Stabilizing Transmission Capacity in Millimeter Wave Links by Q-Learning-Based Scheme", *Hindawi, Mobile Information Systems,* vol. 2020, pp. 1-17, 2020.

[56] A. Maltsev, R. Maslennikov, A. Sevastyanov, A. Khoryaev, and A. Lomayev, "Experimental Investigations of 60 GHz WLAN Systems in Office Environment", *IEEE J. Sel. Areas Commun.*, vol. 27, pp. 1488–1499, 2009.

[57] F. Fuschini, S. Häfner, M. Zoli, R. Müller, E. M. Vitucci, D. Dupleich,M. Barbiroli, J. Luo, E. Schulz , V. Degli-Esposti, and R. S. Thomä , "Analysis of In-Room mm-Wave Propagation: Directional Channel Measurements and Ray Tracing Simulations", *J Infrared Milli Terahz Waves,* vol. 38, pp. 727–744, 2017.

[58] M. Wang, Y. Liu, S. Li, and Z. Chen, "60 GHz Millimeter-Wave Propagation Characteristics in Indoor Environment", *9th IEEE International Conference on Communication Software and Networks,* pp. 1-4, 2017.

[59] S. Yang, Y. Liu, S. Li, and D. Sun. "Simulation and Analysis of 60 GHz Millimeter Wave Propagation Characteristics in Laboratory Environment", *2020 International Conference on Microwave and Millimeter Wave Technology (ICMMT)*, pp. 1-3, 2020.

[60] X. Bian, Y. Liu, and S. Li, "Analysis of Millimeter-Wave Channel Characteristics in Urban Microcell Environment Based on the SBR Method", *International Conference on Microwave and Millimeter Wave Technology (ICMMT)*, pp. 1-3, 2020.

[61] G. R. MacCartney, Jr., T. S. Rappaport, S. Sun, and S. Deng, "Indoor Office Wideband Millimeter-Wave Propagation Measurements and Channel Models at 28 GHz And 73 GHz for Ultra-Dense 5G Wireless Networks", *IEEE Access,* vol. 3, pp. 2388–2424,2015.

[62] G. R. Maccartney, T.S. Rappaport, M.K. Samimi, and S. Sun, “Millimeter-Wave Omnidirectional Path Loss Data for Small Cell 5G Channel Modeling”, Special Section On Ultra-Dense Cellular Networks, *IEEE Access*, vol. 3, pp. 1573-1580, 2015.

[63] S. Sun, T. A. Thomas, T. S. Rappaport, H. Nguyen, I. Z. Kovacs and I. Rodriguez, "Path Loss, Shadow Fading, and Line-of-Sight Probability Models for 5G Urban Macro-Cellular Scenarios," *2015 IEEE Globecom Workshops (GC Wkshps)*, pp.1-7, 2015.

[64] S. Sun, T. S. Rappaport, T. A. Thomas, A. Ghosh, H. C. Nguyen, I. Z. Kovács, I.Rodriguez, O.Koymen, and A.Partyka, “Investigation of Prediction Accuracy, Sensitivity, and Parameter Stability of Large-Scale Propagation Path Loss Models for 5G Wireless Communications”, *IEEE Transactions on Vehicular Technology,* vol. 65, pp. 2843-2860, 2016.

[65] K. Haneda, L. Tian, H. Asplund, J. Li, Y. Wang, D. Steer, C. Li, T. Balercia, S. Lee, Y. Kim, A. Ghosh, T. Thomas, T. Nakamura, Y. Kakishima, T.Imai, H. Papadopoulas, T.S Rappaport,G.R MacCartney Jr,M.K Samimi, A. Ghosh, “Indoor 5G 3GPP-like Channel Models for Office and Shopping Mall Environments”, *2016 IEEE International Conference on Communications (ICC),* pp. 694-699, 2016.

[66] A. I. Sulyman, A. T. Nassar, M. K. Samimi, G. R. MacCartney, T. S. Rappaport, and A. Alsanie, “Radio Propagation Path Loss Models for 5G Cellular Networks in The 28 GHz and 38 GHz Millimeter-Wave Bands”, *IEEE Communications Magazine, IEEE,* vol. 52, pp. 78-86, 2014.

[67] G. R. MacCartney, and T.S. Rappaport, “Rural Macrocell. Path Loss Models for Millimeter Wave Wireless Communications”, *IEEE Journal On Selected Areas in Communications,* vol. 35, pp. 1663 - 1677, 2017.

[68] A. M. Al-Samman, T.A. Rahman, M.H. Azmi, M.N Hindia, I. Khan, E. Hanafi, “Statistical Modeling and Characterization of Experimental mm-Wave Indoor Channels for Future 5G Wireless Communication Networks”, *PLoS ONE,* vol. 11, pp. 1-29, 2016.

[69] A. M. Al-Samman, T. A. Rahman, M. Hadri, M.N. Hinrai, “Path Loss and RMS Delay Spread Model for 5G Channel at 19 GHz”, *IEEE,15th International Colloquium on Signal Processing and its Applications (CSPA 2017)* , pp.1-6, 2017.

[70] M. B. Majed , T. A. Rahman , O. A. Aziz, M.N.Hindia , and E.Hanafi, “Channel Characterization and Path Loss Modeling in Indoor Environment at 4.5, 28, and 38GHz for 5G Cellular Networks”, *International Journal of Antennas and Propagation,* vol. 2018, pp. 1-14, 2018.

[71] S. Deng, G. R. MacCartney, T. S. Rappaport, “Indoor and Outdoor 5G Diffraction Measurements and Models at 10, 20, and 26 GHz”, *IEEE Global Communications Conference, GLOBECOM 2016 - Proceedings. Institute of Electrical and Electronics Engineers Inc.* pp. 1-7, 2016.

[72] M. Khatun, H. Mehrpouyan, D. Matolak, “60-GHz Millimeter-Wave Path loss Measurements in Boise Airport”, *IEEE Global Conference on Signal and Information Processing (GlobalSIP),* pp. 1276-1280, 2018.

[73] A. M. Al-Samman, T. A. Rahman, M. H.Azmi, A. Sharaf, Y. Yamada, A. Alhammadi, “Path Loss Model in Indoor Environment at 40 GHz for 5G Wireless Network”, *IEEE 14th International Colloquium on Signal Processing & its Applications (CSPA 2018)*, pp. 1-6, 2018.

[74] K. Naruke, N. Honma, K. Kikuchi, Y. Sugawara, H. Minamizawa, "Indoor Localization Method Using Path Loss-Distance Relationship with Handset Sensor Information", *2018 IEEE International Symposium on Antennas and Propagation and URSI-USNC National Radio Science Meeting,* pp. 761-762, 2018.

[75] A. Alwarafy, A.I. Al-Sulyman, A. Alsanie, S.A. Alshebeili, and H.M. Behairy, "Path-Loss Channel Models for Receiver Spatial Diversity Systems at 2.4 GHz", *International Journal of Antennas and Propagation,* vol. 2017, pp. 1-12, 2017.

[76] P. Zhang, H. Wang, and W. Hong, "Empirical Analysis of Millimeter-Wave Propagation in Indoor Transitional Environments", *IEEE International Symposium on Antennas and Propagation and North American Radio Science Meeting,* pp.1189-1190, 2020.

[77] D. Zhang, Z. Zhou, C. Xu, Y. Zhang, J. Rodriguez and T. Sato, "Capacity Analysis of NOMA With mm Wave Massive MIMO Systems", *IEEE Journal on Selected Areas in Communications,* vol. 35, pp. 1606-1618, 2017.

[78] S. S. Sarma and R. Hazra, "Path Loss Attenuation Analysis for D2D Communication in 5G Mmwave Networks", *2020 Advanced Communication Technologies and Signal Processing (ACTS),* pp. 1-6, 2020.

[79] M. Giordani, M. Mezzavilla, and M, Zorzi, "Initial access in 5G mmWave cellular networks". *IEEE Commun. Mag.,* vol. 54, pp.40–47, 2016.

[80] D. P. Valle , Luis Mendo , J.M. Riera and P.G.Pino "Indoor LOS Propagation Measurements and Modelling at 26, 32, and 39 GHz Millimeter Wave Frequency Bands", *Electronics*, vol. 9, pp. 1-16, 2020.

[81] Q. Faizan, "Enhancing QOS Performance of the 5G Network by Characterizing mm-Wave Channel and Optimizing Interference Cancellation Scheme", *A Thesis Submitted for Doctor of Philosophy*, *University of Malaysia*, 2020.

[82] T. A. Thomas, M. Rybakowski, S. Sun, T. S. Rappaport, H. C. Nguyen, I. Z. Kovacs, and I. R. Larrad, "A Prediction Study of Path Loss Models from 2–73.5 GHz in an Urban-Macro Environment", *Proc. IEEE 83rd VTC Spring,* Nanjing, China, pp. 1-5, 2016.

[83] S. Sun, T. S. Rappaport, S. Rangan, T. A. Thomas, A. Ghosh, I.Z. Kovacs, I. Rodriguez, O. Koymen, A. Partyka, J. Jarvelainen "Propagation path loss models for 5G urban micro- and macro-cellular scenarios*", Proc. IEEE 83rd VTC Spring,* pp. 1-6, 2016.

[84] S. Sun, G. R. MacCartney, Jr., and T. S. Rappaport, "Millimeter-Wave Distance-Dependent Large-Scale Propagation Measurements and Path Loss Models for Outdoor and Indoor 5G Systems", *Proc. 10th EuCAP,* pp. 1-6, 2016.

[85] Spatial Channel Model for Multiple Input Multiple Output (MIMO) Simulations, *3GPP TR 25.996,* 2012.

[86] Study on 3D Channel Model for LTE, (Rel. 12), *3GPP TR 36.873*, V12.1.0, 2015.

[87] U. Schilcher, S. Toumpis, M. Haenggi, A. Crismani, G. Brandner, and C. Bettstetter, "Interference Functionals in Poisson Networks", *IEEE Transactions On Information Theory,* vol. 62, pp 371-384, 2016.

[88] T. S. Rappaport, G. R. MacCartney, M. K. Samimi, and S. Sun, "Wideband Millimeter-Wave Propagation Measurements and Channel Models for Future Wireless Communication System Design", *IEEE Trans. Communication.,* pp. 1-6, 2015.

[89] EE/TE 4367 Telecommunications Switching & Transmission Schedule, by Prof. Murat Torlak, Spring 2008 Semester. https://personal.utdallas.edu/~torlak/courses/ee4367/lectures/

[90] J. Yang, B. Ai, D. He, L. Wang, Z. Zhong, and A. Hrovat, "A Simplified Multipath Component Modeling Approach for High-Speed Train Channel Based on Ray Tracing", *Wireless Communications and Mobile Computing,* vol. 2017, pp. 1-14, 2017.

[91] Z. Xiao, T.He, P.Xia, and X. Xia, "Hierarchical Codebook Design for Beamforming Training in Millimeter-Wave Communication", *IEEE Transactions on Wireless Communications,* vol. 16, pp 141–153, 2017.

[92] A. A. M. Saleh and R. A. Valenzuela, "A statistical model for indoor multipath propagation", *IEEE Journal on Selected Areas in Communications,* vol. 5, pp. 128–137,1987.

[93] J. Foerster, Ed., "Channel Modeling Sub-Committee Report Final", *IEEE, Document* IEEE P802.15-02/490r1-SG3a, 2003.

[94] X. Wu, C. Wang, J. Sun, J. Huang, R. Feng, Y. Yang, and X. Ge, "60 GHz Millimeter-Wave Channel Measurements and Modeling for Indoor Office Environments", *IEEE Transactions on Antennas and Propagation,* vol. 65, pp 1912- 1924, 2017.

[95] S. Qu and Z. Zhe, "Wide-Angle Scanning Lens at 28 GHz Fed by Antenna Array", *IEEE Transactions on Antennas and Propagation*, vol. 68, pp. 3635 – 3643, 2020.

[96] P. Wang, Y. Li, L. Song, and B. Vucetic, "Multi-Gigabit Millimeter Wave Wireless Communications for 5G: From Fixed Access to Cellular Networks", *IEEE Communications Magazine,* vol. 53, pp. 168-178, 2014.

[97] B. Nin, Z. Chen, W. Chen, Y. Du, and J. Fang, "Channel Estimation and Hybrid Beam forming for Reconfigurable Intelligent Surfaces Assisted THz Communications", *ICC 2020 IEEE International Conference on Communications (ICC),* pp. 1-7, 2020.

[98] A.A. Althuwayb, "MTM- and SIW-Inspired Bowtie Antenna Loaded with AMC for 5G mm-Wave Applications". *Int. J. Antennas Propag.*, vol. 2021, pp, 1–7, 2021.

[99] A. A. Althuwayb, "Low-Interacted Multiple Antenna Systems Based on Metasurface-Inspired Isolation Approach for MIMO Applications". *Arab. J. Sci. Eng*, vol. *47*, pp. 2629–2638, 2021.

[100] A. A. Althuwayb, "On-Chip Antenna Design Using the Concepts of Metamaterial and SIW Principles Applicable to Terahertz Integrated Circuits Operating over 0.6–0.622 THz". *Int. J. Antennas Propag.,* vol. 2020, pp. 1–9, 2020.

[101] M. Alibakhshikenari, et al, "A Comprehensive Survey on Antennas On-Chip Based on Metamaterial, Metasurface, and Substrate Integrated Waveguide Principles for Millimeter-Waves and Terahertz Integrated Circuits and Systems". *IEEE Access*, vol. *10*, pp. 3668–3692, 2022.

[102] M. Zarastvand, M. Asadijafari, and R. Talebitooti, "Acoustic wave transmission characteristics of stiffened composite shell systems with double curvature". *Compos. Struct.*, vol. *292*, 115688, 2022.

[103] M. R. Akdeniz, Y. Liu, M. K. Samimi, S. Sun, S. Rangan, T. S. Rappaport, and E. Erkip, "Millimeter wave channel modeling and cellular capacity evaluation". *IEEE J. Selected Areas Commun*, vol.*32*, pp. 1164–1179, 2014.

[104] M. Lecci, P. Testolina, M. Giordani, M. Polese, T. Ropitault, and C. Gentile, "Simplified Ray Tracing for the Millimeter Wave Channel: A Performance Evaluation"; *National Institute of Technology (NIST), Information Theory and Applications Workshop (ITA):* Gaithersburg, MD, USA, 2020.

[105] J. Caruso, *Copper 10 Gigabit Ethernet NICs Unveiled*; Network World: Needham, MA, USA, 2007.

[106] K.C. Huang, and Z. Wang, "Millimeter Wave Communication Systems"*; Institute of Electrical and Electronics Engineers; John Wiley & Sons, Inc.; IEEE Press:* Piscataqay, NJ, USA, 2011.

[107] M. H. Alsharif, and R. Nordin, "Evolution towards fifth generation (5G) wireless networks: Current trends and challenges in the deployment of millimetre wave, massive MIMO, and small cells". *Telecommun. Syst*, vol.*64*, pp.617–637, 2016.

[108] M.M. Shirkolaei, and M. Jafari, "A new class of wideband microstrip falcate patch antennas with reconfigurable capability at circular-polarization". *Microw. Opt. Technol. Lett.*, vol.*62*, pp.3922–3927, 2020.

[109] M. M. Shirkolaei, "Wideband linear microstrip array antenna with high efficiency and low side lobe level". *Int. J. RF Microw. Comput. Aided Eng*, vol.*30*, pp. 1-7, 2020.

[110] J. I. E. Huang, Y. Cao, X. Raimundo, A. Cheema, "Rain Statistics Investigation and Rain Attenuation Modeling for Millimeter Wave Short-Range Fixed Links", *IEEE Access*, vol. 7, pp.156110–156120, 2019.

[111] A. Sari, and A. Alzubi. "Security and Resilience in Intelligent Data-Centric Systems and Communication Networks"; *Intelligent Data-Centric Systems; Elsevier:* Amsterdam, The Netherlands, pp. 285–313, 2018.

[112] Y. Wang, W. Lu, and H. Zhu, "An Empirical Path-Loss Model for Wireless Channels in Indoor Short-Range Office Environment". *Int. J. Antennas Propag.*, vol. 2012, pp. 1–7, 2012.

[113] A. Al-Hourani, S. Chandrasekharan, and S. Kandeepan, "Path loss study for millimeter wave device-to-device communications in urban environment". *In Proceedings of the IEEE International Conference on Communications Workshops*, pp. 102–107, 2014.

[114] S. S. Sarma, and R. Hazra, "Interference management for D2D communication in mmWave 5G network: An Alternate Offer Bargaining Game theory approach". *In Proceedings of the 2020 7th International Conference on Signal Processing and Integrated Networks (SPIN),* pp.202–207, 2020.

[115] R. G. Donmez, "A Study on Path Loss for Indoor Wireless Communication Networks". *Master's Thesis, Middlesex University: London,* UK, pp. 1–70, 2013.

[116] M. Khatuny, H. Mehrpouyany, and D. Matolakz, "60-GHz Millimeter-Wave Path Loss Measurements in Boise Airport". *In Proceedings of the IEEE Global Conference on Signal and Information Processing (GlobalSIP)*, pp. 1276–1280, 2018.

[117] S. J. Howard, and K. Pahlavan, "Measurement and analysis of the indoor radio channel in the frequency domain. *IEEE Transactions on Instrumentation and Measurement*, vol. 39; pp. 751–755, 1990.

[118] D. Cassioli, M. Win, and A. Molisch, "The ultra-wide bandwidth indoor channel: From statistical model to simulations". *IEEE J. Sel. Areas Commun.*, vol. *20*, 1247–1257, 2002.

[119] S. S. Ghassemzadeh, R. Jana, C. W. Rice, W. Turin, and V. Tarokh, "Measurement and modeling of an ultra-wide bandwidth indoor channel". *IEEE Transactions on Communications,* vol. 52; pp. 1786–1796, 2004.

[120] P. Handayani, L. Mubarokah, and G. Hendrantoro, "Path loss and Shadowing Characteristics in Indoor Environment at 2.4 GHz Band". *In Proceedings of the IEEE International Seminar on Intelligent Technology and Its Applications (ISITIA),* pp.1-6,2015.

[121] J. Qiao, X. S. Shen, J. W. Mark, Q. Shen, Y. He, and L. Lei, "Enabling device-to-device communications in millimeter-wave 5G cellular networks". *IEEE Commun. Mag.*, vol. *53*, pp. 209–215, 2015.

[122] D. P. Domingo, L. Mendo, J. M. Riera, and P. G. Pino. "Indoor LOS Propagation Measurements and Modeling at 26, 32, and 39 GHz Millimeter Wave Frequency Bands". *Electronics*, vol.*9*, 1867, 2020.

[123] F. Qamar, "Enhancing QOS Performance of the 5G Network by Characterizing mm-Wave Channel and Optimizing Interference Cancellation Scheme". *Ph.D. Thesis, University of Malaysia, Kuala Lumpur,* Malaysia, 2020.

[124] J. B. Andersen, T. S. Rappaport, and S. Yoshida, "Propagation measurements and models for wireless communications channels". *IEEE Commun. Mag.*, vol. *33*, pp.42–49, 1995.

[125] F. Qamar, M. N. Hindia, T. A. Rahman, R. Hassan, K. Dimyati, and Q. N. Nguyen, "Propagation Characterization and Analysis for 5G mmWave Through Field Experiments". *Comput. Mater. Contin.*, vol.*68*, pp. 2249–2264, 2021.

[126] T. Oladimeji, P. Kumar, and M. K. Elmezughi, "Path loss measurements and model analysis in an indoor corridor environment at 28 and 38 GHz*". Sensors*, vol. 22, pp. 1-30, 2022.

[127] A. K. Jain, Acharya, R. S Jakhar, and T. Mishra, "Fifth Generation (5G) Wireless Technology Revolution in Telecommunication*", 2018 Second International Conference on Inventive Communication and Computational Technologies (ICICCT*), pp. 1867-1872, 2018.

[128] C.X. Wang, F. Haider, X. Gao, X. H You, Y. Yang, D. Yuan, H. M Aggoune, H. Haas, S. Fletcher, and E. Hepsaydir, "Cellular architecture and key technologies for 5G wireless communication networks", *IEEE Commun. Mag.* vol. 52, pp. 122 – 130, 2014.

[129] B. Xu, D. Zhang, Y. Wang, B. Hong, G. Shu, and W. He, "Characterization of millimeter wave photonic crystal circulator with a ferrite sphere", *Results in Physics*, vol. 34, pp. 1-5, 2022.

[130] T. T. Oladimeji, P. Kumar, and NO Oyie, "Propagation Path Loss Prediction Modelling in Enclosed Environments for 5G Networks: A Review", *Heliyon,* vol. 8, pp.1-16, 2022.

[131] Industry Proposal for a Public Private Partnership (PPP) in Horizon 2020 (Draft Version 2.1), Horizon 2020 Advanced 5G Network Infrastructure for the Future Internet PPP, 2020. Available: http://www.networks-etp-eu/_leadmin/user_upload/Home/ draft-PPP-proposal.pdf

[132] A.M. Al-Samman, T. A Rahman, M. H.Azmi, and S.A. Al-Gailani, "Millimeter-wave propagation measurements and models at 28 and 38 GHz in a dining room for 5G wireless networks", *Measurement*, vol. 130,pp. 71-81, 2018.

[133] https://www.everythingrf.com/community/what-are-millimeter-waves, retrieved on 27th August 2022 ;11.27am.

[134] http://www.eng.tau.ac.il/~dbl/mmw.htm. Retrieved 10th August 2021; 10.59am.

[135] L. Pometcu, and R. D'Errico, "An Indoor Channel Model for High Data- Rate Communications in D-Band", *IEEE Access,* vol. 8, pp. 9420–9433. 2019.

[136] M. Aborahama *e*t al, "Large-scale channel characterization at 28 GHz on a university campus in the United Arab Emirates", *Telecommun. Sys.*, vol. 1, pp. 1–15, 2020.

[137] Kleine-Ostmann.T.et al, "Measurement of channel and propagation properties at 300 GHz". *2012 Conf. Precision electromagn. Measurements*, pp. 258–259, 2012.

[138] N.V. Dien, N. V. Tuan, L.T. P Mai, N.V. Hieu, V.Q Phuoc, N.Q.N. Quynh, N.T Hung, "Tolerance of SCM nyquist and OFDM signals for heterogeneous fiber-optic and millimeter-wave mobile backhaul links under the effect of power amplifier saturation induced clipping", *Computer Networks,* vol. 204, pp. 1-8, 2022.

[139] T.S. Rappaport, S. Sun, R. Mayzus, H. Zhao, Y. Azar, K. Wang, G.N. Wong, J.K. Schulz, M. Samimi, and F. Gutierrez, "Millimeter wave mobile communications for 5G cellular: It will work!" *IEEE Access,* vol. 1, pp.335–349, 2013.

[140] FCC. http://transition.fcc.gov/bureaus/oet/tac/--tacdocs/meeting61313/ TACPresentations6-13-13.pdf.

[141] Z. Qingling, and J. Li, "Rain attenuation in millimeter wave ranges", in Antennas, Propagation EM Theory, 2006. *ISAPE '06. 7th International Symposium,* pp. 1–4, 2006.

[142] A. Osseiran, J. F. Monserratand, and P. Marsch, "5G mobile and wireless communications technology", *Int. J. Satell. Commun. and Networ.,* vol. 34, pp. 351-360, 2016.

[143] C. L. Cheng, S. Kim, and A. Zaji, "Comparison of path loss models for indoor 30 GHz, 140 GHz, and 300 GHz channels", *2017 11th European Conf. Antennas Propag. (EUCAP),* pp. 716–720, 2017.

[144] G. Zhang, K. Saito, W. Fan, X. Cai, P. Hanpinitsak, J.I. Takada, and G. F. Pedersen, "Experimental characterization of millimeter-wave indoor propagation channels at 28 GHz", *IEEE Access,* vol. 6, pp. 76516-76526, 2018.

[145] M. Marcus, and B. Pattan, "Millimeter wave propagation: spectrum management implications", *IEEE Microwave Magazine,* vol. 6, pp. 54– 62, 2005.

[146] M. K. Samimi, T.S. Rappaport, and G. R. Maccartney, "Probabilistic Omnidirectional Path Loss Models for Millimeter-Wave Outdoor Communications", *IEEE Wirel. Commun. Lett.*, vol. 4, pp. 357–360, 2015.

[147] Z. Pi. and Khan. F. "An introduction to millimeter-wave mobile broadband systems", *IEEE Commun. Mag.*, vol. 49, pp. 101–107, 2011.

[148] M. K. Elmezughi, and T. J. Afullo, "Proposal of a Probabilistic Path Loss Model for Wireless Communications in Indoor Corridors", *International Conference on Electrical, Computer and Energy Technologies (ICECET)*, pp. 1-5, 2021.

[149] A. M. Al-Samman, M. N. Hindia, and T. A. Rahman, "Path loss model in outdoor environment at 32 GHz for 5G system", *2016 IEEE 3rd Int. Symp. Telecommun. Technol. ISTT,* pp. 9–13. 2016.

[150] Haneda. et al. "5G 3GPP-like channel models for outdoor urban microcellular and macro cellular environments", *IEEE Veh. Technol. Conf.*, pp. 1-7, 2016.

[151] N. O. Oyie, and T. J. O. Afullo, "A Comparative Study of Dual-Slope Path Loss Model in Various Indoor Environments at 14 to 22 GHz", *Prog. Electromagn. Res. Symp.*, pp. 121–128, 2018.

[152] S. Hur, S. Baek, B. Kim, Y. Chang, A. F. Molisch, T.S. Rappaport, K. Haneda, and J. Park, "Proposal on millimeter-wave channel modeling for 5G cellular system", *IEEE J. Sel. Top. Signal Process.*, vol. 10, pp. 454–469, 2016.

[153] M. Peter, R. J. Weiler, W. Keusgen, T. Eichler, M. Kottkamp, and A. Nähring, "Characterization of mm-wave channel sounders up to W-band and validation of measurement results", *in 2016 10th European Conference on Antennas and Propagation (EuCAP),* pp. 1–5, 2016.

[154] M. N. Hindia, A.M. Al-Samman, T. A. Rahman, and T. M. Yazdani, "Outdoor large-scale path loss characterization in an urban environment at 26, 28, 36, and 38 GHz", *Physical Communication,* vol. 27, pp. 150–160, 2018.

[155] S. Deng, M.K. Samimi, and T. S. Rappaport, "28 GHz and 73 GHz millimeter-wave indoor propagation measurements and path loss models", *2013 IEEE Global Communications Conference (GLOBECOM),* pp. 1244–1250, 2015.

[156] T. Abbas, F. Qamar, I. Ahmed, K. Dimyati, and M.B. Majed, "Propagation channel characterization for 28 and 73 GHz millimeter-wave 5G frequency band", *2017 IEEE 15th Student Conference on Research and Development (SCOReD),* pp. 297–302, 2017.

[157] F. Qamar, M. H. Siddiqui, K. Dimyati, K. A. Noordin, and M. B. Majed, "Channel characterization of 28 and 38 GHz MM-wave frequency band spectrum for the future 5G network", *2017 IEEE 15th Student Conference on Research and Development (SCOReD),* pp. 291–296, 2017.

[158] T. Zwick, T. J. Beukema, and H. Nam, "Wideband channel sounder with measurements and model for the 60 GHz indoor radio channel", *IEEE Trans. Veh. Technol.,* vol. 54, pp. 1266–1277,2005.

[159] M. Cheffena, and M. Mohamed, "Empirical Path Loss Models for Wireless Sensor Network Deployment in Snowy Environments", *IEEE Antennas Wirel. Propag. Lett.,* vol. 16, pp. 2877–2880, 2017.

[160] P. F. M. Smulders, "Statistical characterization of 60-GHz indoor radio channels", *IEEE Trans. Antennas Propag.,* vol. 57, pp. 2820-2829, 2009.

[161] M. K. Elmezughi, and T. J. Afullo, "Investigations into the Effect of High-Ordering the Log-Distance Dependency of Path Loss Models for Indoor Wireless Channels", *International Journal on Communications Antenna and Propagation (I.Re.C.A.P.),* vol. 12, pp.1-13, 2022.

[162] S. Ali, M.I. Aslam, and I. Ahmed, "Uplink coverage probability and spectral efficiency for downlink uplink decoupled dense heterogeneous cellular network using multi-slope path loss model". *Telecommun Syst* vol. 72, pp. 505–516, 2019.

[163] S. Ali, M.I. Aslam, I. Ahmed, et al. "Analysis of the decoupled uplink downlink technique for varying path loss exponent in multi-tier HetNet". *Telecommun Syst* vol. 74, pp. 497–510, 2020.

[164] S. Sun, T. S. Rappaport, R. W. Heath, A. Nix, and S. Rangan, "MIMO for millimeter-wave wireless communications: Beamforming, spatial multiplexing, or both?" *IEEE Commun. Mag.,* vol. 52, pp. 110–121, 2014.

[165] T. S. Rappaport et al., "Millimeter wave mobile communications for 5G cellular: It will work!" *IEEE Access,* vol. 1, pp. 335–349, 2013.

[166] T. T. Oladimeji, P. Kumar, and M. K. Elmezughi. "Performance Analysis of Improved Path Loss Models for Millimeter-Wave Wireless Network Channels at 28 GHz and 38 GHz". *PLOS ONE*, vol. 18, pp. 1-27, 2023

[167] T. Oladimeji, P. Kumar and M. Elmezughi. "Performance Analysis of High Order Close-In Path Loss Model at 28 and 38 GHz", *2023 Conference on Information Communications Technology and Society (ICTAS 2023)*, pp.1-52023.

[168] H. Song, and M. Brandt-Pearce, "A Discrete-Time Polynomial Model of Single Channel Long-Haul Fiber Optic Communication Systems", *IEEE International Conference on Communications (ICC)*, pp. 1–6, 2011.

[169] O. Ahmadien, H.F. Ateş, T. Baykas, and B.K. Gunturk, "Predicting Path Loss Distribution of an Area from Satellite Images Using Deep Learning". *IEEE Access, vol. 8*, pp. 64982-64991, 2020.

[170] S.I. Popoola, A.A. Atayero, O.D Arausi, and V.O. Matthews, "Path loss Dataset for Modeling Radio Wave Propagation in Smart Campus Environment." *Elsevier Data Brief*, vol. 17, pp.1062–1073, 2018.

[171] S. Salous, J. Lee, M. D. Kim, M. Sasaki, W. Yamada,X. Raimundo, and A.A. Cheema, "Radio Propagation Measurements and Modeling for Standardization of the Site General Path Loss Model in International Telecommunications Union Recommendations for 5G Wireless Networks" *Radio Sci.,* vol. 55, pp. 1-12, 2020.

[172] N. Shabbira, L. Kütta, M .M Alamb, P. Roosipuub, M. Jawadc, M. B Qureshic,A. R Ansarid, and R. Nawaze, "Vision Towards 5G: Comparison of Radio Propagation Models for Licensed and Unlicensed Indoor Femtocell Sensor Networks". *Elsevier Phys. Commun,* vol. 47, pp. 1-11, 2021.

[173] P. D. Casillas, G. C. Camacho, F. S. Jiménez-Fernandez, F. J A. Portilla, and S. S Salcedo, "Weighted ABG: A General Framework for Optimal Combination of ABG Path-Loss Propagation Models". *IEEE Access,* vol. 8, pp. 101758–101769, 2020.

[174] H. K. Rath, S. Timmadasari, B. Panigrahi, and A. Simha, ``Realistic indoor path loss modeling for regular WiFi operations in India," in *Proc. 23rd Nat. Conf. Commun. (NCC)*, pp. 1-6, 2017.

[175] G. Zhang, P. Hanpinitsak, X. Cai, W. Fan, K. Saito, J. Takada, and G.F. Pedersen, "Millimeter-wave channel characterization in large hall scenario at the 10 and 28 GHz bands". *in Proceedings of the 2019 13th European Conference on Antennas and Propagation (EuCAP),* pp. 1–4, 2019.

[176] W. Fan, I. Carton, J. Ø. Nielsen, K. Olesen, and G. F. "Pedersen Measured wideband characteristics of indoor channels at centimetric and millimetric bands*". J Wireless Com Network*, vol. 58, pp. 1-13, 2016.

[177] A. M. Al-Samman, T. A. Rahman, and M.H. Azmi, "Indoor corridor wideband radio propagation measurements and channel models for 5G millimeter wave wireless communications at 19 GHz, 28 GHz, and 38 GHz bands". *Wirel. Commun. Mobile Comput,* vol. 2018, pp. 1-12, 2018.

[178] A. M. Al-Samman, T. Al-Hadhrami, A. Daho, M. Hindia, M. H. Azmi, K. Dimyati, and M.Alazab, "Comparative study of indoor propagation model below and above 6 GHz for 5G wireless networks", *Electronics,* vol. 8, pp. 1-16, 2019.

[179] M. K. Elmezughi and T. J. Afullo, "Proposal of a Measurement-Based Propagation Channel Model for Future Indoor Wireless Networks," *Southern Africa 2022 Telecommunication Networks and Applications Conference (SATNAC 2022)*, pp. 1-5, 2022.

[180] I. F Akyildiz., C. Han, and S. Nie, "Combating the Distance Problem in the Millimeter Wave and Terahertz Frequency Bands", *IEEE Communications Magazine,* vol. 56, pp. 102 – 108, 2018.

[181] B. T. Ahmed, J.L. Masa Campos, and J.M Lalueza Mayordomo. "Propagation Path Loss and Materials Insertion Loss in Indoor Environment at WiMAX Band of 3.3 to 3.6 GHz". *Wireless Pers Commun.*, vol.66, pp.251–260, 2012.

[182] C. M. K. Swain, and S. Das, "Proposed Prediction Framework for Improving the Accuracy of Path Loss Models of WiMAX Network". *Wireless Pers Commun.,* vol.117, pp. 1079–1101, 2021.

[183] A. Gupta, and R.K Jha, "A survey of 5G network: architecture and emerging technologies", *IEEE Access*, vol. 3, pp. 1206– 1232, 2015.

[184] Y. A. Al-Gumaei, N. Aslam, A. M. Al-Samman, T. Al-Hadhrami, K. Noordin, and Y. Fazea, "Non-cooperative power control game in D2D underlying networks with variant system conditions", *Electronics,* vol. 8, pp 1-15, 2019.

[185] R. Li, Z. Zhao, C. Qi, and H. Zhang "Characterizing and Learning the Mobile Data Traffic in Cellular Network"5G Networks: Fundamental Requirements, Enabling Technologies, and Operations Management, *John Wiley & Sons, Inc.,* pp. 453-498,2018.

[186] H. Tataria, K. Haneda, A. F Molisch, M. Shafi, and F. Tufvesson, "Standardization of Propagation Models: 800 MHz to 100 GHz, A Historical Perspective", *IEEE Invited paper, arXiv Signal Processing*, pp. 1-19, 2020

[187] 3GPP TR 36.104 "Technical specification of radio access network: Base station radio transmission and reception", 2019.

[188] R. Steele, "Mobile Radio Communications", *Pentech Press,* 1992.

[189] M. Shafi, H. Tataria, A. F. Molisch, F. Tufvesson, and G. Tunnicliffe., "Real-time deployment aspects of C-band and millimeter-wave 5G-NR systems", *in Proc. IEEE ICC*, pp. 1-7, 2020.

[190] ITU-R M.1225, Guidelines for evaluation of radio transmission, *ITUR*, 1997.

[191] M. Stefanovic, S .R. Panic, R. A.A Souza, and J. Reig "Recent Advances in RF Propagation Modelling for 5G Systems", *Hindawi, International Journal of Antennas and Propagation*, vol.2017, pp.1-5, 2017.

[192] Channel Modelling for Higher Frequency Bands, document RP 151306, *3GPP*, 2015.

[193] METIS Deliverables D1.2, "Initial Channel Models Based on Measurements." Accessed: Nov. 5, 2017.

[194] N. Moraitis, and P. Constantinou, "Indoor Channel Measurements and Characterization at 60 GHz for Wireless Local Area Network Applications", *IEEE Transactions on Antennas and Propagation,* vol. 52, pp 3180- 3189,2004.

[195] M. K. Elmezughi, O. Salih, T. J Afullo, and K.J. Duffy,"Comparative Analysis of Major Machine-Learning Based Path Loss Models for Enclosed Indoor Channels". *Sensors*, vol. 22, pp.1-25,2022.

[196] C. Nguyen, and A. A. Cheema, A.A. "A Deep Neural Network-Based Multi-Frequency Path Loss Prediction Model from 0.8 GHz to 70 GHz", *Sensors* vol. 21, pp. 1-24, 2021.

[197] N. Faruk, S.I. Popoola, N. T. Surajudeen-Bakinde, A. A. Oloyede, A. Abdulkarim, L.A. Olawoyin, M. Ali, C.T. Calafate, and A.A. Atayero, "Path Loss Predictions in the VHF and UHF Bands within Urban Environments: Experimental Investigation of Empirical, Heuristics and Geospatial Models", *IEEE Access*, vol. 7, pp. 77293–77307, 2019.

[198] H.S. Jo, C. Park, E. Lee, H. K. Choi, and J. Park, "Path Loss Prediction Based on Machine Learning Techniques: Principal Component Analysis, Artificial Neural Network and Gaussian Process". *Sensors*, vol. 20, pp.1-23, 2020.

[199] Beauvarlet. D, and Virga.K.L, "Measured characteristics of 30-GHz indoor propagation channels with low-profile directional antennas", *IEEE Antennas Wirel. Propag. Lett.,* vol.1, pp, 87–90, 2002.

[200] R. He, Y.Gong, W. Bai, Y. Li, X. Wang, "Random Forests Based Path Loss Prediction in Mobile Communication Systems". *In Proceedings of the 2020 IEEE 6th International Conference on Computer and Communications (ICCC)*, pp. 3029–3056,2020.